TOWARDS AN UNDERSTANDING OF THE CLOUD FORMATION POTENTIAL OF CARBONACEOUS AEROSOL: LABORATORY AND FIELD STUDIES

A Thesis
Presented to
The Academic Faculty

by

Luz Teresa Padró Martínez

In Partial Fulfillment
of the Requirements for the Degree
Doctor of Philosophy in the
School of Chemical and Biomolecular Engineering

Georgia Institute of Technology
December 2009

TOWARDS AN UNDERSTANDING OF THE CLOUD FORMATION POTENTIAL OF CARBONACEOUS AEROSOL: LABORATORY AND FIELD STUDIES

Approved by:

Dr. Athanasios Nenes, Advisor
School of Chemical and Biomolecular Engineering and School of Earth and Atmospheric Sciences
Georgia Institute of Technology

Dr. Amyn Teja
School of Chemical and Biomolecular Engineering
Georgia Institute of Technology

Dr. Greg Huey
School of Earth and Atmospheric Sciences
Georgia Institute of Technology

Dr. Rodney J. Weber
School of Earth and Atmospheric Sciences
Georgia Institute of Technology

Dr. Carson Meredith
School of Chemical and Biomolecular Engineering
Georgia Institute of Technology

Date Approved: July 10, 2009

To my family for always believing in me and
in memory of my grandparents, Cuca and Urbano

ACKNOWLEDGEMENTS

I would like to thank everyone who has helped and supported me throughout this experience. To my advisor Dr. Athanasios Nenes, for his assistance and guidance through out the years. I am truly grateful for all the support, advice, and opportunities you have given me. To my committee members, Dr. Greg Huey, Dr. Carson Meredith, Dr. Amyn Teja, and Dr. Rodney Weber, for their support throughout this experience. To my group members, Dr. Rafaella Sotoripoulus, Dr. Sara Lance, Dr. Christos Fountoukis, Dr. Akua Asa-Awuku, Dr. Wei-Chun Hsieh, Donifan Barahona, Richard Moore, Shannon Capps, Terry Lathem, Prashant Kumar, Ricardo Morales, Kate Cerully, Ryan Morrison, and Daniel Tkacik, for making the work environment so enjoyable.

In addition, I would like to thank my collaborators for the different field campaigns, Dr. Chris Hennigan and Dr. Amy Sullivan (MILAGRO), Dr. Armin Sorooshian, Shane Murphy, Harmony Gates, Dr. Richard C. Flagan, and Dr. John H. Seinfeld at California Institute of Technology (MASE II), and Xialou Zhang and Dr. Neeraj Rastogi at Georgia Institute of Technology (AMIGAS). I would also like to extend my gratitude to Dr. Gayle Hagler, Dr. Mike Bergin, Evan Cobb, and Dr. Armisted Rusell for allowing me to use their instruments for my chemical composition analysis. To the NASA Earth System Science (ESS) Fellowship Program, I am grateful for providing me with the financial support in the last two years.

Finally this work could have not been possible without the love and encouragement of my biggest supporters, my friends and family. I extend my deepest gratitude to my parents, Héctor Jaime and Luz Teresa, and siblings, Margarita y Jaimito, for all the love and support you have given me and for always believing in me. Thanks for all the sacrifice you have made; I love you all so much. To my uncles, aunts, cousins, and grandparents, thank you for being my cheerleaders. To my husband and best friend, Roel Sigifredo, thanks for all your love, patience, and support throughout grad school;

you have made this journey easier and enjoyable. To his family, for accepting me as one of their own and showing me their continuous support. To Ana Fernández, Enrique Michel Sánchez, and Gerardo Orozco Valdés, thanks for making my first year in grad school so much fun. It was a pleasure hanging out and getting to know you all. I wish you could have stayed here longer. To Swati Rane, for being such a good roommate, listener, and friend through out this last two years. To Juan Manfredo and Juan José, thank you for being my friends all these years no matter the distance. And lastly, I would like to thank God for all the blessings he has given me and for making this a reality; without him nothing would be possible.

TABLE OF CONTENTS

Page

ACKNOWLEDGEMENTS iv

LIST OF TABLES x

LIST OF FIGURES xii

LIST OF SYMBOLS xix

LIST OF ABBREVIATIONS xxv

SUMMARY xxvii

CHAPTER 1: INTRODUCTION 1

1.1 Aerosols, clouds, and climate change 1

1.2 Aerosols as cloud condensation nuclei 3

1.3 Thesis outline 4

1.4 References 5

CHAPTER 2: CLOUD DROPLET ACTIVATION: SOLUBILITY REVISITED 9

2.1 Motivation 9

2.2 Theory of CES and its impact on CCN activity 12

2.2.1 Traditional Köhler theory 12
2.2.2 The effect of solute core curvature 13
2.2.3 When is bulk solubility not enough to explain CCN activity? 14
2.2.4 Introducing CES in Köhler theory 15
2.2.5 When can CES affect CCN activity? 17

2.3 Obtaining interfacial energy: the contact angle method 21

2.4 CES for single-component organic CCN 22

2.4.1 Interfacial energy for the compounds studied 24
2.4.2 Impact of CES on Köhler curves 27
2.4.3 Sensitivity of critical supersaturation to CES and interfacial energy 29
2.4.4 Does CES improve predictions of CCN activity? 31

2.5 Conclusions 31

2.6 References 34

CHAPTER 3: INFERRING THERMODYNAMIC PROPERTIES FROM CCN ACTIVATION EXPERIMENTS: SINGLE-COMPONENT AND BINARY AEROSOLS 37

3.1 Motivation 37

3.2 Köhler theory analysis 39

3.2.1 Single component CCN 39
3.2.2 Multicomponent CCN 40
3.2.3 Köhler theory analysis: inferring molar volume 41
3.2.4 Molar volume uncertainty analysis 43
3.2.5 Köhler theory analysis: inferring solubility 43

3.3 Experimental procedure 46

3.3.1 Surface tension measurements 46
3.3.2 CCN activity measurements 47
3.3.3 Compounds considered in this study 50

3.4 Results 51

3.4.1 Surface tension measurements 51
3.4.2 CCN measurements 53
3.4.3 Evaluation of inferred molar volumes 57

3.5 Conclusions 63

3.6 References 63

CHAPTER 4: INVESTIGATION OF CCN RELEVANT PROPERTIES AND DROPLETGROWTH KINETICS OF WATER-SOLUBLE ORGANIC CARBON IN MEXICO CITY 68

4.1 Motivation 68

4.2 Location description, sample collection, and experimental methods 70

4.2.1 Location, meteorology, and air masses sampled 70
4.2.2 Particle collection and extraction 71
4.2.3 Chemical composition 73

4.2.3.1 TOC analyzer 73
4.2.3.2 Ion chromatography 75

4.2.4 Surface tension 75
4.2.5 CCN activity and growth kinetic measurements 76
4.2.6 Effects of electrolyte addition on surface tension and CCN activity 79

4.3 Experimental analysis 79
4.3.1 Köhler theory analysis 79
4.3.2 κ-Köhler theory 83
4.4 Results and discussion 85
4.4.1 Surfactant characteristics 85
4.4.2 CCN activity and hygroscopicity 85
4.4.3 Growth kinetics 93
4.4.4 Average organic molar mass 95
4.5 Conclusions 96
4.6 References 99
CHAPTER 5: MIXING STATE, CCN ACTIVITY, AND DROPLET GROWTH KINETICS OF SIZE RESOLVED CCN IN AN URBAN ENVIRONMENT 106
5.1 Motivation 107
5.2 Experimental methods 110
5.2.1 Chemical composition 110
5.2.2 Particle size distribution and total aerosol concentration 111
5.2.3 CCN activity and growth kinetic measurements 112
5.3 Experimental analysis 115
5.3.1 Sigmoidal fit of CCN activity spectrum 115
5.3.2 CCN distribution 116
5.3.3 CCN closure and mixing state 117
5.4 Results and discussion 122
5.4.1 Total CN concentration comparison 122
5.4.2 HYSPLIT trajectories 124
5.4.3 CCN closure 125
5.4.4 Mixing state as a function of dry diameter 131
5.4.5 Droplet growth kinetics 133
5.5 Conclusions 137
5.6 References 138
CHAPTER 6: CCN MEASUREMENTS ABOARD THE CIRPAS TWIN OTTER DURING THE 2007 MASE II CAMPAIGN 143
6.1 Motivation 144
6.2 Observation platform and instruments 145

6.2.1 Particle size distribution and total aerosol concentration 146
6.2.2 Aerosol chemical composition 148
6.2.3 CCN and growth kinetic measurements 148

6.3 CCN closure 151

6.4 Results and discussion 153

6.4.1 CCN closures 153
6.4.2 Growth kinetics 159

6.5 Conclusions 161

6.6 References 164

CHAPTER 7: SUMMARY AND IMPLICATIONS 169

7.1 Synopsis 169

7.2 References 173

VITA 175

LIST OF TABLES

Page

Table 2. 1: Compounds considered in this study. 23

Table 2. 2: Value of Φ (ratio solute moles required for activation over those allowed by bulk solubility) at various supersaturations. Bold numbers denote cases where bulk solubility alone is insufficient for activating CCN. 24

Table 2. 3: Surface tension at saturation point, contact angle, and interfacial energy for organic/saturated aqueous system interface at 25 °C. Uncertainty in measured quantities corresponds to one standard deviation. 25

Table 3. 1: Formulas used for computing the sensitivity of molar volume to σ, ω, and υ_j. 44

Table 3. 2: Properties of compounds considered in this study. Organics are sorted in order of decreasing solubility. 51

Table 3. 3: Szyskowski-Langmuir constants (298 K) for computing the surface tension of aqueous organic solutions. The same parameters apply for pure organic solutions and mixtures with $(NH_4)_2SO_4$ (up to 10 % salt mole fraction). C_{max} is the maximum concentration of organic used in the measurements. 55

Table 3. 4: Szyskowski-Langmuir constants (298 K) for computing the surface tension of aqueous organic solutions mixed with $(NH_4)_2SO_4$ for larger than 10 % salt mole fraction. 56

Table 3. 5: Results of Köhler theory analysis for the compounds and mixtures considered in this study. Organics are arranged in order of decreasing solubility. 59

Table 3. 6: Molar volume uncertainty analysis and total uncertainty as percent of molar volume for the compounds and mixtures considered in this study. 62

Table 4. 1: Summary of T0 site filter grouping with extracted WSOC concentration (C_{WSOC}) and hygroscopicity parameter (κ). 73

Table 4. 2: Summary of T1 site filter grouping with extracted WSOC concentration (C_{WSOC}), inferred average organic molar mass (M_{org}), and hygroscopicity parameter (κ). 74

Table 4. 3: Properties of inorganic salts potentially present in the extracted filters. 81

Table 4. 4: Organic and inorganic mass fraction for Mexico City T0 site samples. Salts shown for each sample were predicted by using ISORROPIA II (Fountoukis and Nenes, 2007). Uncertainties in all mass fractions are smaller than 0.2%..... 82

Table 4. 5: Organic and inorganic mass fractions for Mexico City T1 site samples. Salts shown for each sample were predicted by using ISORROPIA II (Fountoukis and Nenes, 2007). Uncertainties in all mass fractions are smaller than 0.2%..... 82

Table 4. 6: Formulas used for computing the sensitivity of molar mass to σ, ω, υ_{org}, υ_{inorg}, ε_{org}, and ε_{inorg}. 84

Table 4. 7: Szyskowski-Langmuir constants (298 K) for computing the surface tension measurements of aqueous Mexico City T0 site samples and mixtures with $(NH_4)_2SO_4$. The measured surface tension depression relative to water at T = 34 °C at a C_{WSOC} = 1000 ppm and the SO_4^{2-} concentration are also shown. 86

Table 4. 8: Szyskowski-Langmuir constants (298 K) for computing the surface tension measurements of aqueous Mexico City T0 site samples and mixtures with $(NH_4)_2SO_4$. The measured surface tension depression relative to water at T = 34 °C and C_{WSOC} = 1000 ppm and the SO_4^{2-} concentration are also shown. 87

Table 4. 9: Molar mass uncertainty analysis and total uncertainty as percent of molar mass for the T1 site samples..... 97

Table 5. 1: CCN closure analysis error metrics for entire AMIGAS campaign. 130

Table 6. 1: Summary of Twin Otter Missions for MASE II campaign..... 147

LIST OF FIGURES

Page

Figure 1. 1: Estimated global average radiative forcing from anthropogenic and natural sources in conjunction with the spatial scale and the level of scientific understanding. 2

Figure 2. 1: Illustration of the importance of solute curvature on solubility..... 11

Figure 2. 2: Algorithm used for introducing CES into Köhler theory..... 16

Figure 2. 3: Regions of thermodynamic stability for the solute-water system as determined from Equation (2.10) for different interfacial energy. The curves correspond to a wet ammonium sulfate CCN with Dp = 0.5 μm, ρs = 1760 kg m-3, Ms = 0.132 kg mol-1, $Cbulk$ = 1g kg-1, $ddry$ = 100 nm, T = 298 K. 17

Figure 2. 4: Regions of thermodynamic stability for the solute-water system as determined from Equation (2.10) when (a) water condenses upon an initially dry particle, and, (b) water evaporates from a particle that is initially wet. 19

Figure 2. 5: Interfacial tension as a function of substance solubility as predicted by the Söhnel correlation (Söhnel, 1982). Blue diamonds correspond to sparingly soluble and soluble substances studied in Söhnel (1982) and pink squares correspond to compounds considered in this study. 26

Figure 2. 6: (a) Comparison of Köhler curves for a leucine particle without curvature enhanced solubility (grey line) and with curvature enhanced solubility (black line), (b) Same as 6a, but for a pinonic acid particle, (c) Same as 6a, but for a pinic acid particle. Predictions used our measured interfacial energy (Table 2. 3) for leucine and γsl = 30 mN m-1 for pinonic and pinic acid. 28

Figure 2. 7: (a) Interfacial energy contribution to CES of pinic acid for zero interfacial energy (black line), 1 mN m-1(dark grey line), 5 mN m-1 (light grey line), 15 mN m-1 (dotted black line), 30 mN m-1 (dotted dark grey line), and 60 mN m-1 (dotted light grey line). Number in parenthesis is the corresponding contact angle when assuming surface tension of water. (b) Interfacial energy contribution to CES of leucine for zero interfacial energy (black line), 31 mN m-1 and 62 mN m-1 interfacial energy (grey line). 30

Figure 2. 8: Measured vs. predicted *dp50* for all species and supersaturations (a) without CES and (b) with CES. Predictions used our measured interfacial energy (Table 2. 3) for azelaic acid, phthalic acid, and leucine; γsl = 30 mN m-1 was used for the remaining compounds. . 32

Figure 3. 1: Example on how CCN activation experiments can be used to infer the solubility of compounds. 45

Figure 3. 2: Experimental setup used to measure CCN activity. 47

Figure 3. 3: Example of procedure used to determine *dp50*. Shown are CCN/CN data obtained at 1.2 % supersaturation for 50 % malonic acid (mole percent) with its sigmoidal fit (light blue line). *dp50* is the dry diameter for which the CCN/CN = 0.5. 49

Figure 3. 4: Surface tension as a function of carbon concentration of mixed organic/inorganic aqueous solutions. Shown are succinic acid (black diamond), azelaic acid (grey triangle), phthalic acid (outlined grey square), malonic acid (black circle), leucine (grey diamond), and fructose (outlined grey triangle). The lines correspond to the Szyskowski-Langmuir fit for each organic. 52

Figure 3. 5: (a) Surface tension as a function of carbon concentration for pure succinic acid (black diamond) and mixtures with (NH4)2SO4 for 99 % (grey square), 95 % (grey triangle), and 90 % (grey circle) succinic acid (mole fraction). The solid black line corresponds to the Szyskowski-Langmuir fit for all high organic fraction mixtures. (b) Surface tension depression as a function of carbon concentration for (NH4)2SO4 – succinic acid mixtures for 50 % (black diamond), 10 % (grey square), and 1% (grey triangle) succinic acid (mole fraction). The solid lines correspond to the Szyskowski-Langmuir fit for each mixture: 50 % (black line), 10 % (dark grey line), and 1 % (light grey line). The dashed black line corresponds to the Szyskowski-Langmuir fit for all three low organic fraction mixtures. 54

Figure 3. 6: Activation curves for pure succinic acid (black diamond) and mixtures with (NH4)2SO4 consisting of 99 % (grey triangle), 95 % (grey circle), 90 % (grey diamond), 50 % (open diamond), 10 % (outlined grey triangle), and 1 % (outlined grey circle) molar fraction of succinic acid. Activation curve for (NH4)2SO4 (black square) is also plotted for comparison. The solid and dash lines (100 % (black dash line), 99 % (dark grey line), 95 % (light grey line), 90 % (dark grey dashed line), and (NH4)2SO4 (black line)) indicates a power fit to the data. 57

Figure 3. 7: (a) Activation curves for pure organic components: succinic acid (black diamond), azelaic acid (grey triangle), phthalic acid (outlined grey square), malonic acid (black circle), leucine (grey diamond), and fructose (outlined grey triangle). The lines correspond to a power law fit to the activation data. (b) Activation curves for 50 % organic fraction mixtures with (NH4)2SO4: azelaic acid (grey triangle), succinic acid (black diamond), and malonic acid (black circle). The lines correspond to a power law fit to the activation data..... 58

Figure 4. 1: Instrument calibration curves used. Critical supersaturation versus delta T. Calibration was performed at a flowrate of 500 cm3 min-1 and at ambient pressure using (NH4)2SO4 aerosol**.**..... 78

Figure 4. 2: Surface tension as a function of concentration for (a) 24 hour integrated samples: MEX-T0-1 (blue diamond), MEX-T0-2 (pink square), MEX-T1-1 (purple triangle), and MEX-T1-2 (maroon circle), (b) 12 hr integration day samples: MEX-T0-4 (blue diamond), MEX-T0-5 (pink square), MEX-T1-11 (purple triangle), and MEX-T1-12 (maroon circle), (c) 12 hr integration night samples: MEX-T1-8 (blue diamond), MEX-T1-9 (pink square), and 12 hr integration day samples: MEX-T1-11 (purple triangle), and MEX-T1-12 (maroon circle). The solid lines correspond to the Szyskowski-Langmuir fit for each sample..... 88

Figure 4. 3: CCN activity for (a) 24 hour integrated samples: MEX-T0-1 (blue diamond), MEX-T0-2 (pink square), MEX-T1-1 (purple triangle), and MEX-T1-2 (maroon circle), (b) 12 hr integration day samples: MEX-T0-3 (blue diamond), MEX-T0-4 (pink square), MEX-T1-11 (purple triangle), and MEX-T1-12 (maroon circle), (c) 12 hr integration night samples: MEX-T1-8 (blue diamond), MEX-T1-9 (pink square), and 12 hr integration day samples: MEX-T1-11 (purple triangle), and MEX-T1-12 (maroon circle) with their corresponding power fit) assuming complete solubility. (NH4)2SO4 (black square) is also shown for comparison..... 89

Figure 4. 4: Activation curves for: MEX-T0-4 with (a) low (blue diamond), medium (pink square), and high (purple triangle) SO42- concentration, MEX-T1-12 (b) low (blue diamond), medium (pink square), and high (purple triangle) SO42- concentration. Pure (NH4)2SO4 (black square) is also shown for comparison. 90

Figure 4. 5: Hygroscopicity parameter versus organic mass fraction: T0 24 hr (red open square), T0 12 hr day (red open circle), T1 24 hr (blue open square), T1 12 hr day (blue open circle), T1 12 hr night (blue open triangle). The black dotted line represents the hygroscopicity parameter for (NH4)2SO4.. 91

Figure 4. 6: Hygroscopicity parameter closure plot. Comparison of κ predicted from the mixing rule to the κ determined experimentally from CCN data assuming the surface tension of water (pink squares) and 15% surface tension depression (blue circles). The black dashed line represents the 1 to 1 line.. 93

Figure 4. 7: Growth curves for 12 hr integration day samples: MEX-T0-3 (blue triangle), MEX-T0-4 (pink square), MEX-T1-11 (purple triangle), MEX-T1-12 (maroon circle), and (NH4)2SO4 (black square). The grey band represents the variability in the average droplet distribution.. 94

Figure 5. 1: AMIGAS experimental setup. From August 1st to August 26th, the CPC 3022A was used for the SMPS; while the CPC 3010 was used from August 26th till the end of the campaign (September 15th). The sheath-to-aerosol ratio in the DMA was run at 10:1 (August 1st till August 8th; Setup A1) and 5:1 (August 8th till September 15th; Setup A2 and B). The dotted box highlights the total CN measurement which was done from August 15th till August 26th. 111

Figure 5. 2: Critical supersaturation versus delta T calibration for (NH4)2SO4 aerosol. Calibration was performed at a flowrate of 700 cm3 min-1 and at ambient pressure..... 114

Figure 5. 3: Example of an ambient CCN activity spectrum (at constant supersaturation) with sigmoid fit and its defined parameters. 114

Figure 5. 4: Visual representation of chemical composition binning to the corresponding scan time. 118

Figure 5. 5: Aerosol mixing state. 120

Figure 5. 6: Scatter plot of total CN obtained from the SMPS distribution versus that measured by the CPC. 123

Figure 5. 7: Total CN and CCN time-series for whole AMIGAS campaign. Periods A and C correspond to “polluted” air masses originating from the continental US; while period B corresponds to “cleaner” air masses originating from either the Atlantic Ocean or Gulf of Mexico. Gaps in data correspond to times where the power was down or there were problems with one of the instruments. 124

Figure 5. 8: NOAA HYSPLIT one day trajectories representative of the three air masses sampled in JST during the AMIGAS campaign. Plots (a) and (c) represent "polluted" air masses which originated from the continental US; while plot (b) represents a "cleaner" air mass which originated from the Gulf of Mexico. During August 24th till the 27th, the air masses originated either from the Atlantic Ocean or Gulf of Mexico. 125

Figure 5. 9: Dry particle size distribution time-series. 126

Figure 5. 10: CCN distribution time-series. 126

Figure 5. 11: *dp50* closure for the internal mixture case. The red, blue, green, and yellow circles correspond to the INT-AS, INT-SALTS, INT-ALLSOL, and INT-ALLSOL-ST cases, respectively. 127

Figure 5. 12: *dp50* closure for the internal mixture case. The red, blue, green, and yellow circles correspond to the EXT-SOL, EXT-ALLSOL, and EXT-ALLSOL-ST cases, respectively. 128

Figure 5. 13: CCN closure plot for the internal mixture case. The red, blue, green, and yellow circles correspond to the INT-AS, INT-SALTS, INT-ALLSOL, and INT-ALLSOL-ST cases, respectively. 129

Figure 5. 14: CCN closure plot for the external mixture case. The red, green, and yellow circles correspond to the EXT-SOL, EXT-ALLSOL, and EXT-ALLSOL-ST cases, respectively. 130

Figure 5. 15: Example of an ambient CCN activity spectrum (at constant dry diameter) with sigmoid fit and its defined parameters..... 132

Figure 5. 16: Example of the activation fraction as a function of particle size for a day (square) and night (circle) sample. The smaller the particles the more externally mixed they become (smaller *E*). 133

Figure 5. 17: CCN closure plot for the size resolved external mixture (SR_EXT). 134

Figure 5. 18: Droplet growth kinetics study analysis. Box plots for droplet size at the point of activation grouped by supersaturation. The whiskers represent the 10th and 90th percentile; therefore capturing 90% of the points. Outliers shown as open circles represent those points that are 1.5 times the interquartile range (box width). The dashed blue line corresponds to the (NH4)2SO4 calibration droplet size at activation at the same supersaturation. The grey band represents the variability in the average droplet distribution. 135

Figure 5. 19: Droplet size distribution versus particle dry diameter for: a) a particle that experiences delayed droplet growth and b) a particle that grows as fast as (NH4)2SO4 at activation. The CCN counts are normalized with the total CCN concentration measured at each time. The black line represents the average droplet size versus particle dry diameter of (NH4)2SO4 calibration aerosol at the same supersaturation as the scan (1.0% nominal). The dashed black line represents the variability (one standard deviation) in the average droplet diameter. 136

Figure 6. 1: Critical supersaturation versus delta T calibration for (NH4)2SO4 aerosol. a) Calibration curve at a constant flowrate of 500 cm3 min-1 and three different pressures: 1000 mb (blue diamonds), 900 mb (pink squares), and 700 mb (purple triangles). b) Calibration curve at a constant flowrate of 1000 cm3 min-1 and three different pressures: 1000 mb (blue diamonds), 900 mb (pink squares), and 800 mb (purple triangles). 150

Figure 6. 2: Mixing state of aerosols. 153

Figure 6. 3: Sulfate ratio as a function of time for Flight A (ship). The areas shaded in gray correspond to the times where we are "in plume".. 154

Figure 6. 4: Example of the effects of water retention by H2SO4 on the aerosol size distributions in Flight A. The wet distribution is shown in blue and the dry distribution is shown in red. 155

Figure 6. 5: Size resolved chemical composition of particles within the plume (Flight A). 156

Figure 6. 6: Flight A "in plume" CCN closure for an internal mixture with size averaged composition. The color scheme refers to the supersaturation in the CCN instrument (Murphy et al., 2009). 157

Figure 6. 7: Flight A "in plume" CCN closure assuming an internal mixture with size resolved composition. The color scheme refers to the supersaturation in the CCN instrument (Murphy et al., 2009). 158

Figure 6. 8: Sulfate ratio as a function of time for Flight B. 158

Figure 6. 9: Flight B "in plume" CCN closure for an external mixture with size averaged composition. The color scheme refers to the supersaturation in the CCN instrument. 159

Figure 6. 10: Flight B "in plume" CCN closure for an internal mixture with size averaged composition. The color scheme refers to the supersaturation in the CCN instrument. 160

Figure 6. 11: Flight A droplet growth curves for the “in plume” (green) and “out of plume” (red) case. The lines correspond to the (NH4)2SO4 calibration droplet diameter at 1000 (blue) and 800 (grey) mb (Murphy et al., 2009). 160

Figure 6. 12: Droplet growth curves for Flight B. The color scheme refers to the pressure (altitude) corresponding to that measurement. 162

Figure 6. 13: Droplet growth curves for Flight C. The color scheme refers to the pressure (altitude) corresponding to that measurement. 162

LIST OF SYMBOLS

A	Kelvin or curvature effect term
B	Raoult or solute effect term
C	slope of CCN activity spectrum
C_{act}	average organic concentration at activation
C_{bulk}	solubility of the compound over a flat surface or bulk solubility
C_{eq}	equilibrium solubility of the compound over the curved interface
C_{max}	maximum concentration of organic used in surface tension measurements
C_{SO4}	concentration of sulfate ions in solution
C_{WSOC}	water soluble organic carbon concentration
d	CCN dry diameter
d^*	critical cluster size or characteristic dry diameter
d_a	aerodynamic diameter
D_c	CCN critical diameter
d_c	activation diameter
d_{core}	diameter of the solute “droplet inclusion”
$d_{core,max}$	maximum diameter of the solute “droplet inclusion”
$d_{core,min}$	minimum diameter of the solute “droplet inclusion”

d_{dry}	dry particle diameter or original core diameter
d_m	electrical mobility diameter
$\frac{dN_{CCN}}{d\log D_p}$	CCN distribution
$\frac{dN_{CN}}{d\log D_p}$	particle size distribution
D_p	CCN wet diameter
d_{p50}	minimum dry size of particles that activate at a given level of supersaturation
d_{pc}	characteristic dry diameter above which all particles with similar composition activate into cloud droplets
E	upper asymptote of CCN activity spectrum
m	mass of dissolved solute
$m_{EXT,ins}$	insoluble aerosol mass
$m_{EXT,sol}$	soluble aerosol mass
m_{INT}	total aerosol mass
m_{inorg}	mass of inorganic
M_i	molar mass of species *i*
M_{inorg}	molar mass of inorganic
$\frac{M_j}{\rho_j}$	molar volume of the water soluble organic carbon component
m_{org}	mass of organic

$m_{org,ins}$	insoluble organic mass
$m_{org,sol}$	soluble organic mass
M_{org}	molar mass of organic
$\left(\frac{M}{\rho}\right)_{org}$	molar volume of the water soluble organic carbon component
m_{salts}	total soluble salt mass
M_s	molar mass of the solute
M_w	molar mass of water
n_{bulk}	number of moles available from bulk solubility at activation
N_{CCN}	total CCN
n_s	number of moles dissolved in the droplet from the soluble species
n_{ss}	number of moles dissolved in the droplet from the sparingly soluble species
n_w	moles of water
P°	saturation vapor pressure for pure water over a flat surface
pKa	logarithmic acid dissociation constant
P_w	droplet water vapor pressure
R	ideal gas constant
S_c	maximum critical saturation ratio
s_c	critical supersaturation, $s_c = S_c - 1$
s_c^*	characteristic critical supersaturation
S_{eq}	equilibrium saturation ratio
T	temperature
V_d	droplet volume

V_{sample}	sample volume
x_i	mass fraction of species *i*
x_{CaCO_3}	mass fraction of calcium carbonate ($CaCO_3$)
x_{CaSO_4}	mass fraction of calcium sulfate ($CaSO_4$)
$x_{H_2SO_4}$	mass fraction of sulfuric acid (H_2SO_4)
$x_{K_2CO_3}$	mass fraction of potassium carbonate (K_2CO_3)
x_{KHSO_4}	mass fraction of potassium bisulfate ($KHSO_4$)
$x_{K_2SO_4}$	mass fraction of potassium sulfate (K_2SO_4)
x_{mole}	inorganic mole fraction
x_{NaCl}	mass fraction of sodium chloride (NaCl)
$x_{Na_2CO_3}$	mass fraction of sodium carbonate (Na_2CO_3)
x_{NaHSO_4}	mass fraction of sodium bisulfate ($NaHSO_4$)
x_{NaNO_3}	mass fraction of sodium nitrate ($NaNO_3$)
$x_{Na_2SO_4}$	mass fraction of sodium sulfate (Na_2SO_4)
$x_{NH_4HSO_4}$	mass fraction of ammonium bisulfate (NH_4HSO_4)
$x_{(NH_4)_3H(SO_4)_2}$	mass fraction of letovicite ($(NH_4)_3H(SO_4)_2$)
$x_{(NH_4)_2SO_4}$	mass fraction of ammonium sulfate ($(NH_4)_2SO_4$)
x_{org}	mass fraction of organics

Greek Letters

α	Szyskowski-Langmuir parameter in mN m^{-1} K^{-1}
β	universal constant (Chapter 2) or Szyskowski-Langmuir parameter in ppm^{-1} (Chapter 3 and 4)
$\Delta\left(\frac{M_j}{\rho_j}\right)$	uncertainty in inferred organic molar volume
ΔM_{org}	uncertainty in inferred organic molar mass
ΔT	temperature gradient
Δx	uncertainty in parameter x
γ_{sl}	solute-aqueous phase interfacial energy
γ_{sv}	solute-vapor phase surface energy
ε_i	volume fraction of solute *i*
ε_{inorg}	inorganic volume fraction
ε_{org}	organic volume fraction
ε_s	volume fraction of solute
κ	hygroscopicity parameter
κ_{CCN}	experimental hygroscopicity parameter (s_c and d_{p50} pair)
κ_{mix}	predicted hygroscopicity parameter (mixing rule)
θ	contact angle
ρ_0	unit density (1 g cm^{-3})
ρ_i	density of solute *i*

ρ_{inorg}	density of inorganic
ρ_{org}	density of organic
ρ_p	particle density
ρ_s	solute density
ρ_w	water density
σ	droplet surface tension at the point of activation
σ_w	surface tension of water
υ	effective van't Hoff factor
υ_i	effective van't Hoff factor of solute *i*
υ_{inorg}	effective van't Hoff factor of inorganic
υ_{org}	effective van't Hoff factor of organic
υ_s	effective van't Hoff factor of soluble species
υ_{ss}	effective van't Hoff factor of sparingly soluble species
Φ	ratio of moles of solute dissolved in the droplet over the number of moles available from bulk solubility
Φ_x	sensitivity of organic molar volume to parameters x (σ, ω, υ_{org}, υ_{inorg}, ε_{org}, ε_{inorg})
ϕ	osmotic coefficient
ω	Fitted CCN Activity (FCA) factor

LIST OF ABBREVIATIONS

CCN	Cloud Condensation Nuclei
CES	Curvature Enhanced Solubility
CN	Condensation Nuclei
CPC	Condensation Particle Counter
C-ToF-AMS	Compact Time of Flight Aerosol Mass Spectrometer
DACAD	Dual Automated Classifier Aerosol Detector
DMA	Differential Mobility Analyzer
EXT	External Mixture
FCA	Fitted CCN Activity
HULIS	HUmic-Like Substances
IC	Ion Chromatography
INT	Internal Mixture
KTA	Köhler Theory Analysis
MC	Mexico City
O/C	Organic to Carbon Ratio
OM/OC	Organic Matter to Organic Carbon Ratio
OPC	Optical Particle Counter
PILS	Particle-Into-Liquid-Sampler
PM2.5	Ambient Aerosols of Aerodynamic Diameter Less Than 2.5 μm
RH	Relative Humidity
SMCA	Scanning Mobility CCN Analysis

SMPS	Scanning Mobility Particle Sizer
SR	Sulfate Ratio
SS	Supersaturation
STGC	Streamwise Thermal Gradient CCN Chamber
SVF	Scaled Water-Soluble Volume Fraction
TOC	Total Organic Carbon
WSOC	Water Soluble Organic Carbon

SUMMARY

It is well known that atmospheric aerosols provide the sites for forming cloud droplets, and can affect the Earth's radiation budget through their interactions with clouds. The ability of aerosols to act as cloud condensation nuclei is a strong function of their chemical composition and size. The compositional complexity of aerosol prohibits their explicit treatment in atmospheric models of aerosol-cloud interactions. Nevertheless, the cumulative impact of organics on CCN activity is still required, as carbonaceous material can constitute up to 90% of the total aerosol, 10-70% of which is water soluble. Therefore it is necessary to characterize the water soluble organic carbon fraction by CCN activation, droplet growth kinetics, and surface tension measurements. In this thesis, we investigate the water soluble properties, such as surface tension, solubility, and molecular weight, of laboratory and ambient aerosols and their effect on CCN formation.

A mechanism called Curvature Enhanced Solubility is proposed and shown to explain the apparent increased solubility of organics. A new method, called Köhler Theory Analysis, which is completely new, fast, and uses minimal amount of sample was developed to infer the molar volume (or molar mass) of organics. Due to the success of the technique in predicting the molar volume of laboratory samples, it was applied to aerosols collected in Mexico City. Additionally the surface tension, CCN activity, and droplet growth kinetics of these urban polluted aerosols were investigated. Studies performed for the water soluble components showed that the aerosols in Mexico City have surfactants present, can readily become CCN, and have growth similar to ammonium sulfate. Finally, aerosols from three different polluted sources, urban, bovine,

and ship emissions, were collected and characterized. The data assembled was used to predict CCN concentrations and access our understanding of the system. From these analyses, it was evident that knowledge of the chemical composition and mixing state of the aerosol is necessary to achieve agreement between observations and predictions. The data obtained in this thesis can be introduced and used as constraints in aerosol-cloud interaction parameterizations developed for global climate models, which could lead to improvements in the indirect effect of aerosols.

CHAPTER 1

INTRODUCTION

Aerosols are solid or liquid particles suspended in air. Atmospheric aerosols range from a few nanometers to micrometers in size and are formed by different mechanisms. Smaller particles (below 2.5 μm) tend to be formed by condensation and coagulation processes while larger ones (above 2.5 μm) are produced by mechanical means (e.g., wave bubble breaking and erosion). Aerosols can be either primary or secondary in nature. Primary aerosols are those that are directly emitted to the atmosphere (e.g., black carbon and dust); while secondary aerosols are formed in the atmosphere by condensation of vapor onto pre-existing particles or by chemical reactions (e.g., Secondary Organic Aerosol or SOA). Particles are important since they affect visibility, human health, and climate. The effect of these particles depends on their size and chemical composition.

1.1 Aerosols, clouds, and climate change

The effect of human activities on climate is being recognized as one of the most important issues facing society (IPCC, 2001). However the impact of anthropogenic aerosols on climate is not well understood. It is currently thought that aerosols potentially have a large climatic cooling effect (IPCC, 2001) that rivals greenhouse gas warming, but quantitative estimates are highly uncertain (Figure 1. 1). This uncertainty originates from poorly understood aerosol-cloud interactions known as the aerosol indirect effect. The greatest challenges associated with the aerosol indirect effect assessments are the various length scales involved. For example, cloud formation and processes are smaller than the grid scale of climate models (meters versus kilometers). Furthermore, aerosol-cloud interactions are multiscale (can span nm when dealing with aerosols to meters when looking at clouds) and are complex.

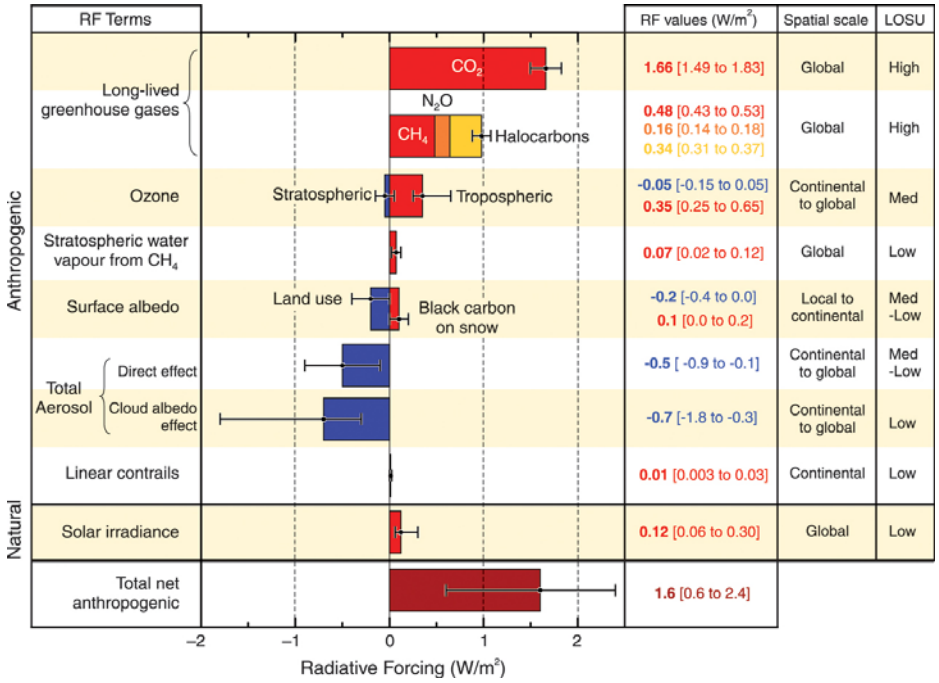

Figure 1. 1: Estimated global average radiative forcing from anthropogenic and natural sources in conjunction with the spatial scale, and the level of scientific understanding.

Aerosols affect the climate indirectly by changing the cloud albedo and lifetime. Increasing the concentrations of aerosols, which occurs under polluted conditions as it is the case in Mexico City and Los Angeles, leads to more reflective and persistent clouds (Twomey, 1977; Albrecht, 1989). Since clouds account for roughly half of the shortwave planetary albedo, fraction of solar radiation reflected back to space, small perturbations in cloud properties can significantly decrease the amount of absorbed solar radiation. Hence, an increase in cloud planetary albedo could cool the Earth's climate system and potentially be as large as the warming effect of the greenhouse gases. Until the aerosol indirect effect is well constrained, society will be incapable of addressing its impact on climate.

1.2 Aerosols as cloud condensation nuclei

The ability of a given aerosol particle to influence cloud properties is a strong function of its size and composition (Seinfeld and Pandis, 1997; Nenes et al., 2002; Dusek et al., 2006). Atmospheric aerosols are formed of a mixture of inorganic and organic material which come from both biogenic and anthropogenic sources (Seinfeld and Pandis, 1998). The ability of inorganic compounds to act as CCN is well understood and explained by Köhler theory (e.g., Raymond and Pandis, 2002). On the other hand, organic compounds, which constitute a significant fraction of the aerosol mass (Zappoli et al., 1999; Decesari et al., 2000; Broekhuizen et al., 2005; Sullivan and Weber, 2006a; Sullivan and Weber, 2006b), and their interactions with water vapor can be more complex (Cruz and Pandis, 1997; Corrigan and Novakov, 1999; Raymond and Pandis, 2002; Hartz et al., 2006). This complexity arises from the large number of organics present in ambient aerosol, each with its own hydrophobicity (i.e., wettability), molecular weight, density, solubility and surfactant characteristics. The presence of inorganic electrolytes introduces further complications for this intricate chemical "soup". Nevertheless, carbonaceous-aerosol can readily act as CCN (Novakov and Penner, 1993; Cruz and Pandis, 1997); hence understanding when and how long it takes for these particles to transform into drops is a necessary requirement for improving the certainty of climate change predictions.

In an effort to study the aerosol organic fraction, a number of studies have focused on studying the physical and chemical properties of the carbonaceous material specifically the water soluble component. For example, Decesari et al. (2001) found the water soluble organic carbon (WSOC) fraction, which constitutes approximately 10-70% of the total organic mass, to be composed of high molecular weight polycarboxylic acids; a heterogeneous mixture containing aromatic, phenolic, and acidic functional groups. These macromolecular WSOC have been termed Humic-Like Substances

(HULIS) due to their resemblance to terrestrial and aquatic humic substances; although differences between them exist (Graber and Rudich, 2006). HULIS have been found to affect CCN activation (Dinar et al., 2006; Svenningsson et al., 2006), hygroscopicity (Brooks et al., 2004; Badger et al., 2006; Svenningsson et al., 2006; Dinar et al., 2007; Wex et al., 2007), and surface tension (Kiss et al., 2005; Taraniuk et al., 2007). For example, studies have found that organics can act as surfactants by decreasing the droplet surface tension (Shulman et al., 1996; Li et al., 1998; Facchini et al., 2000) therefore facilitating the formation of cloud droplets by lowering the critical supersaturation needed for the particle to activate. Additionally, studies have shown that organics can modify particles CCN activity by altering the aerosols hygroscopicity (i.e., wettability; Cruz and Pandis, 1997) and delaying growth of particles due to their lower solubility (Giebl et al., 2002; Kumar et al., 2003).

1.3 Thesis outline

The thesis will focus in understanding the effects of organics on cloud formation by studying laboratory and ambient aerosols in an effort to improve our understanding of the role of organics on CCN activation. Attention is given to organics since they can affect CCN activity (cloud formation) by lowering the surface tension, altering the particle hygroscopicity, and delaying the growth of particles due to their low solubility. Special attention will be given to the water soluble properties of the particles, such as surface tension and solubility, as well as the molecular weight of laboratory and ambient aerosols. The aerosols studied cover laboratory (Chapters 2 and 3) and urban polluted aerosols (Chapters 4, 5 and, 6). In Chapter 2, we present a modeling study which proposes a mechanism to explain the apparent increased solubility of organics observed in laboratory studies. We then develop a method, Köhler Theory Analysis, to determine the molecular weight of organics by coupling CCN activity, surface tension, and composition measurements which will allow us to get a better understanding of the water

soluble components present. Köhler Theory Analysis was applied to known organic/inorganic laboratory mixtures (Chapter 3) and ambient aerosols collected in a polluted environment (Chapter 4) successfully. Size resolved CCN were measured in Atlanta, GA and studied further in Chapter 5. In Chapters 5 and 6, we explore the CCN activity and growth kinetics of CCN particles in polluted environments and address how changes in composition and mixing state can affect these properties. Lastly in Chapters 5 and 6, we couple size distribution, chemical composition, and CCN measurements to predict CCN concentrations and compared the results to actual CCN measurements to assess our understanding of the aerosol cloud interactions. The data obtained, CCN formation and growth kinetics, from laboratory and ambient aerosols can then be introduced into aerosol-cloud interaction parameterizations which could lead to improvements in the assessment of the indirect effect of aerosols.

1.4 References

Albrecht, B. A.: Aerosols, cloud microphysics, and fractional cloudiness, Science, 245, 1227-1230, 1989.

Badger, C. L., George, I., Griffiths, P. T., Braban, C. F., Cox, R. A. and Abbatt, J. P. D.: Phase transitions and hygroscopic growth of aerosol particles containing humic acid and mixtures of humic acid and ammonium sulphate, Atmos. Chem. Phys., 6, 755-768, 2006.

Broekhuizen, K., Chang, R. Y.-W., Leaitch, W. R., Li, S.-M. and Abbatt, J. P. D.: Closure between the measured and modeled cloud condensation nuclei (CCN) using size-resolved aerosol compositions in downtown Toronto, Atmos. Chem. Phys. Discuss., 5, 6263-6293, 2005.

Brooks, S. D., DeMott, P. J. and Kreidenweis, S. M.: Water uptake by particles containing humic materials and mixtures of humic materials with ammonium sulfate, Atmos. Environ., 38, 1859-1868, 2004.

Corrigan, C. E. and Novakov, T.: Cloud condensation nucleus activity of organic compounds: a laboratory study, Atmos. Environ., 33(17), 2661-2668, 1999.

Cruz, C. N. and Pandis, S. N.: A study of the ability of pure secondary organic aerosol to act as cloud condensation nuclei, Atmos. Environ., 31(15), 2205-2214, 1997.

Decesari, S., Facchini, M. C., Fuzzi, S. and Tagliavini, E.: Characterization of water-soluble organic compounds in atmospheric aerosol: A new approach, J. Geophys. Res.-A., 105(D1), 1481-1489, 2000.

Decesari, S., Facchini, M. C., Matta, E., Lettini, F., Mircea, M., Fuzzi, S., Tagliavini, E. and Putaud, J. P.: Chemical features and seasonal variation of fine aerosol water-soluble organic compounds in Po Valley, Italy, Atmos. Environ., 35, 3691-3699, 2001.

Dinar, E., Taraniuk, I., Graber, E. R., Anttila, T., Mentel, T. F. and Rudich, Y.: Hygroscopic growth of atmospheric and model humic-like substances, Journal of Geophysical Research - Atmospheres, 112, D05211, doi:10.1029/2006JD007442, 2007.

Dinar, E., Taraniuk, I., Graber, E. R., Katsman, S., Moise, T., Anttila, T., Mentel, T. F. and Rudich, Y.: Cloud Condensation Nuclei properties of model and atmospheric HULIS, Atmos. Chem. Phys., 6, 2465-2482, 2006.

Dusek, U., Frank, G. P., Hildebrandt, L., Curtius, J., Schneider, J., Walter, S., Chand, D., Drewnick, F., Hings, S., Jung, D., Borrmann, S. and Andreae, M. O.: Size matters more than chemistry for cloud-nucleating ability of aerosol particles, Science, 312(5778), 1375-1378, 2006.

Facchini, M. C., Decesari, S., Mircea, M., Fuzzi, S. and Loglio, G.: Surface tension of atmospheric wet aerosol and cloud/fog droplets in relation to their organic carbon content and chemical composition, Atmos. Environ., 34(28), 4853-4857, 2000.

Giebl, H., Berner, A., Reischl, G., Puxbaum, H., Kasper-Giebl, A. and Hitzenberger, R.: CCN activation of oxalic and malonic acid test aerosols with the University of Vienna cloud condensation nuclei counter, J. Aerosol Sci., 33(12), 1623-1634, 2002.

Graber, E. R. and Rudich, Y.: Atmospheric HULIS: How humic-like are they? A comprehensive and critical review, Atmos. Chem. Phys., 6, 729-753, 2006.

Hartz, K. E. H., Tischuk, J. E., Chan, M. N., Chan, C. K., Donahue, N. M. and Pandis, S. N.: Cloud condensation nuclei activation of limited solubility organic aerosol, Atmos. Environ., 40(4), 605-617, 2006.

IPCC: Climate Change (2001): The Scientific Basis, ed, Cambridge University Press, United Kingdom, 2001.

Kiss, G., Tombacz, E. and Hansson, H. C.: Surface tension effects of humic-like substances in the aqueous extract of tropospheric fine aerosol, J. Atmos. Chem., 50(3), 279-294, 2005.

Kumar, P. P., Broekhuizen, K. and Abbatt, J. P. D.: Organic acids as cloud condensation nuclei: Laboratory studies of highly soluble and insoluble species, Atmos. Chem. Phys., 3, 509-520, 2003.

Li, Z. D., Williams, A. L. and Rood, M. J.: Influence of soluble surfactant properties on the activation of aerosol particles containing inorganic solute, Journal of the Atmospheric Sciences, 55(10), 1859-1866, 1998.

Nenes, A., Charlson, R. J., Facchini, M. C., Kulmala, M., Laaksonen, A. and Seinfeld, J. H.: Can chemical effects on cloud droplet number rival the first indirect effect?, Geophys. Res. Lett., 29(17), Art. No. 1848, doi:10.1029/2002GL015295, 2002.

Novakov, T. and Penner, J. E.: Large Contribution of Organic Aerosols to Cloud-Condensation-Nuclei Concentrations, Nature, 365(6449), 823-826, 1993.

Raymond, T. M. and Pandis, S. N.: Cloud activation of single-component organic aerosol particles, J. Geophys. Res.-A., 107(D24), Art. No. 4787, doi:10.1029/2002JD002159, 2002.

Seinfeld, J. H. and Pandis, S.: Atmospheric Chemistry and Physics, ed, John Wiley, New York, 1997.

Seinfeld, J. H. and Pandis, S.: Atmospheric Chemistry and Physics, ed, John Wiley, New York, 1998.

Shulman, M. L., Jacobson, M. C., Carlson, R. J., Synovec, R. E. and Young, T. E.: Dissolution behavior and surface tension effects of organic compounds in nucleating cloud droplets, Geophys. Res. Lett., 23(3), 277-280, 1996.

Sullivan, A. P. and Weber, R. J.: Chemical characterization of the ambient organic aerosol soluble in water: 1. Isolation of hydrophobic and hydrophilic fractions with a

XAD-8 resin, J. Geophys. Res.-A., 111(D5), Art. D05314,doi:10.1029/2005JD006485, 2006a.

Sullivan, A. P. and Weber, R. J.: Chemical characterization of the ambient organic aerosol soluble in water: 2. Isolation of acid, neutral, and basic fractions by modified size-exclusion chromatography, J. Geophys. Res.-A., 111(D5), Art. No. D05315, doi:10.1029/2005JD006486, 2006b.

Svenningsson, B., Rissler, J., Swietlicki, E., Mircea, M., Bilde, M., Facchini, M. C., Decesari, S., Fuzzi, S., Zhou, J., Monster, J. and Rosenorn, T.: Hygroscopic growth and critical supersaturations for mixed aerosol particles of inorganic and organic compounds of atmospheric relevance, Atmos. Chem. Phys., 6, 1937-1952, 2006.

Taraniuk, I., Graber, E. R., Kostinski, A. and Rudich, Y.: Surfactant properties of atmospheric and model humic-like substances (HULIS), Geophys. Res. Lett., 34, L16807, doi:10.1029/2007GL029576, 2007.

Twomey, S.: Minimum size of particle for nucleation in clouds, J. Atmos. Sci., 34(11), 1832-1835, 1977.

Wex, H., Hennig, T., Salma, I., Ocksay, R., Kiselev, A., Henning, S., Massling, A., Wiedensohler, A. and Stratmann, F.: Hygroscopic growth and measured and modeled critical supersaturations of an atmospheric HULIS sample, Geophys. Res. Lett., 34, L02818,doi:10.1029/2006GL028260, 2007.

Zappoli, S., Andracchio, A., Fuzzi, S., Facchini, M. C., Gelencser, A., Kiss, G., Krivacsy, Z., Molnar, A., Meszaros, E., Hansson, H. C., Rosman, K. and Zebuhr, Y.: Inorganic, organic and macromolecular components of fine aerosol in different areas of Europe in relation to their water solubility, Atmos. Environ., 33(17), 2733-2743, 1999.

CHAPTER 2

CLOUD DROPLET ACTIVATION: SOLUBILITY REVISITED[1]

In this study, the impact of particle curvature on solubility is explored and expressed in terms of a Kelvin enhancement. The augmented solubility, termed "Curvature Enhanced Solubility" (CES), is then introduced into Köhler theory for assessment of its impact on CCN activity for several organic compounds with a wide range of aqueous solubility. The interfacial energy between solute and aqueous phase required for quantification of CES is determined from existing correlations based on bulk solubility, and concurrent measurements of contact angle and surface tension. A number of important findings arise from this study: *i*) CES can substantially increase solubility and impact CCN activity but only if the aerosol is initially wet, and *ii*) CES can stabilize highly supersaturated solutions, and provide a mechanism for retention of an aerosol aqueous phase even at very low relative humidity (RH).

2.1 Motivation

Theory suggests that solubility in water is an important property controlling CCN activity (Corrigan and Novakov, 1999; Kumar et al., 2003; Broekhuizen et al., 2004). In fact, there is a finite solubility range within which CCN activity can be strongly affected (Nenes et al., 2002); outside this range, the organic is effectively insoluble or always dissolved at the point of activation; in the latter, further increase in solubility would not affect its contribution of solute and CCN activity. Nevertheless, predictions of CCN activity based on limited solubility often disagree with experiments (Hori et al., 2003; Bilde and Svenningsson, 2004; Henning et al., 2005; Padró et al., 2007). Raymond and

[1]Under review: Padró, L. T. and Nenes, A.: Cloud droplet activation: solubility revisited, Atmos. Chem. Phys. Discuss., 7, 2325-2355, 2007.

Pandis (2002) found that most often, the activation of sparingly soluble compounds were consistent with the assumption of complete solubility if the limited solubility compounds tend to spread water (i.e., have a small contact angle with water). This behavior was seen in subsequent studies (Broekhuizen et al., 2004; Henning et al., 2005; Hartz et al., 2006; Padró et al., 2007) and was attributed to incomplete drying of the particle, where significantly more solute was dissolved in the preexisting water of the particles than predicted by solubility.

The above studies illustrate the importance of knowing the aerosol phase prior to their activation, but attribute the retention of residual water to the existence of a thermodynamically metastable state. Although possible, very high supersaturation levels develop in these concentrated solutions, suggesting that homogeneous nucleation would likely be spontaneous. Enhancing the thermodynamic stability of the aqueous phase may in fact be responsible for the retention of residual water. For example, Marcolli et al. (2004) show that the presence of multiple water-soluble organics can form eutectic mixtures with low deliquescence points. Just as for multicomponent inorganic aerosol (Wexler and Seinfeld, 1991), eutectic points can favor the presence of a thermodynamically stable aqueous phase even at very low relative humidity. Although directly relevant for ambient multicomponent carbonaceous aerosol, eutectics cannot explain the presence of aerosol water seen in the simple aerosol systems examined in the Hori et al. (2003), Bilde and Svenningsson (2004), Henning et al. (2005) and Raymond and Pandis (2002) studies.

This paper proposes an alternate mechanism for stabilizing highly concentrated aqueous solutions, which we term Curvature-Enhanced Solubility (CES). When a fully hydrated aerosol is exposed to a low relative humidity environment (for example during the drying phase of a typical aerosol generation apparatus in the laboratory), it eventually forms a supersaturated solution that tends to form stable nucleation clusters, upon which subsequent condensation of solute eventually leads to the formation of a dry particle. The

curvature of the initial solute cluster however can raise the solute chemical potential in the solid phase; in other words, the solute in the curved particle can have a higher solubility than its "bulk" value. The property that controls the magnitude of CES is the interfacial energy (otherwise known as "interfacial tension") between the solid nucleus and surrounding liquid solution. Therefore, if the curvature and interfacial energy is high enough (which is certainly possible for nanometer-scale particles), this enhanced solubility may inhibit the subsequent condensation of solute from the aqueous phase, which results in a thermodynamically stable aqueous phase even at very low relative humidity's (Figure 2. 1).

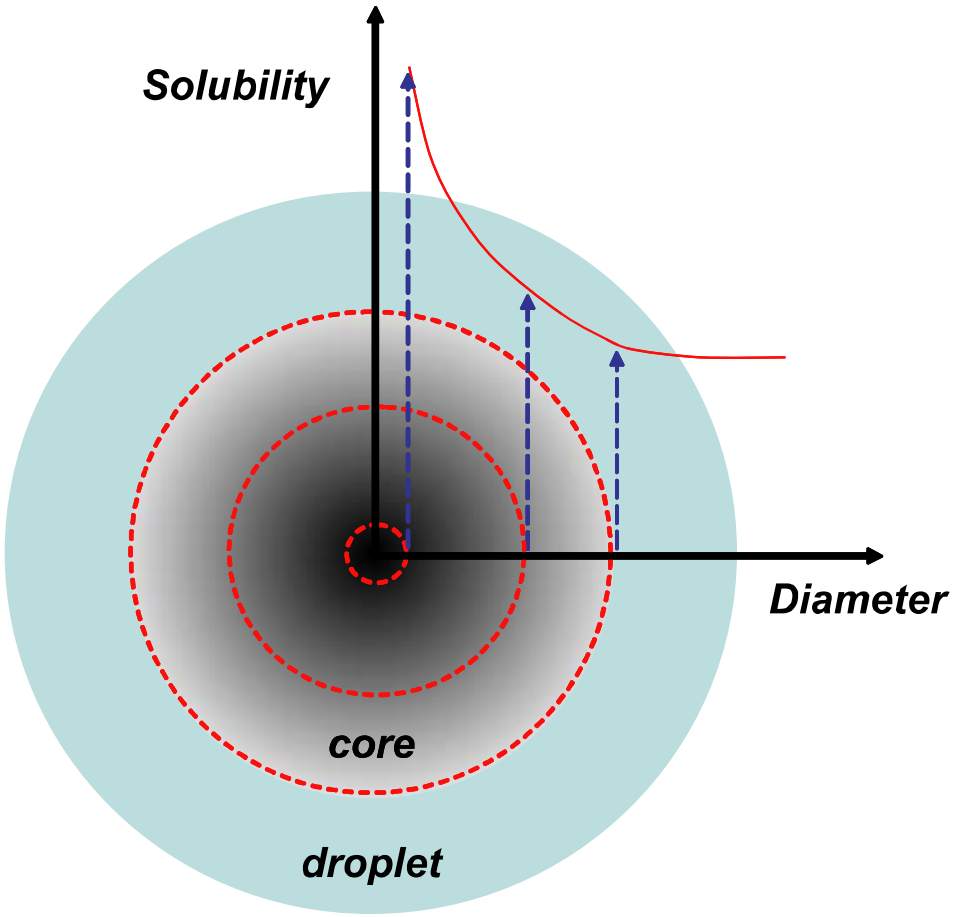

Figure 2. 1: Illustration of the importance of solute curvature on solubility.

In order to assess the relevance of curvature enhanced solubility (CES) for CCN activation and water retention at low RH, we studied nine organic compounds that exhibit a wide range of solubility. For each compound, its interfacial tension with water is determined based on measurements of aqueous solution surface tension, wettability (contact angle with water) and an equation of state (Spelt and Li, 1996). The interfacial tension is introduced into Köhler theory and the equilibrium saturation vapor pressure is calculated with and without CES. For each case, predictions of CCN activity are compared with observations and the results are discussed.

2.2 Theory of CES and its impact on CCN activity

2.2.1 Traditional Köhler theory

The Köhler equation expresses the equilibrium saturation ratio, S_{eq}, (defined as the ratio of the droplet water vapor pressure and the saturation water vapor pressure over a flat surface) of the CCN with its environment. For a deliquescent single-component CCN, S_{eq} is approximated by,

$$S_{eq} = \frac{P_w}{P^\circ} = \exp\left(\frac{4M_w\sigma_w}{RT\rho_w D_p} - \frac{6\upsilon\phi n_s M_w}{\pi\rho_w D_p^3} \right) \tag{2.1}$$

where P_w is the droplet water vapor pressure, D_p is the CCN wet diameter, P° is the saturation vapor pressure for pure water over a flat surface at temperature T, M_w is the molar mass of water, σ_w is the surface tension of water, R is the ideal gas constant, ρ_w is the density of water, υ is the effective van't Hoff factor, ϕ is the osmotic coefficient, and n_s is the moles of solute. The Kelvin (or "curvature") effect in Equation (2.1) is governed by the D_p^{-1} term, while the solute effect is governed by the D_p^{-3} term. The

maximum of Equation (2.1) corresponds to the minimum (or "critical") saturation ratio required for the CCN to become an unstable cloud droplet.

If the CCN is composed of a soluble fraction, *s*, and a partially soluble fraction, *ss*, and is diluted ($\phi = 1$) then Equation (2.1) can be expressed as (Shulman et al., 1996),

$$S_{eq} = \exp\left(\frac{4M_w\sigma_w}{RT\rho_w D_p} - \frac{6n_s M_w \upsilon_s}{\pi\rho_w D_p^3} - \frac{6n_{ss} M_w \upsilon_{ss}}{\pi\rho_w D_p^3} \right) \tag{2.2}$$

where n_s, n_{ss} represent the moles of solute dissolved in the droplet from the soluble and sparingly soluble species, respectively; υ_s, υ_{ss} are the corresponding "effective" van't Hoff factors. If not all the *ss* is dissolved and dissolution kinetics (Asa-Awuku and Nenes, 2007) are unimportant, then the equilibrium solubility, C_{eq}, can be used to compute n_{ss}. Expressing C_{eq} in moles m^{-3}, Equation (2.2) becomes,

$$S_{eq} = \exp\left(\frac{4M_w\sigma_w}{RT\rho_w D_p} - \frac{6n_s M_w \upsilon_s}{\pi\rho_w D_p^3} - \frac{M_w}{\rho_w} C_{eq} \upsilon_{ss} \right) \tag{2.3}$$

2.2.2 The effect of solute core curvature

For a substance that partitions between a solid and aqueous phase, curvature of the solid-aqueous interface and non-zero interfacial energy tends to affect this partitioning (i.e., the solubility); this is expressed by the Kelvin equation as

$$\frac{C_{eq}}{C_{bulk}} = \exp\left(\frac{4}{RT} \frac{M_s}{\rho_s} \frac{\gamma_{sl}}{d_{core}} \right) \tag{2.4}$$

where C_{eq} is the equilibrium solubility of the compound over the curved interface, C_{bulk} is the solubility of the compound over a flat surface ("bulk solubility"), M_s is the molar mass of the solute, ρ_s is the solute density, γ_{sl} is the solute-aqueous phase interfacial energy and d_{core} is the diameter of the solute "droplet inclusion". Equation (2.4) suggests

that the solubility enhancement depends strongly on the size of d_{core} and γ_{sl}. Most often $\gamma_{sl} \geq 0$ (Spelt and Li, 1996), hence $\frac{C_{eq}}{C_{bulk}} \geq 1$. Negative interfacial energies, which have been reported for sparingly soluble minerals (Wu and Nancollas, 1999) and some polymers (Holmberg et al., 2003), would result in $\frac{C_{eq}}{C_{bulk}} < 1$; however such cases are rare and not considered in this study.

2.2.3 When is bulk solubility not enough to explain CCN activity?

As the amount of water available at the critical point depends on critical supersaturation, it is important to assess the conditions for which bulk solubility alone is insufficient to characterize the observed CCN activity. This is accomplished by theoretically estimating the moles of solute required for activating CCN for a given critical supersaturation; the required moles are then compared to those available from solubility. Compounds and supersaturation conditions are then identified for which CES can potentially be important.

Assuming that a CCN is composed of a single compound, critical supersaturation, s_c, is related to CCN physical properties by (Seinfeld and Pandis, 1998),

$$s_c = \frac{2}{3}\left(\frac{4M_w\sigma_w}{RT\rho_w}\right)^{3/2}\left(\frac{18n_sM_w\upsilon_s}{\pi\rho_w}\right)^{-1/2} \tag{2.5}$$

from which the number of moles, n_s, required for the CCN to activate at s_c is

$$n_s = \frac{2}{81}\frac{\pi\rho_w}{\upsilon_s M_w}\left(\frac{4M_w\sigma_w}{RT\rho_w}\right)^3 s_c^{-2} \tag{2.6}$$

If the bulk solubility of a compound, C_{bulk}, is given in moles solute per m^3 solution, then the number of moles available from bulk solubility, n_{bulk}, at the point of

activation is $n_{bulk} = \frac{\pi}{6} D_c^3 C_{bulk}$, where D_c is the CCN critical diameter (here we assume that at the point of activation, the CCN is mostly composed of water, hence the volume of water available for dissolution is $\frac{\pi}{6} D_c^3$). Since $D_c = \frac{2}{3}\left(\frac{4M_w\sigma_w}{RT\rho_w}\right)\frac{1}{s_c}$ (Seinfeld and Pandis, 1998), n_{bulk} is given by

$$n_{bulk} = \frac{4}{81}\pi\left(\frac{4M_w\sigma_w}{RT\rho_w}\right)^3 s_c^{-3} C_{bulk} \tag{2.7}$$

The ratio, Φ, of n_s over n_{bulk} is then calculated from Equations (2.6) and (2.7),

$$\Phi = \frac{n_s}{n_{bulk}} = \frac{1}{2}\frac{\rho_w}{\upsilon_s M_w}\frac{s_c}{C_{bulk}} \tag{2.8}$$

Φ < 1 indicates that bulk solubility alone is sufficient to explain CCN activity of compounds, while Φ > 1 requires an enhancement of solubility that could be a result of CES.

2.2.4 Introducing CES in Köhler theory

Introduction of CES into Köhler theory is relatively straightforward. For a given wet diameter, C_{eq} from Equation (2.4) is calculated and then introduced into Equation (2.3). The application of Equation (2.4) however requires knowledge of the solute core diameter, d_{core}, and γ_{sl}. The latter is determined from contact angle and surface tension measurements (see 2.3), and d_{core} is computed from the solute mass balance, as follows. As the mass of solute in the core must equal the mass of solute in the dry particle minus the amount dissolved in water,

$$d_{core}^3\rho_s = d_{dry}^3\rho_s - D_p^3 M_s C_{eq} \tag{2.9}$$

where d_{dry} is the dry particle diameter (original core diameter). Introducing the modified solubility (Equation (2.4)) into Equation (2.9) yields,

$$d_{core}^3 + \frac{D_p^3 M_s C_{bulk}}{\rho_s} \exp\left(\frac{4}{RT}\frac{M_s}{\rho_s}\frac{\gamma_{sl}}{d_{core}}\right) - d_{dry}^3 = 0 \qquad (2.10)$$

which is a nonlinear equation, the solution of which yields the value of d_{core} for a given D_p. Figure 2. 2 shows the algorithm used for "mapping out" Köhler curves influenced by CES.

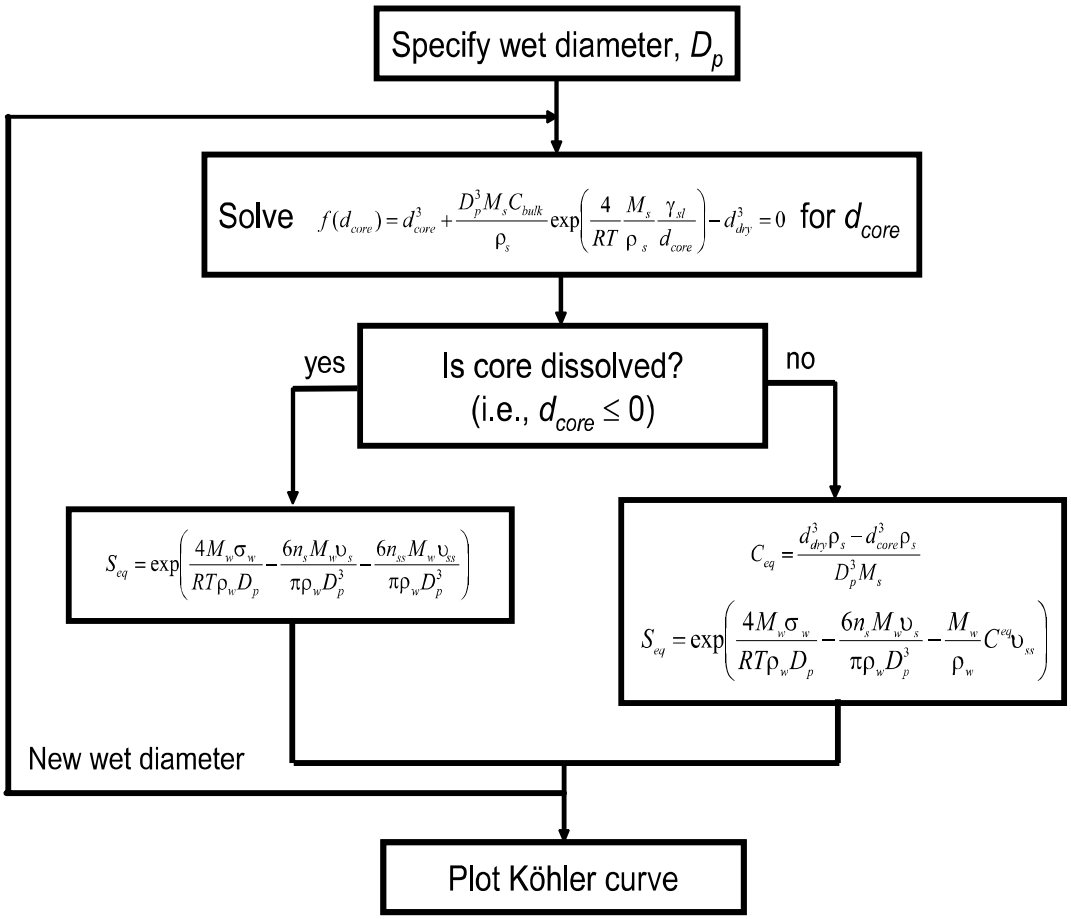

Figure 2. 2: Algorithm used for introducing CES into Köhler theory.

2.2.5 When can CES affect CCN activity?

CES can considerably facilitate CCN activation, as far more solute can be in solution than based on "bulk" solubility alone. However, for this to happen, the "droplet inclusion" needs to be small enough for the exponential increase in solubility (Equation (2.4)) to create an instability that spontaneously dissolves most of the solute core. Equation (2.10) thus has multiple solutions, one for when d_{core} is relatively large (i.e., the exponential is close to unity), and one for when d_{core} is relatively small (i.e., the exponential is very large); this is illustrated in Figure 2. 3, which presents the value of

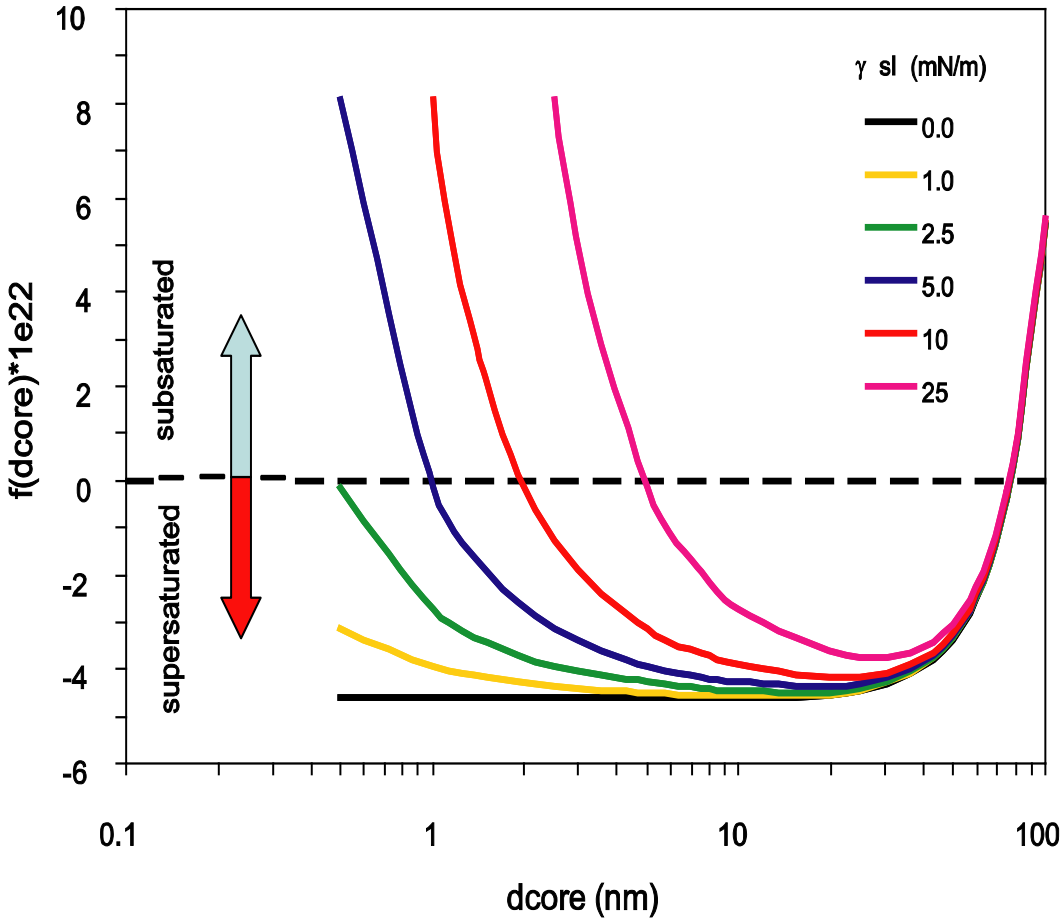

Figure 2. 3: Regions of thermodynamic stability for the solute-water system as determined from Equation (2.10) for different interfacial energy. The curves correspond to a wet ammonium sulfate CCN with D_p = 0.5 μm, ρ_s = 1760 kg m-3, M_s = 0.132 kg mol-1, C_{bulk} = 1g kg-1, d_{dry} = 100 nm, T = 298 K.

$f(d_{core})$ (where f denotes the left hand side of Equation (2.10)) for a wet ammonium sulfate CCN with D_p = 0.5 μm, ρ_s = 1760 kg m^{-3}, M_s = 0.132 kg mol^{-1}, C_{bulk} = 1g kg^{-1}, d_{dry}= 100 nm, T = 298 K. As expected, $f(d_{core}) = 0$ yields one solution for $\gamma_{sl} = 0$. For non-zero interfacial tension, $f(d_{core}) = 0$ yields two solutions, one when d_{core} is large (i.e., CES is small); this solution, $d_{core,max}$, can be approximated from Equation (2.6), assuming that $\exp\left(\frac{4}{RT}\frac{M_s}{\rho_s}\frac{\gamma_{sl}}{d_{core}}\right) \approx 1$,

$$d_{core,\max} \approx \left(d_{dry}^3 - \frac{D_p^3 C_{bulk}}{\rho_s}\right)^{1/3} \tag{2.11}$$

In the region where CES dominates (small d_{core}), $f(d_{core}) = 0$ yields another solution, $d_{core,min}$, and can be approximated from Equation (2.10), assuming that $d_{core} << d_{dry}$,

$$d_{core,\min} \approx \frac{4}{RT}\frac{M_s \gamma_{sl}}{\rho_s}\left(\ln\frac{\rho_s d_{dry}^3}{D_p^3 C_{bulk}}\right)^{-1} \tag{2.12}$$

The sign of $f(d_{core})$ also determines the saturation state of the aqueous phase surrounding the solute core; if an excessive amount of solute is dissolved, $f(d_{core}) < 0$ and the solution is supersaturated, and vice versa (Figure 2. 3). With this in mind, one could then understand the dynamics of the CCN when some water condenses upon it. We consider two initial states: *i*) the CCN is dry, and, *ii*) the CCN is completely wet (i.e., all solute is dissolved).

- If the particle is initially dry, then $d_{core} = d_{dry}$. Adding a small amount of water on to the CCN (Figure 2. 4a, black line) would then result in an initially unsaturated aqueous phase (i.e., $f(d_{core}) > 0$, to the right of $d_{c,max}$). Solute will then dissolve (i.e., d_{core} shifts leftward) until $d_{core} = d_{core,max}$ (Equation (2.11)). $d_{core,max}$ is a stable equilibrium point, as small fluctuations in d_{core} would result

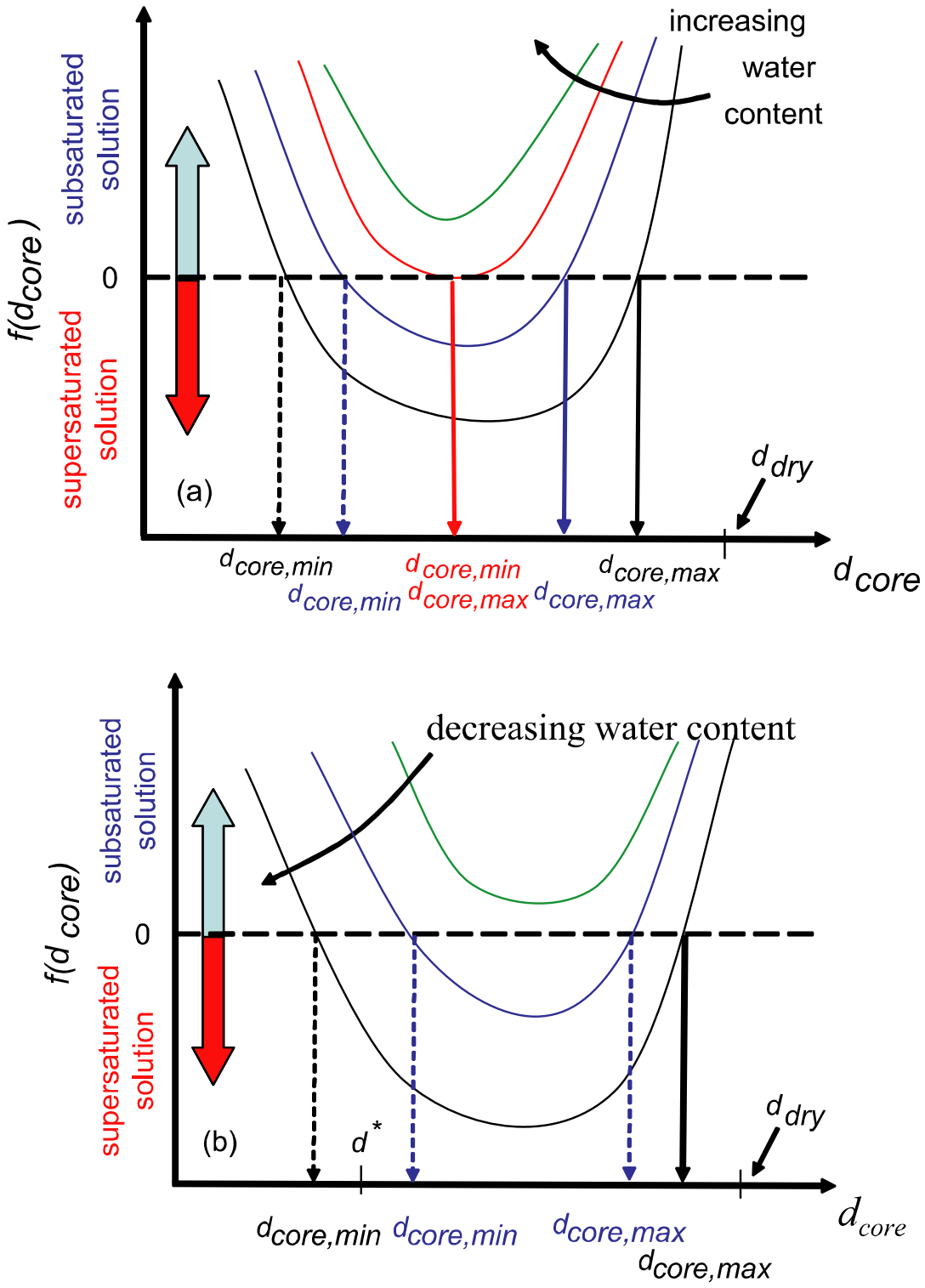

Figure 2. 4: Regions of thermodynamic stability for the solute-water system as determined from Equation (2.10) when (a) water condenses upon an initially dry particle, and, (b) water evaporates from a particle that is initially wet.

in mass transfer to/from the aqueous phase that would restore d_{core} to $d_{core,max}$. Further addition of water to the CCN would always result initially in an unsaturated aqueous phase (i.e., $f(d_{core}) > 0$, to the right of $d_{core,max}$) after which some solute is dissolved until a new equilibrium is reached (Figure 2. 4a, blue line). However, every time some water is added to the CCN, $d_{core,max}$ and $d_{core,min}$ approach each other until they become equal (Figure 2. 4a, red line); at this point, further addition of water would result in $f(d_{core}) > 0$ for all values of d_{core}, hence the solution is always subsaturated (because of CES) and the core spontaneously dissolves (Figure 2. 4a, green line).

- If the particle is initially wet, then $d_{core} = 0$, as the solution is subsaturated with solute (Figure 2. 4b, green line). Removing a small amount of water from the CCN (Figure 2. 4b, blue line) results in a supersaturated aqueous phase which favors the formation of a solid core, by nucleation of a core embryo of size d^* and subsequent condensation of solute. If $d^* < d_{core,min}$ (Figure 2. 4b, blue line) then CES is substantial, the solution becomes subsaturated with solute (i.e., $f(d_{core}) > 0$), the nucleation cluster re-dissolves and a solute core would not appear. If $d^* > d_{core,min}$, (Figure 2. 4b, black line) then CES is not substantial, and the aqueous phase is always supersaturated with respect to solute (i.e., $f(d_{core}) < 0$); solute then continuously condenses upon the core embryo, until a equilibrium is reached, i.e., $d_{core} = d_{core,max}$. The above suggests that $d_{core,min}$ is an unstable equilibrium point, as small fluctuations in d_{core} would result in either complete dissolution of the core (if d_{core} fluctuates to a size slightly smaller than $d_{core,min}$) or spontaneous growth to $d_{core,max}$ (if d_{core} fluctuates to a size slightly greater than $d_{core,min}$).

From the discussion above, the following implications arise:

- CES may not substantially enhance CCN activity if the aerosol is initially dry. When enough water is added to the aerosol (so that $d_{core} \sim d_{core,min}$), CES enhances

solubility enough to spontaneously dissolve the core. The wet diameter for spontaneous dissolution corresponds to the minimum of the red curve in Figure 2. 4a which can be found by solving the system $\frac{\partial f(d_{core})}{\partial d_{core}} = 0;\ f(d_{core}) = 0$ for d_{core} and $D_{p.}$

- Aerosol that is initially wet can retain its water at very low relative humidity, as long as the nucleation embryo size $d^* < d_{core,min}$. When $d^* > d_{core,min}$, CES is not strong enough to maintain a thermodynamically stable state. Therefore, $d^* = d_{core,min}$ denotes the transition point between a completely wet and (primarily) dry aerosol, when applied to Equation (2.12), gives the minimum wet size, $D_{p,min}$ for a thermodynamically stable wet aerosol:

$$D_{p,\min} \approx d_{dry}\left\{\frac{\rho_s}{C_{bulk}}\exp\left(\frac{4}{RT}\frac{M_s\gamma_{sl}}{\rho_s d^*}\right)\right\}^{1/3} \tag{2.13}$$

The magnitude of d^* depends strongly on the interfacial tension, the geometry of the nucleation cluster and the level of solute supersaturation (Nielsen, 1964; Wu and Nancollas, 1999) and vary from a few nm to the particle dry size.

2.3 Obtaining interfacial energy: the contact angle method

γ_{sl} is related to the surface tension and contact angle, θ, between organic and aqueous solution, according to the Young-Laplace equation (Spelt and Li, 1996),

$$\gamma_{sl} = \gamma_{sv} - \sigma\cos\theta \tag{2.14}$$

where γ_{sv} is the solute-vapor phase surface energy. It can be shown (Spelt and Li, 1996) that an equation of state exists relating σ, γ_{sl}, and γ_{sv},

$$\gamma_{sl} = \sigma + \gamma_{sv} - 2\sqrt{\sigma\gamma_{sv}}e^{-\beta(\sigma-\gamma_{sv})^2} \quad (2.15)$$

where β is a "universal constant". From least-squares fit to contact angle and liquid surface tension measurements of many compounds, β = 0.000115 $(m^2\ mJ^{-1})^2$ (Spelt and Li, 1996). Equations (2.14) and (2.15), combined with measurements of σ and θ can be used to determine γ_{sl} and is known as the "contact angle method". Two other methods can be used to determine γ_{sl}, *i*) solubility-size measurements, and, *ii*) crystallization and dissolution kinetics. The former method is subject to significant uncertainty while the latter gives values consistent with those calculated through the contact angle method (Wu and Nancollas, 1999). Studies have shown that for inorganic and organic compounds, solubility increases as the interfacial energy decreases (Söhnel, 1982; Wu and Nancollas, 1998; Wu and Nancollas, 1999). Therefore, sparingly soluble compounds with hydrophobic characteristics, because of the expected high γ_{sl}, may present enhanced solubility from CES if in the form of small particle inclusions in the aqueous solution.

2.4 CES for single-component organic CCN

The importance of CES on solubility and CCN activity is assessed for nine organic compounds: adipic acid, glutamic acid, glutaric acid, norpinic acid, pinic acid, pinonic acid, azelaic acid, phthalic acid and leucine (Table 2. 1). These compounds were selected for their atmospheric relevance, their wide range of solubility in water and for some (adipic acid and glutaric acid) their well-studied CCN characteristics (Cruz and Pandis, 1997; Corrigan and Novakov, 1999; Prenni et al., 2001; Raymond and Pandis, 2002; Hori et al., 2003; Kumar et al., 2003; Bilde and Svenningsson, 2004; Broekhuizen et al., 2004; Hartz et al., 2006).

In Table 2. 2, the values of Φ for the nine organics and four levels of supersaturation (0.3, 0.6, 1.0, and 1.2 %) are shown. When Φ < 1, bulk solubility alone is

Table 2. 1: Compounds considered in this study.

Compound	ρ_s (kg m^{-3})	M_s (kg mole^{-1})	C_{bulk} (kg kg^{-1})
Adipic Acid	1360[a]	0.146[b]	1.825×10^{-2}[b]
Azelaic Acid	1225[c]	0.188[c]	2.447×10^{-3}[c]
Glutamic Acid	1538[a]	0.147[b]	6.95×10^{-3}[b]
Glutaric Acid	1424[a]	0.132[b]	1.235[b]
Leucine	1293[c]	0.131[c]	2.3×10^{-2}[a]
Norpinic Acid	800[a]	0.172[b]	4.7×10^{-2}[b]
Phthalic Acid	2180[c]	0.166[c]	1.415×10^{-3}[c]
Pinic Acid	800[a]	0.186[b]	8.46×10^{-2}[b]
Pinonic Acid	786[a]	0.184[b]	6.75×10^{-3}[b]

[a] CRC Handbook (2002) at 298 K.

[b]Raymond and Pandis (2002) at 293 K.

[c] Yaws (1999) at 298 K.

sufficient to explain the CCN activity of the compounds (see 2.2.3), while an enhancement in solubility is required when $\Phi > 1$. Of the compounds studied, only the CCN activity of glutaric acid and pinic acid is always consistent with their bulk solubility ($\Phi < 1$). For the other seven compounds, conditions exist for which bulk solubility alone is insufficient ($\Phi > 1$) to explain the CCN activity of the compound (Table 2. 2). $\Phi > 1$ occurs more often at high supersaturations, as less water is available at the point of activation (because the critical diameter is small) for dissolution of solute (Equation (2.7).

Table 2. 2: Value of Φ (ratio solute moles required for activation over those allowed by bulk solubility) at various supersaturations. Bold numbers denote cases where bulk solubility alone is insufficient for activating CCN.

Compound	SS = 0.3 %[a]	SS = 0.6 %[b]	SS = 1 %[a]	SS = 1.2 %[b]
Adipic Acid	0.66	N/A	**2.21**	N/A
Azelaic Acid	N/A	**12.78**	N/A	**25.49**
Glutamic Acid	**1.76**	N/A	**5.85**	N/A
Glutaric Acid	0.01	N/A	0.03	N/A
Leucine	0.47	0.95	**1.58**	**1.89**
Norpinic Acid	0.31	N/A	**1.01**	N/A
Phthalic Acid	N/A	**19.51**	N/A	**38.90**
Pinic Acid	0.18	N/A	0.61	N/A
Pinonic Acid	**2.27**	N/A	**7.54**	N/A

[a]Critical supersaturations from Raymond and Pandis (2002).

[b]Critical supersaturations measured during this study.

2.4.1 Interfacial energy for the compounds studied

For three of the compounds considered in this study (azelaic acid, phthalic acid, and leucine), we determined interfacial energy using the contact angle method (see Section 2.3). Surface tension and contact angle for each compound were measured using a KSV Inc. CAM 200 Optical Contact Angle Meter. With this instrument, the shape of the pendant drops are fit to the Young-Laplace equation (Spelt and Li, 1996) from which surface tension is determined. The contact angle is determined from a sessile drop upon a flat substrate of compound. The substrate was applied by evaporation of a solution of the compound upon a glass plate and placing the plate within a diffusional dryer for one day.

The concentration of the solution had a significant impact on the surface roughness; it was found that using solutions diluted down to ¼ their saturation value gave the smoothest surface. Contact angles were measured for sessile drops composed of pure water and of saturated solution, and surface tension was measured for pure water and for saturated solutions of organic.

Table 2. 3 shows the surface tension, contact angle and calculated interfacial energy for organic/water and organic/saturated aqueous solution systems. Contact angle measurements were repeated at least ten times, and surface tension measurements were repeated at least fifty. Larger contact angles are consistently obtained when a saturated solution is placed upon the substrate. This phenomenon is likely from the dissolution of the substrate layer by the pure water; if so, the underlying hydrophilic glass will come into contact with the water drop and reduce the contact angle (this is consistent with the observation that contact angle changes slowly with time). Dissolution of substrate is less likely to happen when placing saturated solution drops on the substrate; this is corroborated by the higher contact angle and their stability with time. Surface heterogeneities are likely not affecting the contact angle because *i*) we did not observe

Table 2. 3: Surface tension at saturation point, contact angle. and interfacial energy for organic/saturated aqueous system interface at 25 °C. Uncertainty in measured quantities corresponds to one standard deviation.

Substrate/Drop System	σ (mN m^{-1})	θ (°)	γ_{sl} (mN m^{-1})
Azelaic/ Azelaic Solution	59.80	26.39 ± 8.11	0.56 ± 0.07
Azelaic/ Water	71.15	21.96 ± 7.48	0.57 ± 0.71
Phthalic/ Phthalic Solution	71.41	22.83 ± 16.11	0.63 ± 0.66
Phthalic/ Water	71.76	12.13 ± 0.62	0.05 ± 0.62
Leucine/ Leucine Solution	69.48	97.09 ± 4.25	30.86 ± 2.72
Leucine/ Water	71.87	57.43 ± 8.26	9.84 ± 3.52

substantial variability between repetition of the measurement, and, *ii*) the angle measured on both sides of the drop cross section were not substantially different. Based on the above, we use only the interfacial energy values obtained from surface tension and contact angle measurements of saturated solutions (Table 2. 3).

Our measurements are compared with the interfacial energy – solubility correlation of Söhnel (1982) to assess their consistency with existing measurement database. Leucine is fairly close to the correlation, while azelaic and phthalic acid substantially deviate from the correlation (Figure 2. 5). The discrepancy of the latter two

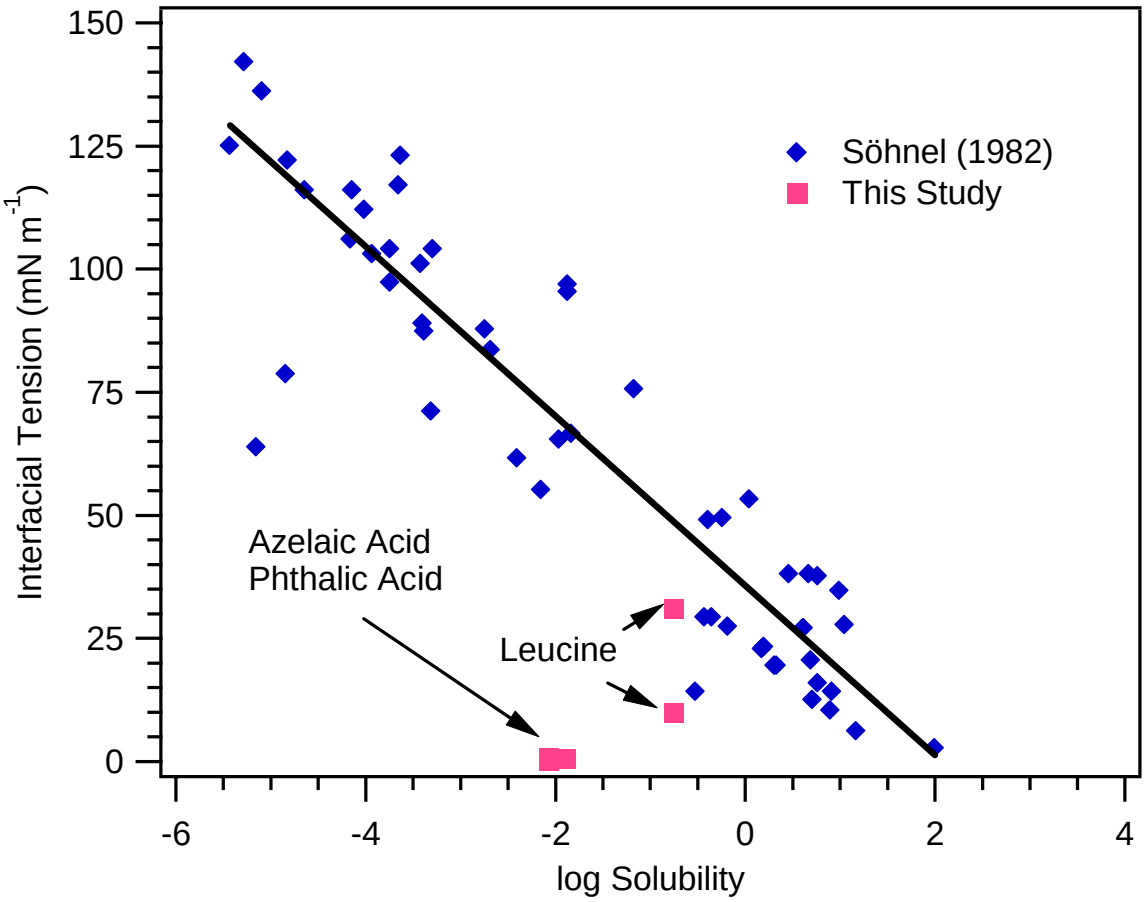

Figure 2. 5: Interfacial tension as a function of substance solubility as predicted by the Söhnel correlation (Söhnel, 1982). Blue diamonds correspond to sparingly soluble and soluble substances studied in Söhnel (1982) and pink squares correspond to compounds considered in this study.

compounds could indicate the presence of small amounts of surfactant impurities which can substantially decrease interfacial energy. For the remaining compounds studied (adipic acid, glutamic acid, glutaric acid, norpinic acid, pinic acid, and pinonic acid), interfacial energy is determined using the solubility-interfacial energy correlation by Söhnel (1982). Given the uncertainty of the correlation, we varied γ_{sl} between 0 and 60 mN m^{-1} consistent with the uncertainty in Söhnel's correlation (Figure 2. 5).

2.4.2 Impact of CES on Köhler curves

Köhler curves are examined for compounds and conditions for which $\Phi > 1$ (Table 2. 2). From the discussion in Section 2.2.5, Köhler curves computed without CES are more representative of particles that are initially completely dry while curves that include CES correspond to particles that are initially wet and subsequently dried (which represents how aerosol are typically generated in laboratory experiments). Köhler curves were computed for leucine, pinonic acid and pinic acid particles with dry diameter ranging from 10 to 500 nm (Figure 2. 6). In all calculations, we take the critical cluster diameter d^* to be 5 nm. CES has a strong impact on the shape of the equilibrium curve for all three compounds examined. For leucine (Figure 2. 6a) and pinic acid (Figure 2. 6c), the CES is strong enough to always keep the solute dissolved in the aqueous phase, consistent with the "complete solubility" behavior seen previously for these compounds (Raymond and Pandis, 2002). As a result, the CCN critical supersaturation substantially decreases, from ~1.5% (without CES) to 0.4% (with CES) for leucine, and ~ 1.1% (without CES) to 0.5% (with CES) for pinic acid. For the sparingly soluble pinonic acid (Figure 2. 6b), not considering CES yields a Köhler curve which is always dominated by the Kelvin effect, in which the critical supersaturation is the equilibrium supersaturation at the dry diameter. Including CES has a notable impact on the Köhler curve, where now two local maxima (one at dry diameter, and one at ~400 nm). Unlike for leucine and pinic acid, introduction of CES increase does not impact the particle critical supersaturation.

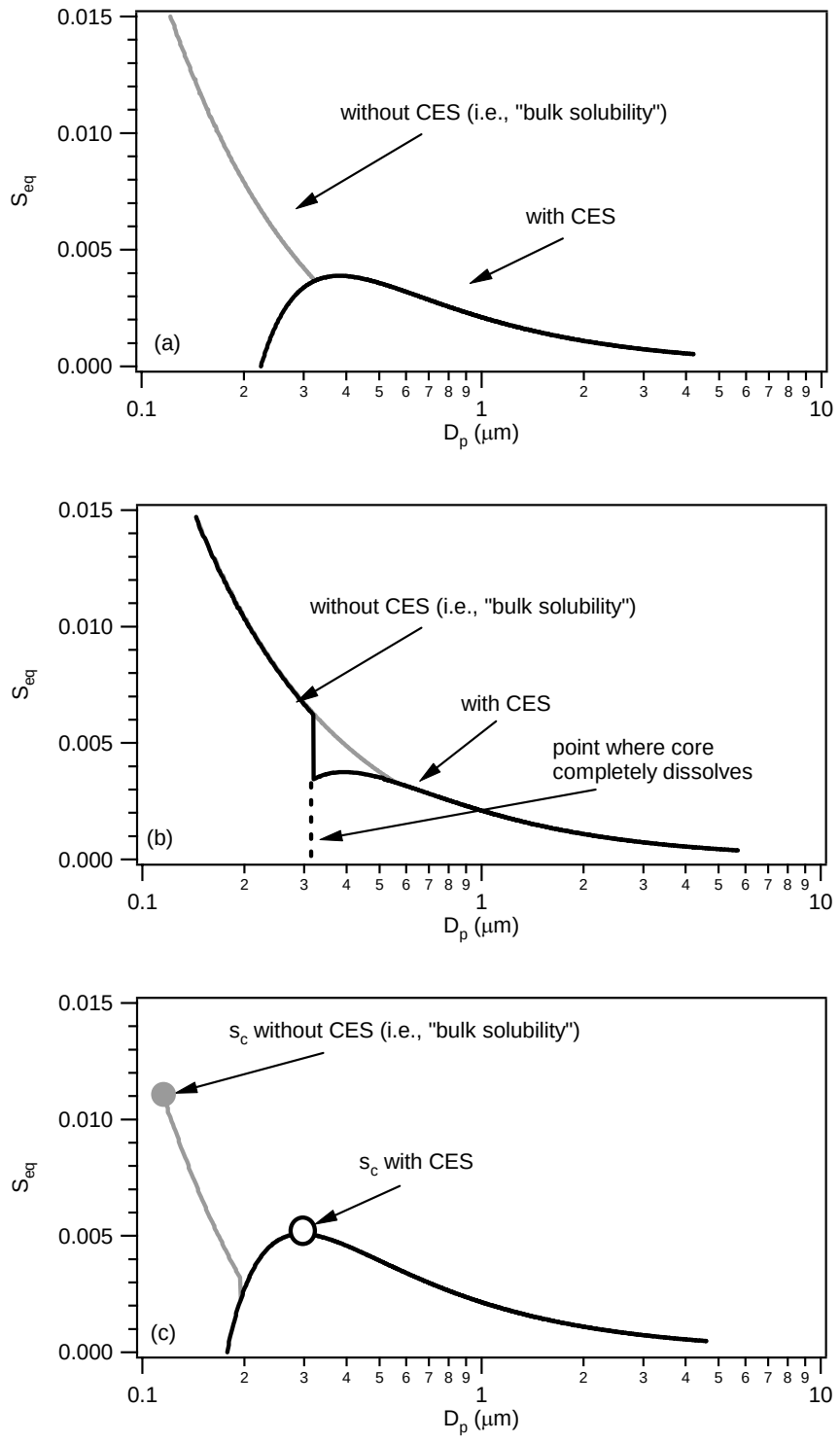

Figure 2. 6: (a) Comparison of Köhler curves for a leucine particle without curvature enhanced solubility (grey line) and with curvature enhanced solubility (black line), (b) Same as 6a, but for a pinonic acid particle, (c) Same as 6a, but for a pinic acid particle. Predictions used our measured interfacial energy (Table 2. 3) for leucine and γ_{sl} = 30 mN m^{-1} for pinonic and pinic acid.

2.4.3 Sensitivity of critical supersaturation to CES and interfacial energy

As seen above, the effect of CES on Köhler curves may (but not always) have an impact on critical supersaturation. In fact, simulations suggest that the impact of interfacial energy on critical supersaturation exhibits a "threshold" type influence; this means that if γ_{sl} is below a characteristic threshold, then the "dry" particle saturation ratio is the global maximum of the Köhler curve and determines the critical supersaturation (this was seen in Figure 2. 6b). However, if γ_{sl} exceeds a characteristic threshold, the solute remains in solution for small wet diameters, and the "second" Köhler curve maximum determines the critical supersaturation (as was seen in Figures 2. 6a and 2. 6c). This threshold behavior is shown clearly in Figure 2. 7a, which presents critical supersaturation of pinic acid particles as a function of dry diameter and γ_{sl}. For a given dry diameter, a jump in critical supersaturation is seen when γ_{sl} changes between 5 and 15 mN m^{-1}; almost no difference is seen when γ_{sl} varies from 0 to 5 mN m^{-1} and 15 to 60 mN m^{-1}. Therefore, the importance of CES on particle critical supersaturation, can be assessed by comparing γ_{sl} with the threshold (if known). For leucine, (Figure 2. 7b) simulations suggest that the threshold γ_{sl} is between 0 and 30 mN m^{-1}; according to our measurements (Table 2. 3) γ_{sl} > 30 mN m^{-1} which mean that CES always reduces the critical supersaturation for this compound.

The simulations carried out in this study suggest that a typical "threshold" for γ_{sl} ranges between 15 and 40 mN m^{-1}. This range covers typical values of organic acid interfacial energy (Miller and Neogi, 1985), which according to the Söhnel (1982) correlation (Figure 2. 5) corresponds to compounds with solubility 10^{-2} M and above. Compounds with a lower solubility do not exhibit enough enhancement in solubility to have a profound impact on critical supersaturation (as was seen for pinonic acid, Figure 2. 6b).

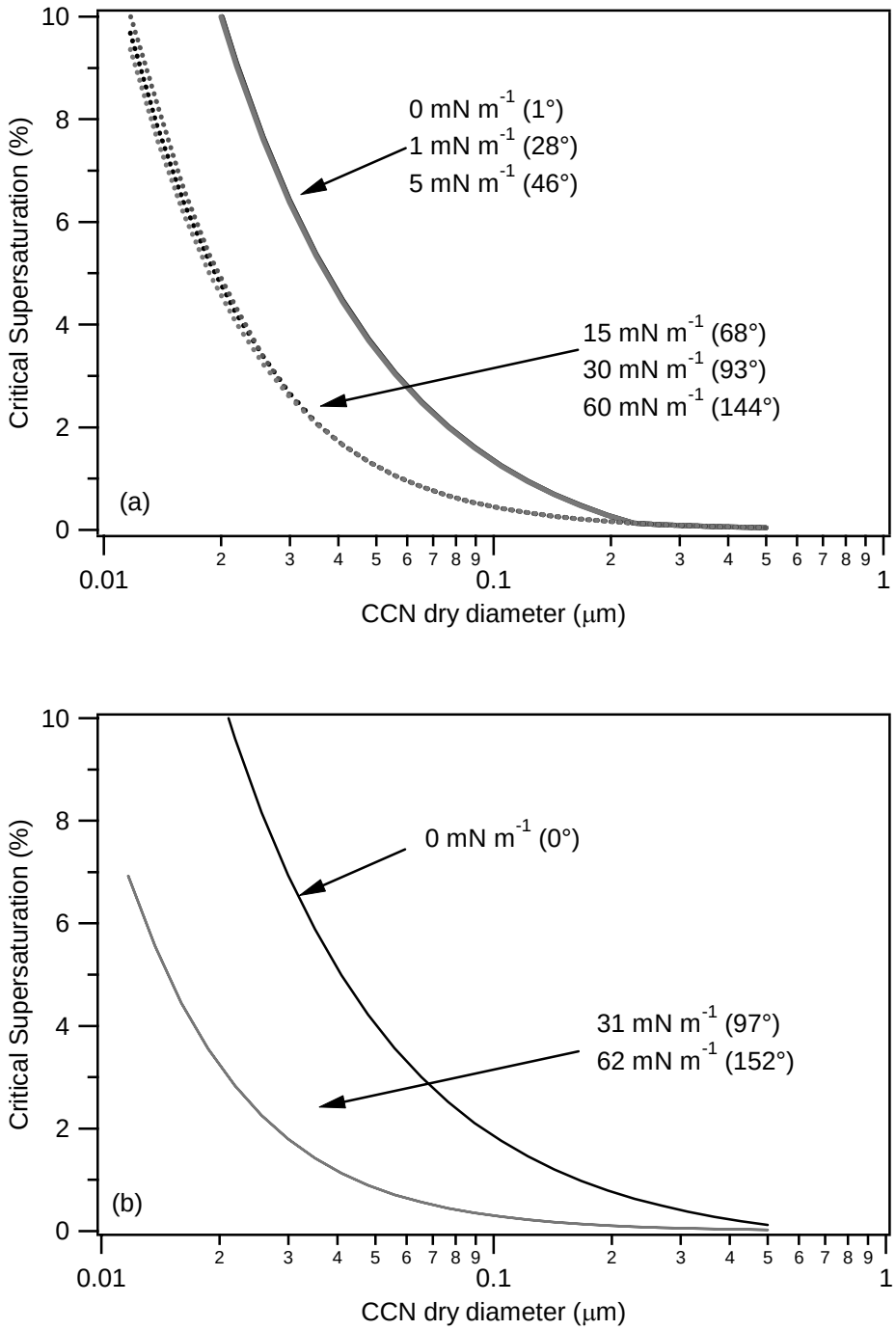

Figure 2. 7: (a) Interfacial energy contribution to CES of pinic acid for zero interfacial energy (black line), 1 mN m^{-1}(dark grey line), 5 mN m^{-1} (light grey line), 15 mN m^{-1} (dotted black line), 30 mN m^{-1} (dotted dark grey line), and 60 mN m^{-1} (dotted light grey line). Number in parenthesis is the corresponding contact angle when assuming surface tension of water. (b) Interfacial energy contribution to CES of leucine for zero interfacial energy (black line), 31 mN m^{-1} and 62 mN m^{-1} interfacial energy (grey line).

2.4.4 Does CES improve predictions of CCN activity?

The proxy we use for CCN activity is the minimum dry size of particles, d_{p50}, that activate at a given level supersaturation of interest. We compare predictions of d_{p50} at 0.3 - 1.2% supersaturation with our measurements and the data from Raymond and Pandis (2002). Our observations of CCN activity were carried out by atomizing an aqueous solution of the compound of interest, drying the particles through a series of two diffusional dryers (residence time ~ 5 s) and then classified with a TSI 6080 electrostatic classifier. The classified aerosol was subsequently introduced into a DMT CCN counter (Roberts and Nenes, 2005; Lance et al., 2006) for measuring its CCN activity. A detailed description of the procedure can be found in Lance et al. (2006). Predictions of d_{p50} are done by determining the dry size of particles with s_c equal to 0.3%, 0.6%, 1.0%, and 1.2%. Predictions are carried out with (i.e., initially wet particles) and without CES (i.e., initially dry particles). For leucine, azelaic and phthalic acid, γ_{sl} is determined from our measurements, while the Söhnel (1982) correlation is used for the rest of the compounds.

The observed vs. predicted d_{p50} (without CES) are shown in Figure 2. 8a; with the exception of cases where $\Phi < 1$ (Table 2. 2), theory does not adequately predict d_{p50}. The discrepancy in the predictions is from insufficient solute being dissolved in the CCN to explain its activity (i.e., $\Phi > 1$). If CES is considered (Figure 2. 8b) all the solute is dissolved at the point of activation and the predictions are much closer to observations. This finding is consistent with the postulation that CES may be important for the activation of aerosol produced by drying atomized aqueous solutions.

2.5 Conclusions

Laboratory and in-situ studies of aerosol-water interactions show that atmospheric hydrophobic particulate matter, if previously wet, may retain significant amounts of water even when exposed to very low relative humidity. We explore the possibility that

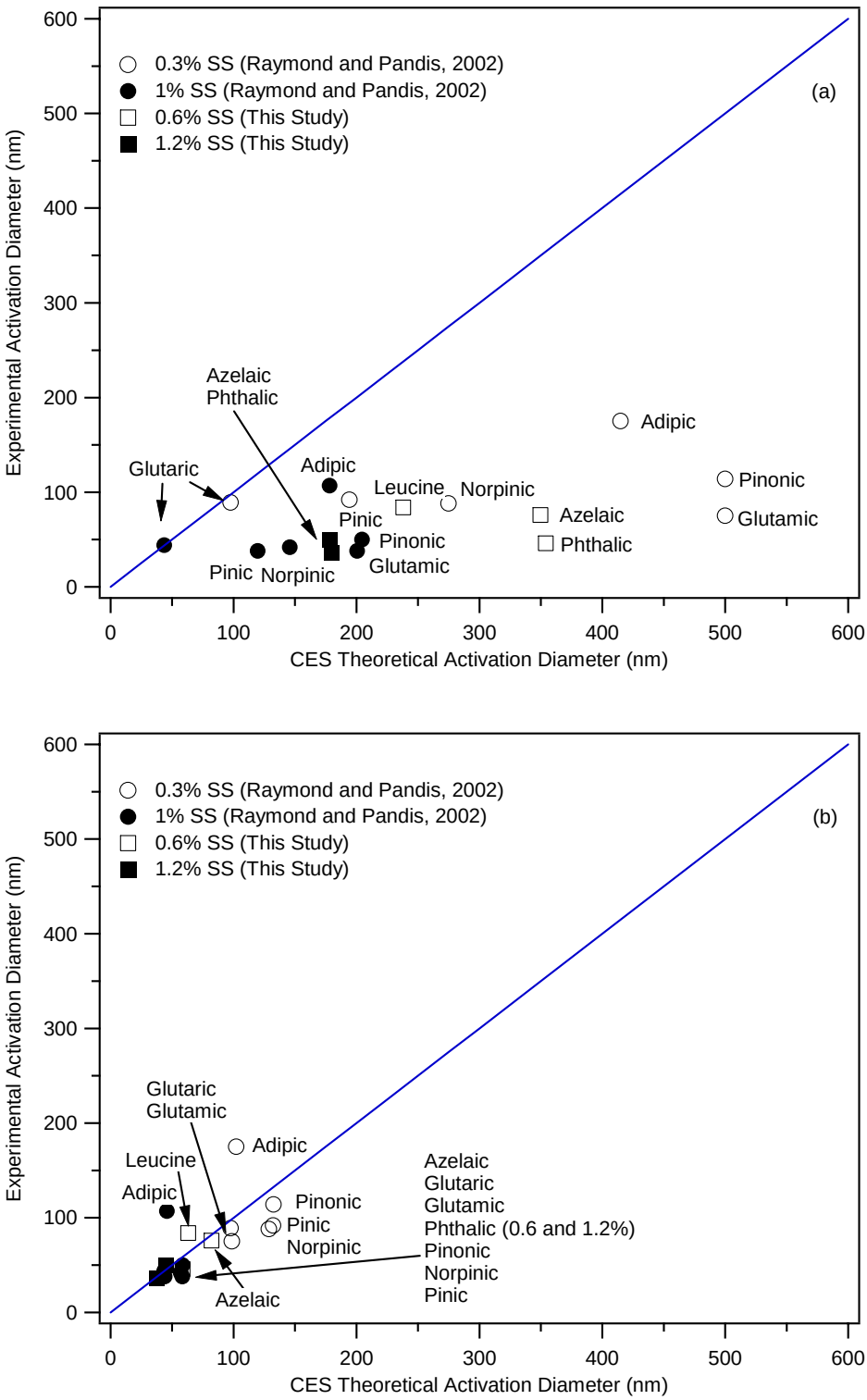

Figure 2. 8: Measured vs. predicted d_{p50} for all species and supersaturations (a) without CES and (b) with CES. Predictions used our measured interfacial energy (Table 2. 3) for azelaic acid, phthalic acid, and leucine; γ_{sl} = 30 mN m^{-1} was used for the remaining compounds.

particle curvature, and its effect on solubility can explain this phenomenon. The augmented solubility, termed "Curvature Enhanced Solubility" (CES), is a strong function of interfacial energy, bulk solubility and nucleation embryo size. A stability analysis of the solute-solution system suggests that if the aerosol is initially wet and the nucleation embryo size of solute is below a threshold, the formation of a solid phase is not favored, even if the solution is supersaturated, giving the "appearance" that the solute is completely soluble. Conversely, particles that are initially dry likely do not experience significant CES, and the amount of solute dissolved in the aqueous phase is consistent with its "bulk" solubility.

CES is introduced into Köhler theory to assess its impact on CCN activity for several organic compounds with a wide range of solubility in water. The interfacial energy between solute and aqueous phase required for quantification of CES is determined from *i*) concurrent measurements of contact angle and surface tension, and, *ii*) semi-empirical correlations based on bulk solubility. We find that the impact of CES on CCN activity (particle critical supersaturation) is not a smooth function of interfacial energy, but that the latter needs to exceed a characteristic threshold to see any impact. Subsequent increases of interfacial energy beyond the threshold would not further increase CCN activity. Measurements of CCN activity of the nine compounds studied here support the above; activation of atomized aerosol using two diffusional dryers (a relatively "soft" method of drying) is consistent with CES. On the contrary, it is known that if "aggressive" drying is used (i.e., heating), the aerosol completely dries and measured critical supersaturation are much higher (Rissman et al., 2007), which is consistent with our expectation that CES is not important.

CES may often occur in ambient particles, since there is almost always water and surfactants present in them. This implies that the concept of "partially soluble" atmospheric organics may not be relevant; even though each of the hundreds of compounds has its own bulk solubility, CES may force compounds above a "bulk"

solubility threshold to always remain in the aqueous phase (i.e., be "completely soluble"), while those below the threshold to act as insoluble. If true, this could greatly simplify the representation of organic impact on CCN activity, as only a characterization of the surface tension depression and average molar mass of the soluble compounds is needed and can be obtained from Köhler theory analysis (Padró et al., 2007; Asa-Awuku et al., 2008).

2.6 References

Asa-Awuku, A. and Nenes, A.: The Effect of Solute Dissolution Kinetics on Cloud Droplet Formation, J. Geophys. Res.-A., 112, D22201, doi:10.1029/2005JD006934, 2007.

Asa-Awuku, A., Nenes, A., Sullivan, A. P., Hennigan, C. and Weber, R. J.: Investigation of Molar Volume and Surfactant Characteristics of Water-Soluble Organic Compounds in Biomass Burning Aerosol Atmos. Chem. Phys., 8, 799 - 812, 2008.

Bilde, M. and Svenningsson, B.: CCN activation of slightly soluble organics: the importance of small amounts of inorganic salt and particle phase, Tellus Series B-Chemical and Physical Meteorology, 56(2), 128-134, 2004.

Broekhuizen, K., Kumar, P. P. and Abbatt, J. P. D.: Partially soluble organics as cloud condensation nuclei: Role of trace soluble and surface active species, Geophys. Res. Lett., 31(1), Art. No. L01107, doi: 10.1029/2003GL018203, 2004.

Corrigan, C. E. and Novakov, T.: Cloud condensation nucleus activity of organic compounds: a laboratory study, Atmos. Environ., 33(17), 2661-2668, 1999.

Cruz, C. N. and Pandis, S. N.: A study of the ability of pure secondary organic aerosol to act as cloud condensation nuclei, Atmos. Environ., 31(15), 2205-2214, 1997.

Hartz, K. E. H., Tischuk, J. E., Chan, M. N., Chan, C. K., Donahue, N. M. and Pandis, S. N.: Cloud condensation nuclei activation of limited solubility organic aerosol, Atmos. Environ., 40(4), 605-617, 2006.

Henning, S., Rosenorn, T., D'Anna, B., Gola, A. A., Svenningsson, B. and Bilde, M.: Cloud droplet activation and surface tension of mixtures of slightly soluble organics and inorganic salt, Atmos. Chem. Phys., 5, 575-582, 2005.

Holmberg, K., Jönsson, B., Kronberg, B. and Lindman, B.: Surfactants and Polymers in Aqueous Solution, 2nd ed, John Wiley & Sons, Ltd, 2003

Hori, M., Ohta, S., Murao, N. and Yamagata, S.: Activation capability of water soluble organic substances as CCN, J. Aerosol Sci., 34(4), 419-448, 2003.

Kumar, P. P., Broekhuizen, K. and Abbatt, J. P. D.: Organic acids as cloud condensation nuclei: Laboratory studies of highly soluble and insoluble species, Atmos. Chem. Phys., 3, 509-520, 2003.

Lance, S., Medina, J., Smith, J. N. and Nenes, A.: Mapping the operation of the DMT continuous flow CCN counter Aerosol Sci. Technol., 40, 242-254, 2006.

Marcolli, C., Luo, B. P. and Peter, T.: Mixing of the organic aerosol fractions: Liquids as the thermodynamically stable phases, J. Phys. Chem. A, 108(12), 2216-2224, 2004.

Miller, C. A. and Neogi, P.: Interfacial Phenomena: Equilibrium and Dynamic Effects, ed, MARCEL DEKKER, INC., New York, 1985.

Nenes, A., Charlson, R. J., Facchini, M. C., Kulmala, M., Laaksonen, A. and Seinfeld, J. H.: Can chemical effects on cloud droplet number rival the first indirect effect?, Geophys. Res. Lett., 29(17), Art. No. 1848, doi:10.1029/2002GL015295, 2002.

Nielsen, A. E.: Kinetics of Precipitation, ed, Macmillan, New York, 1964.

Padró, L. T., Morrison, R., Asa-Awuku, A. and Nenes, A.: Inferring Thermodynamic Properties from CCN Activation Experiments: Single-component and Binary Aerosols, Atmos. Chem. Phys., 7, 5263 - 5274, 2007.

Prenni, A. J., DeMott, P. J., Kreidenweis, S. M., Sherman, D. E., Russell, L. M. and Ming, Y.: The effects of low molecular weight dicarboxylic acids on cloud formation, J. Phys. Chem. A, 105(50), 11240-11248, 2001.

Raymond, T. M. and Pandis, S. N.: Cloud activation of single-component organic aerosol particles, J. Geophys. Res.-A., 107(D24), Art. No. 4787, doi:10.1029/2002JD002159, 2002.

Rissman, T. A., Varutbangkul, V., Surratt, J. D., Topping, D. O., McFiggans, G., Flagan, R. C. and Seinfeld, J. H.: Cloud condensation nucleus (CCN) behavior of organic aerosol particles generated by atomization of water and methanol solutions, Atmos. Chem. Phys., 7, 2949-2971, 2007.

Roberts, G. C. and Nenes, A.: A continuous-flow streamwise thermal-gradient CCN chamber for atmospheric measurements, Aerosol Sci. Technol., 39(3), 206-211, 2005.

Seinfeld, J. H. and Pandis, S.: Atmospheric Chemistry and Physics, ed, John Wiley, New York, 1998.

Shulman, M. L., Jacobson, M. C., Carlson, R. J., Synovec, R. E. and Young, T. E.: Dissolution behavior and surface tension effects of organic compounds in nucleating cloud droplets, Geophys. Res. Lett., 23(3), 277-280, 1996.

Söhnel, O.: Electrolyte Crystal Aqueous-Solution Interfacial-Tensions from Crystallization Data, J. Cryst. Growth, 57(1), 101-108, 1982.

Spelt, J. K. and Li, D.: Applied Surface Thermodynamics, ed, A. W. Neumann and J. K. Spelt, Marcel Dekker, New York, 1996.

Wexler, A. S. and Seinfeld, J. H.: Second-Generation Inorganic Aerosol Model, Atmospheric Environment Part a-General Topics, 25(12), 2731-2748, 1991.

Wu, W. J. and Nancollas, G. H.: The dissolution and growth of sparingly soluble inorganic salts: A kinetics and surface energy approach, Pure Appl. Chem., 70(10), 1867-1872, 1998.

Wu, W. J. and Nancollas, G. H.: Determination of interfacial tension from crystallization and dissolution data: a comparison with other methods, Adv. Colloid Interface Sci., 79(2-3), 229-279, 1999.

CHAPTER 3

INFERRING THERMODYNAMIC PROPERTIES FROM CCN ACTIVATION EXPERIMENTS: SINGLE-COMPONENT AND BINARY AEROSOLS[2]

This study presents a new method, Köhler Theory Analysis (KTA), to infer the molar volume and solubility of organic aerosol constituents. The method is based on measurements of surface tension, chemical composition, and CCN activity coupled with Köhler theory. KTA is evaluated by inferring the molar volume of six known organics (four dicarboxylic acids, one amino acid, and one sugar) in pure form and in mixtures with ammonium sulfate ($(NH_4)_2SO_4$). The average error in inferred molar volumes are to within 18 % of their expected value for organic fractions between 50 and 90 %. This suggests that KTA is a potentially powerful tool for determining the CCN characteristics of ambient water soluble organic carbon (WSOC), providing physically-based constraints for aerosol-cloud interaction parameterizations.

3.1 Motivation

Aerosols in the atmosphere are composed of inorganic and organic compounds which influence their ability to act as CCN. Past studies have shown that particulate matter composed of water soluble inorganic salts and low molecular weight dicarboxylic organic acids can act as efficient CCN (Cruz and Pandis, 1997; Facchini et al., 1999a; Giebl et al., 2002; Kumar et al., 2003; Raymond and Pandis, 2003) which is adequately modeled by Köhler theory (Köhler, 1936). Köhler theory can also predict, with

[2]Appeared in publication: Padró, L. T., Morrison, R., Asa-Awuku, A. and Nenes, A.: Inferring thermodynamic properties from CCN activation experiments: single-component and binary aerosols, Atmos. Chem. Phys., 7, 11240-11248, 2007.

appropriate modifications, the CCN activity of higher molecular weight organic compounds (such as some polycarboxylic acids, fatty acids, alcohols, and amines (Raymond and Pandis, 2002; Hartz et al., 2006)) which constitute a significant fraction of water soluble species (Zappoli et al., 1999; Decesari et al., 2000; Broekhuizen et al., 2006; Sullivan and Weber, 2006a; Sullivan and Weber, 2006b).

Organics primarily influence CCN activity by contributing solute and depressing surface tension; both affect the equilibrium water vapor pressure needed for droplet activation (Shulman et al., 1996; Facchini et al., 1999b; IPCC, 2001; Feingold and Chuang, 2002; Nenes et al., 2002; Kanakidou et al., 2005). A modified version of Köhler theory, incorporating both limited solute solubility and surface tension depression for slightly soluble species was first presented by Shulman et al. (1996); subsequently, Facchini et al. (2000) showed that the surface tension depression could be important for water soluble organic carbon (WSOC) typically found in polluted environments. Decesari et al. (2000) found that WSOC is composed of a complex mixture of neutral and acidic polar compounds, the most hydrophobic of which are responsible for the surface tension depression. Organics may also impact the droplet growth kinetics of CCN (Feingold and Chuang, 2002; Nenes et al., 2002), but this is not the subject of the current study.

Apart from surface tension depression, the solute thermodynamic properties such as the molar volume (molar mass over density), solubility, and effective van't Hoff factor affect CCN activity. Such parameters are very difficult to compute for ambient aerosols, as they are a complex and highly variable mixture of organic/inorganic compounds. As challenging as it may be, this characterization is required to establish a physically-based link between organic aerosol and cloud droplet formation. In this work, we propose and develop a new methodology called Köhler Theory Analysis (KTA) to address this need. KTA is based on using Köhler theory to infer molar volume and solubility from CCN activation measurements (measurements of chemical composition and surface tension may be required as well). In subsequent sections, we present the theoretical basis of KTA

and its application. KTA is then evaluated by inferring the molar volume of six known organics (four dicarboxylic acids, one amino acid, and one sugar) in pure form and in mixtures with $(NH_4)_2SO_4$.

3.2 Köhler theory analysis

3.2.1 Single component CCN

Köhler theory is based on thermodynamic equilibrium arguments and computes the equilibrium saturation ratio, S_{eq}, of a wet particle of diameter, D_p, from the contribution of curvature (Kelvin) and solute (Raoult) terms,

$$S_{eq} = \frac{P_w}{P^\circ} = \exp\left(\frac{A}{D_p} - \frac{\upsilon\phi n_s}{n_w}\right) \tag{3.1}$$

where $A = \frac{4M_w\sigma}{RT\rho_w}$, P_w is the droplet water vapor pressure, P° is the saturation water vapor pressure over a flat surface at the temperature T, M_w is the molar mass of water, σ is the droplet surface tension at the point of activation, R is the ideal gas constant, ρ_w is the density of water, υ is the effective van't Hoff factor of the solute, ϕ is the osmotic coefficient, n_s is the moles of solute, and n_w is the moles of water contained in the particle. The Kelvin or curvature effect (A term) is dependent on the droplet surface tension and tends to increase the saturation ratio; the Raoult (or solute) effect tends to decrease the saturation ratio by contribution of solute to the growing droplet.

If the CCN is composed of a single component that completely dissolves in water and is dilute ($\phi = 1$), Equation (3.1) reduces to the well known Köhler curve (Seinfeld and Pandis, 1998),

$$S_{eq} = \frac{P_w}{P^\circ} = \exp\left(\frac{A}{D_p} - \frac{B}{D_p^3}\right) \tag{3.2}$$

where:

$$B = \frac{6 n_s M_w \upsilon}{\pi \rho_w} \tag{3.3}$$

The maximum ("critical") saturation ratio of the Köhler curve is given by (Seinfeld and Pandis, 1998),

$$S_c = \exp\left(\frac{4A^3}{27B}\right)^{1/2} \tag{3.4}$$

S_c corresponds to the minimum level of water vapor saturation required for a CCN to develop into a cloud droplet. Since critical saturations are always higher than unity, the critical supersaturation, s_c (defined as S_c-1) is often used in its place. For each s_c, there is a characteristic dry diameter (d_{pc}), above which all particles with similar composition activate into cloud droplets.

3.2.2 Multicomponent CCN

If the aerosol is composed of more than one component (e.g., organic and inorganic), Köhler theory can still be applied with appropriate modifications to the Raoult (solute) term (e.g., Raymond and Pandis, 2003; Bilde and Svenningsson, 2004):

$$B = \sum_i B_i = \sum_i \left(\frac{\rho_i}{\rho_w}\right)\left(\frac{M_w}{M_i}\right)\varepsilon_i \upsilon_i d^3 = d^3 \left(\frac{M_w}{\rho_w}\right)\sum_i \left(\frac{\rho_i}{M_i}\right)\varepsilon_i \upsilon_i \tag{3.5}$$

where d is the dry diameter of the CCN, and ρ_i, ε_i, υ_i, and M_i are the density, volume fraction, effective van't Hoff factor and molar mass of the solute i, respectively. ε_i is related to the mass fraction of i, x_i, as:

$$\varepsilon_i = \frac{x_i/\rho_i}{\sum_i x_i/\rho_i} \tag{3.6}$$

where x_i is assumed to be known from measurements. For a single component aerosol, ε_i = 1, and Equation (3.5) reduces to Equation (3.3).

3.2.3 Köhler theory analysis: inferring molar volume

If the CCN is a mixture of completely soluble organic and inorganic material then theory gives,

$$s_c = \left(\frac{256M_w^3\sigma^3}{27R^3T^3\rho_w^3}\right)^{1/2}\left[\sum_i\left(\frac{M_w}{\rho_w}\right)\left(\frac{\rho_i}{M_i}\right)\varepsilon_i\upsilon_i\right]^{-1/2} d^{-3/2} \tag{3.7}$$

where

$$\omega = \left(\frac{256M_w^3\sigma^3}{27R^3T^3\rho_w^3}\right)^{1/2}\left[\sum_i\left(\frac{M_w}{\rho_w}\right)\left(\frac{\rho_i}{M_i}\right)\varepsilon_i\upsilon_i\right]^{-1/2} \tag{3.8}$$

is termed the "Fitted CCN Activity" (FCA) factor. If FCA is known from CCN activity measurements, the molar volume of the water soluble organic carbon component, $\frac{M_j}{\rho_j}$, can be inferred if the surface tension at the point of activation, organic and inorganic fraction as well as the effective van't Hoff factor of the components present are known. $\frac{M_j}{\rho_j}$ can be explicitly solved by rearranging Equation (3.8) as follows:

$$\frac{M_j}{\rho_j} = \frac{\varepsilon_j\upsilon_j}{\frac{256}{27}\left(\frac{M_w}{\rho_w}\right)^2\left(\frac{1}{RT}\right)^3\sigma^3\omega^{-2} - \sum_{i\neq j}\frac{\rho_i}{M_i}\varepsilon_i\upsilon_i} \tag{3.9}$$

where *j* is used to denote the organic component of the aerosol and *i* refers to all compounds (organic, inorganic, except "*j*") present in the particle.

Equation (3.9) is the basis of Köhler Theory Analysis, and can be applied in a variety of ways, depending on the amount of inorganic and surfactants present (which affect the scaling of CCN critical supersaturation with dry diameter). If CCN are composed of an internal mixture of a completely soluble electrolyte with insoluble material, and their proportion does not change with size, Köhler theory states that the critical supersaturation of CCN scales with $d^{3/2}$ (this scaling relationship can change of course if partially soluble substances are present, if composition varies with size, or if strong surfactants are present). Based on the above, Equation (3.9) can be applied as follows:

a. If there are no strong surfactants present (i.e., surface tension of the CCN at the point of activation does not depend on the solute concentration since it essentially stays constant): ω does not depend on d (surface tension depends on concentration and therefore size) and its value can be determined by a power law fit to the CCN activation curves. Equation (3.9) is then applied to infer the WSOC molar volume, given that the volume fractions and composition of organics and inorganic presents are known. This method is applied primarily in this study.

b. However if there are strong surfactants present (i.e., surface tension of the CCN at the point of activation is strongly affected by the solute concentration), the critical supersaturation – dry particle diameter curve can be divided into two regions: one in which the CCN is dilute at the point of activation and surface tension does not vary much (low critical supersaturation, or, large dry particle diameters), and, one which surface tension varies substantially (high critical supersaturation, or, small dry particle diameters). For each regime, Equation (3.9) can be applied differently as follows:

b_1. Dilute regime: Since the CCN is dilute at the point of activation at low supersaturations (i.e., ω does not depend on d since surface tension is relatively constant), hence method "a" can be applied for this range. The

appropriate supersaturation range can be determined by examining the slope (*d* exponent) of the activation curves.

b_2. Concentrated regime: In this case, the CCN can not be assumed to be dilute at the point of activation (high supersaturations), the WSOC molar volume is inferred at each supersaturation (dry diameter), using the relevant value of surface tension. We then compute the average molar volume over the range of supersaturations considered.

3.2.4 Molar volume uncertainty analysis

The uncertainty in inferred organic molar volume, $\Delta\left(\frac{M_j}{\rho_j}\right)$, can be estimated as

$$\Delta\left(\frac{M_j}{\rho_j}\right) = \sqrt{\sum_{\text{for all } x} \left(\Phi_x \Delta x\right)^2} \tag{3.10}$$

where Φ_x is the sensitivity of molar volume to each of the measured parameters x (i.e., any of σ, ω, and υ_j)

$$\Phi_x = \frac{\partial}{\partial x}\left(\frac{M_j}{\rho_j}\right) \tag{3.11}$$

and Δx is the uncertainty in x. The Φ_x for Equation (3.10) are obtained by differentiating Equation (3.9) and are shown in Table 3. 1.

3.2.5 Köhler theory analysis: inferring solubility

From Equation (3.7), s_c for completely soluble CCN scales with $d^{-3/2}$. However, if an aerosol exhibits limited solubility, s_c will change its scaling dependence at a characteristic dry diameter, d^* (Figure 3. 1). This is because when $d < d^*$, the amount of water available at the point of activation is insufficient to dissolve all available solute

Table 3. 1: Formulas used for computing the sensitivity of molar volume to σ, ω, and υ_j.

Property	Sensitivity, $\Phi_x = \frac{\partial}{\partial x}\left(\frac{M_j}{\rho_j}\right)$
σ	$\Phi_\sigma = \frac{768}{27}\left(\frac{M_w}{\rho_w}\right)^2\left(\frac{1}{RT}\right)^3\left(\frac{M_j}{\rho_j}\right)^2\frac{\sigma^2}{\varepsilon_j\upsilon_j\omega^2}$
ω	$\Phi_\omega = -\frac{512}{27}\left(\frac{M_w}{\rho_w}\right)^2\left(\frac{1}{RT}\right)^3\left(\frac{M_j}{\rho_j}\right)^2\frac{\sigma^3}{\varepsilon_j\upsilon_j\omega^3}$
υ_j	$\Phi_{\upsilon_j} = -\frac{256}{27}\left(\frac{M_w}{\rho_w}\right)^2\left(\frac{1}{RT}\right)^3\left(\frac{M_j}{\rho_j}\right)^2\frac{\sigma^3}{\varepsilon_j\upsilon_j^2\omega^2} + \sum_{i\neq j}\frac{\left(\frac{\rho_i}{M_i}\right)\varepsilon_i\upsilon_i}{\varepsilon_j\upsilon_j^2}\left(\frac{M_j}{\rho_j}\right)^2$

(which gives a much steeper dependence of s_c vs. d). For $d > d^*$, all solute is dissolved and s_c scales with $d^{-3/2}$. Hence, $d = d^*$ corresponds to the solubility limit of the solute. Using Köhler theory, the solubility, C_{eq}, of the compound can be approximated as follows. The mass of dissolved solute, m, at the point of complete dissolution is:

$$m = \frac{\pi}{6}\varepsilon_s\rho_s d^{*3} \tag{3.12}$$

where ρ_s and ε_s is the density and volume fraction of solute, respectively. From Köhler theory, the droplet volume, V_d, at the critical diameter, D_c, is:

$$V_d = \frac{\pi}{6}D_c^3 = \frac{\pi}{6}\frac{8}{27}\frac{A^3}{s_c^{*3}} \tag{3.13}$$

where s^*_c is the critical supersaturation of the particle with dry diameter d^*. Assuming that V_d is approximately equal to the volume of water in the activated droplet, C_{eq} (in kg

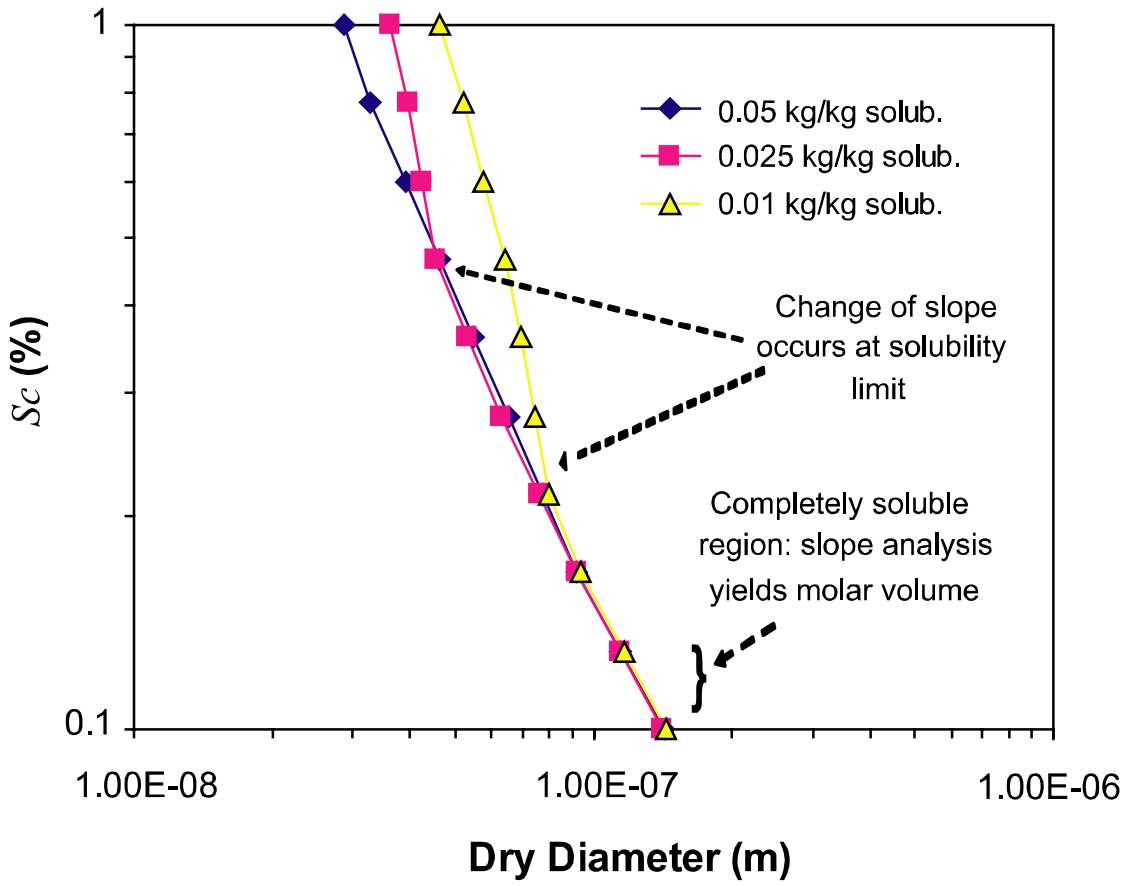

Figure 3. 1: Example on how CCN activation experiments can be used to infer the solubility of compounds.

kg^{-1}) can be estimated as:

$$C_{eq} = \frac{m}{\rho_w V_d} \tag{3.14}$$

Introducing Equation (3.12) and (3.13) into (3.14) yields the solubility of the organic, C_{eq} ($kg\ kg^{-1}$),

$$C_{eq} = \frac{27}{8}\varepsilon_s \frac{\rho_s}{\rho_w}\frac{d^{*3}s_c^{*3}}{A^3} \tag{3.15}$$

3.3 Experimental procedure

3.3.1 Surface tension measurements

Surface tension is measured using a pendant drop tensiometer (CAM 200 Optical Contact Angle Meter, by KSV Inc.). A mechanically-controlled micro-syringe slowly drops the solution into a chamber where a snapshot of the droplet at the tip of a stainless steel needle is taken. The droplet shape is fit to the Young-Laplace equation (Spelt and Li, 1996) from which the sample surface tension is obtained. Approximately seventy pictures (ten pictures per droplet) of seven different droplets (right before they fall off the tip of the needle) were taken in order to obtain averages and standard deviations for each solution. Carbon concentration was chosen as a basis for expressing surfactant concentration (Facchini et al., 1999b). Surface tension depression depends on the amount of dissolved carbon; therefore it is measured over a range of concentrations, starting at near the bulk solubility limit and then 1:2, 1:4, 1:8 dilutions with ultrafine pure water. Finally, one more "pure water" measurement was done corresponding to a "zero" carbon concentration solution, obtained by infinite dilution of the original sample. A plot of the solution surface tension versus the water soluble organic carbon concentration (C_{WSOC}) was obtained for each inorganic/organic mixture and the data fitted to the Szyskowski-Langmuir equation (Langmuir, 1917),

$$\sigma = \sigma_w - \alpha T \ln\left(1 + \beta C_{WSOC}\right) \tag{3.16}$$

where σ_w is the surface tension of water at temperature T and the parameters α and β are obtained by least squares minimization.

In order to introduce the measured surface tension into KTA, the conditions at the point of activation is determined for each supersaturation. Similar to Equation (3.15), the average concentration of the organic at activation, C_{act}, is determined by:

$$C_{act} = \frac{27}{8}\varepsilon_s \rho_s \frac{d^3 s_c^3}{A^3} \tag{3.17}$$

C_{act} is then substituted into Equation (3.16) to obtain the surface tension at the point of activation.

3.3.2 CCN activity measurements

The setup used for measurement of CCN activity consists of three sections: aerosol generation, particle size selection, and CCN/CN measurement (Figure 3. 2). In the aerosol generation step, an aqueous solution of organic/inorganic is atomized with a controlled high velocity air stream atomizer. Compressed filtered air is introduced into the atomizer, the pressure of which controls the size distribution and flow rate of

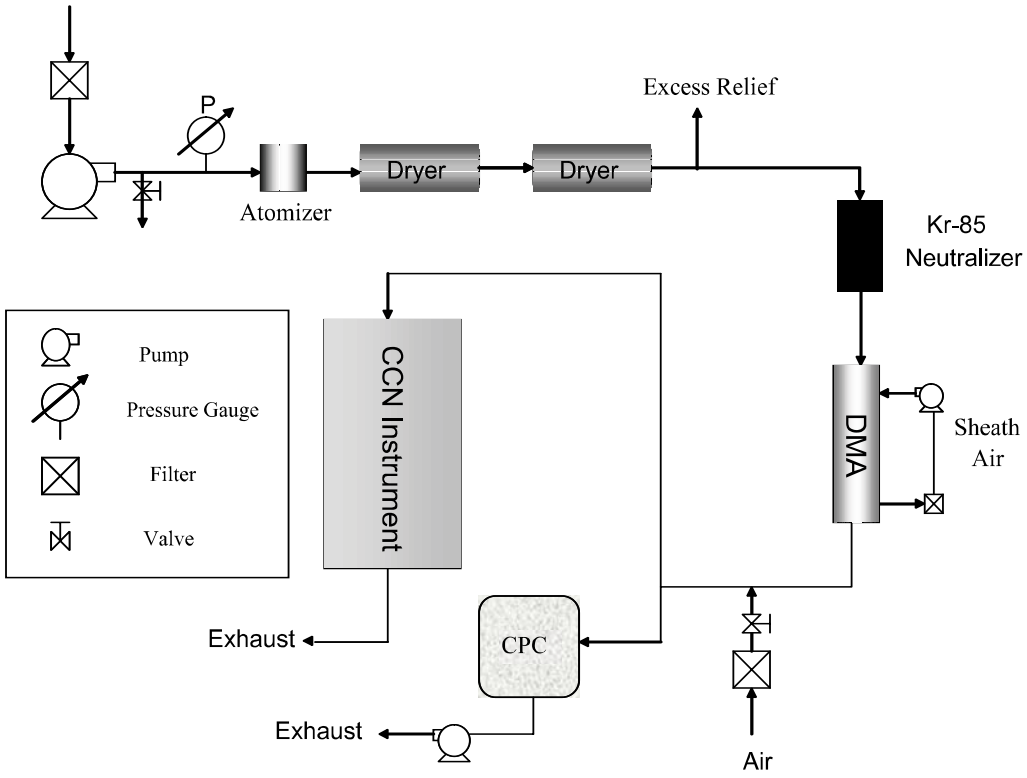

Figure 3. 2: Experimental setup used to measure CCN activity.

atomized droplets. A polydisperse aerosol is subsequently produced by drying the droplet stream by passing it through two silica-gel diffusional dryers.

The dry aerosol is then sent to the electrostatic classifier for particle size selection (TSI Model 3080) with a Differential Mobility Analyzer (DMA, TSI Model 3081). Before entering the classifier, the aerosols are passed through an impactor to remove supermicron particles; the remaining aerosol passes through a Kr-85 neutralizer which charges the particles. The particle size is then selected by a Differential Mobility Analyzer by allowing particles of the selected size (charge) to pass through producing a monodisperse aerosol. The monodisperse flow exiting the DMA at 1 l min^{-1} is mixed with filtered air and then sampled by a Condensation Particle Counter (CPC, TSI Model 3010) and a Continuous Flow Thermal Gradient Cloud Condensation Nuclei (CCN, DMT Inc.) Counter.

The CPC measures the total number concentration of condensation nuclei (CN) present for the specified aerosol size while the CCN counter counts the total number of particles that become activated as the aerosol is exposed to a constant water supersaturation. The CCN instrument operates by applying a linear temperature gradient across a wetted column; water vapor diffuses more quickly than heat, resulting in a constant water supersaturation along a streamline (Roberts and Nenes, 2005). CCN flowing about the column centerline activate and grow into cloud droplets (D_p > 1 μm) and are counted at the exit with an optical particle counter (OPC). For our studies, particles ranging between 7 and 325 nm dry mobility diameters were selected and exposed to 0.2 %, 0.4 %, 0.6 % and 1.2 % supersaturation (SS) to obtain CCN activation curves (Figure 3. 3). The CCN instrument is calibrated daily with $(NH_4)_2SO_4$ to verify that it is operating properly.

Two approaches were applied to perform the particle size selection. In the first approach, called “stepping mode”, the DMA voltage (i.e., monodisperse aerosol diameter) is constant for a period of time, during which the average CN and CCN

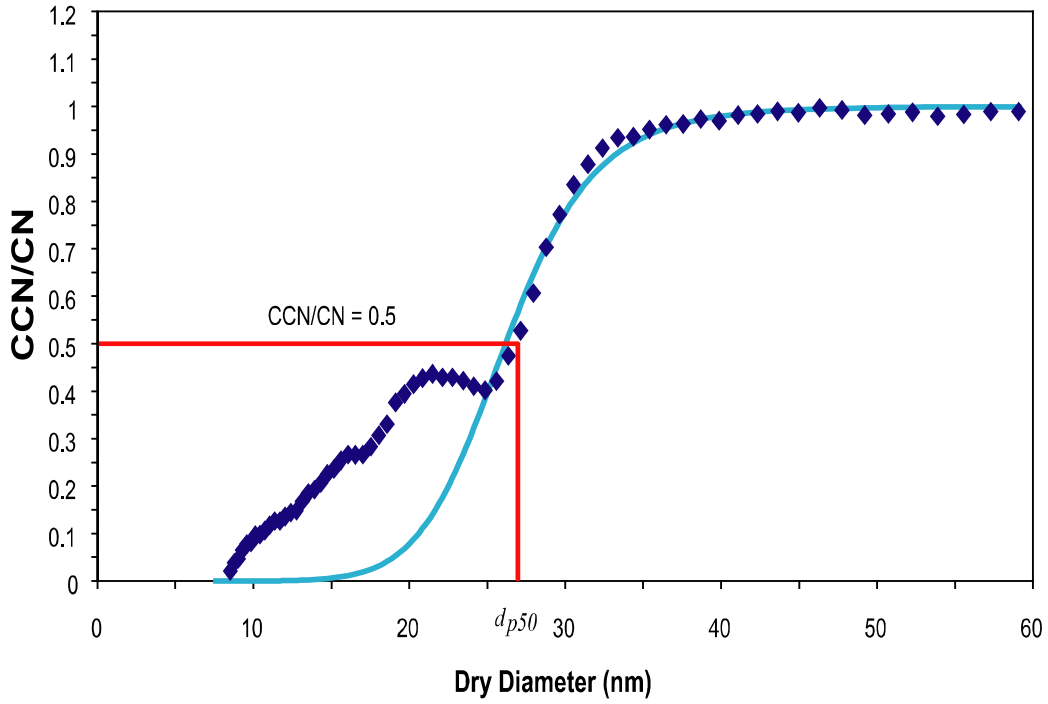

Figure 3. 3: Example of procedure used to determine dp_{50}. Shown are CCN/CN data obtained at 1.2 % supersaturation for 50 % malonic acid (mole percent) with its sigmoidal fit (light blue line). dp_{50} is the dry diameter for which the CCN/CN = 0.5.

concentrations are measured. This procedure is repeated over many particle sizes and CCN supersaturations. In the second approach, called Scanning Mobility CCN Analysis or SMCA (Nenes and Medina, in review[3]), the DMA voltage is changed over time, so that the complete size range of dry particle size is "scanned" over 2 minutes. The time series of CN, CCN and voltage is then converted into activation curves using an inversion method (Nenes and Medina, in review[3]). SMCA greatly reduces the time required for CCN activity measurements and the amount of sample required for its complete characterization.

CCN activity is characterized by the minimum dry particle diameter, d_{p50}, that activates at the supersaturation of interest. d_{p50} is found by plotting the ratio of CCN to

[3] Nenes, A. and Medina, J.: Scanning Mobility CCN Analysis – A new method for fast measurements of size-resolved CCN activity and growth kinetics, In Review.

CN concentration as a function of dry particle diameter and determining the dry diameter for which the CCN/CN ratio equals 0.50. To facilitate with the analysis, the data is fit to a sigmoid curve which then avoids considering the impact of multiply-charged particles (shown in Figure 3. 3 as a "hump" left to the sigmoid curve).

3.3.3 Compounds considered in this study

Table 3. 2 summarizes the properties of the seven compounds (one inorganic salt and six organics) used in the experiments. Because of its atmospheric relevance, $(NH_4)_2SO_4$ was chosen as the inorganic salt. The organics include four carboxylic acids (succinic acid, azelaic acid, phthalic acid, and malonic acid), one amino acid (leucine), and one sugar (fructose). Succinic, azelaic, and malonic acids are dicarboxylic acids of varying chain length, while phthalic acid is a dicarboxylic acid with a benzene ring. Leucine is a branched six carbon amino acid with a carboxylic acid group and an amine group. Finally, fructose is a six carbon sugar that exists interchangeably between a chain and a 5-carbon ring structure. All of these compounds are representative of various biogenic and anthropogenic compounds found in atmospheric particles (Saxena and Hildemann, 1996), all with varying water solubility, carbon chain length, and surfactant characteristics.

For each organic compound, we characterized the surfactant properties and CCN activity for organic-$(NH_4)_2SO_4$ mixtures with the following organic/inorganic molar ratios: 100:0, 99:1, 95:5, 90:10, 50:50, 10:90, and 1:99. By varying the organic mass fraction, we assess the applicability of KTA over a wide range of organic/inorganic interaction strength. This is a particularly important test, as it will largely determine its applicability for complex mixtures typical of atmospheric aerosols. In applying KTA, we assume $\upsilon_j \sim 1$ for organics (Cruz and Pandis, 1997; Raymond and Pandis, 2002; Broekhuizen et al., 2004; Abbatt et al., 2005; Hartz et al., 2006) and $\upsilon_j \sim 2.5$ for $(NH_4)_2SO_4$ (e.g., Brechtel and Kreidenweis, 2000). Finally, we quantify the uncertainty of

Table 3. 2: Properties of compounds considered in this study. Organics are sorted in order of decreasing solubility.

Compound Name	Chemical Formula	Molar Mass (g mol^{-1})	Density (g cm^{-3})	Solubility (g/100g H_2O)	Molar Volume (cm^3 mol^{-1})	pKa[g]
Fructose	$C_6H_{12}O_6$	180.16	1.600[c]	407.4[c]	113	N/A
Malonic Acid	$C_3H_4O_4$	104.06	1.619[a]	154[d]	64	2.9 (5.7)
Succinic Acid	$C_4H_6O_4$	118.09	1.566[b]	8.76[b]	75	4.2 (5.6)
Leucine	$C_6H_{13}NO_2$	131.17	1.293[e]	2.3[e]	101	2.4 (5.98) (acid) 9.60 (amine)
Azelaic Acid	$C_9H_{16}O_4$	188.22	1.225[f]	0.2447[f]	154	N/A
Phthalic Acid	$C_8H_6O_4$	166.13	1.593[b]	0.1415[f]	104	2.9 (5.4)
Ammonium Sulfate	$(NH_4)_2SO_4$	132.14	1.77[d]	41.22[d]	75	

[a] Abbat et al. (2005).

[b] Hartz et al. (2006).

[c] Rosenørn et al. (2006).

[d] Material Safety Data Sheet.

[e] CRC Handbook (2002).

[f] Yaws' Handbook (2003).

[g] Solomons and Fryhle (2000).

the inferred molar volume from uncertainties in σ, ω, υ_j for all mixtures considered.

3.4 Results

3.4.1 Surface tension measurements

Surface tension was measured for all pure organic and mixtures with $(NH_4)_2SO_4$ as a function of C_{WSOC}; the data was subsequently fit to the Szyskowski-Langmuir equation for use in KTA. Figure 3. 4 shows the surface tension dependence of C_{WSOC} for

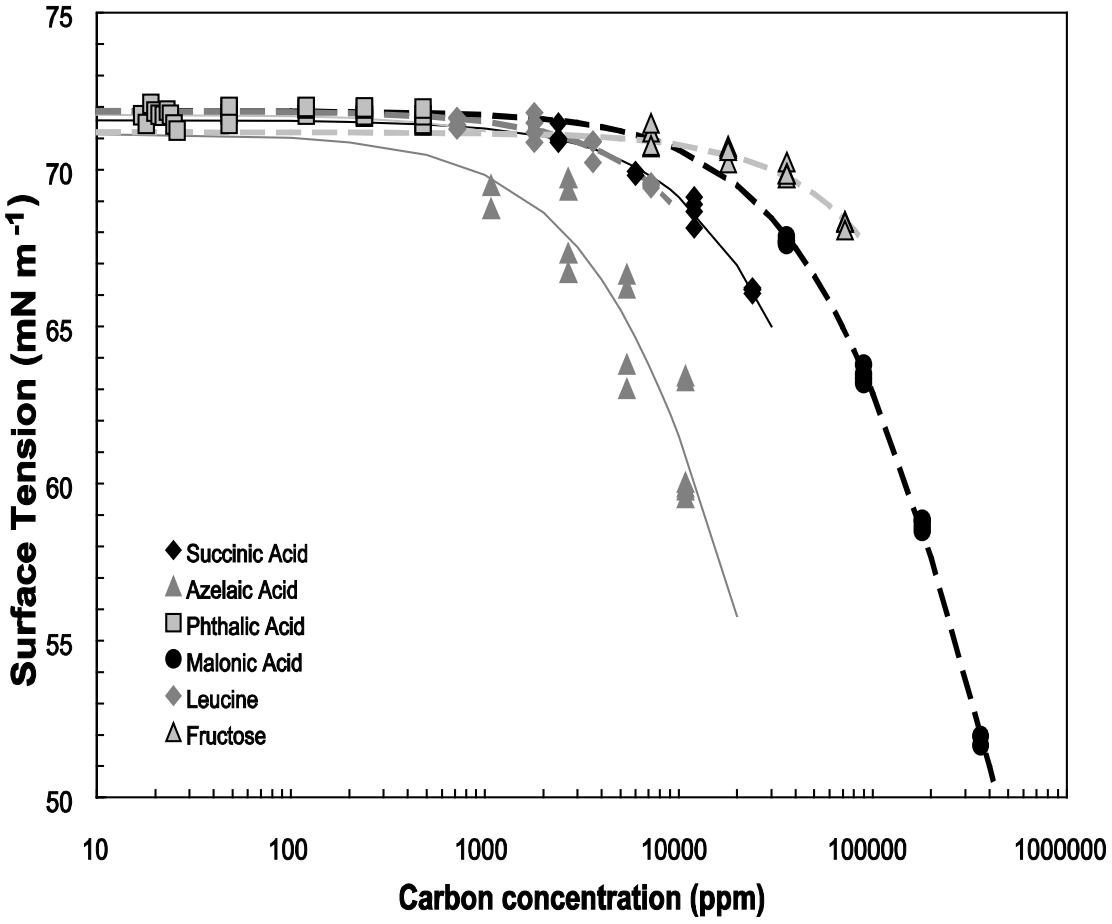

Figure 3. 4: Surface tension as a function of carbon concentration of mixed organic/inorganic aqueous solutions. Shown are succinic acid (black diamond), azelaic acid (grey triangle), phthalic acid (outlined grey square), malonic acid (black circle), leucine (grey diamond), and fructose (outlined grey triangle). The lines correspond to the Szyskowski-Langmuir fit for each organic.

all organic species (high organic fraction) each fitted to the Szyskowski- Langmuir equation. All compounds were found to depress surface tension except for phthalic acid in the range of concentration studied. The strongest surface active compounds were malonic acid and azelaic acid; fructose, leucine and succinic acid showed moderate surfactant behavior in the range of concentrations considered.

To address the effects of salts in the surfactant behavior of organics, we compared the surface tension depression of each organic when dissolved in water alone and mixed

with $(NH_4)_2SO_4$. Examples of the surface tension dependence of pure succinic acid and mixtures with $(NH_4)_2SO_4$ are shown in Figure 3. 5a (high organic fractions) and 3. 5b (low organic fractions). Adding small amounts of $(NH_4)_2SO_4$ does not affect the surfactant behavior of succinic acid at high organic fractions (Figure 3. 5a). At low organic concentrations, introduction of greater amounts of $(NH_4)_2SO_4$ to the succinic acid solution can further decrease the surface tension beyond that of the pure organic (Figure 3. 5b). As an example, for a C_{WSOC} of 2000 ppm, the surface tension for pure succinic acid (100 %) is 71 mN m^{-1} while for a 1 % succinic acid solution, at the same concentration, the surface tension is depressed down to 66.5 mN m^{-1}. The observed decrease in surface tension with salt concentration increase could be explained by the interaction between ammonium sulfate and organic molecules. The presence of the inorganic electrolyte at high concentrations forces the "organic" to partition to the surface creating a surfactant rich layer; this "salting out" effect decreases the surface tension beyond that of the pure organic component (Kiss et al., 2005).

Since the addition of $(NH_4)_2SO_4$ did not substantially affect the droplet surface tension for the high organic fraction solutions considered (90 % - 100 %), all molar fraction solutions of each species were fit to Equation (3.16) in order to obtain average α and β parameters (Table 3. 3), which subsequently can be introduced to KTA. For low organic fractions (50 %, 10 %, and 1 %), $(NH_4)_2SO_4$ has an important impact on surface tension, so α and β must be determined at each ammonium sulfate concentration (Table 3. 4; Figure 3.5b).

3.4.2 CCN measurements

Activation curves for pure succinic acid and mixtures with $(NH_4)_2SO_4$ are shown in Figure 3. 6. As the organic mass fraction decreases from 100 % to 50 %, the activation curves of the mixtures move towards the $(NH_4)_2SO_4$ curve. Therefore, small amounts of salt present notably impact the CCN activity of the organic material. On the other hand,

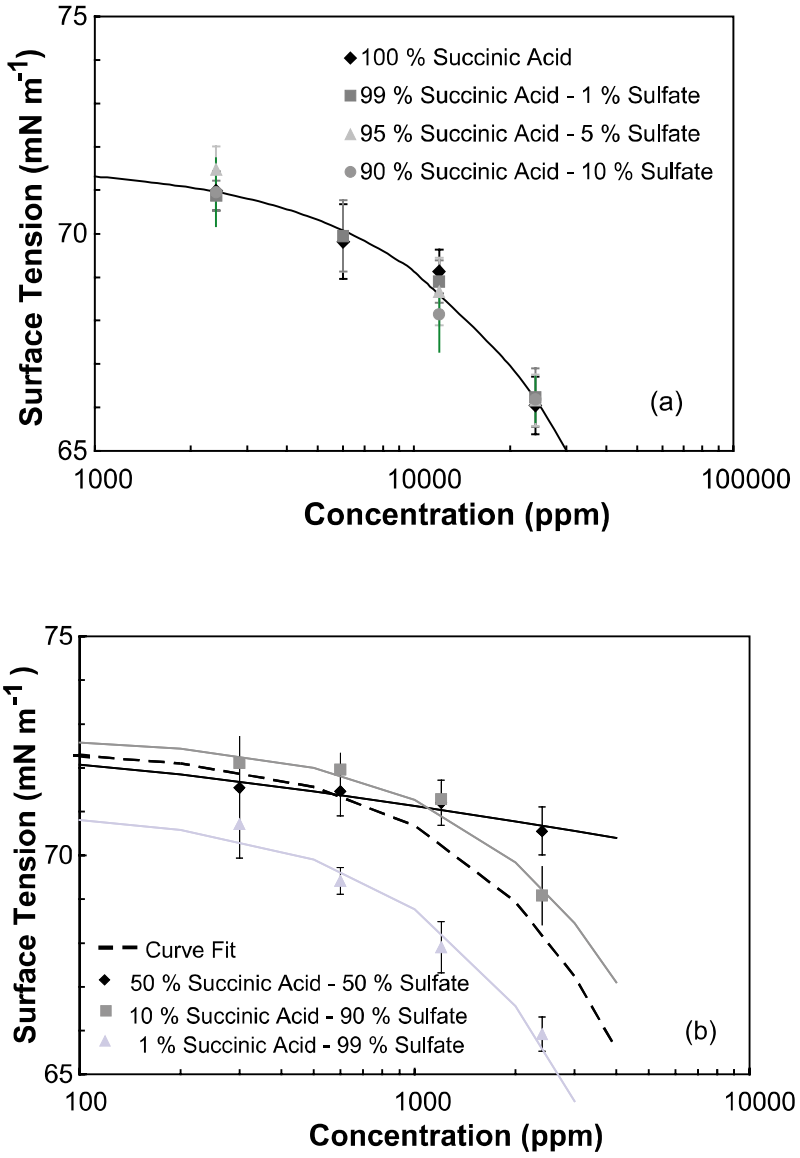

Figure 3. 5: (a) Surface tension as a function of carbon concentration for pure succinic acid (black diamond) and mixtures with $(NH_4)_2SO_4$ for 99 % (grey square), 95 % (grey triangle), and 90 % (grey circle) succinic acid (mole fraction). The solid black line corresponds to the Szyskowski-Langmuir fit for all high organic fraction mixtures. (b) Surface tension depression as a function of carbon concentration for $(NH_4)_2SO_4$ – succinic acid mixtures for 50 % (black diamond), 10 % (grey square), and 1% (grey triangle) succinic acid (mole fraction). The solid lines correspond to the Szyskowski-Langmuir fit for each mixture: 50 % (black line), 10 % (dark grey line), and 1 % (light grey line). The dashed black line corresponds to the Szyskowski-Langmuir fit for all three low organic fraction mixtures.

Table 3. 3: Szyskowski-Langmuir constants (298 K) for computing the surface tension of aqueous organic solutions. The same parameters apply for pure organic solutions and mixtures with $(NH_4)_2SO_4$ (up to 10 % salt mole fraction). C_{max} is the maximum concentration of organic used in the measurements.

Compound	$\alpha \times 10^1$ (mN $m^{-1}K^{-1}$)	$\beta \times 10^5$ (ppm^{-1})	$C_{max} \times 10^{-3}$ (ppm)
Fructose	1.896	0.0709	180
Malonic Acid	0.434	1.0039	1040
Succinic Acid	0.652	1.3383	59
Leucine	1.947	0.5702	13
Azelaic Acid	0.484	9.4885	1.9
Phthalic Acid	1.930	0.9170	0.831

when small amounts of organic are introduced to a $(NH_4)_2SO_4$ particle, the aerosol has a higher CCN activity than pure $(NH_4)_2SO_4$; the surface tension depression from the presence of organics allows the droplet activation to occur at lower supersaturations. The same behavior was observed for all mixtures.

Comparison of CCN activity (activation curves) are presented in Figures 3. 7a and 3. 7b for organic aerosol mixed with $(NH_4)_2SO_4$. The observed CCN activity was not consistent with solubility reported in Table 3. 2; in fact, all cases studied behaved as if they were completely soluble, possibly because of aerosol metastability or the effect of curvature-enhanced solubility (Padró and Nenes, 2007). As the measurements suggest that most compounds studied are not strong surfactants (Figure 3. 4), we expect CCN activity to correlate with the number of moles at the point of activation, i.e., the effective van't Hoff factor (the moles of ions released per mol of solute) over the molar volume. Thus, phthalic acid should produce better CCN than fructose; the two have comparable

Table 3. 4: Szyskowski-Langmuir constants (298 K) for computing the surface tension of aqueous organic solutions mixed with $(NH_4)_2SO_4$ for larger than 10 % salt mole fraction.

Compound	Organic Mole Fraction (%)	$\alpha \times 10^1$ (mN m^{-1} K^{-1})	$\beta \times 10^5$ (ppm^{-1})
Malonic Acid	50	5.3316	1.381
	10	5.3316	1.381
	1	0.5000	1.946
Succinic Acid	50	0.0185	1004
	10	1.8031	2.756
	1	3.4842	2.202
Azelaic Acid	50	0.2045	454.4
	10	21.322	2.404
	1	23.917	3.012

molar volumes (Table 3. 2) but the carboxyl groups in phthalic acid dissociate substantially (low pKa, i.e. van't Hoff factor > 1), while fructose does not dissociate at all (i.e. van't Hoff factor = 1). Using this approach, one can rank the compounds in terms of decreasing CCN activity as follows: ammonium sulfate, phthalic acid, malonic acid, succinic acid, leucine, azelaic acid, and fructose. Our measurements support this ranking.

The high CCN activity of leucine in our study is in disagreement with other published data (e.g., Hartz et al., 2006). We attribute this difference to the phase state of the aerosol introduced in the CCN instrument: our atomized particles were "softly" dried down to ~ 10% RH (as measured using a RH probe inline); under such conditions aerosol tends to retain water (Padró and Nenes, 2007) and leucine does not crystallize out of solution. In contrast, other studies used more aggressive drying methods (for example,

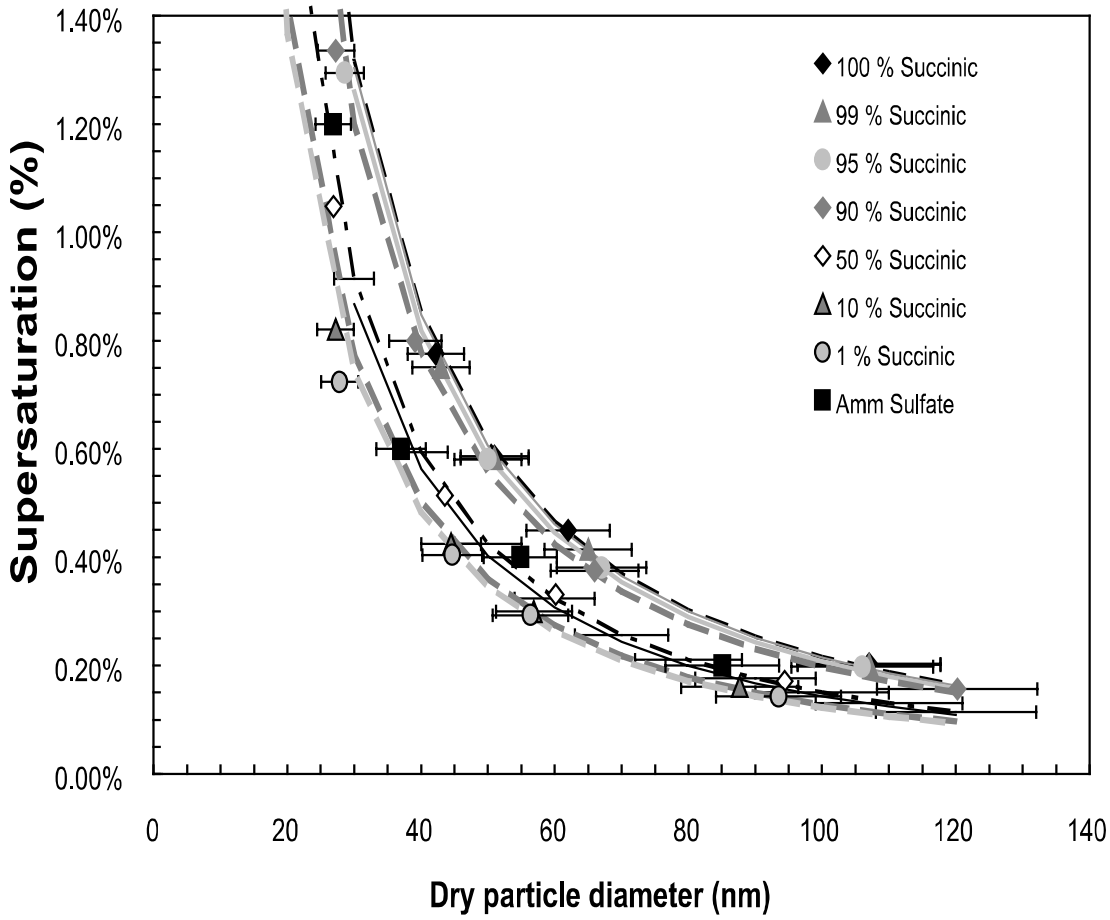

Figure 3. 6: Activation curves for pure succinic acid (black diamond) and mixtures with $(NH_4)_2SO_4$ consisting of 99 % (grey triangle), 95 % (grey circle), 90 % (grey diamond), 50 % (open diamond), 10 % (outlined grey triangle), and 1 % (outlined grey circle) molar fraction of succinic acid. Activation curve for $(NH_4)_2SO_4$ (black square) is also plotted for comparison. The solid and dash lines (100 % (black dash line), 99 % (dark grey line), 95 % (light grey line), 90 % (dark grey dashed line), and $(NH_4)_2SO_4$ (black line)) indicates a power fit to the data.

Hartz et al., 2006 used a silica gel dryer followed by an activated carbon dryer) which likely resulted in much drier leucine particles.

3.4.3 Evaluation of inferred molar volumes

Köhler theory analysis requires knowledge of the parameters α, β (Tables 3. 3 and 3. 4), and ω (Table 3. 5), which are introduced into Equation (3.9). The

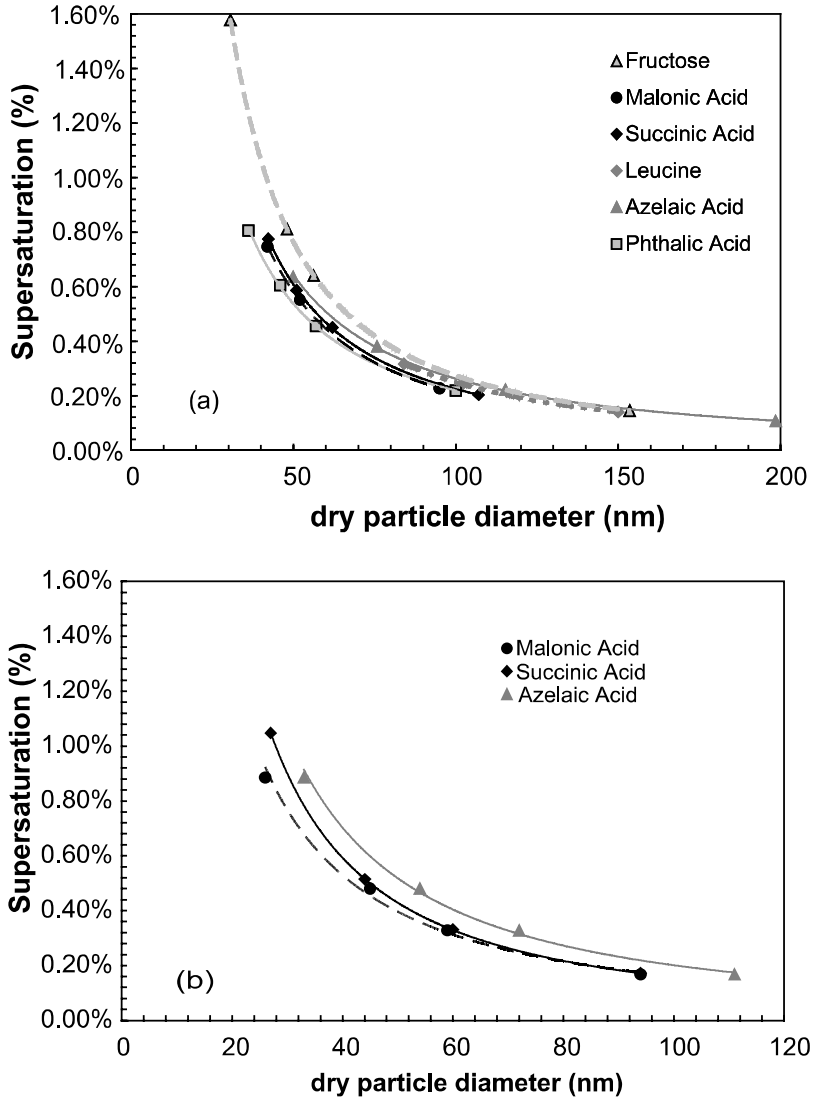

Figure 3. 7: (a) Activation curves for pure organic components: succinic acid (black diamond), azelaic acid (grey triangle), phthalic acid (outlined grey square), malonic acid (black circle), leucine (grey diamond), and fructose (outlined grey triangle). The lines correspond to a power law fit to the activation data. (b) Activation curves for 50 % organic fraction mixtures with $(NH_4)_2SO_4$: azelaic acid (grey triangle), succinic acid (black diamond), and malonic acid (black circle). The lines correspond to a power law fit to the activation data.

calculated $\left(\frac{M_j}{\rho_j}\right)$ as well as its error with respect to expected values are shown in Table 3. 5. Predicted molar volume of each organic was closest to literature values when the organic mass fraction is 50 % and above; under such conditions, the average error in

Table 3. 5: Results of Köhler theory analysis for the compounds and mixtures considered in this study. Organics are arranged in order of decreasing solubility.

Compound (Molar Volume)	Organic Mole Fraction (%)	$\omega \times 10^{14}$ ($m^{3/2}$)	Inferred Molar Volume ($cm^3\ mol^{-1}$)	Molar Volume Error (%)
Fructose ($113\ cm^3\ mol^{-1}$)	100	8.478	112.868	0.2
	99	8.527	115.207	2
	95	8.075	111.447	1
	90	7.587	106.600	5
Malonic Acid ($64\ cm^3\ mol^{-1}$)	100	6.473	66.150	3
	99	6.398	65.089	1
	95	6.195	63.531	1
	90	5.944	62.145	3
	50	4.588	68.328	6
	10	3.965	3.082	95
	1	3.904	0.016	100
Succinic Acid ($75\ cm^3\ mol^{-1}$)	100	6.839	89.368	19
	99	6.777	88.680	18
	95	6.548	81.394	8
	90	6.227	76.909	2
	50	4.753	58.130	23
	10	4.024	7.313	90
	1	3.863	0.099	100
Leucine ($101\ cm^3\ mol^{-1}$)	100	7.807	139.106	37
	99	7.960	183.440	81
	95	7.435	125.739	24
	90	7.054	113.670	12
Azelaic Acid ($154\ cm^3\ mol^{-1}$)	100	8.146	281.794	83
	99	7.867	190.044	23
	95	7.062	135.549	12
	90	6.804	131.878	14
	50	3.986	212.967	38
	10	2.462	161.931	5
	1	4.099	691.836	349
Phthalic Acid ($104\ cm^3\ mol^{-1}$)	100	5.787	90.024	14
	99	5.605	82.449	21
	95	5.617	89.298	14
	90	5.630	107.624	3

inferred molar volume was found to be 18 %. In terms of the molar volume error dependence with organic fraction (Table 3. 5), addition of some deliquescent material (ammonium sulfate) enhances the amount of water in the CCN and facilitates complete dissolution of the organic fraction (which can be further enhanced from curvature enhanced solubility, Padró and Nenes, 2007). As a result, the inferred molar volume error decreases as s_c more closely scales with $d^{-3/2}$. When the organic fraction is low (< 50%), the CCN at the point of activation becomes concentrated in ammonium sulfate and the organic may "salt out" (i.e., precipitate out of solution). This affects the solution surface tension and number of dissolved moles, which eventually increases the error in molar volume (Table 3. 5). Phthalic acid is in less error compared to leucine and azelaic acid (despite the "bulk" solubility of the former), two types of patters are seen: *i*) for the soluble non-surfactant compounds (fructose, malonic acid) error is almost zero for the pure compound and increases as the organic mass fraction decreases, *ii*) for sparingly-soluble and surface-active species (leucine, phthalic acid, succinic acid and azelaic acid), errors tends to be larger when (almost) pure compound is activated, reaches a minimum at the 90-50% organic fraction range, and then increases again at lower organic factions. In both pattern types, the error at small organic fractions is consistent with the expectation that molar volume uncertainty is inversely proportional to organic fraction (Equation (3.10), Table 3. 1). In pattern type (*ii*), the simple form of Köhler theory used when applying KTA (Equations (3.1) -(3.4)) does not consider the effect of surface layer partitioning on critical supersaturation (Sorjamaa et al., 2004; Sorjamaa and Laaksonen, 2006); this may introduce a bias in inferred molar volume which becomes maximum when the organic mass fraction is high. Furthermore, since surfactants are not very soluble (Table 3. 2), they may not completely dissolve at the point of activation (when they constitute most of the CCN dry mass), which leads to an overestimation of solute molar volume (Table 3. 5). Addition of some deliquescent material (ammonium sulfate) enhances the amount of water in the CCN and facilitates complete dissolution of the

organic fraction (the solubility of which can be further enhanced from curvature-enhanced solubility, Padró and Nenes, 2007). As a result, the inferred molar volume error decreases as s_c more closely scales with $d^{-3/2}$. When the organic fraction becomes low (< 50%), the CCN at the point of activation becomes concentrated in ammonium sulfate and the organic may "salt out" (i.e., precipitate out of solution). This affects the solution surface tension and number of dissolved moles, which eventually increases the error in molar volume (Table 3. 5). Phthalic acid is in less error compared to leucine and azelaic acid (despite the "bulk" solubility of the former being lower than the latter two), likely because it is the least surface-active of the type (*ii*) compounds, hence least subject to surface-partitioning effects. Overall, the assumption of complete solubility used in KTA seems to work well, particularly for cases where organics are mixed with some sulfate.

Estimating average molar volume uncertainty requires computing its sensitivity with respect to σ, ω, υ_j and the estimated uncertainty in those parameters (Table 3. 6). Of the three parameters, ω and υ_j were found to introduce the greatest uncertainty; while the uncertainty in σ is rather small. The greater uncertainty (~ 55 %) for all the compounds arises from the van't Hoff factor (dissociation in water). The uncertainty in this parameter is high since we assumed $\upsilon_j = 1$ when in reality it is larger (since most of the dicarboxylic acids we studied dissociate, pKa < 3). Error estimates increase as the organic fraction decreases, since the sensitivities, Φ_x, depend inversely on the organic mass fraction (Table 3. 1).

From our assessment of KTA, the new method applies best for relatively high organic mass fractions but with some deliquescent material to insure sufficient water uptake for complete dissolution of constituents. It is suggested that the method should not be used for the low organic fraction aerosols because: i) salting out effects can become very important and ii) the sensitivities scale with ε_j^{-1} and uncertainties are magnified substantially for volume fractions below 20%. The uncertainty estimated from Equation

Table 3. 6: Molar volume uncertainty analysis and total uncertainty as percent of molar volume for the compounds and mixtures considered in this study.

Compound	Organic Mole Fraction (%)	Uncertainty to σ ($cm^3\ mol^{-1}$)	Uncertainty to ω ($cm^3\ mol^{-1}$)	Uncertainty to υ_{org} ($cm^3\ mol^{-1}$)	Total Uncertainty ($cm^3\ mol^{-1}$)	Total Uncertainty (%)
Fructose	100	0.048	4.042	5.613	9.703	8.6
	99	0.063	4.057	5.634	9.754	8.6
	95	0.061	4.697	6.524	11.282	10.0
	90	0.060	5.647	7.843	13.550	12.0
Malonic Acid	100	0.021	2.214	3.075	5.267	8.2
	99	0.019	2.303	3.199	5.483	8.6
	95	0.012	2.588	3.594	6.170	9.6
	90	0.021	2.979	4.137	7.095	11.1
	50	0.057	3.817	10.602	14.362	22.4
	10	0.217	58.691	56.433	114.907	179.5
	1	3.704	658.918	866.996	1522.208	2378.4
Succinic Acid	100	0.026	2.012	3.143	5.129	6.8
	99	0.026	2.066	3.229	5.269	7.0
	95	0.031	2.511	3.923	6.402	8.5
	90	0.042	3.106	4.853	7.917	10.6
	50	0.091	13.004	14.778	27.691	36.9
	10	0.642	31.213	86.702	117.272	156.4
	1	7.124	696.943	967.975	1657.794	2210.4
Leucine	100	0.046	2.843	3.949	6.746	6.7
	99	0.031	2.112	2.934	5.015	5.0
	95	0.043	3.682	5.114	8.752	8.7
	90	0.075	4.999	6.943	11.868	11.8
Azelaic Acid	100	0.057	3.462	4.555	7.960	5.2
	99	0.065	4.715	6.203	10.854	7.0
	95	0.120	6.976	9.178	16.034	10.4
	90	0.113	8.873	11.675	20.435	13.3
	50	0.238	12.749	26.560	39.071	25.4
	10	1.906	122.662	180.385	301.142	195.5
	1	17.549	3327.155	3080.696	6390.317	4149.6
Phthalic Acid	100	0.109	10.200	14.167	24.477	23.5
	99	0.105	11.259	15.637	27.002	26.0
	95	0.109	11.666	16.203	27.978	26.9
	90	0.118	12.949	17.984	31.050	29.9

(3.10) (Table 3. 6) is usually larger than the actual molar volume (Table 3. 5), which suggests that Equation (3.10) can be used as an upper limit estimate.

3.5 Conclusions

This study presents a new method, Köhler Theory Analysis, to infer the molar volume, solubility, and surfactant characteristics of water soluble atmospheric organic matter. This is done by combining Köhler theory with measurements of surface tension, chemical composition, and CCN activity. In addition to presenting KTA, we evaluate the method by comparing inferred molar volumes to their expected values for particles composed of six organics (azelaic acid, malonic acid, phthalic acid, succinic acid, leucine, and fructose) in pure form or mixed with $(NH_4)_2SO_4$. CCN activation experiments were done at 0.2 %, 0.4 %, 0.6 %, and 1.2 % supersaturation.

Köhler theory analysis was found to predict the average error in molar volume to within 18 % of the expected value when the organic mass fraction ranges between 50 and 90 %. The estimated molar volume error was found to be larger than its actual value (most likely from surface partitioning and partial solubility effects). KTA is a potentially powerful tool for characterizing the droplet formation potential of ambient water soluble organic carbon, as it can provide much needed constraints for physically-based assessments of the aerosol indirect effect.

3.6 References

CRC handbook of Chemistry and Physics, 83 ed, D. R. Lide, CRC Press, New York, 2002.

Abbatt, J. P. D., Broekhuizen, K. and Kumal, P. P.: Cloud condensation nucleus activity of internally mixed ammonium sulfate/organic acid aerosol particles, Atmos. Environ., 39(26), 4767-4778, 2005.

Bilde, M. and Svenningsson, B.: CCN activation of slightly soluble organics: the importance of small amounts of inorganic salt and particle phase, Tellus Series B-Chemical and Physical Meteorology, 56(2), 128-134, 2004.

Brechtel, F. J. and Kreidenweis, S. M.: Predicting particle critical supersaturation from hygroscopic growth measurements in the humidified TDMA. Part I: Theory and sensitivity studies, Journal of Atmospheric Science, 57(12), 1854-1871, 2000.

Broekhuizen, K., Chang, R. Y.-W., Leaitch, W. R., Li, S.-M. and Abbatt, J. P. D.: Closure between measured and modeled cloud condensation nuclei (CCN) using size-resolved aerosol compositions in downtown Toronto, Atmos. Chem. Phys., 6, 2513-2524, 2006.

Broekhuizen, K., Kumar, P. P. and Abbatt, J. P. D.: Partially soluble organics as cloud condensation nuclei: Role of trace soluble and surface active species, Geophys. Res. Lett., 31(1), Art. No. L01107, doi: 10.1029/2003GL018203, 2004.

Cruz, C. N. and Pandis, S. N.: A study of the ability of pure secondary organic aerosol to act as cloud condensation nuclei, Atmos. Environ., 31(15), 2205-2214, 1997.

Decesari, S., Facchini, M. C., Fuzzi, S. and Tagliavini, E.: Characterization of water-soluble organic compounds in atmospheric aerosol: A new approach, J. Geophys. Res.-A., 105(D1), 1481-1489, 2000.

Facchini, M. C., Decesari, S., Mircea, M., Fuzzi, S. and Loglio, G.: Surface tension of atmospheric wet aerosol and cloud/fog droplets in relation to their organic carbon content and chemical composition, Atmos. Environ., 34(28), 4853-4857, 2000.

Facchini, M. C., Fuzzi, S., Zappoli, S., Andracchio, A., Gelencser, A., Kiss, G., Krivacsy, Z., Meszaros, E., Hansson, H. C., Alsberg, T. and Zebuhr, Y.: Partitioning of the organic aerosol component between fog droplets and interstitial air, J. Geophys. Res.-A., 104(D21), 26821-26832, 1999a.

Facchini, M. C., Mircea, M., Fuzzi, S. and Charlson, R. J.: Cloud albedo enhancement by surface-active organic solutes in growing droplets, Nature, 401(6750), 257-259, 1999b.

Feingold, G. and Chuang, P. Y.: Analysis of the influence of film-forming compounds on droplet growth: Implications for cloud microphysical processes and climate, J. Atmos. Sci., 59(12), 2006-2018, 2002.

Giebl, H., Berner, A., Reischl, G., Puxbaum, H., Kasper-Giebl, A. and Hitzenberger, R.: CCN activation of oxalic and malonic acid test aerosols with the University of Vienna cloud condensation nuclei counter, J. Aerosol Sci., 33(12), 1623-1634, 2002.

Hartz, K. E. H., Tischuk, J. E., Chan, M. N., Chan, C. K., Donahue, N. M. and Pandis, S. N.: Cloud condensation nuclei activation of limited solubility organic aerosol, Atmos. Environ., 40(4), 605-617, 2006.

IPCC: Climate Change (2001): The Scientific Basis, ed, Cambridge University Press, United Kingdom, 2001.

Kanakidou, M., Seinfeld, J. H., Pandis, S. N., Barnes, I., Dentener, F. J., Facchini, M. C., Van Dingenen, R., Ervens, B., Nenes, A., Nielsen, C. J., Swietlicki, E., Putaud, J. P., Balkanski, Y., Fuzzi, S., Horth, J., Moortgat, G. K., Winterhalter, R., Myhre, C. E. L., Tsigaridis, K., Vignati, E., Stephanou, E. G. and Wilson, J.: Organic aerosol and global climate modeling: a review, Atmos. Chem. Phys., 5, 1053-1123, 2005.

Kiss, G., Tombacz, E. and Hansson, H. C.: Surface tension effects of humic-like substances in the aqueous extract of tropospheric fine aerosol, J. Atmos. Chem., 50(3), 279-294, 2005.

Köhler, H.: The nucleus in and the growth of hygroscopic droplets, Transactions of the Faraday Society, 32(2), 1152-1161, 1936.

Kumar, P. P., Broekhuizen, K. and Abbatt, J. P. D.: Organic acids as cloud condensation nuclei: Laboratory studies of highly soluble and insoluble species, Atmos. Chem. Phys., 3, 509-520, 2003.

Langmuir, I.: The constitution and fundamental properties of solids and liquids. II. Liquids., J. Am. Chem. Soc., 39, 1848-1906, 1917.

Nenes, A., Charlson, R. J., Facchini, M. C., Kulmala, M., Laaksonen, A. and Seinfeld, J. H.: Can chemical effects on cloud droplet number rival the first indirect effect?, Geophys. Res. Lett., 29(17), Art. No. 1848, doi:10.1029/2002GL015295, 2002.

Padró, L. T. and Nenes, A.: Cloud droplet activation: solubility revisited, Atmos. Chem. Phys. Discuss., 7, 2325-2355, 2007.

Raymond, T. M. and Pandis, S. N.: Cloud activation of single-component organic aerosol particles, J. Geophys. Res.-A., 107(D24), Art. No. 4787, doi:10.1029/2002JD002159, 2002.

Raymond, T. M. and Pandis, S. N.: Formation of cloud droplets by multicomponent organic particles, J. Geophys. Res.-A., 108(D15), 2003.

Roberts, G. C. and Nenes, A.: A continuous-flow streamwise thermal-gradient CCN chamber for atmospheric measurements, Aerosol Sci. Technol., 39(3), 206-211, 2005.

Rosenørn, T., Kiss, G. and Bilde, M.: Cloud droplet activation of saccharides and levoglucosan particles, Atmos. Environ., 40(10), 1794-1802, 2006.

Saxena, P. and Hildemann, L. M.: Water-soluble organics in atmospheric particles: A critical review of the literature and application of thermodynamics to identify candidate compounds, J. Atmos. Chem., 24(1), 57-109, 1996.

Seinfeld, J. H. and Pandis, S.: Atmospheric Chemistry and Physics, ed, John Wiley, New York, 1998.

Shulman, M. L., Jacobson, M. C., Carlson, R. J., Synovec, R. E. and Young, T. E.: Dissolution behavior and surface tension effects of organic compounds in nucleating cloud droplets, Geophys. Res. Lett., 23(3), 277-280, 1996.

Solomons, G. and Fryhle, C.: Organic Chemistry, 7th ed, John Wiley & Sons, Inc., New York, 2000.

Sorjamaa, R. and Laaksonen, A.: The influence of surfactant properties on critical supersaturations of cloud condensation nuclei, J. Aerosol Sci., 37(12), 1730-1736, 2006.

Sorjamaa, R., Svenningsson, B., Raatikainen, T., Henning, S., Bilde, M. and Laaksonen, A.: The role of surfactants in Köhler theory reconsidered, Atmos. Chem. Phys., 4, 2107-2117, 2004.

Spelt, J. K. and Li, D.: Applied Surface Thermodynamics, ed, A. W. Neumann and J. K. Spelt, Marcel Dekker, New York, 1996.

Sullivan, A. P. and Weber, R. J.: Chemical characterization of the ambient organic aerosol soluble in water: 1. Isolation of hydrophobic and hydrophilic fractions with a XAD-8 resin, J. Geophys. Res.-A., 111(D5), Art. D05314,doi:10.1029/2005JD006485, 2006a.

Sullivan, A. P. and Weber, R. J.: Chemical characterization of the ambient organic aerosol soluble in water: 2. Isolation of acid, neutral, and basic fractions by modified size-exclusion chromatography, J. Geophys. Res.-A., 111(D5), Art. No. D05315, doi:10.1029/2005JD006486, 2006b.

Yaws, C. L.: Yaw's handbook of thermodynamic and physical properties of chemical compounds, ed, Knovel, New York, 2003.

Zappoli, S., Andracchio, A., Fuzzi, S., Facchini, M. C., Gelencser, A., Kiss, G., Krivacsy, Z., Molnar, A., Meszaros, E., Hansson, H. C., Rosman, K. and Zebuhr, Y.: Inorganic, organic and macromolecular components of fine aerosol in different areas of Europe in relation to their water solubility, Atmos. Environ., 33(17), 2733-2743, 1999.

CHAPTER 4

INVESTIGATION OF CCN RELEVANT PROPERTIES AND DROPLET GROWTH KINETICS OF WATER-SOLUBLE ORGANIC CARBON IN MEXICO CITY [4]

In this study, we characterize the hygroscopic and CCN-relevant properties of the water-soluble fraction of Mexico City (MC) aerosol collected during the MILAGRO (Megacity Initiative: Local and Global Research Observations) campaign during March 2006. Emphasis is placed on the contribution of water-soluble organics to the observed CCN activity, their potential impact on the droplet activation kinetics and their variation over time and location. Soluble material was obtained from water extraction of aerosol samples collected upon Hi-Volume quartz filters at the downtown Mexico City (T0), and, the Universidad Tecnológica de Tecámac (T1) sites. Köhler theory analysis (KTA) was used to infer the molar volume and surfactant characteristics of the extracted water-soluble samples and in mixture with ammonium sulfate, $(NH_4)_2SO_4$. Finally κ- Köhler theory was used to study the overall hygroscopic properties of the extracted samples.

4.1 Motivation

It is well known that the ability of aerosols to act as cloud condensation nuclei (CCN) is a strong function of their size, chemical composition, and supersaturation levels in ambient clouds. The compositional complexity of aerosol, being a mixture of inorganic salts and numerous organic species, poses a challenge for their description in atmospheric models of aerosol-cloud interactions. Knowledge of their cumulative impact on CCN

[4] Under preparation for submission: Padró, L. T., Tkacik, D., Lathem, T., Hennigan, C., Sullivan, A. P., Weber, R. J., Huey, L. G. and Nenes, A.: Investigation of CCN relevant properties and droplet growth kinetics of water-soluble organic carbon in Mexico City, Manuscript in Preparation.

activity is important, as carbonaceous material can constitute up to 90% of the total aerosol (e.g., Andreae and Crutzen, 1997;Lance et al., 2006;Lance et al., 2004;Moffet et al., 2008;Stone et al., 2008), 10-70% of which is water soluble (Facchini et al., 2000;Hagler et al., 2007;Sullivan et al., 2004;Zappoli et al., 1999).

Many studies have focused on understanding the processes involving the interactions of water soluble organic compounds with water vapor, such as CCN activity (e.g., Asa-Awuku et al., 2008;Dinar et al., 2006b;Svenningsson et al., 2006), hygroscopicity (e.g., Badger et al., 2006;Brooks et al., 2004;Dinar et al., 2007;Svenningsson et al., 2006;Wex et al., 2007), droplet activation kinetics (e.g., Asa-Awuku et al., 2009; Engelhart et al., 2008; Ruehl et al., 2008; Ruehl et al., in press) and surfactant characteristics (e.g., Asa-Awuku et al., 2008;Kiss et al., 2005;Taraniuk et al., 2007). Chemical characterization of the organics in ambient samples using analytical techniques such as size exclusion chromatography and mass spectrometry (Kiss et al., 2003;Samburova et al., 2005;Zappoli et al., 1999) has met with limited success, as it often does not identify the majority of compounds present. Even if complete speciation were possible, the amount of information involved excludes its facile implementation in models of aerosol-cloud interactions. Alternatively, indirect methods can be used to parameterize the CCN properties of the organic fraction. Petters and Kreidenweis (2007) proposed the use of a hygroscopicity parameter, κ (which is a parameterized term of the Raoult effect from dissolved solute), which has been widely used to characterize the aerosol water uptake characteristics and CCN activity of a variety of compounds as well as mixtures. Wex et al. (2007) suggested another single-parameter approach, the ionic density, ρ_{ion}, to model the hygroscopic growth of HUmic-LIke Substances (HULIS) by combining physical properties of these compounds into a single parameter. ρ_{ion} can be determined by adjusting it value to reproduce measured hygroscopic growth factors for RH < 100%. Köhler Theory Analysis (KTA) (Padró et al., 2007; Asa-Awuku et al., 2007; Asa-Awuku et al., 2008; Moore et al., 2008; Engelhart et al., 2008) is another

approach to understand the average molar properties and surfactant characteristics of the desired organics, and is most successful whenever the organic fraction in the aerosol is large and detailed measurements of water soluble organic carbon (WSOC) and inorganic composition is available.

In this study we characterize the CCN-relevant properties (e.g., CCN activity, hygroscopicity parameter, surface tension, molar volume, and droplet activation kinetics) of the water soluble fraction of Mexico City aerosol collected during March 2006. The emphasis of the analysis is placed on constraining the impact of water-soluble organics on hygroscopicity and droplet formation, and their temporal variation. Mexico City was selected for sample collection, as it represents an environment with strong anthropogenic influences (e.g., biomass burning, fossil fuel, dust); collection at two sites allows comparison of aged/background properties against fresh emissions.

4.2 Location description, sample collection, and experimental methods

4.2.1 Location, meteorology, and airmasses sampled

The main goal of MILAGRO (Megacity Initiative: Local and Global Research Observations; http://www.eol.ucar.edu/projects/milagro/) was to study the evolution of the Mexico City (MC) plume as it aged and quantify its impact on local and regional scales. Mexico City was chosen owing to its size, pollution level, meteorology, and geography. The field campaign took place in March, which is characterized by dry, clear sky conditions with strong photochemistry observed (Jáuregui Ostos, 2000) and a low frequency of biomass burning events. By selecting this period, the evolution of the Mexico City plume could be studied without the complications from regional biomass burning events (Fast et al., 2007). To study the evolution of the Mexico City plume, measurements were performed at three ground sites and on board of aircrafts. The ground sites were located: *i*) at the Instituto Mexicano de Petróleo (T0, 19.488° N, 99.147° W)

located in the northern part of Mexico City, *ii*) at the Universidad Tecnológica de Tecámac (T1 19.703° N, 98.982° W) in Tecámac, Estado de México located at the northeast of the city, and *iii*) further northeast at Pachuca (T2 20.010° N, 98.909° W). The T0 site was chosen in the metropolitan area to represent fresh emissions while the T1 site was chosen outside of the city limits to study the effects of transport mixing and chemical aging on plume properties.

Field campaign measurements and large-scale analysis performed during the MILAGRO campaign defined three periods that characterized the overall meteorological conditions throughout the mission (Fast et al., 2007). The first period was prior to March 14th, where clear sky and persistently dry conditions (relative humidity (RH) < 50%). The second period (March 14th till the 23rd) was characterized by a sharp increase in RH (55 – 85%) and the development of late afternoon convection associated with the passage of a weak cold front on March 14th. The last and third period (after March 23rd) began with the passage of a strong cold front which led to an increase in RH, afternoon convection, and precipitation events that were much stronger than those observed during the second period. As a result, the frequency and intensity of fires within the vicinity of Mexico City during this period diminished (Fast et al., 2007), so that interaction between Mexico City and biomass burning plumes occurred mostly during the first 3 weeks of MILAGRO.

Tracer simulations using the WRF-chem model suggest that the most direct transport between the T0 and T1 sites occurred from March 9 -10 and March 18 – 20 (Fast et al., 2007). Further analysis of measurements and large scale analysis of the winds suggested favorable days of transport from T0 to T1 to have occurred from March 8 – 12 and from March 17 – 30 (Fast et al., 2007).

4.2.2 Particle collection and extraction

Ambient aerosols of aerodynamic diameter less than 2.5 μm (PM 2.5) were collected on quartz filters with Thermo Andersen Hi-Volume samplers. Three Hi-Volume

samplers were used for aerosol collection. One was located at T0, on the rooftop of a building approximately 20 meters above ground level; two samplers were located at ground level at the T1 site. Twenty-four and twelve hour integrated samples at T0 were collected from March 18 to 21, and, from March 22 to 30, respectively. At T1, twenty-four and twelve hour samples were obtained from March 9 to 19, and, from March 20 to 30. At T1, twelve hour integrated samples were collected during daytime (6:00 to 18:00, Local Standard Time, LST) and nighttime (18:00 to 6:00, LST); only daytime samples were collected at T0. Aerosol collection for the twenty-four hour samples started at 10:00 LST at both locations.

The Hi-Volume samplers draw 1.16 m^3 min^{-1} of air over a two stage impactor assembly to separately collect particles from 10 – 2.5 μm and below 2.5 μm diameter. The quartz filters used in our study were pretreated to remove organic residue and excess water vapor by baking them using the procedure of Sullivan and Weber (2006). After particle collection in the field, the filters were stored in a freezer to limit losses of volatile components until the WSOC is analyzed in the laboratory. Processing of the filter samples involve extraction of the WSOC fraction in water. For the extraction, the filters were placed in a Nalgene HDPE bottle with 125 mL of dionized (DI) water. Since a high concentration sample is needed to perform the surface tension measurements, two to three filters are extracted together at a time resulting in a sample with ~ 400 ppm of WSOC. Filters were grouped by integration periods (Tables 4. 1 and 4. 2). For 24 hr filters, two were extracted in 125 mL of DI water; while for 12 hr measurements, three were needed. After the addition of water, the bottle was placed on a sonicator and heated for 75 minutes; the solution was then allowed to cool down for 3 hours and filtered to remove quartz fibers and insoluble particles suspended in solution. The organic carbon concentration (C_{WSOC}) in all of the extracts was measured with a Total Organic Carbon (TOC) analyzer (Section 4.2.3.1).

Table 4. 1: Summary of T0 site filter grouping with extracted WSOC concentration (C_{WSOC}) and hygroscopicity parameter (κ).

Sample Name (sample period)	Collection Date (March 2006)	C_{WSOC} (ppm)	κ
MEX-T0-1 (24 hr)	18 - 19	287.5 ± 1.44	0.319 ± 0.055
MEX-T0-2 (24 hr)	20 - 21	310 ± 0	0.288 ± 0.073
MEX-T0-3 (12 hr day)	22 - 24	246.25 ± 0.43	0.271 ± 0.046
MEX-T0-4 (12 hr day)	25 - 27	715 ± 5.2	0.252 ± 0.019
MEX-T0-5 (12 hr day)	28 - 30	237.75 ± 3.08	0.290 ± 0.107

Although grouping the filters allowed us to have enough mass for CCN measurements, the extract was not concentrated enough for direct measurement of surface tension representative of the conditions at the point of activation (1000 – 10000 ppm). This is addressed by concentrating the samples using a rotavapor (Büchi R-124), which removes water from the samples by placing them in a rotating evaporation flask under vacuum submerged in a hot water bath. The water removed from the sample was collected at the top of the column on the condensation flask, while the concentrated WSOC solution remains in the evaporation flask. A carbon balance calculation shows that most of the WSOC remain in the concentrated sample (84 – 98%).

4.2.3 Chemical composition

4.2.3.1 TOC analyzer

WSOC concentration for all samples was measured with a portable TOC analyzer (Sievers 900). The TOC analyzer determines the organic carbon concentration in the sample by subtracting the inorganic carbon concentration from the total carbon concentration. Inorganic and total carbon concentration is determined by measuring the

Table 4. 2: Summary of T1 site filter grouping with extracted WSOC concentration (C_{WSOC}), inferred average organic molar mass (M_{org}), and hygroscopicity parameter (κ).

Sample Name (sample period)	Collection Date (March 2006)	C_{WSOC} (ppm)	M_{org} (g mol^{-1})	κ
MEX-T1-1 (24 hr)	9, 11	392.5 ± 1.44	158.31 ± 56.41	0.339 ± 0.094
MEX-T1-2 (24 hr)	13, 16	317.5 ± 1.44	141.81 ± 11.73	0.316 ± 0.052
MEX-T1-3 (24 hr)	17 - 18	115.5 ± 0.95	161.92 ± 11.79	0.329 ± 0.024
MEX-T1-4 (24 hr)	15 - 16	217 ± 0.63	222.71 ± 15.67	0.297 ± 0.029
MEX-T1-5 (24 hr)	17 - 18	110.5 ± 0.80	527.32 ± 146.85	0.311 ± 0.025
MEX-T1-6 (24 hr)	19	117.5 ± 2.5	61.93 ± 6.18	0.366 ± 0.017
MEX-T1-7 (12 hr night)	20 - 22	114.5 ± 0.72	N/A[a]	0.220 ± 0.017
MEX-T1-8 (12 hr night)	23 - 25	76.75 ± 3.48	431.35 ± 210.28	0.221 ± 0.023
MEX-T1-9 (12 hr night)	26 -28	140.75 ± 1.42	344.64 ± 117.61	0.275 ± 0.030
MEX-T1-10 (12 hr day)	21 - 23	382.5 ± 1.44	380.82 ± 97.00	0.214 ± 0.013
MEX-T1-11 (12 hr day)	24 -26	352.5 ± 1.44	221.97 ± 8.08	0.263 ± 0.010
MEX-T1-12 (12 hr day)	27 -29	362.5 ± 1.44	267.89 ± 13.94	0.256 ± 0.006

[a]N/A: Not available.

amount of carbon dioxide formed during the acidification (for inorganic carbon) and oxidation (for total carbon) of the sample streams. Prior to each measurement, samples were diluted by a factor of 250 or 1000 to ensure the WSOC concentration would be within the dynamic range of the instrument (0.20 ppb to 10 ppm). Measurement of WSOC was repeated three times for each sample.

4.2.3.2 Ion chromatography

Ion chromatography (IC) was used to measure the concentration of the major ions in solution. The IC used in this study (Dionex Model DX500) has two channels, allowing for the measurement of anions and cations. An assessment of the instrument can be found in Butler (2000) and Cobb (2006). Anions measured were acetate ($C_2H_3O_2^-$), chloride (Cl^-), formate ($HCOO^-$), nitrate (NO_3^-), nitrite (NO_2^-), oxalate ($C_2O_4^{2-}$), and sulfate (SO_4^{2-}). The cations measured were ammonium (NH_4^+), calcium (Ca^{2+}), potassium (K^+), and sodium (Na^+). The samples were diluted by a factor of 50 to be within the dynamic range of the standards used for the IC calibration. The ion concentrations obtained from the IC measurement were then used as input for the ISORROPIA-II thermodynamic equilibrium code (Fountoukis and Nenes, 2007; http://nenes.eas.gatech.edu/ISORROPIA) to predict the mixture of inorganic salts dissolved in the samples (used in the application of KTA and κ-Köhler theory).

4.2.4 Surface Tension

The surface tension of each sample was measured with a pendant drop tensiometer (CAM 200 Optical Contact Angle Meter, by KSV Inc.). A mechanically-controlled micro-syringe was used to produce a droplet of the solution at the tip of a stainless steel needle; a picture of it is then taken at the point where the drop is ready to fall from the tip. The sample surface tension, σ, is then determined by fitting the droplet shape to the Young-Laplace equation (Spelt and Li, 1996). Approximately 10 pictures per droplet were taken to obtain an average and standard deviation for surface tension.

Surface tension depression depends on the surfactant concentration (expressed by C_{WSOC}, the concentration of dissolved carbon), and is measured for each extract concentration on the rotavapor, and at 3:1, 2:1, 1:1, 1:3, and 1:∞ dilutions with ultrafine pure water (Fisher). σ is then expressed against C_{WSOC} for each sample and fit to the Szyskowski-Langmuir equation (Langmuir, 1917),

$$\sigma = \sigma_w - \alpha T \ln\left(1 + \beta C_{WSOC}\right) \tag{4.1}$$

where σ_w is the surface tension of water at temperature T of measurement, and the parameters α and β are obtained by least squares minimization of Equation (4.1) to the data.

4.2.5 CCN activity and growth kinetic measurements

The laboratory setup employed to characterize the CCN activity of the dissolved material and the impact of organic material on the droplet activation kinetics is described in Padró et al. (2007) and Asa-Awuku et al. (2008). The system consists of an aerosol generation, size classification, and CCN measurement section. Polydisperse aerosols are generated by atomizing the filter extracts. The droplets are subsequently dried by flowing them through multiple diffusion driers and charged with a Kr-85 bipolar charger (TSI Model 3077). Then, a Differential Mobility Analyzer (DMA, TSI Model 3081) is used for size mobility selection of the dry particles. The classified aerosol flow is split into two streams, one sent to a Condensation Particle Counter (CPC, TSI Model 3022A) to measure their concentration (CN) and the other to a Continuous Flow Streamwise Thermal Gradient CCN Chamber (CFSTGC, Lance et al., 2006;Roberts and Nenes, 2005) to measure the number of which act as CCN. The activated droplets in the CCN are counted and sized at the exit with an Optical Particle Counter (OPC, 660 nm) with a dynamic range of 0.75 to 10 μm with 0.5 μm bin resolution.

In this work, CCN activation data is obtained using Scanning Mobility CCN Analysis or SMCA (Nenes and Medina, in review[5]); instead of "stepping" through the DMA voltage to obtain CCN concentrations at discrete values of mobility diameter, the DMA voltage is continuously changed over time, so that the dynamic mobility range of the DMA is "scanned" over 2 min. During a size scan, the supersaturation in the

[5]Nenes A. and Medina J., in review. Scanning Mobility CCN Analysis – A method for fast measurements of size resolved CCN activity and growth kinetics, Aerosol Science and Technology.

CFSTGC is maintained constant. The timeseries of activated droplet size, CCN, and CN counts are then inverted to obtain size-resolved CCN activity and activation kinetics. In this study, the aerosol size was ranged between 7 and 260 nm, and 0.2% to 1.2% supersaturation (nominal). CCN activity of the aerosol is characterized by determining the minimum dry diameter, d_{p50}, of particles that activate into cloud droplets at each supersaturation (i.e., those particles with a critical supersaturation equal to the instrument supersaturation). d_{p50} is found by expressing the ratio of CCN to CN concentration with respect to dry particle diameter and determining the dry diameter for which the $\frac{CCN}{CN} = 0.5$. To facilitate with the analysis, the activation data is fit to a sigmoid curve which neglects the impact of multiply-charged particles. Once the d_{p50} at each supersaturation is known, a "CCN spectrum" (s_c versus d_{p50}) can be obtained and used to characterize the average properties of WSOC using Köhler Theory Analysis or the hygroscopicity parameter using κ-Köhler Theory.

The CCN instrument used in this study was calibrated with $(NH_4)_2SO_4$ using a procedure similar to that of Sorooshian et al. (2008), Asa-Awuku et al., (2009), and Rose et al., (2008). The calibration procedure consisted of generating particles by atomizing a $(NH_4)_2SO_4$ solution; the polydisperse aerosol was then dried, charged, and size selected with a DMA operated in scanning voltage mode. Once d_{p50} is determined, the effective supersaturation in the column was determined using traditional Köhler theory by assuming $(NH_4)_2SO_4$ has a van't Hoff factor of 2.5 (Brechtel and Kreidenweis, 2000; Rose et al., 2008) and the surface tension of water (calculated at the average column temperature). The standard deviation in the supersaturation from Köhler theory was determined from the standard deviation observed in the d_{p50}. This procedure is repeated for multiple values of ΔT and calibration curves of instrument supersaturation versus ΔT are generated. The resulting calibration curves are shown in Figure 4. 1.

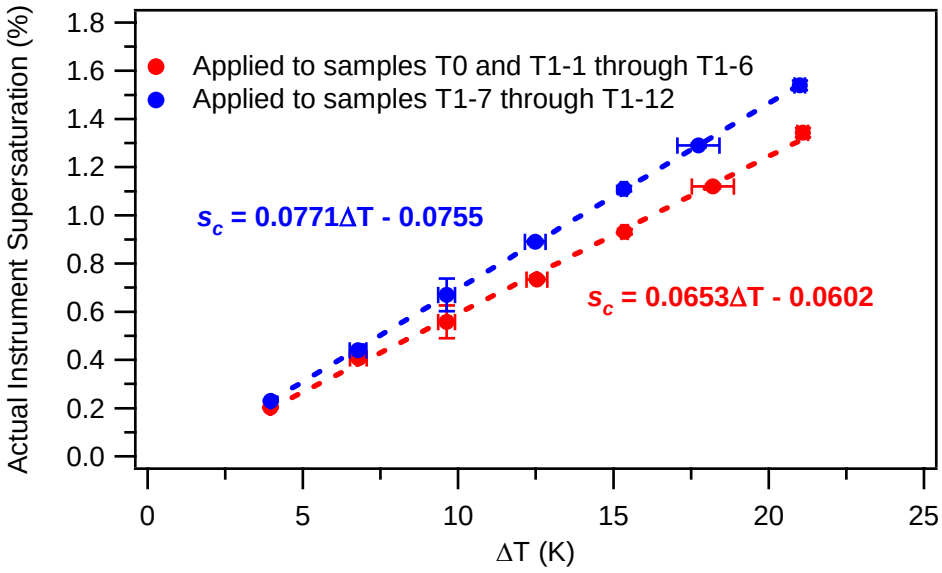

Figure 4. 1: Instrument calibration curves used. Critical supersaturation versus delta T. Calibration was performed at a flowrate of 500 cm^3 min^{-1} and at ambient pressure using $(NH_4)_2SO_4$ aerosol.

CCN activation kinetics and changes thereof from the presence of organics can also be determined from the CCN measurements; this is done by monitoring the droplet size measured at the OPC for particles of critical supersaturation equal to the instrument supersaturation (i.e., dry size equal to d_{p50}). For particles composed of pure deliquescent electrolytes (e.g., $(NH_4)_2SO_4$ calibration aerosol), CCN activation kinetics is rapid (corresponding to an uptake coefficient of ~ 0.1) and the wet droplet size, D_w, for d_{p50} particles is used as a reference (for the given conditions of pressure, ΔT, and flow). Comparing D_w against the corresponding wet diameter (i.e. same critical supersaturation) of activated particles generated from the extracted filters can reveal whether organic compounds slow activation kinetics. When combined with a computational fluid dynamics model of the CCN instrument (Lance et al., 2006), changes in growth kinetics can be parameterized in terms of an uptake coefficient (Asa-Awuku et al., 2009;Engelhart et al., 2008;Ruehl et al., 2008;Ruehl et al., in press).

4.2.6 Effects of electrolyte addition on surface tension and CCN activity

The presence of inorganic solute at high concentrations may force organics to the surface, creating a surfactant rich layer; this "salting out" effect may then decrease the surface tension of the droplet and notably affect surface tension (Asa-Awuku et al., 2008;Kiss et al., 2005). To explore this potential, prescribed amount of $(NH_4)_2SO_4$, m_{AS}, as multiples of the existing organic mass, is added to the sample:

$$m_{AS} = f * m_{org} \tag{4.2}$$

where f is the "mass multiplication factor" (ranging between 1 and 9), m_{org} is the mass of dissolved organic matter in the sample, given by $m_{org} = \left[\frac{OM}{OC}\right] C_{WSOC} V_{sample}$, V_{sample} is the sample volume, and OM and OC is the concentration of organic matter and organic carbon, respectively. The $\frac{OM}{OC}$ was assumed 1.5 and 2.3 for T0 and T1 (DeCarlo et al., 2008), respectively.

4.3 Experimental analysis

4.3.1 Köhler theory analysis

Köhler Theory Analysis is a method used to infer average thermodynamic properties (e.g., molar volume) of the water soluble organic fraction of the aerosol. The method is based on combining Köhler theory with size-resolved CCN, chemical composition, and surface tension measurements (Padró et al., 2007). When combined with SMCA (Nenes and Medina, in review[1]), KTA allows the characterization of the CCN relevant properties of ambient WSOC from small amount of sample typically collected on filters. KTA has been evaluated for laboratory generated particles composed of inorganic-organic mixtures of known composition (Padró et al., 2007), biomass burning WSOC (Asa-Awuku et al., 2008), secondary organic aerosol (Asa-Awuku et al.,

2009;Asa-Awuku et al., 2007;Engelhart et al., 2008) and primary marine organic matter (Moore et al., 2008). According to KTA, the average molar volume, $\frac{M_{org}}{\rho_{org}}$, of the soluble organic fraction of an aerosol is given by,

$$\frac{M_{org}}{\rho_{org}} = \frac{\varepsilon_{org}\upsilon_{org}}{\frac{256}{27}\left(\frac{M_w}{\rho_w}\right)^2\left(\frac{1}{RT}\right)^3\sigma^3\varpi^{-2} - \sum_{inorg}\left(\frac{\rho}{M}\right)_{inorg}\varepsilon_{inorg}\upsilon_{inorg}} \tag{4.3}$$

where M_{org}, ε_{org}, υ_{org}, ρ_{org} is the molar mass, dry volume fraction, effective van't Hoff factor and density of the organic fraction, respectively; M_{inorg}, ρ_{inorg}, ε_{inorg}, and υ_{inorg} are the molecular weight, density, volume fraction, and effective van't Hoff factor of the inorganic compounds (Table 4. 3), respectively. M_w and ρ_w is the molar mass and density of water, respectively, R is the ideal gas constant, T is the temperature, and σ is the surface tension of the solution at the point of activation. The Pitzer activity coefficient model (Clegg and Brimblecombe, 1988;Pitzer and Mayorga, 1973) is used to calculate the υ_{inorg} for all inorganic salts present in the samples, at the appropriate concentration corresponding to the critical wet diameter of the CCN (Padró et al., 2007). ω is the "Fitted CCN Activity" (FCA) parameter (Padró et al., 2007) obtained by expressing CCN activity measurements by the power-law expression $s_c = \omega d_{50}^{-3/2}$. ε is related to the mass fraction of the compound of interest (*j*, organic or inorganic), x_i (Tables 4.4 and 4.5), as:

$$\varepsilon_i = \frac{x_i/\rho_i}{\sum_j (x/\rho)_j} \tag{4.4}$$

The ionic composition of each sample (obtained from the IC) is converted into a mixture

Table 4. 3: Properties of inorganic salts potentially present in the extracted filters.

Compound Name	Chemical Formula	M_{inorg} (g mol^{-1})	ρ_{inorg}[a] (g cm^{-3})	κ_{inorg}
Ammonium Bisulfate	NH_4HSO_4	115.11	1.79	0.53
Ammonium Chloride	NH_4Cl	53.49	2.165	1.46
Ammonium Nitrate	NH_4NO_3	80.04	1.5	0.64
Ammonium Sulfate	$(NH_4)_2SO_4$	132.14	1.77[b]	0.60
Calcium Carbonate	$CaCO_3$	100.09	2.71	~0
Calcium Chloride	$CaCl_2$	110.98	2.15	0.70
Calcium Nitrate	$Ca(NO_3)_2$	164	1.82	0.40
Calcium Sulfate	$CaSO_4$	136.14	2.32	~0
Letovicite	$(NH_4)_3H(SO_4)_2$	247.25	1.83	0.60
Potassium Bisulfate	$KHSO_4$	136.17	2.24	0.59
Potassium Carbonate	K_2CO_3	138.21	2.29	~0
Potassium Sulfate	K_2SO_4	174.27	2.66	0.69
Sodium Bisulfate	$NaHSO_4$	120.06	2.742	0.82
Sodium Carbonate	Na_2CO_3	105.99	2.5	~0
Sodium Sulfate	Na_2SO_4	142.04	2.68	0.85
Sulfuric Acid	H_2SO_4	98.08	1.84	0.81

[a]Unless noted values are from the Material Safety Data Sheet.

[b]Svenningsson et al. (2006).

[c]Cruz and Pandis (1997).

Table 4. 4: Organic and inorganic mass fraction for Mexico City T0 site samples. Salts shown for each sample were predicted by using ISORROPIA II (Fountoukis and Nenes, 2007). Uncertainties in all mass fractions are smaller than 0.3%.

Sample	x_{org}	$x_{Na_2SO_4}$	x_{NaHSO_4}	$x_{(NH_4)_2SO_4}$	$x_{NH_4HSO_4}$	$x_{(NH_4)_3H(SO_4)_2}$	x_{CaSO_4}	$x_{K_2SO_4}$	x_{KHSO_4}	$x_{H_2SO_4}$
MEX-T0-1	0.22	0	0.21	0	0.29	0	0.11	0	0.02	0.16
MEX-T0-2	0.27	0	0.19	0	0.30	0	0.10	0	0.02	0.12
MEX-T0-3	0.25	0.07	0.13	0	0.41	0	0.11	0.03	0	0
MEX-T0-4	0.55	0.11	0	0.13	0	0.12	0.08	0.02	0	0
MEX-T0-5	0.35	0.17	0	0.36	0	0	0.10	0.02	0	0

Table 4. 5: Organic and inorganic mass fractions for Mexico City T1 site samples. Salts shown for each sample were predicted by using ISORROPIA II (Fountoukis and Nenes, 2007). Uncertainties in all mass fractions are smaller than 0.3%.

Sample	x_{org}	$x_{(NH_4)_2SO_4}$	$x_{NH_4NO_3}$	x_{NH_4Cl}	x_{CaSO_4}	$x_{Ca_2(NO_3)_2}$	x_{CaCl_2}	$x_{Na_2CO_3}$	x_{CaCO_3}	$x_{K_2CO_3}$	$x_{Na_2SO_4}$	$x_{K_2SO_4}$
MEX-T1-1	0.72	0.08	0	0	0.10	0	0	0.02	0	0	0.06	0.03
MEX-T1-2	0.67	0.12	0	0	0.06	0	0	0.06	0.08	0.02	0	0
MEX-T1-3	0.49	0.17	0	0	0.02	0	0	0.07	0.21	0.04	0	0
MEX-T1-4	0.57	0.12	0.03	0.02	0	0	0	0.07	0.16	0.03	0	0
MEX-T1-5	0.39	0.21	0.01	0	0	0.06	0	0.12	0.17	0.04	0	0
MEX-T1-6	0.44	0.12	0	0	0.14	0	0	0.17	0.09	0.06	0	0
MEX-T1-7	0.50	0.14	0.05	0	0	0.01	0	0.16	0.11	0.03	0	0
MEX-T1-8	0.52	0.09	0.02	0	0	0.02	0	0.20	0.11	0.02	0	0
MEX-T1-9	0.59	0.09	0.06	0.01	0	0	0.03	0.17	0.04	0.02	0	0
MEX-T1-10	0.70	0.09	0.02	0	0	0.01	0	0.10	0.07	0.02	0	0
MEX-T1-11	0.68	0.06	0.04	0.01	0	0	0.003	0.14	0.07	0.01	0	0
MEX-T1-12	0.74	0.06	0.05	0	0	0	0.01	0.09	0.04	0.01	0	0

of salts by applying the ISORROPIA-II model as described in Section 4.2.3.2. For the *OM* density, two different values were used to reflect the compositional change between the two sites: *i*) 1.6 g cm^{-3} (Dinar et al., 2006a) at MC, and, *ii*) 1.5 g cm^{-3} at the T1 site (Cross et al., 2008).

The uncertainty in the inferred organic molar mass, ΔM_{org}, can be estimated from the total uncertainty from each parameter as follows:

$$\Delta M_{org} = \sqrt{\sum_{forallx} \left(\Phi_x \Delta x\right)^2} \tag{4.5}$$

where Φ_z is the sensitivity of the organic molar mass to each of the parameters z (that affect M_{org}, σ, ω, υ_{org}, υ_{inorg}, ε_{org}, and ε_{inorg}), $\Phi_z = \frac{\partial M_{org}}{\partial z}$ and Δz is the uncertainty on z. The formulas used to compute the sensitivity of the organic molar mass to z are shown in Table 4. 6.

4.3.2 κ-Köhler theory

κ-Köhler theory was developed by Petters and Kreidenweis (2007) to quantitatively represent aerosol hygroscopic water uptake and CCN activity through the hygroscopicity parameter, *κ*, without the usage of individual component density, molar mass, or water activity coefficients. *κ* values range from 0.01 to 2, with hygroscopic inorganic species such as $(NH_4)_2SO_4$ and NaCl having *κ* ranging from 0.5 to 2 and organic species and mixtures ranging from 0.01 to 0.5 (Petters and Kreidenweis, 2007). For $\kappa > 0.01$, the hygroscopicity parameter can be obtained from s_c and d_{p50} pairs as

$$\kappa = \frac{4A^3}{27 d_{p50}^3 \ln^2 s_c} \tag{4.6}$$

Table 4. 6: Formulas used for computing the sensitivity of molar volume to σ, ω, υ_{org}, υ_{inorg}, ε_{org}, and ε_{inorg}.

Parameter, x	Sensitivity, $\Phi_x = \frac{\partial M_{org}}{\partial x}$
σ	$\Phi_\sigma = \frac{768}{27}\left(\frac{M_w}{\rho_w}\right)^2\left(\frac{1}{RT}\right)^3\frac{\sigma^2 M_{org}^2}{\varepsilon_{org}\upsilon_{org}\rho_{org}\omega^2}$
ω	$\Phi_\omega = \frac{512}{27}\left(\frac{M_w}{\rho_w}\right)^2\left(\frac{1}{RT}\right)^3\frac{\sigma^3 M_{org}^2}{\varepsilon_{org}\upsilon_{org}\rho_{org}\omega^3}$
υ_{org}	$\Phi_{\upsilon_{org}} = \frac{256}{27}\left(\frac{M_w}{\rho_w}\right)^2\left(\frac{1}{RT}\right)^3\frac{\sigma^3 M_{org}^2}{\varepsilon_{org}\rho_{org}\upsilon_{org}^2\omega^2} + \frac{M_{org}^2}{\varepsilon_{org}\rho_{org}\upsilon_{org}^2}\left(\sum_{inorg}\left(\frac{\rho_{inorg}}{M_{inorg}}\right)\varepsilon_{inorg}\upsilon_{inorg}\right)$
υ_{inorg} [a]	$\Phi_{\upsilon_{inorg}} = \left(\frac{\rho_{inorg}}{M_{inorg}}\right)\frac{\varepsilon_{inorg}M_{org}^2}{\varepsilon_{org}\rho_{org}\upsilon_{org}}$
ε_{org}	$\Phi_{\varepsilon_{org}} = \frac{256}{27}\left(\frac{M_w}{\rho_w}\right)^2\left(\frac{1}{RT}\right)^3\frac{\sigma^3 M_{org}^2}{\upsilon_{org}\rho_{org}\varepsilon_{org}^2\omega^2} + \frac{M_{org}^2}{\upsilon_{org}\rho_{org}\varepsilon_{org}^2}\left(\sum_{inorg}\left(\frac{\rho_{inorg}}{M_{inorg}}\right)\varepsilon_{inorg}\upsilon_{inorg}\right)$
ε_{inorg} [a]	$\Phi_{\varepsilon_{inorg}} = \left(\frac{\rho_{inorg}}{M_{inorg}}\right)\frac{\upsilon_{inorg}M_{org}^2}{\varepsilon_{org}\upsilon_{org}\rho_{org}}$

[a]Inorganics present at T0 are: Na_2SO_4, $NaHSO_4$, $(NH_4)_2SO_4$, NH_4HSO_4, $(NH_4)_3H(SO_4)_2$, $CaSO_4$, K_2SO_4, $KHSO_4$, $H2SO_4$; Inorganics present at T1 are: NaCl, $NaNO_3$, Na_2SO_4, $CaSO_4$, K_2SO_4, Na_2CO_3, K_2CO_3, $CaCO_3$.

where $A = \frac{4M_w\sigma_w}{RT\rho_w}$ and s_c is the instrument supersaturation. The reported hygroscopicity parameters have been evaluated at a surface tension of water; however the surface tension can be different especially if strong surfactants (e.g., HUmic-LIke Substance, HULIS) are present (Dinar et al., 2007;Kiss et al., 2005), which can introduce notable uncertainty in calculation of the parameter, if it is based solely on compositional data.

4.4 Results and discussion

4.4.1 Surfactant characteristics

Tables 4. 7 and 4. 8 present the Szyskowski-Langmuir adsorption constants α and β (Equation (4.1)), the maximum C_{WSOC} of the extracted and concentrated sample, and the concentration of SO_4^{2-} ions in solution (C_{SO4}). The surface tension depression is also presented at C_{WSOC} = 1000 ppm for comparison purposes. Even though organics at both locations depress σ, stronger depression is seen at T0 (24 hr samples, Figure 4. 2a; 12 hr day samples, Figure 4. 2b) consistent with having a higher hydrophobic fraction (lower O/C ratio) very near emission sources (DeCarlo et al., 2008;Kleinman et al., 2008). Furthermore, the observed surface tension depression at the T0 site (for both sample periods) could be enhanced by the higher salt concentration present at this site (Tables 4. 4 and 4. 5).

Differences were observed in surfactant characteristics between the day and night samples at T1 (Figure 4. 2c), with nightime samples being slightly more surface active than the day samples (Figure 4. 2c). The higher σ depression observed for the night samples could originate from local emissions, which tend to be hydrophobic, or, ageing of organics in the aqueous phase to form humic-like substances (Hoffer et al., 2004). This is consistent with a source apportionment study performed for the fine organic aerosol for T0 and T1 sites, which found the T1 site to be influenced by local sources rather than from the Mexico City outflow (Stone et al., 2008). Addition of more electrolytes further depressed the surface tension of activated CCN (compared to CCN from the original sample); consistent with the "salting out" effect (Tables 4.6 and 4.7; Kiss et al., 2005).

4.4.2 CCN activity and hygroscopicity

The CCN activity (embodied in the s_c versus d_{p50} relationship) of aerosol generated from some of the extracted samples is presented in Figure 4. 3. The curves

Table 4. 7: Szyskowski-Langmuir constants (298 K) for computing the surface tension measurements of aqueous Mexico City T0 site samples and mixtures with $(NH_4)_2SO_4$. The measured surface tension depression relative to water at T = 34 °C at a C_{WSOC} = 1000 ppm and the SO_4^{2-} concentration are also shown.

Sample Name	Mixture with $(NH_4)_2SO_4$, f	C_{SO4} (ppm)	$\alpha \times 10^1$ (mN m^{-1}K^{-1})	$\beta \times 10^5$ (ppm^{-1})	Surface Tension Depression (%)
MEX-T0-1	0	1320	8.22	6.35	21.93
	1	1786	2.29	24.7	21.91
	9	5159	2.64	22.9	23.59
MEX-T0-2	0	1066	6.39	6.68	17.91
	1	1604	3.99	11.8	19.29
	9	4527	3.38	14.8	20.22
MEX-T0-3	0	893	5.09	5.17	11.12
	1	1257	6.26	5.83	15.37
	9	4121	12.20	3.77	19.57
MEX-T0-4	0	654	5.18	4.97	10.89
	1	1687	2.93	8.27	10.09
	9	100018	6.28	4.90	13.02
MEX-T0-5	0	342	5.84	5.43	13.38
	1	691	4.95	5.70	11.89
	9	3453	2.98	11.6	14.18

shown are grouped by sites and integration period (Figures 4. 3a and 4. 3b) as well as the time of day for the T1 samples (Figure 4. 3c). As a first approximation, the extracts were found to have similar CCN activity regardless of the site (Figures 4. 3a and 4. 3b). Compared to T1 samples, T0 samples tend to have somewhat higher CCN activity (i.e., the s_c-d_{p50} curve is closer to that of $(NH_4)_2SO_4$) due to the presence of stronger surfactants and the high salt fraction in the latter samples (Tables 4. 4 and 4. 5). The CCN activity of 12 hr (day and night) samples collected at T1 (Figure 4. 3c) exhibit little variability. Electrolytes were added to the extracted samples to study the surfactant characteristics of the aerosol independently of direct surface tension measurements. The increase in CCN activity observed for the salted samples (Figure 4. 4) is consistent with the increase in soluble material (from the salts) and the depression in surface tension from the organics present in the aerosol which facilitates CCN formation as defined by Köhler

Table 4. 8: Szyskowski-Langmuir constants (298 K) for computing the surface tension measurements of aqueous Mexico City T0 site samples and mixtures with $(NH_4)_2SO_4$. The measured surface tension depression relative to water at T = 34 °C and C_{WSOC} = 1000 ppm and the SO_4^{2-} concentration are also shown.

Sample Name	Mixture with $(NH_4)_2SO_4$, f	C_{AS} (ppm)	$\alpha \times 10^1$ (mN m^{-1}K^{-1})	$\beta \times 10^5$ (ppm^{-1})	Surface Tension Depression (%)
MEX-T1-1	0	235	3.33	6.92	9.66
	1	802	2.60	8.83	9.54
	9	5367	3.34	8.26	11.49
MEX-T1-2	0	140	4.74	6.06	12.09
	1	605	1.50	16.9	10.15
	9	4298	1.51	8.99	5.63
MEX-T1-3	0	74	2.32	9.34	8.98
	1	249	1.14	19.7	8.89
	9	1586	6.00	4.10	10.45
MEX-T1-4	0	76	1.47	18.2	10.65
	1	396	1.95	9.92	7.99
	9	2911	9.24	4.39	17.21
MEX-T1-5	0	101	1.44	19.5	11.12
	1	261	1.29	13.8	7.23
	9	1541	1.28	19.7	9.98
MEX-T1-6	0	116	0.037	2400	5.16
	1	290	3.60	5.25	7.98
	9	1657	0.44	50.9	7.85
MEX-T1-7	0	54	3.39	3.40	4.91
	1	221	3.93	3.38	5.66
	9	1552	5.43	5.23	12.00
MEX-T1-8	0	22	5.62	3.89	9.30
	1	134	5.80	5.18	12.70
	9	1027	3.61	8.46	12.71
MEX-T1-9	0	35	4.37	4.22	7.83
	1	240	2.09	8.60	7.47
	9	1877	3.23	7.04	9.52
MEX-T1-10	0	78	14.9	1.85	11.84
	1	634	5.45	5.04	11.62
	9	5083	9.09	2.66	10.34
MEX-T1-11	0	56	3.58	5.66	8.54
	1	583	3.58	7.02	10.53
	9	4799	2.58	8.78	9.41
MEX-T1-12	0	48	4.46	4.03	7.64
	1	575	3.43	4.73	6.87
	9	4791	3.51	4.68	6.96

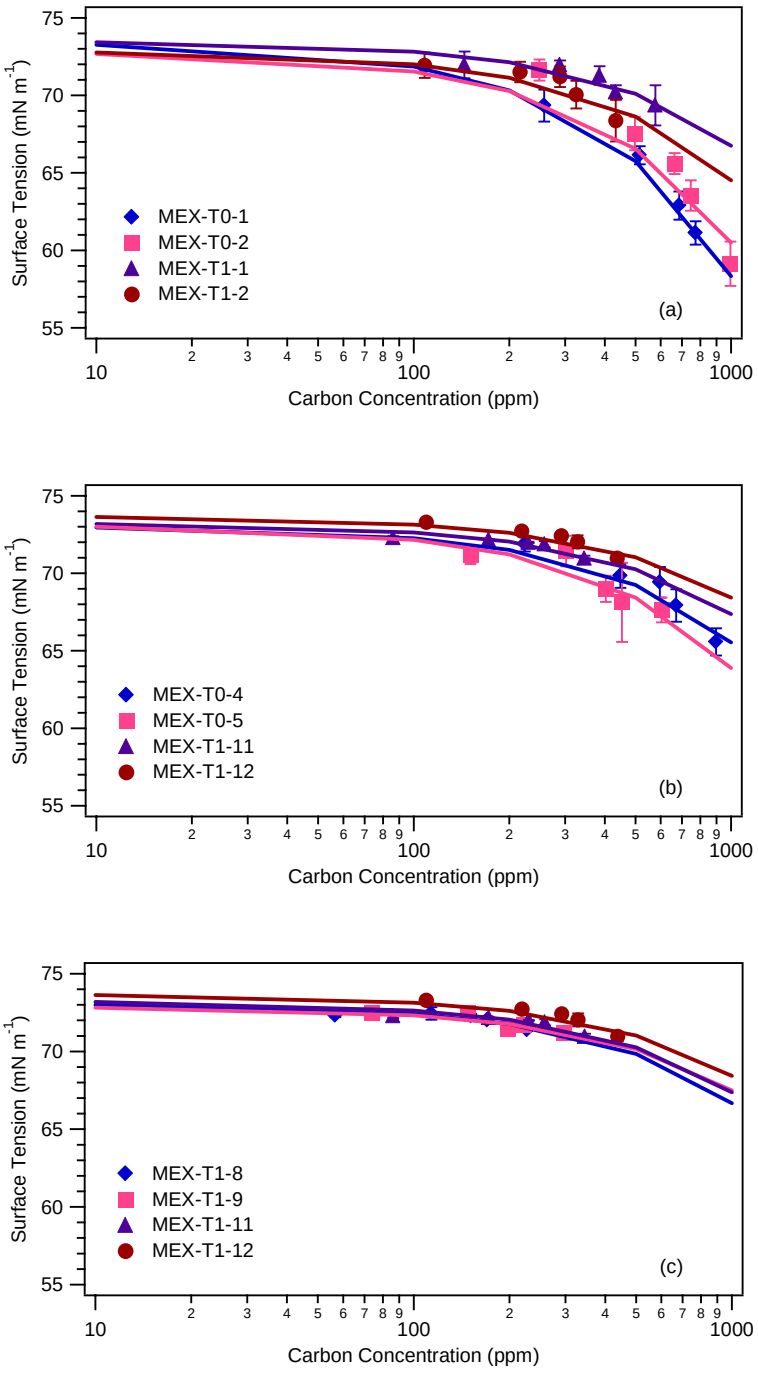

Figure 4. 2: Surface tension as a function of concentration for (a) 24 hour integrated samples: MEX-T0-1 (blue diamond), MEX-T0-2 (pink square), MEX-T1-1 (purple triangle), and MEX-T1-2 (maroon circle), (b) 12 hr integration day samples: MEX-T0-4 (blue diamond), MEX-T0-5 (pink square), MEX-T1-11 (purple triangle), and MEX-T1-12 (maroon circle), (c) 12 hr integration night samples: MEX-T1-8 (blue diamond), MEX-T1-9 (pink square), and 12 hr integration day samples: MEX-T1-11 (purple triangle), and MEX-T1-12 (maroon circle). The solid lines correspond to the Szyskowski-Langmuir fit for each sample.

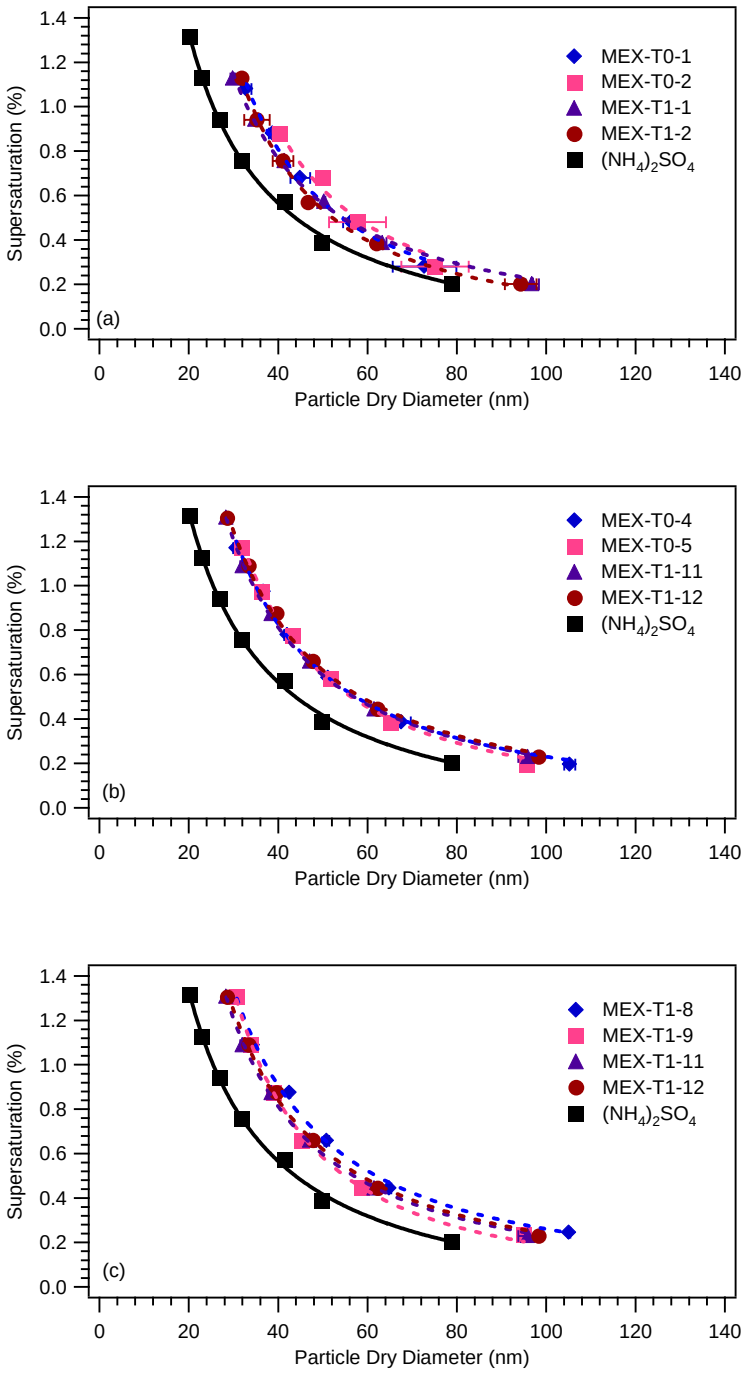

Figure 4. 3: CCN activity for (a) 24 hour integrated samples: MEX-T0-1 (blue diamond), MEX-T0-2 (pink square), MEX-T1-1 (purple triangle), and MEX-T1-2 (maroon circle), (b) 12 hr integration day samples: MEX-T0-3 (blue diamond), MEX-T0-4 (pink square), MEX-T1-11 (purple triangle), and MEX-T1-12 (maroon circle), (c) 12 hr integration night samples: MEX-T1-8 (blue diamond), MEX-T1-9 (pink square), and 12 hr integration day samples: MEX-T1-11 (purple triangle), and MEX-T1-12 (maroon circle) with their corresponding power fit) assuming complete solubility. $(NH_4)_2SO_4$ (black square) is also shown for comparison.

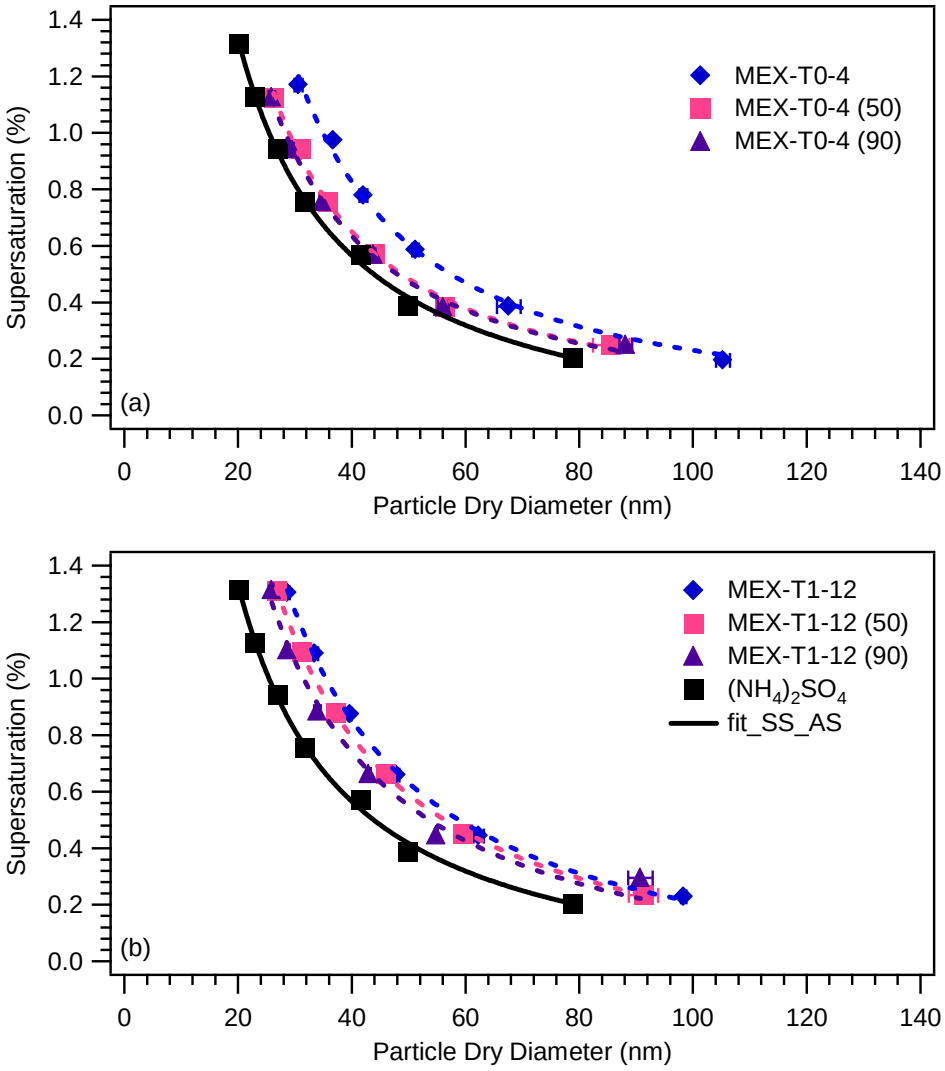

Figure 4. 4: Activation curves for: (a) pure MEX-T0-4 (blue diamond), 50% (pink square), and 90% (purple triangle) $(NH_4)_2SO_4$ mixtures, (b) pure MEX-T1-12 (blue diamond), 50% (pink square), and 90% (purple triangle) $(NH_4)_2SO_4$ mixtures. Pure $(NH_4)_2SO_4$ (black square) is also shown for comparison.

theory.

κ was calculated from application of Equation (4.6) to the s_c and d_{p50} pairs (Tables 4. 1 and 4. 2), κ ranged for the T0 site samples between 0.29 – 0.32 and 0.25 – 0.39 for the 24 and 12 hr samples, respectively; κ for the T1 site ranged from 0.30 – 0.37, 0.21 – 0.26, and 0.22 – 0.28 for the 24, 12 hr day, and 12 hr night samples,

respectively. κ values obtained at the T1 site are consistent with in situ measurements performed at that site (Lance, 2007) and is an indication that filter processing does not significantly affect the hygroscopic properties of the filter-extracted WSOC. No significant correlation was found between κ and the organic mass fraction (Figure 4. 5; $R^2 = 0.01$) as well as the sampling site (overall average of 0.28 ± 0.06). The κ values reported in this study are within the range reported in previous studies and correspond to values typical of soluble salts and very hygroscopic organics (Carrico et al., 2008;Koehler et al., 2009;Petters and Kreidenweis, 2007;Shantz et al., 2008). The invariance of κ with respect to organic fraction although counter intuitive, provides insight on the nature of the WSOC. First, the water soluble components extracted from both sites have about the same hygroscopicity, meaning that ageing processes may not

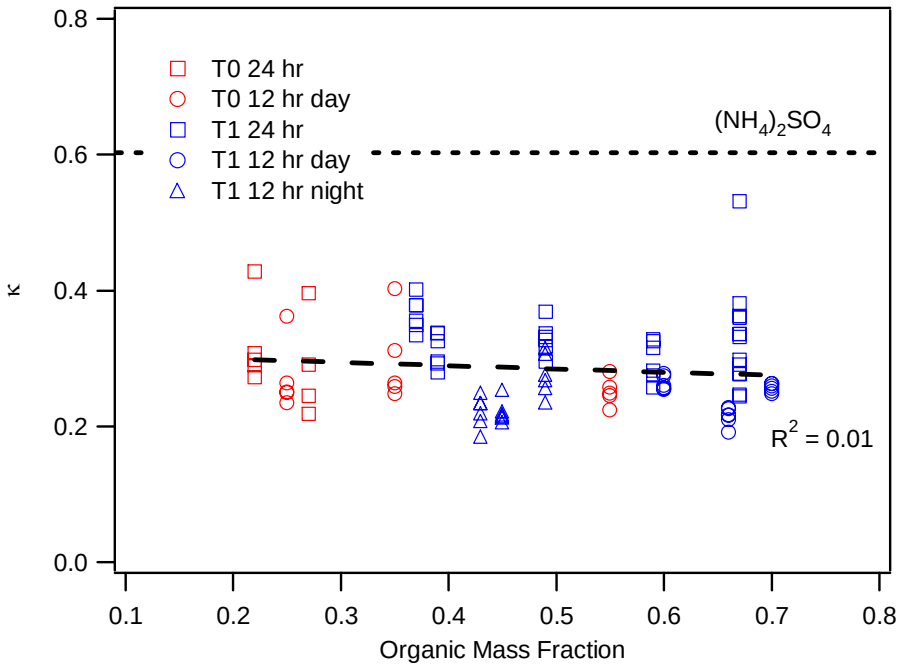

Figure 4. 5: Hygroscopicity parameter versus organic mass fraction: T0 24 hr (red open square), T0 12 hr day (red open circle), T1 24 hr (blue open square), T1 12 hr day (blue open circle), T1 12 hr night (blue open triangle). The black dotted line represents the hygroscopicity parameter for $(NH_4)_2SO_4$.

affect the nature of the hygroscopic fraction, but only their relative amount in the aerosol. Second, the water-soluble organic and inorganic fractions exhibit about the same level of hygroscopicity; given that inorganic salts are by nature more hygroscopic than organics (due to their dissociation and relatively low molar volumes), this invariance may be a combined effect of solute and surface tension depression. This may also explain why some CCN closure studies may seem to be insensitive to assumptions of chemical composition.

A "κ closure" analysis was performed to compare predicted (κ_{mix}) versus measured (κ_{CCN}) hygroscopicity parameter values. κ_{CCN} was determined from the s_c and d_{p50} pairs as detailed in Section 4.3.2. κ is sensitive to the assumption of surface tension used (Equation (4.6)), and this sensitivity is evaluated by calculating κ_{CCN} assuming: *i*) the surface tension of water and *ii*) 15% surface tension from the contribution of organics (an expected value, based on Figures 4. 2a and 4. 2b). κ can also be predicted, if the aerosol composition is known, by applying a mixing rule (Petters and Kreidenweis, 2007),

$$\kappa_{mix} = \sum_i \varepsilon_i \kappa_i \tag{4.7}$$

where κ_i is the hygroscopicity parameter of component *i*

$$\kappa_i = \frac{M_w \rho_i \upsilon_i}{\rho_w M_i} \tag{4.8}$$

κ for the water-soluble organics were calculated using the properties determined by KTA (Section 4.4.4). κ for salts potentially present in the extracted filters are presented in Table 4.3.

From the κ closure, it was determined that neglecting the effects of surface tension depression of organics leads to underestimation of the κ_{CCN} (Figure 4.6). From

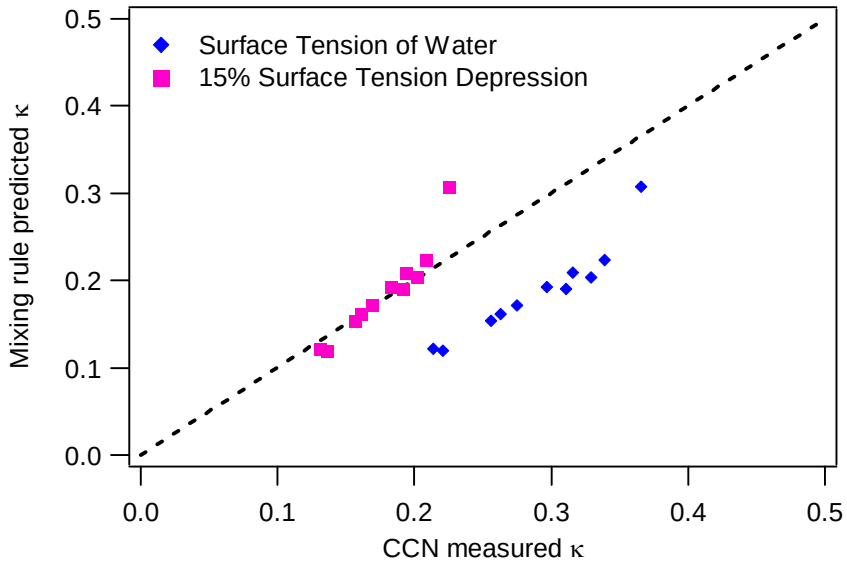

Figure 4. 6: Hygroscopicity parameter closure plot. Comparison of κ predicted from the mixing rule to the κ determined experimentally from CCN data assuming the surface tension of water (pink squares) and 15% surface tension depression (blue circles). The black dashed line represents the 1 to 1 line.

our analysis, we found the $\frac{\kappa_{mix}}{\kappa_{CCN}} = 0.6$. This discrepancy is due to the assumption that the surface tension is equal to that of water. When κ_{CCN} is calculated allowing for the surface tension depression observed (~15%), excellent agreement was obtained. This implies that neglecting surfactant characteristics of the aerosol can results in overestimation of κ by about a factor of 2 and therefore may need to be taken into account.

4.4.3 Growth kinetics

The impact of organics on the CCN activation kinetics were studied by looking at the resulting droplet diameter of activated CCN with s_c equal to the instrument supersaturation (i.e., for particles with dry diameter of d_{p50}) and comparing against that of $(NH_4)_2SO_4$ calibration aerosol. If the droplet sizes from ambient aerosols are smaller than those from calibration aerosol, the activation kinetics can be said to be affected by organics. However, if activated droplet sizes are indistinguishable from $(NH_4)_2SO_4$ data

(to within experimental uncertainty), they are said to exhibit activation kinetics similar to $(NH_4)_2SO_4$ aerosol.

Activated droplet sizes obtained for the pure Mexico City samples at both sites (12 hr day integration) are shown in Figure 4. 7; droplet sizes are indistinguishable from $(NH_4)_2SO_4$, hence the water soluble organics present in the Mexico City samples do not delay activation kinetics. This is consistent with the findings of Asa-Awuku et al. (2007), Moore et al. (2008), Engelhart et al. (2008), Sorooshian et al. (2008), Asa-Awuku et al.(2009), Murphy et al. (2009), and Bougiatioti et al., (in review[6]) where delayed activation kinetics is not observed for aerosol containing a significant fraction of water-soluble organics. However, growth kinetics performed in situ at the T1 site, suggest that

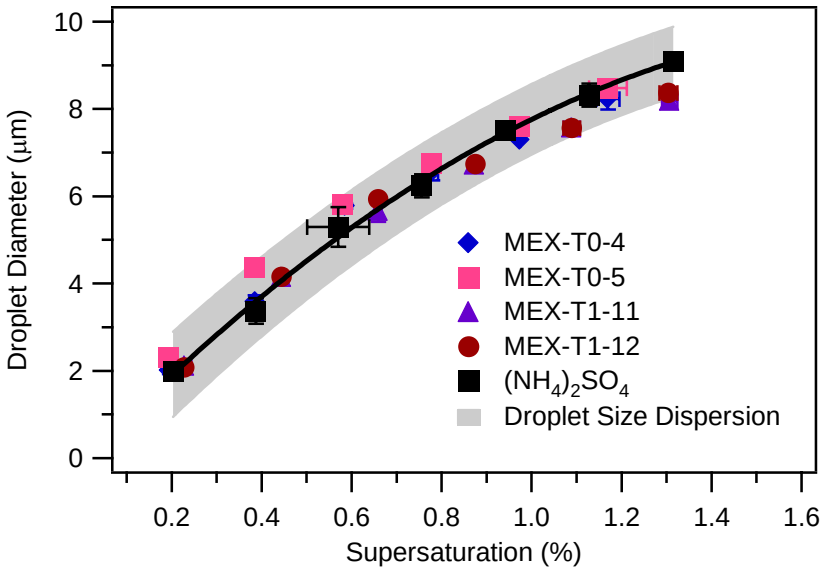

Figure 4. 7: Growth curves for 12 hr integration day samples: MEX-T0-3 (blue triangle), MEX-T0-4 (pink square), MEX-T1-11 (purple triangle), MEX-T1-12 (maroon circle), and $(NH_4)_2SO_4$ (black square). The grey band represents the variability in the average droplet distribution.

[6]Bougiatioti A., Fountoukis C., Kalivitis N., Pandis S. N., Nenes A. and Mihalopoulos N., 2009. Cloud condensation nuclei measurements in the eastern Mediterranean marine boundary layer: CCN closure and droplet growth kinetics. Atmospheric Chemistry and Physics Discussions 9, 10303 – 10336.

kinetic inhibitions may be related to the less hygroscopic fraction of the aerosol (Lance, 2007).

4.4.4 Average organic molar mass

KTA is used to infer the average organic molar volume based on Equation (4.3), measured surface tension (Tables 4. 7 and 4. 8), FCA factor, and chemical composition (Tables 4. 4 and 4. 5). From the molar volume, the average molar mass can be inferred by multiplying with the organic density, ρ_{org}. During application of KTA, we assume that υ_{org} = 1. For all samples collected at T1 there was an excess of cations present in the extracted samples. It was determined that the presence of excess cations (Ca^{2+}, Na^{+}, and K^{+}) were associated with dust, where excess Ca^{2+} is bound to CO_3^{-}. Excess K^{+} and Na^{+} is also associated with re-suspension of dry lake bed salt from Lake Texcoco (Vega et al., 2001, located southwest of the T1 site). Metereological data (De Foy et al., 2008;Fast et al., 2007) support this, since on these dates a high pressure system present over the Gulf of Mexico causing southwesterly winds over the MC area that favored the transport of salt-rich dust from the dry lake to the site.

The organic mass fraction in the T0 site samples was low and KTA is subject to large uncertainty (Padró et al., 2007). Hence molar mass estimates are calculated only for T1 site samples where the organic mass fraction is highest. Higher molecular weight organics were found for the 12 hr samples relative to the 24 hr samples. The higher molecular weights found could have been formed through condensed-phase chemistry (which forms oligomers and therefore increases the organic molecular weight) taking place on the days for which the 12 hr samples were collected. These were collected during the third period which had higher relative humidity and evening rain events than the previous periods (before March 23; De Foy et al., 2008;Fast et al., 2007), which likely

enhanced the formation of higher molecular weight organics. Diurnal changes in oxidant levels (O_3 and OH) did not vary substantially, hence not likely responsible for this change (Case Hanks, 2008). For the 12 hr samples in T1 (day and night), a lower organic molecular weight (on average) was observed for the day samples (Table 4. 2). The day samples have lower organic molecular weight which is consistent with condensation of fresh SOA during peak photochemical activity, which agrees with in-situ size-resolved CCN activity measurements carried out during the same time period (Lance et al., 2007). While the apparent increase in average molecular weight during the night could be due to olgomerization processes occurring throughout the night when the RH increases. This is consistent with hydrocarbon-like organic aerosols dominating in the early morning (during peak traffic emissions) and oxygenated organic aerosols dominating in the afternoon indicating strong photochemical formation (de Gouw et al., 2009).

A sensitivity analysis was performed to determine the greatest source of uncertainty in the organic molar mass calculations. Of the six parameters (σ, ω, υ_{org}, υ_{inorg}, ε_{org}, and ε_{inorg}) considered, the greatest source of uncertainty arises from the van't Hoff factor (dissociation of ions in water), followed by the FCA parameter. The total estimated uncertainty in molar mass for all the samples is ~ 20% (Table 4. 9) which is comparable with estimates from other KTA studies (e.g., Asa-Awuku et al., 2007, 2008, 2009;Englehart et al., 2008; Moore et al., 2008;Padró et al., 2007).

4.5 Conclusions

Ambient aerosols were collected with Hi-Volume samplers on March 2006 during the MILAGRO field campaign in Mexico City. Particles were collected at the T0 (downtown) and T1 (northeast of the city) sites. 12 and 24 hr filter samples were collected to contrast daytime versus nighttime characteristics. Characterization of the water soluble fraction was possible by measuring its CCN activity and growth kinetics, surface tension, and ionic composition. Köhler Theory Analysis (Padró et al., 2007) was

Table 4. 9: Molar mass uncertainty analysis and total uncertainty as percent of molar mass for the T1 site samples.

Sample Name	Uncertainty to σ (g mol^{-1})	Uncertainty to ω (g mol^{-1})	Uncertainty to υ_{org} (g mol^{-1})	Uncertainty to υ_{inorg} (g mol^{-1})	Uncertainty to ε_{org} (g mol^{-1})	Uncertainty to ε_{inorg} (g mol^{-1})	Total Uncertainty (%)
MEX-T1-1	0.105	4.813	15.749	20.892	0.0004	0[a]	14.5
MEX-T1-2	0.047	6.472	3.178	6.674	85.145	0[a]	44.0
MEX-T1-3	0.080	3.740	6.137	17.009	0.001	0[a]	10.8
MEX-T1-4	0.098	7.212	10.057	34.513	0.001	0[a]	22.3
MEX-T1-5	0.758	57.782	95.883	381.184	0.006	0.001	289.4
MEX-T1-6	0.011	0.930	1.032	1.918	0[a]	0[a]	3.3
MEX-T1-7	N/A[b]	N/A[b]	N/A[b]	N/A[b]	N/A[b]	N/A[b]	N/A[b]
MEX-T1-8	0.109	21.291	29.332	96.639	0.001	0[a]	41.4
MEX-T1-9	0.082	15.620	23.676	93.514	0.002	0[a]	28.1
MEX-T1-10	0.045	7.776	16.986	50.696	0.001	0[a]	18.6
MEX-T1-11	0.019	5.316	6.871	19.369	0.001	0[a]	10.0
MEX-T1-12	0.244	5.872	9.498	28.946	0.001	0[a]	10.3

[a]Values are much smaller than 10^{-5} g mol^{-1}.

[b]N/A: Not available.

used to infer the average molecular weight of the organics by coupling it to parameters obtained from the offline analysis methods employed here. κ -Köhler theory analysis was also carried out to examine the variability of the soluble mass hygroscopicity and its sensitivity to the surfactant characteristics of the particulate matter.

From our analysis, we found the water soluble organics present in Mexico City act as surfactants; the organics at T1 depress surface tension to a lesser degree than those at T0 consistent with having more hydrophobic organics present in the latter (fresh emissions), further promoted by higher salt concentrations. The most surprising result is that the water-soluble fraction, regardless of sampling site and period, exhibit similar CCN activity and hygroscopicity. As a result, κ is fairly constant over a wide range of water soluble organic mass fractions, which implies that the CCN activity of the parent aerosol depends solely on its soluble fraction (inorganic and organic combined) and its dry particle diameter. When closure in predicted κ is attempted, neglecting surfactants may lead to a 50% overestimation. Given that this overprediction corresponds to a 15% surface tension depression (which is typical for most aerosol containing surfactants), studies that use a κ-based approach to parameterize compositional impacts on CCN activity need to account for this variability (in terms of a sensitivity study) in simulations.

Application of KTA to the T1 site samples suggests that the organic molar mass varies between night and day samples by twofold, exhibiting the lowest molar mass during the day. The observed increase in molar mass during the nighttime is consistent with local primary emissions condensing upon the particles, combined with aqueous reactions that could form HULIS. Finally, the growth kinetics of the activated CCN at both sites was found to be similar to $(NH_4)_2SO_4$.

In conclusion, this study suggests that the properties of the water-soluble fraction of aerosol as complex as that found in Mexico City can be described in terms of a few parameters. Surfactants are important for affecting CCN activity, and should be considered, either in terms of a sensitivity study, as a “modified” hygroscopicity

parameter may introduce uncertainty in CCN predictions. The remarkably constant hygroscopicity, if also seen in other locations, is an exciting prospect for atmospheric models of aerosol-cloud interactions.

4.6 References

Andreae, M. O. and Crutzen, P. J.: Atmospheric Aerosols: Biogeochemical Sources and Role in Atmospheric Chemistry, Science, 276, 1052-1058, 1997.

Asa-Awuku, A., Engelhart, G. J., Lee, B. H., Pandis, S. N. and Nenes, A.: Relating CCN activity, volatility, and droplet growth kinetics of β-caryophyllene secondary organic aerosol, Atmos. Chem. Phys., 9, 795-812, 2009.

Asa-Awuku, A. and Nenes, A.: The Effect of Solute Dissolution Kinetics on Cloud Droplet Formation, J. Geophys. Res.-A., 112, D22201, doi:10.1029/2005JD006934, 2007.

Asa-Awuku, A., Nenes, A., Gao, S., Flagan, R. C. and Seinfeld, J. H.: Alkene ozonolysis SOA: inferences of composition and droplet growth kinetics from Köhler theory analysis, Atmos. Chem. Phys. Discuss., 7, 8983-9011, 2007.

Asa-Awuku, A., Nenes, A., Sullivan, A. P., Hennigan, C. and Weber, R. J.: Investigation of Molar Volume and Surfactant Characteristics of Water-Soluble Organic Compounds in Biomass Burning Aerosol Atmos. Chem. Phys., 8, 799 - 812, 2008.

Badger, C. L., George, I., Griffiths, P. T., Braban, C. F., Cox, R. A. and Abbatt, J. P. D.: Phase transitions and hygroscopic growth of aerosol particles containing humic acid and mixtures of humic acid and ammonium sulphate, Atmos. Chem. Phys., 6, 755-768, 2006.

Brechtel, F. J. and Kreidenweis, S. M.: Predicting particle critical supersaturation from hygroscopic growth measurements in the humidified TDMA. Part I: Theory and sensitivity studies, Journal of Atmospheric Science, 57(12), 1854-1871, 2000.

Brooks, S. D., DeMott, P. J. and Kreidenweis, S. M.: Water uptake by particles containing humic materials and mixtures of humic materials with ammonium sulfate, Atmos. Environ., 38, 1859-1868, 2004.

Butler, A. J.: Temporal and spatial analysis of PM2.5 mass and composition in Atlanta, School of Civil and Environmental Engineering, Georgia Institute of Technology, Atlanta, 226, 2000.

Carrico, C. M., Petters, M. D., Kreidenweis, S. M., Collett, J. L., Engling, G. and Malm, W. C.: Aerosol hygroscopicity and cloud droplet activation of extracts of filters from biomass burning experiments, J. Geophys. Res.-A., 113(D8), 2008.

Case Hanks A. T.: Formaldehyde instrument development and boundary layer sulfuric acid: implications for photochemistry, Earth and Atmospheric Sciences, Georgia Institute of Technology, Atlanta, GA, 2008.

Clegg, S. L. and Brimblecombe, P.: Equilibrium partial pressures of strong acids over concentrated saline solutions -- I. HNO3., Atmos. Environ., 1, 91-100, 1988.

Cobb, C. E.: Spatial and temporal variations of PM2.5 mass and composition in Atlanta: ASACA 1999 - 2006, School of Civil and Environmental Engineering, Georgia Institute of Technology, Atlanta, 84, 2006.

Cross, E. S., Onasch, T. B., Canagaratna, M., Jayne, J. T., Kimmel, J., Yu, X.-Y., Alexander, M. L., Worsnop, D. R. and Davidovits, P.: Single particle characterization using a light scattering module coupled to a time-of-flight aerosol mass spectrometer, Atmos. Chem. Phys. Discuss., 8, 21313-21381, 2008.

Cruz, C. N. and Pandis, S. N.: A study of the ability of pure secondary organic aerosol to act as cloud condensation nuclei, Atmos. Environ., 31(15), 2205-2214, 1997.

De Foy, B., Fast, J. D., Paech, S. J., Phillips, D., Walters, J. T., Coulter, R. L., Martin, T. J., Pekour, M. S., Shaw, W. J., Kastendeuch, P. P., Marley, N. A., Retama, A. and Molina, L. T.: Basin-scale wind transport during the MILAGRO field campaign and comparison to climatology using cluster analysis, Atmos. Chem. Phys., 8, 1209-1224, 2008.

de Gouw J. A., Welsh-Bon D., Warneke C., Kuster W. C., Alexander L., Baker A. K., Beyersdorf A. J., Blake D. R., Canagaratna M., Celada A. T., Huey L. G., Junkermann W., Onasch T. B., Salcido A., Sjostedt S. J., Sullivan A. P., Tanner D. J., Vargas O., Weber R. J., Worsnop D. R., Yu X. Y. and Zaveri R.: Emission and chemistry of organic carbon in the gas and aerosol phase at a sub-urban site near Mexico City in March 2006 during the MILAGRO study. Atmospheric Chemistry and Physics 9, 3425 – 3442, 2009.

DeCarlo, P. F., Dunlea, E. J., Kimmel, J. R., Aiken, A. C., Sueper, D., Crounse, J., Wennberg, P. O., Emmons, L., Shinozuka, Y., Clarke, A., Zhou, J., Tomlinson, J., Collins, D. R., Knapp, D., Weinheimer, A. J., Montzka, D. D., Campos, T. and Jimenez, J. L.: Fast Airborne Aerosol Size and Chemistry Measurements with the High Resolution Aerosol Mass Spectrometer during the MILAGRO Campaign, Atmos. Chem. Phys., 8, 4027 - 4048, 2008.

Dinar, E., Mentel, T. F. and Rudich, Y.: The density of humic acids and humic like substances (HULIS) from fresh and aged wood burning and pollution aerosol particles, Atmos. Chem. Phys., 6, 5213-5224, 2006a.

Dinar, E., Taraniuk, I., Graber, E. R., Anttila, T., Mentel, T. F. and Rudich, Y.: Hygroscopic growth of atmospheric and model humic-like substances, Journal of Geophysical Research - Atmospheres, 112, D05211, doi:10.1029/2006JD007442, 2007.

Dinar, E., Taraniuk, I., Graber, E. R., Katsman, S., Moise, T., Anttila, T., Mentel, T. F. and Rudich, Y.: Cloud Condensation Nuclei properties of model and atmospheric HULIS, Atmos. Chem. Phys., 6, 2465-2482, 2006b.

Engelhart, G. J., Asa-Awuku, A., Nenes, A. and Pandis, S. N.: CCN activity and droplet growth kinetics of fresh and aged monoterpene secondary organic aerosol, Atmos. Chem. Phys., 8, 3937 - 3949, 2008.

Facchini, M. C., Decesari, S., Mircea, M., Fuzzi, S. and Loglio, G.: Surface tension of atmospheric wet aerosol and cloud/fog droplets in relation to their organic carbon content and chemical composition, Atmos. Environ., 34(28), 4853-4857, 2000.

Fast, J. D., De Foy, B., Acevedo Rosas, F., Caetano, E., Carmichael, G., Emmons, L., McKenna, D., Mena, M., Skamarock, W., Tie, X., Coulter, R. L., Barnard, J. C., Wiedinmyer, C. and Madronich, S.: A meteorological overview of the MILAGRO field campaigns, Atmos. Chem. Phys., 7, 2233-2257, 2007.

Feingold, G. and Chuang, P. Y.: Analysis of the influence of film-forming compounds on droplet growth: Implications for cloud microphysical processes and climate, J. Atmos. Sci., 59(12), 2006-2018, 2002.

Fountoukis, C. and Nenes, A.: ISORROPIA II: a computationally efficient thermodynamic equilibrium model for K^+ -Ca^{2+} -Mg^{2+} -$NH4^+$ -Na^+ -SO_4^{2-} -NO_3^- -Cl^- -H_2O aerosols, Atmos. Chem. Phys., 7, 4639-4659, 2007.

Hagler, G. S. W., Bergin, M. H., Smith, E. A. and Dibb, J. E.: A summer time series of particulate carbon in the air and snow at Summit, Greenland, Journal of Geophysical Research - Atmospheres, 112, D21309, doi:10.1029/2007JD008993, 2007.

Hoffer, A., Kiss, G., Blazsó, M. and Gelencsér, A.: Chemical characterization of humic-like substances (HULIS) formed from a lignin-type precursor in model cloud water, Geophysical Research Letters, 31, L06115, doi:10.1029/2003GL018962, 2004.

Jáuregui Ostos, E.: El clima de la Ciudad de México, 1st ed, P. y. Valdés, Instituto de Geografía - UNAM, México, D.F., 131, 2000.

Kiss, G., Tombacz, E. and Hansson, H. C.: Surface tension effects of humic-like substances in the aqueous extract of tropospheric fine aerosol, J. Atmos. Chem., 50(3), 279-294, 2005.

Kiss, G., Tombacz, E., Varga, B., Alsberg, T. and Persson, L.: Estimation of the average molecular weight of humic-like substances isolated from fine atmospheric aerosol, Atmos. Environ., 37(27), 3783-3794, 2003.

Kleinman, L. I., Springston, S. R., Daum, P. H., Lee, Y.-N., Nunnermacker, L. J., Senum, G. I., Wang, J., Weinstein-Lloyd, J., Alexander, M. L., Hubbe, J., Ortega, J., Canagaratna, M. and Jayne, J.: The time evolution of aerosol composition over the Mexico City plateau, Atmos. Chem. Phys., 8, 1559-1575, 2008.

Koehler, K. A., Kreidenweis, S. M., DeMott, P. J., Petters, M. D., Prenni, A. J. and Carrico, C. M.: Hygroscopicity and cloud droplet activation of mineral dust aerosol, Geophys. Res. Lett., 36, 2009.

Lance, S.: Quantifying compositional impacts of ambient aerosol on cloud droplet formation, School of Earth and Atmospheric Sciences, Georgia Institute of Technology, Atlanta, 166, 2007.

Lance, S., Medina, J., Smith, J. N. and Nenes, A.: Mapping the operation of the DMT continuous flow CCN counter Aerosol Sci. Technol., 40, 242-254, 2006.

Lance, S., Nenes, A. and Rissman, T. A.: Chemical and dynamical effects on cloud droplet number: Implications for estimates of the aerosol indirect effect, Journal of Geophysical Research - Atmospheres, 109(D22208), doi:10.1029/2004JD004596, 2004.

Langmuir, I.: The constitution and fundamental properties of solids and liquids. II. Liquids., J. Am. Chem. Soc., 39, 1848-1906, 1917.

Moffet, R. C., de Foy, B., Molina, L. T., Molina, M. J. and Prather, A.: Measurement of ambient aerosols in northern Mexico City by single particle mass spectrometry, Atmos. Chem. Phys., 8, 4499-4516, 2008.

Moore, R. H., Ingall, E. D., Sorooshian, A. and Nenes, A.: Molar mass, surface tension, and droplet growth kinetics of marine organics from measurements of CCN activity, Geophys. Res. Lett., 35, L07801, doi:10.1029/2008GL033350, 2008.

Murphy, S. M., Agrawal, H., Sorooshian, A., Padro, L. T., Gates, H., Hersey, S., Welch, W. A., Jung, H., Miller, J. W., Cocker III, D. R., Nenes, A., Jonsson, H. H., Flagan, R. C. and Seinfeld, J. H.: Comprehensive simultaneous shipboard and airborne characterization of exhaust from a modern container ship at sea, Environmental Science & Technology, doi:10.1021/es802413j, 2009.

Padró, L. T., Morrison, R., Asa-Awuku, A. and Nenes, A.: Inferring Thermodynamic Properties from CCN Activation Experiments: Single-component and Binary Aerosols, Atmos. Chem. Phys., 7, 5263 - 5274, 2007.

Petters, M. D. and Kreidenweis, S. M.: A single parameter representation of hygroscopic growth and cloud condensation nucleus activity, Atmos. Chem. Phys., 7, 1961-19711, 2007.

Pitzer, K. S. and Mayorga, G.: Thermodynamics of electrolytes -- II. Activity and osmotic coefficients for strong electrolytes with one or both ions univalent, J. Phys. Chem., 77, 2300-2308, 1973.

Roberts, G. C. and Nenes, A.: A continuous-flow streamwise thermal-gradient CCN chamber for atmospheric measurements, Aerosol Sci. Technol., 39(3), 206-211, 2005.

Rose, D., Frank, G. P., Dusek, U., Gunthe, S. S., Andreae, M. O. and Pöschl, U.: Calibration and measurement uncertainties of a continuous-flow cloud condensation nuclei counter (DMT-CCNC): CCN activation of ammonium sulfate and sodium chloride aerosol particles in theory and experiment, Atmos. Chem. Phys., 8, 1153-1179, 2008.

Ruehl C. R., Chuang P. Y. and Nenes A.: How quickly do cloud droplets form on atmospheric particles?, Atmos. Chem. Phys., 8, 1043 – 1055, 2008.

Ruehl C. R., Chuang P. Y. and Nenes A.: Distinct CCN activation kinetics above the marine boundary layer along the California coast, Geophys. Res. Lett., in press.

Samburova, V., Zenobi, R. and Kalberer, M.: Characterization of high molecular weight compounds in urban atmospheric particles, Atmos. Chem. Phys., 5, 2163-2170, 2005.

Shantz, N. C., Leaitch, W. R., Phinney, L., Mozurkewich, M. and Toom-Sauntry, D.: The effect of organic compounds on the growth rate of cloud droplets in marine and forest settings, Atmos. Chem. Phys., 8, 5869-5887, 2008.

Sorooshian, A., Murphy, S. M., Hersey, S., Gates, H., Padro, L. T., Nenes, A., Brechtel, F. J., Jonsson, H., Flagan, R. C. and Seinfeld, J. H.: Comprehensive airborne characterization of aerosol from a major bovine source, Atmos. Chem. Phys., 8, 5489 - 5520, 2008.

Spelt, J. K. and Li, D.: Applied Surface Thermodynamics, ed, A. W. Neumann and J. K. Spelt, Marcel Dekker, New York, 1996.

Stone, E. A., Snyder, D. C., Sheesley, R. J., Sullivan, A. P., Weber, R. J. and Schauer, J. J.: Source apportionment of fine organic aerosol in Mexico City during the MILAGRO Experiment 2006, Atmos. Chem. Phys., 8, 1249-1259, 2008.

Sullivan, A. P. and Weber, R. J.: Chemical characterization of the ambient organic aerosol soluble in water: 2. Isolation of acid, neutral, and basic fractions by modified size-exclusion chromatography, J. Geophys. Res.-A., 111(D5), Art. No. D05315, doi:10.1029/2005JD006486, 2006.

Sullivan, A. P., Weber, R. J., Clements, A. L., Turner, J. R., Bae, M. S. and Schauer, J. J.: A method for on-line measurement of water-soluble organic carbon in ambient aerosol particles: Results from an urban site, Geophys. Res. Lett., 31, L13105, doi:10.1029/2004GL019681, 2004.

Svenningsson, B., Rissler, J., Swietlicki, E., Mircea, M., Bilde, M., Facchini, M. C., Decesari, S., Fuzzi, S., Zhou, J., Monster, J. and Rosenorn, T.: Hygroscopic growth and critical supersaturations for mixed aerosol particles of inorganic and organic compounds of atmospheric relevance, Atmos. Chem. Phys., 6, 1937-1952, 2006.

Taraniuk, I., Graber, E. R., Kostinski, A. and Rudich, Y.: Surfactant properties of atmospheric and model humic-like substances (HULIS), Geophys. Res. Lett., 34, L16807, doi:10.1029/2007GL029576, 2007.

Vega, E., Mugica, V., Reyes, E., Sánchez, G., Chow, J. C. and Watson, J. G.: Chemical composition of fugitive dust emitters in Mexico City, Atmos. Environ., 35, 4033-4039, 2001.

Wex, H., Hennig, T., Salma, I., Ocksay, R., Kiselev, A., Henning, S., Massling, A., Wiedensohler, A. and Stratmann, F.: Hygroscopic growth and measured and modeled critical supersaturations of an atmospheric HULIS sample, Geophys. Res. Lett., 34, L02818,doi:10.1029/2006GL028260, 2007.

Zappoli, S., Andracchio, A., Fuzzi, S., Facchini, M. C., Gelencser, A., Kiss, G., Krivacsy, Z., Molnar, A., Meszaros, E., Hansson, H. C., Rosman, K. and Zebuhr, Y.: Inorganic, organic and macromolecular components of fine aerosol in different areas of Europe in relation to their water solubility, Atmos. Environ., 33(17), 2733-2743, 1999.

CHAPTER 5

MIXING STATE, CCN ACTIVITY, AND DROPLET GROWTH KINETICS OF SIZE-RESOLVED CCN IN AN URBAN ENVIRONMENT[7]

The effects of aerosol composition (especially from organic species) on the cloud droplet formation process is highly variable and uncertain, but can be largely constrained by size-resolved Cloud Condensation Nuclei (CCN) measurements. A fast method for size-resolved CCN measurements is Scanning Mobility CCN Analysis (SMCA; Nenes and Medina, in review), where the monodisperse aerosol output from a Differential Mobility Analyzer (operated in scanning voltage mode), sampling ambient aerosol, is concurrently introduced into a Streamwise Thermal Gradient CCN Chamber (STGC, Roberts and Nenes, 2005) and a Condensation Particle Counter. Inversion of the concentration time-series from both instruments yields the activation ratio and size of activated droplets, as a function of dry mobility diameter and supersaturation. In this study, we performed SMCA for aerosols sampled at Atlanta, GA in August and September 2008. We quantify the predictive uncertainty associated with simplifying compositional assumptions (e.g., size-invariant composition and mixing state, organic insoluble/soluble with constant hygroscopicity) when used to predict CCN concentrations as well as droplet growth kinetics.

[7] Under preparation for submission: Padró, L. T., Moore, R. H., Zhang, X., Rastogi, N., Weber, R. J. and Nenes, A.: Mixing state, CCN activity, and droplet growth kinetics of size-resolved CCN in an urban environment, Manuscript in Preparation.

5.1 Motivation

It is well accepted that atmospheric aerosols affect climate directly by reflecting incoming solar radiation (IPCC, 2001) and indirectly through their role as cloud condensation nuclei (CCN) (Twomey, 1977; Albrecht, 1989; IPCC, 2001). Understanding the cloud droplet formation potential of aerosols is a requirement for predicting their impact on clouds but suffers from a large uncertainty in climate change predictions.

The ability of a given aerosol particle to act as a CCN and activate into a cloud droplet is a strong function of its size and composition. Köhler theory (Köhler, 1936) adequately describes CCN composed of inorganic compounds and soluble low molecular weight organic compounds (Cruz and Pandis, 1997; Raymond and Pandis, 2002). CCN containing high molecular weight organic compounds can exhibit complex interactions with water vapor, (Corrigan and Novakov, 1999; Raymond and Pandis, 2002; Hartz et al., 2006) which can be further complicated in the presence of inorganic electrolytes, (especially bivalent ions, such as sulfate (SO_4^{-2})) typically found in ambient aerosol. There is a need to unravel this complexity for aerosol-cloud interaction studies, particularly because ambient carbonaceous aerosol can readily act as CCN (Novakov and Penner, 1993).

One way to access our understanding of CCN activation is through CCN closures. The idea is to compare measured and predicted CCN concentrations in order to determine how well Köhler theory can predict CCN formation. CCN predictions are performed by combining particle size distributions, chemical composition, and CCN measurements. Numerous CCN closure studies have been performed in ground based (Bigg, 1986; Quinn et al., 1993; Liu et al., 1996; Covert et al., 1998; Cantrell et al., 2001; Roberts et al., 2002; Roberts et al., 2003; Broekhuizen et al., 2006; Chang et al., 2007; Ervens et al., 2007; Medina et al., 2007; Stroud et al., 2007; Vestin et al., 2007; Cubison et al., 2008;

Bougiatioti et al., 2009), ship (Zhou et al., 2001), and airborne platforms (Martin et al., 1994; VanReken et al., 2003; Rissman et al., 2006, Asa-Awuku et al., in review[8], Lance et al., in review[9]; Roberts et al., 2006; Wang et al., 2008; Murphy et al., 2009) in which the effects of chemical composition and mixing state have been addressed.

Some CCN closure studies (Bigg, 1986; Quinn et al., 1993; Martin et al., 1994; VanReken et al., 2003; Vestin et al., 2007) have predicted CCN concentrations by assuming that the particles are composed of only ammonium sulfate or sodium chloride (no chemical composition measurements) and have achieved reasonable closures. For example, Bigg (1986) found reasonable results for low particle concentrations, while Martin (1994) and VanReken et al. (2003) achieved it for maritime air masses. It should be noted that VanReken et al. (2003) was the first airborne campaign to achieve closure even with the simplified composition scheme used. However, that was not the case for Quinn et al. (1993) and Vestin et al. (2007). Quinn et al. (1993) overpredicted CCN concentrations by a factor of two whereas Vestin et al. (2007) underpredicted by 15 – 20% the measured CCN concentrations. The results obtained from these groups made it evident that a more detailed chemical composition data is needed in order to get a more accurate prediction of CCN.

Chemical composition data for CCN closures has been obtained recently from filters (Liu et al., 1996), Micro Orifice Uniform Deposit Impactor (MOUDI) cascade impactors (Cantrell et al., 2001; Roberts et al., 2002; Roberts et al., 2003), hygroscopic growth measurements (Covert et al., 1998; Zhou et al., 2001; Ervens et al., 2007), and aerosol mass spectrometers (AMS; Broekhuizen et al., 2006, Asa-Awuku et al., in review[8], Lance et al., in review[9]; Medina et al., 2007; Stroud et al., 2007). Even though

[8] Asa-Awuku, A., Moore, R. H., Brock, C. A., Bahreini, R., Middlebrook, A. M., Schwarz, J. P., Spackman, J. R., Holloway, J. S., Stickel, R., Tanner, D. J., Huey, L. G. and Nenes, A.: Airborne cloud condensation nuclei measurements during the 2006 Texas Air Quality Study, In Review.

[9] Lance, S., Gates, H., Varutbangkul, V., Rissman, T., Murphy, S., Sorooshian, A. Brechtel, F., Flagan, R. C., Seinfeld, J. H. and Nenes, A.: CCN activity, closure, and droplet growth kinetics of Houston aerosol during the Gulf of Mexico Atmospheric Composition and Climate Study (GoMACCS), In Review.

good closures have been achieved with all the methods some provide a more accurate chemical composition (e.g., AMS) due to their ability to provide size resolved chemical composition which becomes important at smaller sizes.

Although introducing chemical composition and the mixing state of the aerosol has been found to improve the CCN closure, there is still a debate as to which is more significant to obtain closure. For example, Ervens et al. (2007) found that knowing the mixing state of the aerosol is more important to achieve closure than the size resolved aerosol chemical composition. Yet other studies (Medina et al., 2007, Asa-Awuku et al., in review[8], Lance et al., in review[9]) have found that knowledge of both chemical composition and mixing state are needed to achieve good closure.

Of all the closure studies done to date, closures have been achieved in places that are not influenced by strong anthropogenic sources and have low organic mass fractions. Thus far only two exceptions to the rule have been observed. Broekhuizen et al. (2006) were the first to achieve closure under conditions of high anthropogenic emissions; while Roberts et al. (2002) were able to achieve closure in an area where the organic concentration (assumed to be insoluble) was high but had no anthropogenic influence.

In this study, we present size-resolved CCN and droplet growth kinetic measurements obtained during the August Mini-Intensive Gas and Aerosol Study (AMIGAS) campaign which took place in Georgia from August 1st till September 15th, 2008. AMIGAS was a ground based study with two locations: *i*) urban Atlanta (Jefferson St.) and *ii*) rural Yorkville (~ 40 mi NW of Atlanta) were SouthEastern Aerosol Research and Characterization (SEARCH; http://www.atmospheric-research.com/index.html) network sites are located. The Jefferson St. (JST) site was chosen because it is affected by both biogenic and anthropogenic emissions; while Yorkville (YRK) is mostly biogenic. The main objective of this campaign was to study the interactions between biogenic and anthropogenic emissions and their contribution to the formation and transformation of particulate matter, mainly Secondary Organic Aerosol (SOA) by

studying both the gas and particle phase. Size-resolved CCN measurements performed at the Jefferson St. site were done using the Scanning Mobility CCN Analysis (see Section 5.3.3). In this paper we present the daily trend of the mixing state and the scaled water-soluble volume fraction as a function of dry particle size. In addition, CCN closures for different mixing states and compositional scenarios as well as droplet growth kinetic studies are discussed.

5.2 Experimental methods

Coarse size aerosols (2.5 – 10 μm) in the ambient sample were separated from the fine particles (≤ 2.5 μm) with a PM 2.5 (particulate matter with aerodynamic diameter less than 2.5 μm) cyclone before being introduced to the instruments for analysis. The incoming filtered stream was then split between the different instruments (discussed below) for analysis.

5.2.1 Chemical composition

Two Particle-Into-Liquid-Samplers (PILS) were used in the campaign to study the chemical composition of the aerosols. The aerosols are exposed to a supersaturation in order to become droplets and are subsequently collected by inertial impaction. The droplets collected in the PILS are then sent to the detectors for analysis. The PILS-IC (Ion Chromatography; Weber et al., 2001) is a PILS coupled with a dual channel Ion Chromatograph which allows the detection of cations and anions in solution simultaneously. The PILS-IC detected inorganics (Ca^{2+}, Mg^{2+}, K^+, Na^+, Cl^-, NH_4^+, NO_3^-, NO_2^-, and SO_4^{2-}) and organics (formate and oxalate) ions present in the aerosol phase by reporting results in ~ 3 and 2 minute intervals for the anions and cations, respectively. The PILS-WSOC (Water Soluble Organic Carbon; Sullivan et al., 2004) is a PILS coupled to a Total Organic Carbon (TOC) Analyzer. Before the WSOC measurements

are performed, the sample stream is filtered to remove any large insoluble particles. The PILS-WSOC reports the soluble organic concentration in ~ 10 minute intervals.

5.2.2 Particle size distribution and total aerosol concentration

A Scanning Mobility Particle Sizer (SMPS) was used to measure the particle size distribution for particles having electrical mobility diameters (d_m) ranging from 6 to 870 nm by placing them in bins, which change depending on the set up (Figure 5. 1; CPC 3022A or CPC 3010; Setup A or B) and sheath-to-aerosol ratio (10:1 or 5:1; Setup A1 or

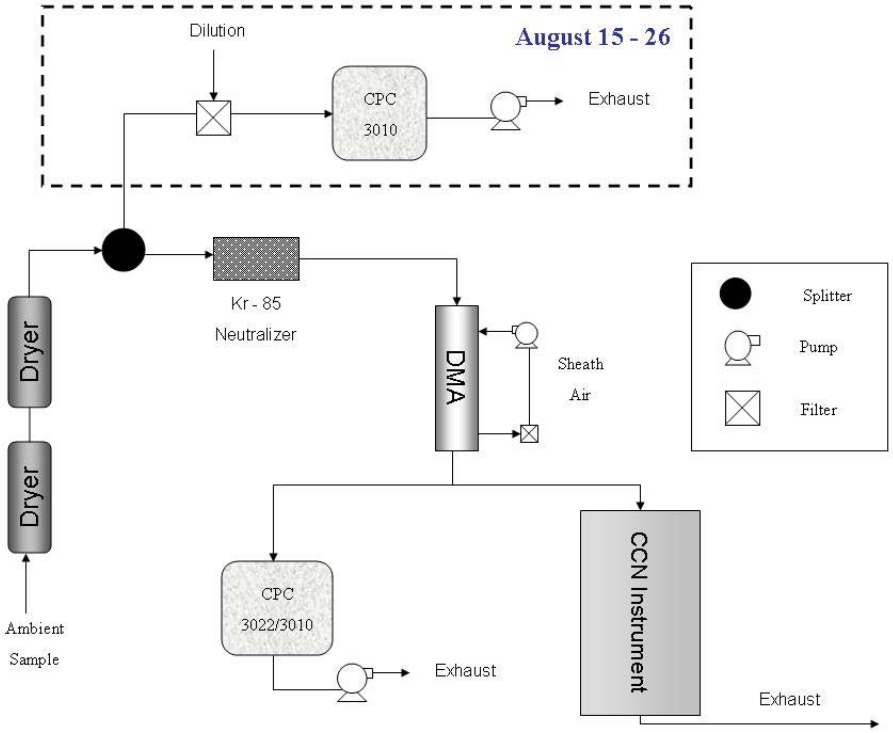

Figure 5. 1: AMIGAS experimental setup. From August 1st to August 26th, the CPC 3022A was used for the SMPS; while the CPC 3010 was used from August 26th till the end of the campaign (September 15th). The sheath-to-aerosol ratio in the DMA was run at 10:1 (August 1st till August 8th; Setup A1) and 5:1 (August 8th till September 15th; Setup A2 and B). The dotted box highlights the total CN measurement which was done from August 15th till August 26th.

Setup A2 and B). The SMPS consists of a scanning Differential Mobility Analyzer (DMA) running in series with a Condensation Particle Counter (CPC) for which a complete distribution is obtained in 2 minutes. Two different CPC's were used during the course of the campaign since one of them (CPC 3022A) stopped working on August 26th. The sheath-to-aerosol ratio was changed to detect larger particles. We assumed the particles sampled in this study to be spherical. This assumption is supported by observations which showed that the most abundant mass of Atlanta aerosol to consist of spherical hygroscopic particles (McMurry et al., 2002).

The total aerosol concentration (CN) was measured by a Condensation Particle Counter with a minimum diameter of 10 nm (TSI model 3010) from August 15th till the 26th. The measured CN reported is based on a 20 s average. Besides the CPC, the total aerosol concentration can be obtained by integrating the SMPS size distributions; however, it is at a lower resolution than the CPC (120 s versus 20 s). The disadvantage of the lower time resolution of the SMPS is its inability to capture plumes; however, this is not expected to be a problem on a ground site as it is the case in this study.

5.2.3 CCN activity and growth kinetic measurements

The setup employed to characterize the CCN activity and droplet growth kinetics of the ambient aerosols consists of a size classification and CCN measurement section (Figure 5. 1). Before size-resolved measurements were performed, polydisperse aerosols sampled (PM 2.5) were dried from ambient relative humidity (RH) to ~ 21% RH to insure "dry" particles were sampled throughout the period, since residual water can affect the aerosol CCN activity. Having residual water allows the particles to become activated at lower diameters. The dried particles were subsequently charged by passing them through a Kr-85 bipolar charger (TSI Model 3077). Then, a Differential Mobility Analyzer (TSI Model 3081) is used for size mobility selection of the dry particles. The classified aerosol is then split into two streams, one sent to a Condensation Particle

Counter (TSI Model 3022A or TSI Model 3010) to measure their concentration and the other to a Continuous Flow Streamwise Thermal Gradient CCN Chamber (Roberts and Nenes, 2005; Lance et al., 2006) to measure the number of particles which act as CCN. The activated droplets in the CCN are counted and sized at the exit with an Optical Particle Counter (OPC, 660 nm). The OPC detects particles with size ranging from 0.625 to 10 μm by dividing them into 20 bins.

In this work, data is obtained using Scanning Mobility CCN Analysis or SMCA (Nenes and Medina, in review[10]), the DMA voltage is changed over time, so that the dynamic mobility range of the DMA is scanned over 2 min. The time-series of CCN and CN counts are then inverted and aligned to obtain size-resolved CCN activity and growth kinetics. The aerosol size, analyzed for this study, ranged from 6 to 868 nm, depending on the sheath-to-aerosol ratio used in the DMA (10:1 or 5:1; the latter of which allowed higher diameters to be selected). A total of five supersaturations were run (each at 6 min) in the following order: 0.2, 0.6, 1.0, 0.8, and 0.4%. Scattering the supersaturations, allows the analysis of all the supersaturations considered, since all are allowed to reach equilibrium within the time allotted for each set supersaturation (6 min or 3 scans). The instrument was calibrated with $(NH_4)_2SO_4$ particles (for setups A1 and B) following the procedure discussed in Section 4.2.5. The resulting calibration curve (s_c versus ΔT; Figure 5. 2) was then interpolated for the temperature gradient to calculate the nominal instrument supersaturation.

The CCN activity of the aerosol is characterized at each supersaturation by determining the minimum dry particle diameter, d_{p50}, at which they can activate. d_{p50} is found by plotting the ratio of CCN to CN concentration as a function of dry particle diameter and determining the dry diameter for which the CCN/CN ratio equals 0.50 (Figure 5. 3). To facilitate with the analysis, the data is fit to a sigmoid curve which

[10] Nenes, A. and Medina, J.: Scanning Mobility CCN Analysis – A new method for fast measurements of size-resolved CCN activity and growth kinetics, In Review.

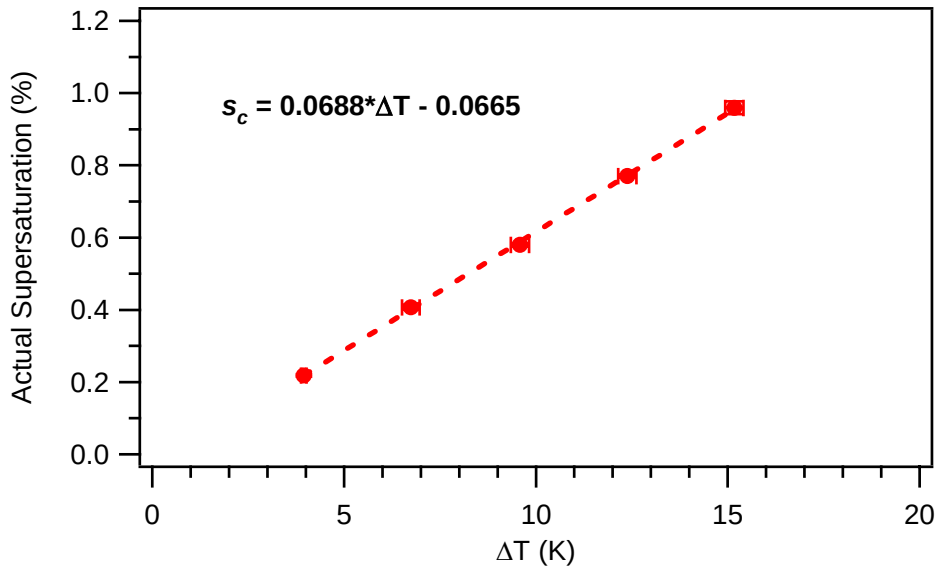

Figure 5. 2: Critical supersaturation versus delta T calibration for $(NH_4)_2SO_4$ aerosol. Calibration was performed at a flowrate of 700 cm^3 min^{-1} and at ambient pressure.

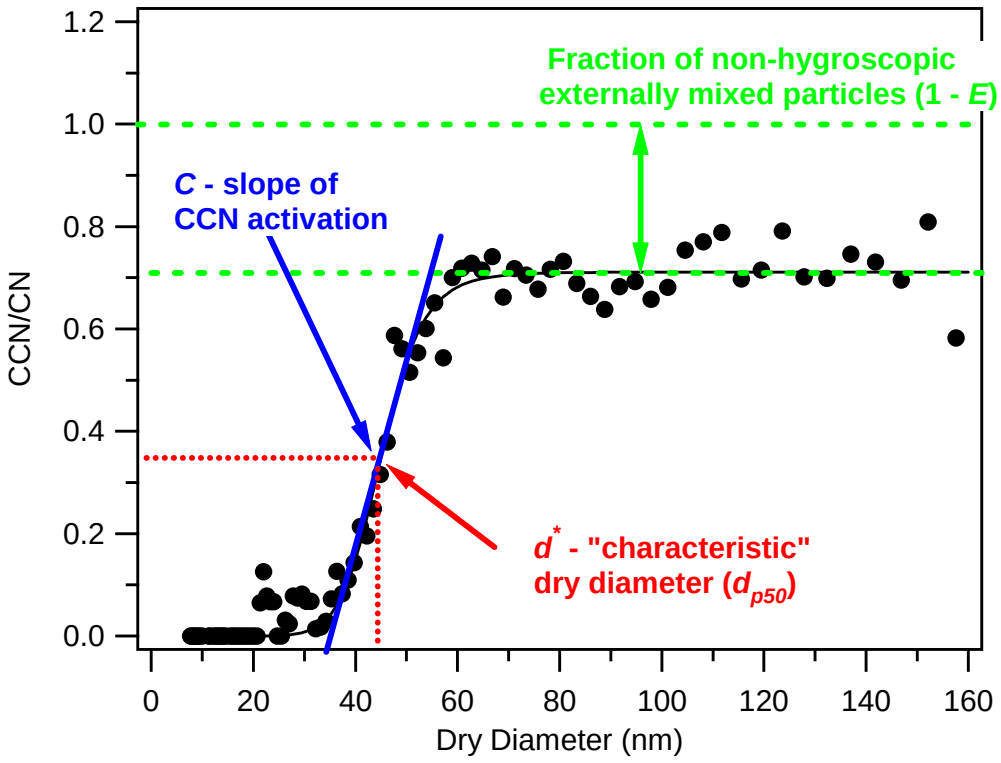

Figure 5. 3: Example of an ambient CCN activity spectrum (at constant supersaturation) with sigmoid fit and its defined parameters.

neglects the impact of multiply-charged particles (see Section 5.3.1). The measured and estimated parameters (s_c, d_{p50}, and CCN/CN ratio) can then be used to obtain the CCN distribution, mixing state, and inferred soluble volume fraction (see Section 5.3).

Growth kinetics of the CCN can be determined from the CCN measurements by monitoring the change in droplet size, as a function of selected dry diameter, measured at the OPC for all supersaturations considered. Growth kinetics can be addressed by comparing the size of the activated, ambient and $(NH_4)_2SO_4$ particles at the same critical supersaturation. In other words, we examine the relationship between supersaturation and droplet diameter (D_w) by determining the at the D_w at d_{p50}. Furthermore, a comparison between the droplet size for ambient and $(NH_4)_2SO_4$ particles (as a function of dry diameter) can also be done.

5.3 Experimental analysis

5.3.1 Sigmoidal fit of CCN activity spectrum

We fit the CCN activity spectrum (CCN/CN ratio) as a function of dry diameter at a specific supersaturation to a sigmoidal fit (Figure 5. 3):

$$\frac{CCN}{CN} = \frac{E}{1+\left(d^*/d\right)^C} \tag{5.1}$$

where E is the upper asymptote of the CCN activity spectrum, d^* is the characteristic dry diameter, d is the particle dry diameter, and C is proportional to the slope (positive since the activation ratio increases with dry particle size). E represents the extent of particle mixing. Therefore when $E = 1$ the particle is internally mixed (all particles for which the asymptote is reached become activated); whereas when $E < 1$ it is externally mixed. The fraction of the particles that are externally mixed is defined by 1 – E. For this analysis, we assumed all particle sizes have the same fraction of externally mixed particles as those

with d > 200 nm which is an underestimation since smaller aerosols tend to be more externally mixed. Although we brought the particle charge distribution to a Boltzmann equilibrium, we rarely observe an obvious "shoulder" in the sampled data that would indicate the presence of multiply-charged aerosols which could be due to the particles varying chemical composition with size.

5.3.2 CCN distribution

Since the size-resolved aerosols are sent simultaneously to the CPC and CCN counter for CN and CCN measurements, the CCN distribution can be acquired. This is done by multiplying the particle size distribution with the CCN/CN ratio. The CCN distribution, $\frac{dN_{CCN}}{d\log D_p}$, is defined:

$$\frac{dN_{CCN}}{d\log D_p} = \frac{CCN}{CN} * \frac{dN_{CN}}{d\log D_p} \tag{5.2}$$

where $\frac{dN_{CN}}{d\log D_p}$ is the particle size distribution. Substituting Equation (5.1) into Equation (5.2) gives:

$$\frac{dN_{CCN}}{d\log D_p} = \frac{E^*}{1+\left(d^*/d\right)^C} * \frac{dN_{CN}}{d\log D_p} \tag{5.3}$$

Integrating Equation (5.3) for all sizes gives the total CCN concentration (N_{CCN}) in cm^{-3}:

$$N_{CCN} = \int_0^\infty \frac{dN_{CCN}}{d\log D_p} * d\log D_p \tag{5.4}$$

5.3.3 CCN closure and mixing state

CCN closure is defined as a comparison between measured (obtained from the integrated CCN distributions) and predicted CCN concentrations. CCN closures are performed to determine how well Köhler theory can predict CCN formation when the chemical composition and mixing state of the aerosol are known. To predict CCN concentrations, the supersaturation, the aerosol size distribution, and aerosol chemical composition (bulk or size resolved) is needed. Data from the SMCA technique (CN and CCN; 120 s), PILS-IC (200 s) and PILS-WSOC (620 s) were used to perform the closure. Since small perturbations in temperature can change the supersaturation in the column (Roberts and Nenes, 2005; Ervens et al., 2007), scans in which there were temperature transients were removed from the analysis. Given that the SMCA and chemical composition measurements have different time resolutions, the chemical composition data was binned to match the SMCA time stamp as shown in Figure 5. 4.

The total CCN concentration at each supersaturation was determined by calculating the minimum aerosol diameter or the activation diameter, d_c, from Köhler theory (Köhler, 1936):

$$d_c = \left(\frac{256 M_w^3 \sigma^3}{27 R^3 T^3 \rho_w^3} \right)^{1/3} \left[\sum_i \left(\frac{M_w}{\rho_w} \right) \left(\frac{\rho_i}{M_i} \right) \varepsilon_i \upsilon_i \right]^{-1/3} s^{-2/3} \tag{5.5}$$

where M_w is the molar mass of water, σ is the surface tension of the solution, R is the ideal gas constant, T is the temperature, ρ_w is the density of water, s is the supersaturation, and ρ_i, ε_i, υ_i, and M_i are the density, volume fraction, effective van't Hoff factor and molar mass of the solute i (sulfuric acid (H_2SO_4), ammonium bisulfate (NH_4HSO_4), ammonium sulfate ($(NH_4)_2SO_4$), and ammonium nitrate(NH_4NO_3), and organic), respectively. The sulfate molar ratio, SR = $[NH_4^+]/[SO_4^{2-}]$, was used to determine which salts (H_2SO_4, NH_4HSO_4, $(NH_4)_2SO_4$, and NH_4NO_3) will be present in

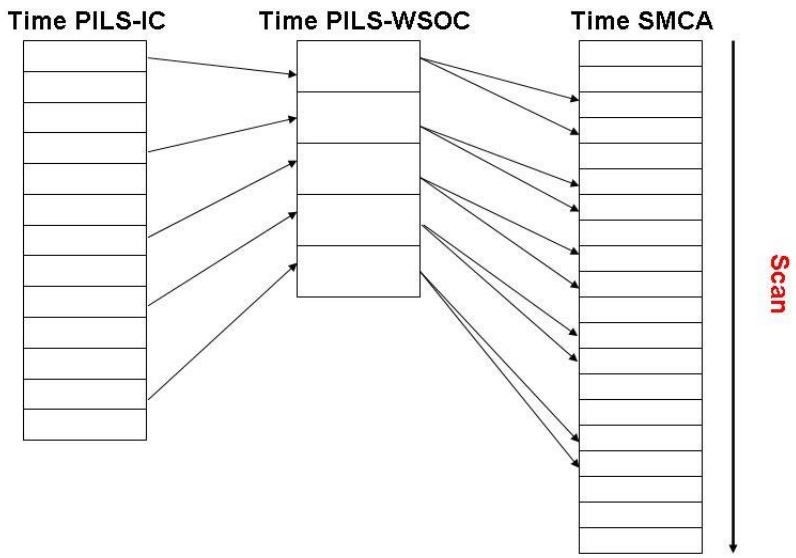

Figure 5. 4: Visual representation of chemical composition binning to the scan times.

the aerosol phase. When SR ≤ 1, the sulfate and ammonium are a mixture of H_2SO_4 and NH_4HSO_4, when 1 < SR < 2, the sulfate and ammonium are a mixture of NH_4HSO_4 and $(NH_4)_2SO_4$ and when SR ≥ 2, the sulfate and ammonium are composed of $(NH_4)_2SO_4$ and NH_4NO_3 (if NH_4^+ is in excess). ε_i is related to the mass fraction of i, x_i, as:

$$\varepsilon_i = \frac{x_i/\rho_i}{\sum_j (x/\rho)_j} \tag{5.6}$$

For the closure, the effective van't Hoff factor of organics was assumed to be 1 (Cruz and Pandis, 1997; Raymond and Pandis, 2002; Broekhuizen et al., 2004; Abbatt et al., 2005; Hartz et al., 2006), while for H_2SO_4, NH_4HSO_4, $(NH_4)_2SO_4$, and NH_4NO_3 values of 2, 2.5, 2.5 and 2 were used, respectively (Svenningsson et al., 2006; Murphy et al., 2009).

The total predicted CCN ($N_{CCN,predicted}$) is obtained by integrating the aerosol size distribution for all diameters greater than d_c:

$$N_{CCN,predicted} = \int_{d_c}^{\infty} \frac{dN_{CCN}}{d\log D_p} * d\log D_p \tag{5.7}$$

Two different CCN closure schemes, EXT and INT, can be performed based on the chemical composition given (bulk) and mixing state of the aerosol observed (E, obtained from the CCN spectrum). Aerosols can be either externally mixed, each aerosol comes from a different source, or internally mixed, aerosols of the same size have a uniform mixture of components or have the same source. For this study, we consider the external particles to be the same size as the internal particles; however, a fraction are considered as completely soluble while the rest are treated as completely insoluble (Figure 5. 5).

In order to determine the chemical composition (salts and organics) present in the soluble and insoluble particles in the external mixture, a mass balance was performed. Based on the degree of particle mixing (assuming all particle sizes have the same degree of mixing), E, we split the aerosol size into E soluble particles and $1 - E$ insoluble particles. The soluble particles are assumed to be composed of salts ($(NH_4)_2SO_4$, NH_4HSO_4, H_2SO_4, and NH_4NO_3) and soluble organics while the insoluble particles are made of only organics. Since mass needs to be conserved:

$$m_{INT} = m_{EXT,sol} + m_{EXT,ins} = E * m_{INT} + (1-E) * m_{INT} \tag{5.8}$$

where m_{INT}, $m_{EXT,sol}$, $m_{EXT,ins}$ are the total aerosol mass, the soluble aerosol mass, and the insoluble aerosol mass, respectively. By the definition of the particles composition above, the total organic mass, m_{org}, is:

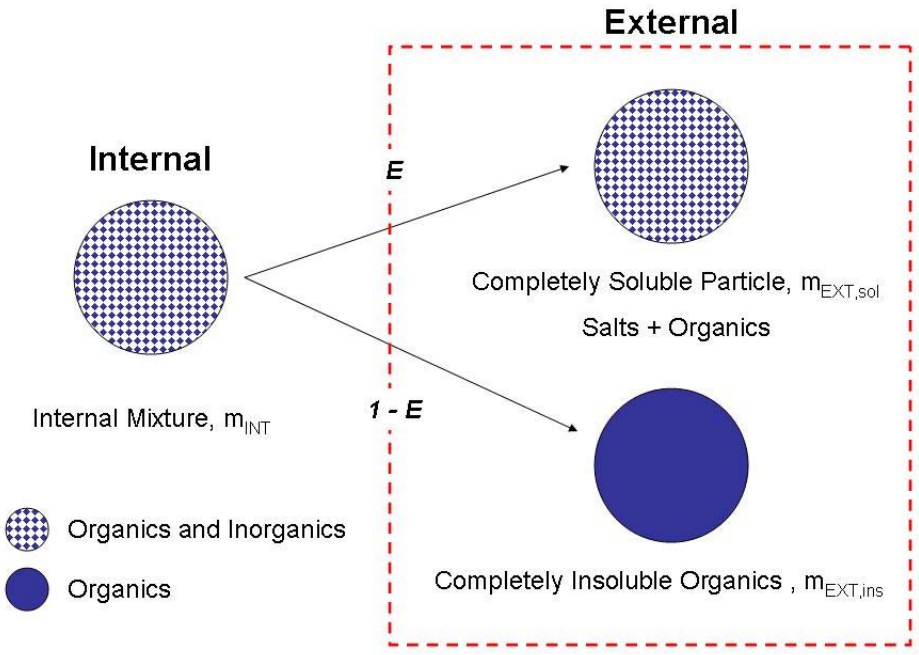

Figure 5. 5: Aerosol mixing state.

$$m_{org} = m_{org,sol} + m_{org,ins} \tag{5.9}$$

where $m_{org,sol}$ and $m_{org,ins}$ are the soluble and insoluble organic mass. Then the insoluble external particle mass is:

$$m_{EXT,ins} = m_{org,ins} = (1-E) * m_{INT} \tag{5.10}$$

while the soluble particle mass is defined by:

$$m_{EXT,sol} = E * m_{INT} = m_{salts} + m_{org,sol} \tag{5.11}$$

where m_{salts} is the total soluble salt mass. By rearranging Equation (5.11), $m_{org,sol}$ can be solved and the mass fraction of each component determined.

The difference between the EXT and INT is in how the mixing state of the aerosol is treated. For the EXT, only the internally soluble particle fraction (within the external mixture) is considered to contribute to particle formation; whereas for the INT, the aerosol is completely internally mixed. In addition to the different aerosol mixing states the effect of chemical composition and surface tension where explored. Within the external mixture closure, three different chemical composition and surface tension scenarios where considered: EXT-SOL, EXT-ALLSOL, and EXT-ALLSOL-ST. For the EXT-SOL scenario, the total predicted CCN is first calculated by assuming the aerosol is composed of pure $(NH_4)_2SO_4$ and then multiplying it by the soluble components (i.e., only inorganic salts). Both EXT-ALLSOL and EXT- ALLSOL-ST assume all components within the particle are soluble but treat the surface tension differently. In EXT-ALLSOL the surface tension of water is used; while in EXT- ALLSOL-ST a 25% surface tension from organics is assumed.

For the internal mixture closure scheme, four different chemical composition and surface tension scenarios are considered: INT-AS, INT-SALTS, INT-ALLSOL, and INT-ALLSOL-ST. For INT-AS, INT-SALTS, and INT-ALLSOL, the surface tension of water is assumed; whereas on INT- ALLSOL-ST a 25% surface tension depression from organics is prescribed. In INT-AS the aerosol is assumed to be composed of pure $(NH_4)_2SO_4$; while on the others it is assumed to be made of inorganics and organics as determined from the PILS measurements. In INT-SALTS only the inorganic salts are considered to contribute solute (e.g., $\upsilon_{org} = 0$) whereas in INT-ALLSOL and INT-ALLSOL-ST all components are treated as soluble (e.g., $\upsilon_{org} = 1$).

The total CCN predicted from the 7 CCN closure scenarios explained above are compared to the total CCN (obtained from SMCA) graphically. The CCN closure agreement between predicted and observed values is performed by a least-squares linear fitting. Besides the correlation that can be obtained from the linear fit, the closure

agreement can be determined in terms of two error metrics, the Normalized Mean Error (NME) and the Normalized Mean Bias (NMB). These two are defined as:

$$NME = \frac{\sum_{i}^{n} |P_i - O_i|}{\sum_{i}^{n} O_i} \tag{5.12}$$

and

$$NMB = \frac{\sum_{i}^{n} P_i - O_i}{\sum_{i}^{n} O_i} \tag{5.13}$$

where P and O are the predicted and measured total CCN obtained for each scan, i. The NME and NMB show the degree of scatter and biases between the predicted and measured CCN concentrations, respectively.

5.4 Results and discussion

5.4.1 Total CN concentration comparison

Since two different CPCs (3022 and 3010) were used in the SMCA setup, a comparison of CN concentration between the two had to be done. The comparison of the CPCs was performed for the data collected from August 15th till the 26th which is the time period in which the CPC 3010 measured total CCN in parallel to the SMCA (Figure 5. 1; Setup A2). In order to compare the two instruments the total CN from the SMCA method was obtained by integrating the particle size distribution. Since both instruments have different particle size detection limits (7 nm and 10 nm for CPC 3022 and CPC 3010, respectively), the particle size distribution obtained from the SMPS (DMA and CPC 3022) was integrated from 10 nm onwards to match the size range of the CPC 3010. In

addition, only scans in which both modes (no partial modes) appear and the total CN remains constant throughout the scan are considered. Based on the measurements, the CPC 3022 was found to undercount the total CN concentration from the CPC 3010 by 37% (Figure 5. 6). The difference in concentration observed between both CPCs comes from a combination of factors: *i*) a bias that exists between the two CPC's and *ii*) the maximum detectable particle size of the instruments. When the CPC 3010 and CPC 3022 were compared by sampling room air in the laboratory, we observed a 15% bias between the two with the CPC 3010 always having the higher concentration. It has been observed that the bias between the two instruments gets worse as the aerosol concentrations increase. This is consistent with the lower particle concentration range of the CPC 3010 which is able to detect 10^4 particles cm^{-3} with little coincidence (< 10%) while the CPC

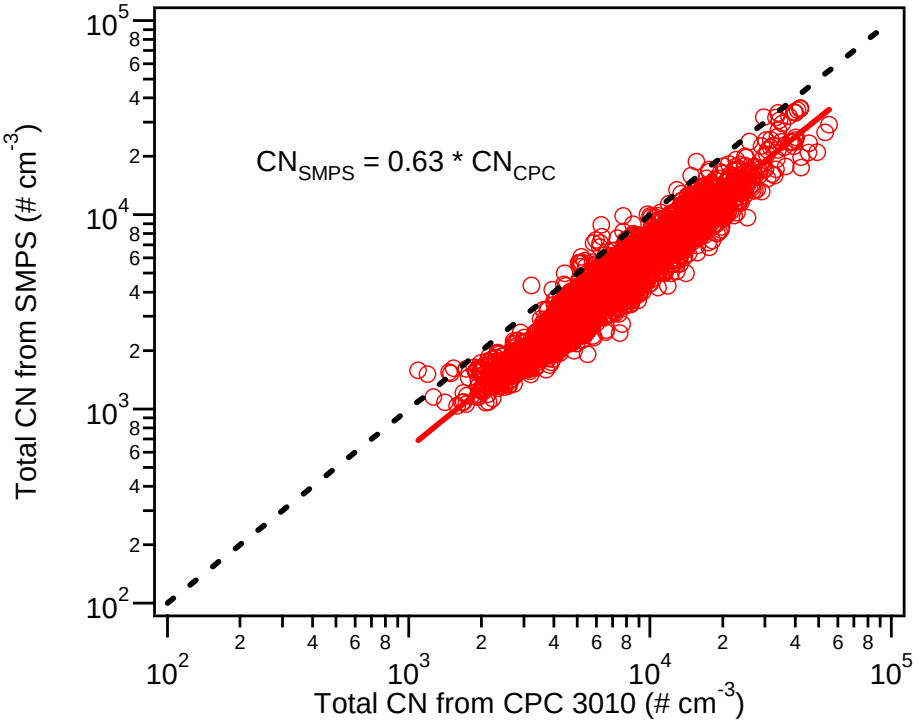

Figure 5. 6: Scatter plot of total CN obtained from the SMPS distribution versus that measured by the CPC.

3022 is able to go to 10^7 particles cm^{-3}. These corrections were applied to the total CN and CCN concentrations obtained for Setup A1 and A2 before the CCN closure analysis was performed. The total CN and CCN time-series (after correction) are shown in Figure 5. 7. Throughout the campaign the CCN was found to correlate well with the CN concentration and increased with supersaturation (Figure 5. 7).

5.4.2 HYSPLIT trajectories

HYSPLIT trajectories (www.arl.noaa.gov/ready/hysplit4.html) were run and used to determine the characteristics and origin of the air masses affecting JST throughout the campaign. From the trajectories results, three periods were determined: Period A, Period B, and Period C (Figure 5. 8). Periods A and C (August 1st till the 23rd and August 29th till September 15th; beginning and end of the campaign) are affected by "polluted" air masses that originate from the continental US (from August 1st till the 23rd and from

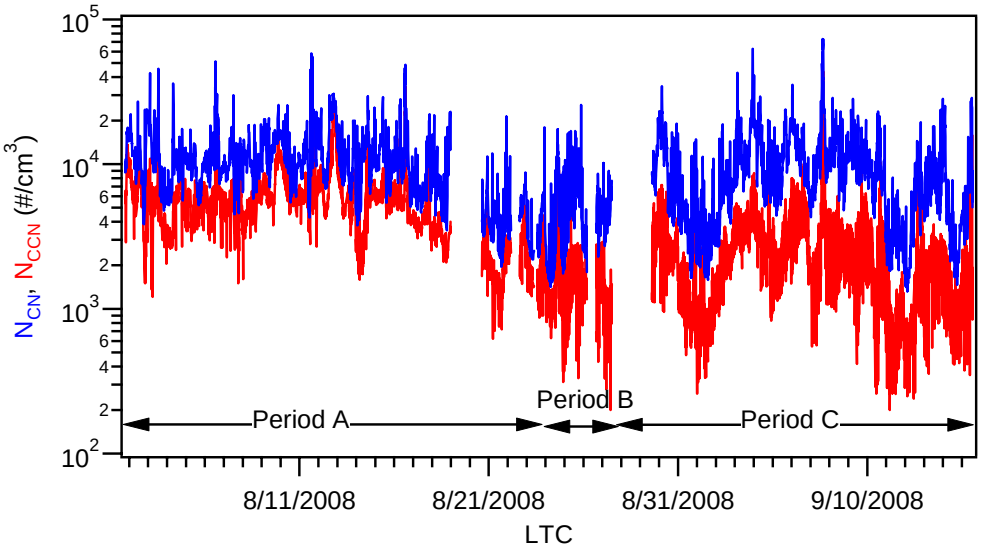

Figure 5. 7: Total CN and CCN time-series for whole AMIGAS campaign. Periods A and C correspond to "polluted" air masses originating from the continental US; while period B corresponds to "cleaner" air masses originating from either the Atlantic Ocean or Gulf of Mexico. Gaps in data correspond to times where the power was down or there were problems with one of the instruments.

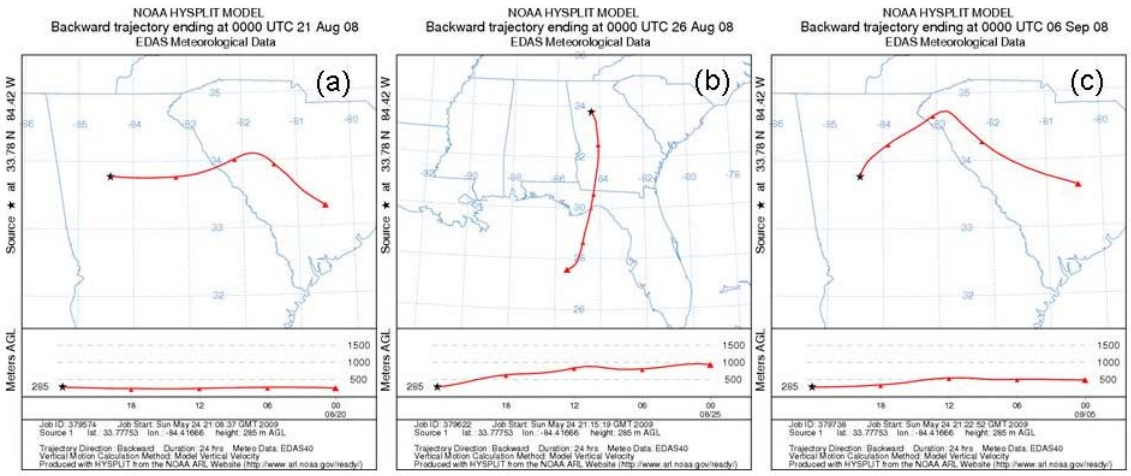

Figure 5. 8: HYSPLIT one day trajectories representative of the three air masses sampled in JST during the AMIGAS campaign. Plots (a) and (c) represent "polluted" air masses which originated from the continental US; while plot (b) represents a "cleaner" air mass which originated from the Gulf of Mexico. During August 24th till the 27th, the air masses originated either from the Atlantic Ocean or Gulf of Mexico.

August 28th till the end of the campaign); while Period B is influenced by "cleaner" air masses that originate either from the Atlantic Ocean or the Gulf of Mexico (August 24th till the 27th). The effect of these different masses on JST site is not only evident in the total CN and CCN concentrations, (Figure 5. 7) which decrease with the "cleaner" air masses, but also in the particle size and CCN distribution (Figures 5. 9 and 5. 10).

5.4.3 CCN closure

A number of CCN closures were performed in which different mixing states and chemical composition scenarios were considered. The different scenarios were run in order to gain a better understanding of the system studied. The CCN closures were performed for internal and external mixtures based on the information obtained from the CCN activity spectrum (Figure 5. 3; 1 – E and supersaturation in the column), particle size distribution, and chemical composition. This data was used to calculate d_c (Equation (5.11)) and consequently the predicted CCN concentration by integrating the CCN

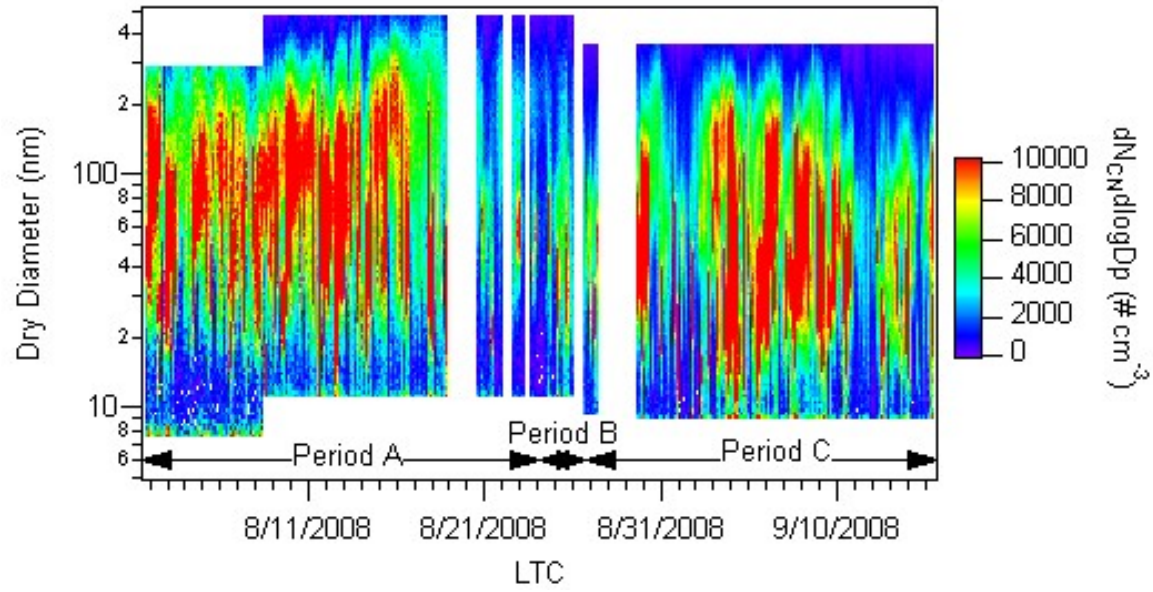

Figure 5. 9: Dry particle size distribution time-series.

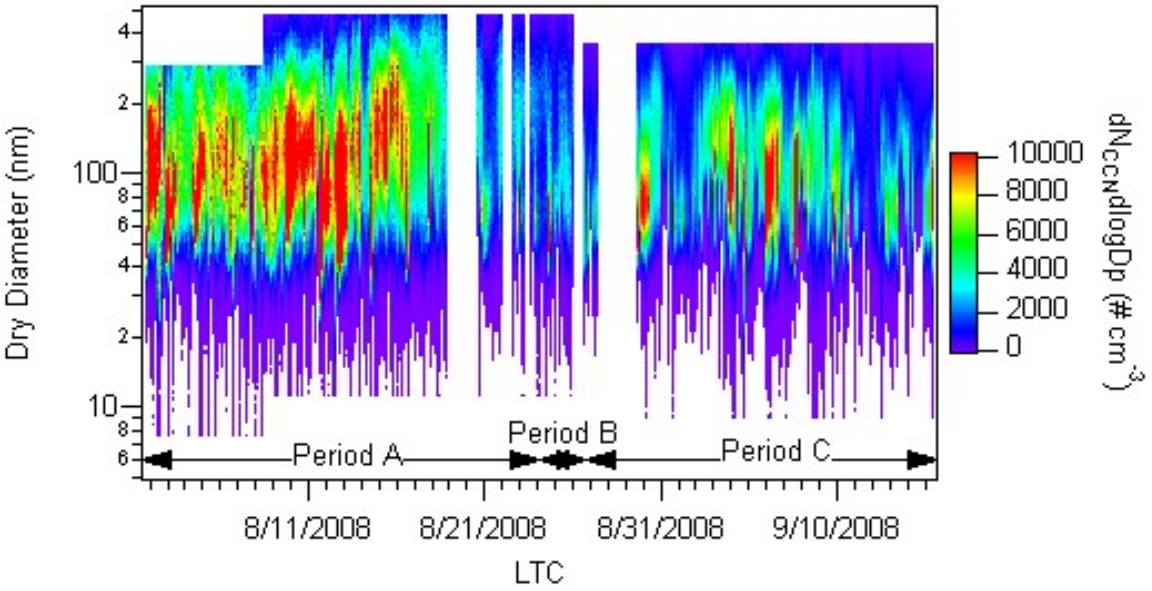

Figure 5. 10: CCN distribution time-series.

distribution from d_c onward (Equation (5.13)).

Since the SMCA technique and the sigmoidal fit (Equation (5.7)) provide us with the characteristic activation diameter, a comparison between the measured and predicted d_{p50} can be performed. For the internal mixture case, a diameter comparison was done for the 4 chemical composition and surface tension scenarios (Figure 5. 11). For all scenarios considered, theory predicts that, a smaller diameter (than that measured) is needed to activate the particles. From all the internal mixture scenarios, INT-SALTS and INT-ALLSOL provide the best closure (d_{p50} is still underpredicted by 20 and 25%, respectively). For the external mixture case, a comparison was done for the EXT-ALLSOL and EXT- ALLSOL-ST cases. As with the internal mixture scenarios, the activation diameter was underpredicted and a better closure was achieved for the former

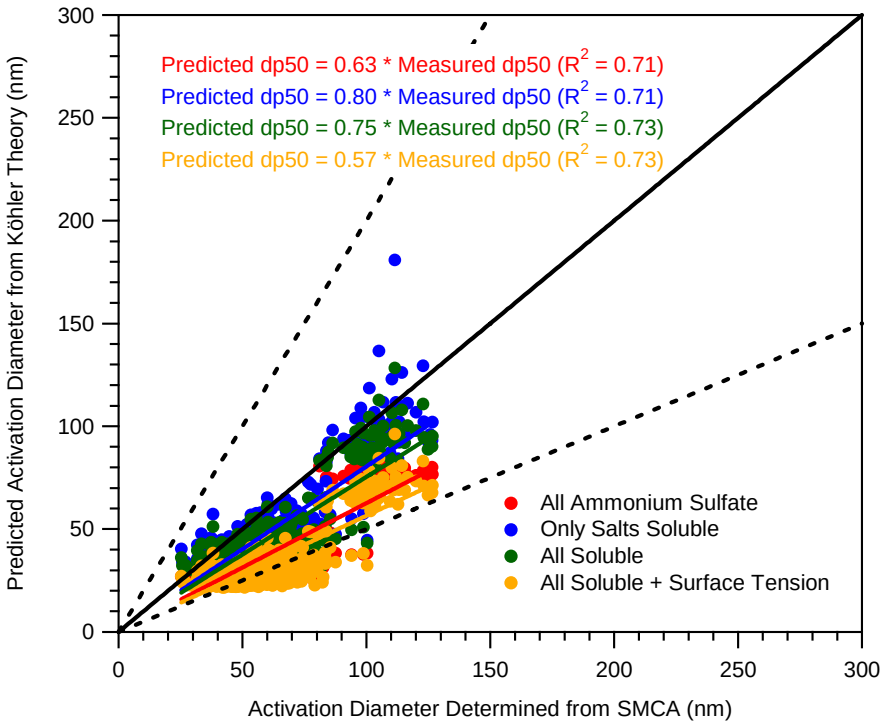

Figure 5. 11: d_{p50} closure for the internal mixture case. The red, blue, green, and yellow circles correspond to the INT-AS, INT-SALTS, INT-ALLSOL, and INT-ALLSOL-ST cases, respectively.

scenario (Figure 5. 12).

The predicted d_{p50} for each case was used to determine the theoretical CCN concentration and compared to that measured. As expected from the activation diameter results (Figures 5. 11 and 5. 12), a discrepancy between the predicted and measured CCN concentration was observed for all scenarios within the internal and external mixture case (Figures 5. 13 and 5. 14). Consistent with the d_{p50} closure plots, the best CCN closures from the internal case where achieved using the INT-SALTS and INT-ALLSOL scenarios (Figure 5. 13); whereas EXT-ALLSOL was for the external case (Figure 5. 14). Based on the closure results and the NBE and NMB values obtained (Table 5. 1), it is evident that the organics present in the particles should not be considered as soluble as $(NH_4)_2SO_4$ or completely insoluble. Therefore it is likely that

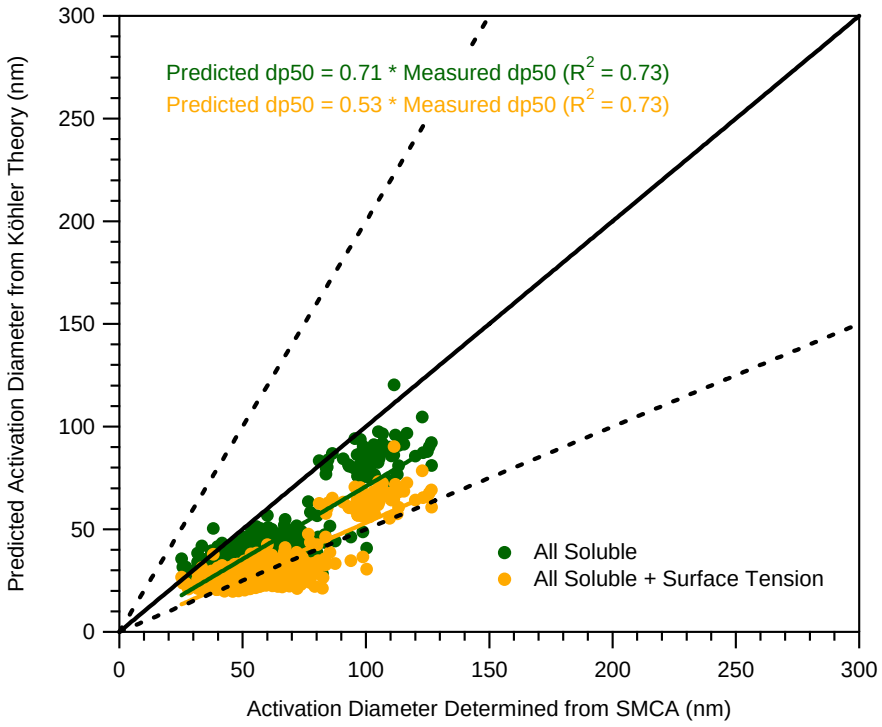

Figure 5. 12: d_{p50} closure for the internal mixture case. The red, blue, green, and yellow circles correspond to the EXT-SOL, EXT-ALLSOL, and EXT-ALLSOL-ST cases, respectively.

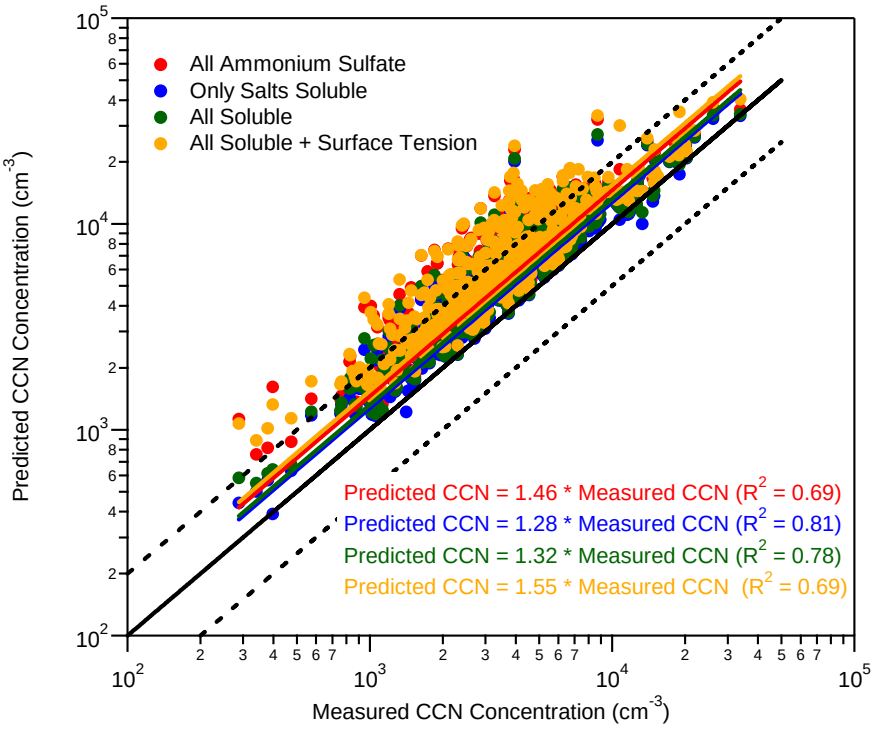

Figure 5. 13: CCN closure plot for the internal mixture case. The red, blue, green, and yellow circles correspond to the INT-AS, INT-SALTS, INT-ALLSOL, and INT-ALLSOL-ST cases, respectively.

some organics do contribute solute and possibly depress surface tension (but not as much as 25%). Not accounting for the size-resolved chemical composition and mixing state in the CCN closure are prime sources of CCN prediction error. Additional error in the CCN closure could be due to the presence of residual water (associated with NH_4NO_3 and NH_4HSO_4, which have efflorescence RH below 15% RH) in the particle, which would translate to a positive CCN prediction bias. Thermodynamic calculations (for the conditions in the experiment) suggests that this bias may not be important (not shown).

For all the CCN closure analysis performed, a uniform external mixture fraction (1- *E* at diameter > 150 nm) was assumed for all particle sizes. This is of course an "upper limit" scenario of external mixing, as larger particles tend to be more internally mixed (have a lower 1- *E*; see Section 5.4.4). Therefore using a uniform external mixture for all sizes will lead to an overestimation in CCN concentration for the external mixture

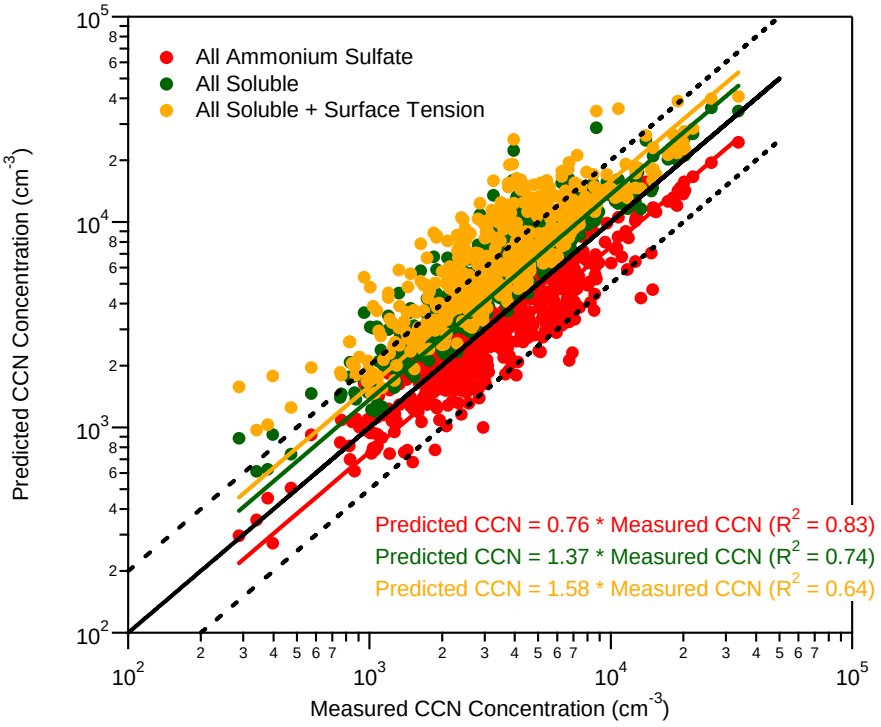

Figure 5. 14: CCN closure plot for the external mixture case. The red, green, and yellow circles correspond to the EXT-SOL, EXT-ALLSOL, and EXT-ALLSOL-ST cases, respectively.

Table 5. 1: CCN closure analysis error metrics for entire AMIGAS campaign.

CCN Closure Scenario	NME	NMB
INT-AS	0.668	0.668
INT-SALTS	0.415	0.406
INT-ALLSOL	0.476	0.472
INT-ALLSOL-ST	0.759	0.759
EXT-SOL	0.267	-0.191
EXT-ALLSOL	0.536	0.534
EXT-ALLSOL-ST	0.819	0.819
SR_EXT	0.139	0.113

cases, EXT-ALLSOL and EXT-ALLSOL-ST, when compared to their equivalent internal mixture scenarios (e.g., INT-ALLSOL and INT-ALLSOL-ST). Therefore a more precise knowledge of mixing state (as function of size; see Section 5.4.4) as well as chemical composition (size-resolved) is needed to achieve closure.

5.4.4 Mixing state as a function of dry diameter

Since the DMA in SMCA provides the dry diameter with time, the external fraction at each dry diameter size can be obtained from our measurements by creating a CCN activity spectrum as a function of supersaturation. In order to do this, we first have to calculate the CCN/CN ratio for specific dry diameters by using the sigmoid parameters (E, C, and d_{50}^{*} obtained from fitting the measured data to Equation (5.1)) obtained from each scan (which correspond to a specific supersaturation). Then a CCN activity spectrum, as a function of supersaturation, can be obtained for a constant dry diameter as shown in Figure 5. 15. Finally a sigmoidal fit similar to that in Equation (5.1) can be fitted to the CCN spectrum:

$$\frac{CCN}{CN} = \frac{E}{1+\left(s_c^{*}/s\right)^{C}} \tag{5.14}$$

where s_c^{*} is the characteristic supersaturation or critical supersaturation needed for the particle to activate. In Equation (5.14), E represents the fraction of particles within a specific size that are internally mixed and C represents the degree of chemical heterogeneity of the particles . This proves to be a powerful method since it demonstrates that information obtained from SMCA can be used to determine the external fraction of all particle sizes as shown in Figure 5. 16, and further improve CCN closures calculations.

An extra CCN closure (SR_EXT) was performed using the size resolved mixing

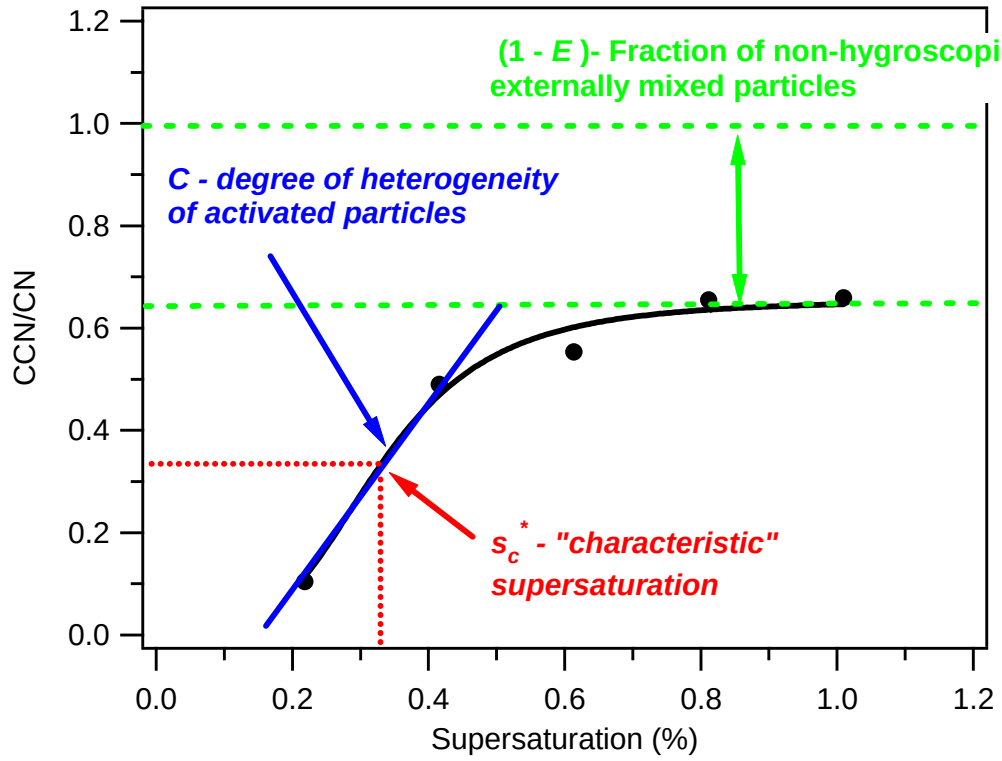

Figure 5. 15: Example of an ambient CCN activity spectrum (at constant dry diameter) with sigmoid fit and its defined parameters.

state obtained from the fitted CCN activity spectrum at a constant dry diameter. For SR_EXT, the activated or internal mixture fraction (E) of the aerosol was assumed to be completely soluble (since it activates) and with the surface tension of water. $N_{CCN,predicted}$ is obtained by applying Equation (5.7), during which total CCN concentration at each size bin is calculated based on its mixing state (E). Compared to the internal and external closure scenarios previously discussed, introducing size-resolved mixing state improves CCN closure significantly (average overprediction = 6%; Figure 5.17). Since size-resolved mixing state was considered here, it is likely that the remaining error is due to the assumption of size average composition.

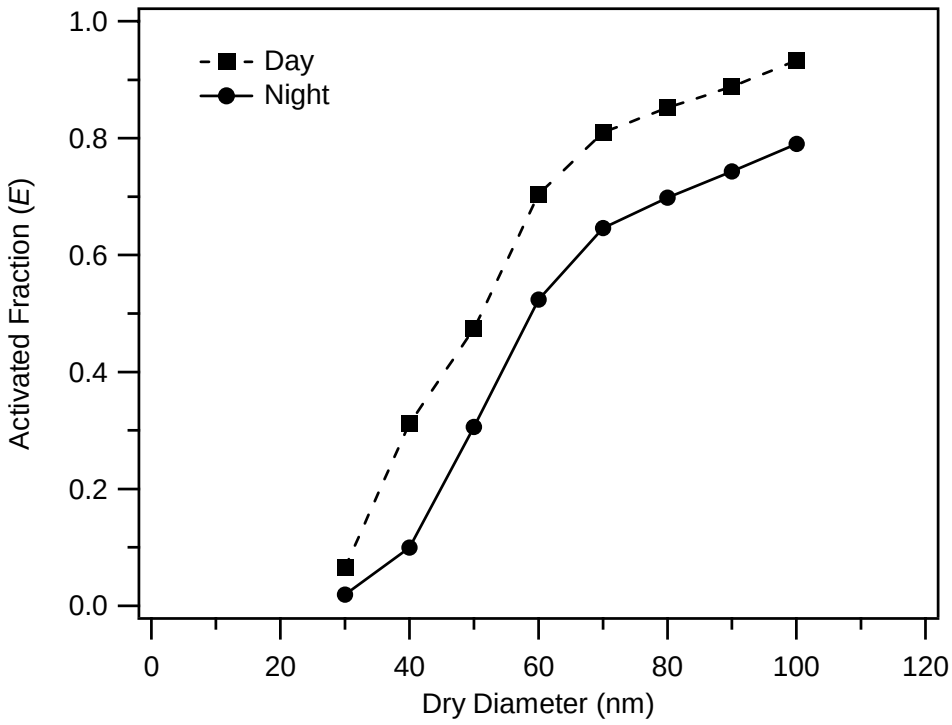

Figure 5. 16: Example of activation fraction as function of particle size for a day (square) and night (circle) sample. The smaller the particles the more externally mixed they become (smaller *E*).

5.4.5 Droplet growth kinetics

The measured activated droplet size as a function of dry diameter was used to assess the effect of organics on activation kinetics (at the point of activation). In Figure 5. 18, the droplet size at the point of activation (D_p corresponding to d_{p50}) for a subset of the ambient data is plotted against the instrument supersaturation. The droplet sizes for ambient aerosol is compared to the droplet size achieved by $(NH_4)_2SO_4$ aerosol at the same supersaturation as that in the instrument. If droplets formed from ambient CCN are smaller than calibrations, it is said that organics can retard the activation process.

From the results of this campaign (Figure 5. 18), it seems that for the most part Atlanta aerosol has similar growth to $(NH_4)_2SO_4$. However, an increase in the amount of particles that exhibit retarded activation kinetics was observed at higher supersaturations.

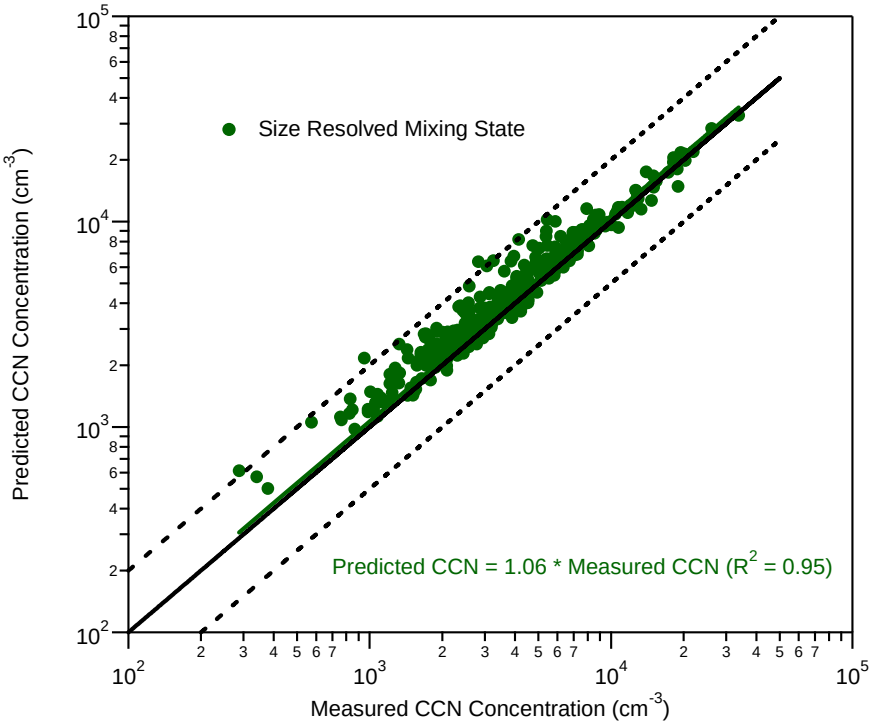

Figure 5. 17: CCN closure plot for the size resolved external mixture (SR_EXT).

The quantity of outliers was shown to increase with supersaturation (e.g., lower activation diameters) from 4% (at 0.2% supersaturation) to 9% (at 1.0% supersaturation) of the total data points. Of these, some points were found to lie within the variability of the average droplet diameter, especially for the lower supersaturations. The apparent growth delay at the higher supersaturations could be related to the externally mixed nature of the smaller particles (see Section 5.4.4), some of which may contain organics that retard CCN activation kinetics. Overall, there was no relationship between the observed smaller droplet diameters and the fraction of organic present in the aerosol; therefore it is likely that a combination of the hygroscopic nature (hygroscopic versus hydrophilic) and mixing state of the aerosols controls the droplet growth.

Additional to the droplet growth curve shown, the droplet size versus dry diameter for particles with different droplet growth kinetics (at the same supersaturation) was addressed. The idea was to compare the droplet size distribution as a function of

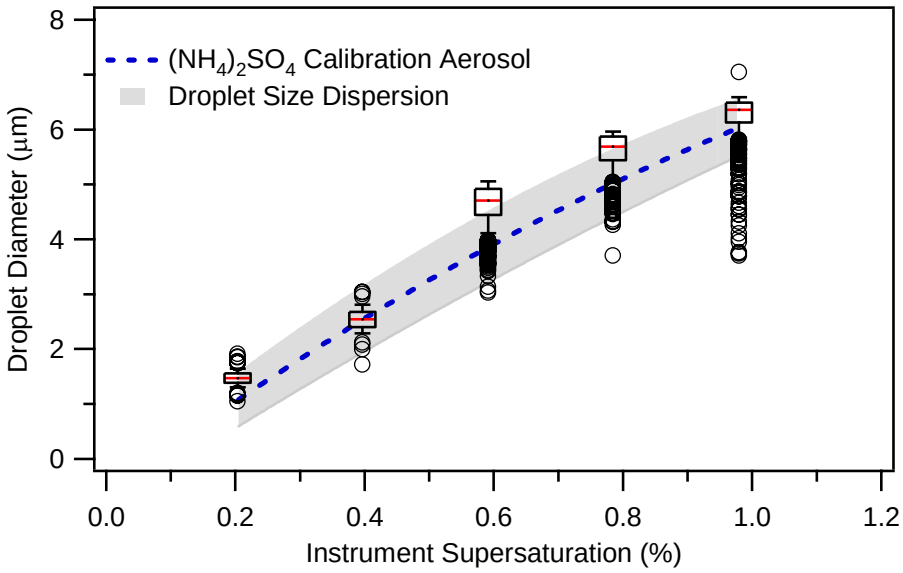

Figure 5. 18: Droplet growth kinetics study analysis. Box plots for droplet size at the point of activation grouped by supersaturation. The whiskers represent the 10th and 90th percentile; therefore capturing 90% of the points. Outliers shown as open circles represent those points that are 1.5 times the interquartile range (box width). The dashed blue line corresponds to the $(NH_4)_2SO_4$ calibration droplet size at activation at the same supersaturation. The grey band represents the variability in the average droplet distribution.

particle size and see if the particles that exhibit delayed growth remained smaller (than the ones that grow as fast as $(NH_4)_2SO_4$) at higher diameters. In Figure 5. 19, the droplet distribution, normalized with the total CCN concentration, is plotted against the particle dry diameter for two scans (one for particles that experience droplet growth delay (a) and one that does not (b)) at the same supersaturation (1.0% SS nominal). By normalizing the droplet counts, the peak of the droplet distribution can be compared against the average droplet sizes from the activation of $(NH_4)_2SO_4$ calibration aerosol. It is evident from Figure 5. 19, that once the CCN activates (diameter is greater that d_{p50}), droplets will grow as fast as calibration aerosol. This implies that once the kinetic activation barrier is overcome, droplets resume growth rates comparable with deliquescent salts.

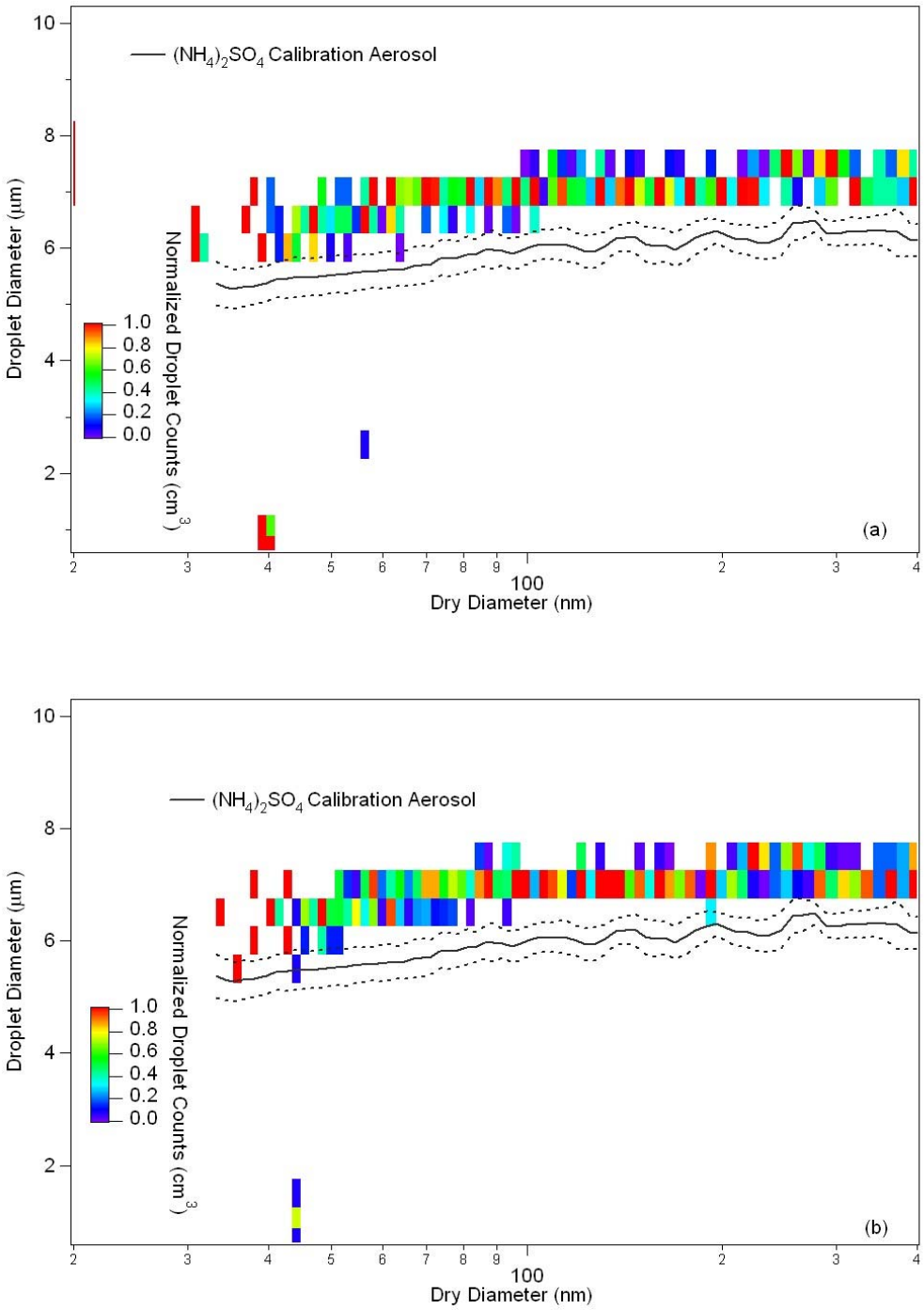

Figure 5. 19: Droplet size distribution versus particle dry diameter for: a) a particle that experiences delayed droplet growth and b) a particle that grows as fast as $(NH_4)_2SO_4$ at activation. The CCN counts are normalized with the total CCN concentration measured at each time. The black line represents the average droplet size versus particle dry diameter of $(NH_4)_2SO_4$ calibration aerosol at the same supersaturation as the scan (1.0% nominal). The dashed line represents the variability (one standard deviation) in the average droplet diameter.

5.5 Conclusions

Size-resolved CCN measurements were performed during the AMIGAS campaign which took place in Atlanta, GA from August 1st till September 15th. The size-resolved data and activation ratio (CCN/CN) was obtained with SMCA. The CCN activity spectrum (CCN/CN versus dry diameter) acquired by the size-resolved measurements provides a lot of information about the aerosol mixing state (activation fraction, CCN/CN), heterogeneity, and activation characteristics (activation diameter and corresponding supersaturation). Additionally, the SMCA data (particle size distribution and CCN measurements) were coupled to chemical composition measurements to perform CCN closures in which different chemical composition and mixing state scenarios were considered.

Three distinct air mass periods were sampled throughout the campaign. Period A and C (beginning and end of the field mission) were characterized by "polluted" air masses originating from the continental US; while Period B was characterized by "cleaner" air masses originating from either the Atlantic Ocean or the Gulf of Mexico. Higher CN and CCN concentrations were consistent with the "polluted" air masses; while lower CN and CCN concentrations were observed during the "clean" air mass period. A change was observed not only in concentration but also in the distributions, when different air masses where affecting the site.

A total of eight CCN closures were performed in which different chemical composition and mixing state scenarios were considered. Of all the cases considered, the best closure was achieved for the size-resolved mixing state scenario (6%) even when a size average chemical composition was considered. It is likely that the CCN closure would further improve with size resolved composition. Based on the results of these analyses, it is important to know the composition and mixing state of aerosols to predict CCN more accurately. As for the activated CCN, most of the aerosols sampled during the

campaign experienced growth similar to $(NH_4)_2SO_4$ although there is evidence of some droplet growth delay. The droplet growth kinetic limitations were the most evident at the higher supersaturations (smaller aerosol size and likely to have more organics). Our results suggest that after activation, CCN assume rapid growth, similar to that of $(NH_4)_2SO_4$.

5.6 References

Abbatt, J. P. D., Broekhuizen, K. and Kumal, P. P.: Cloud condensation nucleus activity of internally mixed ammonium sulfate/organic acid aerosol particles, Atmos. Environ., 39(26), 4767-4778, 2005.

Albrecht, B. A.: Aerosols, cloud microphysics, and fractional cloudiness, Science, 245, 1227-1230, 1989.

Bigg, E. K.: Discrepancy between observation and prediction of concentrations of cloud condensation nuclei, Atmospheric Research, 20, 82 - 86, 1986.

Bougiatioti, A., Fountoukis, C., Kalivitis, N., Pandis, S. N., Nenes, A. and Mihalopoulos, N.: Cloud condensation nuclei measurements in the eastern Mediterranean marine boundary layer: CCN closure and droplet growth kinetics, Atmos. Chem. Phys. Discuss., 9, 10303 - 10336, 2009.

Broekhuizen, K., Chang, R. Y.-W., Leaitch, W. R., Li, S.-M. and Abbatt, J. P. D.: Closure between measured and modeled cloud condensation nuclei (CCN) using size-resolved aerosol compositions in downtown Toronto, Atmos. Chem. Phys., 6, 2513-2524, 2006.

Broekhuizen, K., Kumar, P. P. and Abbatt, J. P. D.: Partially soluble organics as cloud condensation nuclei: Role of trace soluble and surface active species, Geophys. Res. Lett., 31(1), Art. No. L01107, doi: 10.1029/2003GL018203, 2004.

Cantrell, W., Shaw, G., Cass, G., Chowdhury, Z., Hughes, L., Prather, K., Guazzotti, S. and Coffee, K.: Closure between aerosol particles and cloud condensation nuclei at Kaashidhoo climate observatory, Journal of Geophysical Research - Atmospheres, 106(D22), 28,711 - 28, 718, 2001.

Chang, R. Y.-W., Liu, P. S. K., Leaitch, W. R. and Abbatt, J. P. D.: Comparison between measured and predicted CCN concentrations at Egbert, Ontario: Focus on the organic aerosol fraction at a semi-rural site, Atmospheric Environment Part a-General Topics, 41(37), 8172 - 8182, 2007.

Corrigan, C. E. and Novakov, T.: Cloud condensation nucleus activity of organic compounds: a laboratory study, Atmos. Environ., 33(17), 2661-2668, 1999.

Covert, D., Gras, J., Wiedensohler, A. and Stratmann, F.: Comparison of directly measured CCN with modeled CCN from the number-size distribution in the marine boundary layer during ACE 1 at Cape Grim, Tasmania, Journal of Geophysical Research - Atmospheres, 103(D13), 16597 - 16608, 1998.

Cruz, C. N. and Pandis, S. N.: A study of the ability of pure secondary organic aerosol to act as cloud condensation nuclei, Atmos. Environ., 31(15), 2205-2214, 1997.

Cubison, M. J., Ervens, B., Feingold, G., Docherty, K. S., Ulbrich, I. M., Shields, L., Prather, K., Hering, S. and Jimenez, J. L.: The influence of chemical composition and mixing state of Los Angeles urban aerosol on CCN number and cloud properties, Atmos. Chem. Phys., 8, 5649-5667, 2008.

Ervens, B., Cubison, M., Andrews, E., Feingold, G., Ogren, J. A., Jimenez, J. L., DeCarlo, P. and Nenes, A.: Prediction of cloud condensation nucleus number concentration using measurements of aerosol size distributions and composition and light scattering enhancement due to humidity, Journal of Geophysical Research - Atmospheres, 112, D10S32, doi:10.1029/2006JD007426, 2007.

Hartz, K. E. H., Tischuk, J. E., Chan, M. N., Chan, C. K., Donahue, N. M. and Pandis, S. N.: Cloud condensation nuclei activation of limited solubility organic aerosol, Atmos. Environ., 40(4), 605-617, 2006.

IPCC: Climate Change (2001): The Scientific Basis, ed, Cambridge University Press, United Kingdom, 2001.

Köhler, H.: The nucleus in and the growth of hygroscopic droplets, Transactions of the Faraday Society, 32(2), 1152-1161, 1936.

Lance, S., Medina, J., Smith, J. N. and Nenes, A.: Mapping the operation of the DMT continuous flow CCN counter Aerosol Sci. Technol., 40, 242-254, 2006.

Liu, P., Leaitch, W., Banic, C., Li, S., Ngo, D. and Megaw, W.: Aerosol observations at Chebogue Point during the 1993 North Atlantic Regional Experiment: Relationships among cloud condensation nuclei, size distribution, and chemistry, Journal of Geophysical Research - Atmospheres, 101, 28971 - 28990, 1996.

Martin, G. M., Johnson, D. W. and Spice, A.: The measurement and parameterization of effective radius of droplets in warm stratocumulus clouds, Journal of Atmospheric Science, 51, 1823 - 1842, 1994.

McMurry, P. H., Wang, X., Park, K. and Ehara, K.: The relationship between mass and mobility for atmospheric particles: A new technique for measuring particle density, Aerosol Sci. Technol., 36(2), 227-238, 2002.

Medina, J., Nenes, A., Sotiropoulou, R. E. P., Cottrell, L. D., Ziemba, L. D., Beckman, P. J. and Griffin, R. J.: Cloud condensation nuclei closure during the International Consortium for Atmospheric Research on Transport and Transformation 2004 campaign: Effects of size-resolved composition, Journal of Geophysical Research - Atmospheres, 112, D10S31, doi:10.1029/2006JD007588, 2007.

Murphy, S. M., Agrawal, H., Sorooshian, A., Padro, L. T., Gates, H., Hersey, S., Welch, W. A., Jung, H., Miller, J. W., Cocker III, D. R., Nenes, A., Jonsson, H. H., Flagan, R. C. and Seinfeld, J. H.: Comprehensive simultaneous shipboard and airborne characterization of exhaust from a modern container ship at sea, Environmental Science & Technology, doi:10.1021/es802413j, 2009.

Novakov, T. and Penner, J. E.: Large Contribution of Organic Aerosols to Cloud-Condensation-Nuclei Concentrations, Nature, 365(6449), 823-826, 1993.

Quinn, P. K., Covert, D. S., Bates, T. S., Kapustin, V. N., Ramsey-Bell, D. C. and McInnes, L. M.: Dimethylsulfide/cloud condensation nuclei/climate system: relevant size-resolved measurements of the chemical and physical properties of atmospheric aerosol particles, Journal of Geophysical Research - Atmospheres, 98, 10411 - 10427, 1993.

Raymond, T. M. and Pandis, S. N.: Cloud activation of single-component organic aerosol particles, J. Geophys. Res.-A., 107(D24), Art. No. 4787, doi:10.1029/2002JD002159, 2002.

Rissman, T. A., VanReken, T. M., Wang, J., Gasparini, R., Collins, D. R., Jonsson, H. H., Brechtel, F. J., Flagan, R. C. and Seinfeld, J. H.: Characterization of ambient aerosol from measurements of cloud condensation nuclei during the 2003 Atmospheric Radiation

Measurement Aerosol Intensive Observational Period at the Southern Great Plains site in Oklahoma, Journal of Geophysical Research - Atmospheres, 111, D05S11,doi:10.1029/2004JD005695, 2006.

Roberts, G., Mauger, G., Hadley, O. and Ramanathan, V.: North American and Asian aerosols over the eastern Pacific Ocean and their role in regulating cloud condensation nuclei, J. Geophys. Res.-A., 111, D13205, doi:10.1029/2005JD006661, 2006.

Roberts, G. C., Artaxo, P., Zhou, J., Swietlicki, E. and Andreae, M. O.: Sensitivity of CCN spectra on chemical and physical properties of aerosol: A case study from the Amazon Basin, Journal of Geophysical Research - Atmospheres, 107, 8070, doi:10.1029/2001JD00583, 2002.

Roberts, G. C. and Nenes, A.: A continuous-flow streamwise thermal-gradient CCN chamber for atmospheric measurements, Aerosol Sci. Technol., 39(3), 206-211, 2005.

Roberts, G. C., Nenes, A., Seinfeld, J. H. and Andreae, M. O.: Impact of biomass burning on cloud properties in the Amazon Basin, Journal of Geophysical Research - Atmospheres, 108(D2), 4062, doi:10.1029/2001JD000985, 2003.

Stroud, C. A., Nenes, A., Jimenez, J. L., DeCarlo, P. F., Huffman, J. A., Bruintjes, R., Nemitz, E., Delia, A. E., Toohey, D. W., Guenther, A. B. and Nandi, S.: Cloud activating properties of aerosol observed during CELTIC, J. Atmos. Sci., 64(2), 441 - 459, 2007.

Sullivan, A. P., Weber, R. J., Clements, A. L., Turner, J. R., Bae, M. S. and Schauer, J. J.: A method for on-line measurement of water-soluble organic carbon in ambient aerosol particles: Results from an urban site, Geophys. Res. Lett., 31, L13105, doi:10.1029/2004GL019681, 2004.

Svenningsson, B., Rissler, J., Swietlicki, E., Mircea, M., Bilde, M., Facchini, M. C., Decesari, S., Fuzzi, S., Zhou, J., Monster, J. and Rosenorn, T.: Hygroscopic growth and critical supersaturations for mixed aerosol particles of inorganic and organic compounds of atmospheric relevance, Atmos. Chem. Phys., 6, 1937-1952, 2006.

Twomey, S.: Minimum size of particle for nucleation in clouds, J. Atmos. Sci., 34(11), 1832-1835, 1977.

VanReken, T. M., Rissman, T. A., Roberts, G. C., Varutbangkul, V., Jonsson, H. H., Flagan, R. C. and Seinfeld, J. H.: Toward aerosol/cloud condensation nuclei (CCN) closure during CRYSTAL-FACE, J. Geophys. Res.-A., 108(D20), 2003.

Vestin, A., Rissler, J., Swietlicki, E., Frank, G. P. and Andreae, M. O.: Cloud-nucleating properties of the Amazonian biomass burning aerosol: Cloud condensation nuclei measurements and modeling, Journal of Geophysical Research - Atmospheres, 112, D14201, doi:10.1029/2006JD008104, 2007.

Wang, J., Lee, Y.-N., Daum, P. H., Jayne, J. and Alexander, M. L.: Effects of aerosol organics on cloud condensation nucleus (CCN) concentration and first indirect aerosol effect, Atmos. Chem. Phys., 8, 6325 - 6339, 2008.

Weber, R. J., Orsini, D., Daun, Y., Lee, Y. N., Klotz, P. J. and Brechtel, F.: A particle-into-liquid collector for rapid measurement of aerosol bulk chemical composition, Aerosol Sci. Technol., 35(3), 718-727, 2001.

Zhou, J., Swietlicki, E., Berg, O. H., Aalto, P. P., Hämeri, K., Nilsson, E. D. and Leck, C.: Hygroscopic properties of aerosol particles over the central Artic Ocean during summer, Journal of Geophysical Research - Atmospheres, 106, 32111 - 32123, 2001.

CHAPTER 6

CCN MEASUREMENTS ABOARD THE CIRPAS TWIN OTTER DURING THE 2007 MASE II CAMPAIGN[11]

In this study, we characterize aerosols sampled onboard the Center for Interdisciplinary Remotely Piloted Aircraft Studies (CIRPAS) Twin Otter during July 2007 in California. We focus our analysis on three of the sixteen flights performed; one downwind of a large ship container off the coast of Monterey and two downwind of a major bovine source in the San Joaquin Valley. The main objective of the study was to assess our understanding of the CCN formation through CCN closure, a comparison between predicted and measured CCN concentration, as well as the droplet growth kinetics. CCN closure was performed by coupling the data obtained from the CCN counter, particle size distribution, and chemical composition measurements with Köhler theory; while the droplet growth kinetic information was obtained from the CCN measurements. CCN closure was performed for two different chemical composition scenarios: size averaged (bulk) and size resolved. For the ship flight, we found an overprediction in CCN of 23% and 16% for the size averaged and size resolved internal mixtures, respectively. The slight improvement in the size resolved CCN closure is due to higher mass fraction of organics found in the smaller size particles which do not contribute solute. For one of the flights downwind of the bovine source, CCN were underpredicted by 14% and overpredicted by 59% for the external and internal size

[11] Data appears in publication: Sorooshian, A., Murphy, S. M., Hersey, S., Gates, H., Padró, L. T., Nenes, A., Brechtel, F. J., Jonsson, H., Flagan, R. C. and Seinfeld, J. H.: Comprehensive airborne characterization of aerosol from a major bovine source, Atmos. Chem. Phys., 8, 5489 – 5520, 2008.

Murphy, S. M., Agrawal, H., Sorooshian, A., Padró, L. T., Gates, H., Hersey, S., Welch, W. A., Jung, H., Miller, J. W., Cocker III, D. R., Nenes, A., Jonsson, H. H., Flagan, R. C. and Seinfeld, J. H.: Comprehensive simultaneous shipboard and airborne characterization of exhaust from a modern container ship at sea, Environ. Sci. Technol., doi:10.1021/es802413j, 2009.

averaged, respectively. Some droplet growth delay was observed for all three flights especially when hydrophobic material was present.

6.1 Motivation

CCN closures have been performed in different locations throughout the world to evaluate our understanding of CCN activation. CCN closures consist of comparing measured and predicted CCN concentrations. CCN predictions are obtained by coupling particle size distributions, chemical composition, and CCN measurements and introducing them into Köhler theory. A number of CCN closure studies (Bigg, 1986; Quinn et al., 1993; Martin et al., 1994; Liu et al., 1996; Covert et al., 1998; Cantrell et al., 2001; Zhou et al., 2001; Roberts et al., 2002; Roberts et al., 2003; VanReken et al., 2003, Asa-Awuku et al., in review[12], Lance et al., in review[13]; Broekhuizen et al., 2006; Rissman et al., 2006; Roberts et al., 2006; Chang et al., 2007; Ervens et al., 2007; Medina et al., 2007; Stroud et al., 2007; Vestin et al., 2007; Cubison et al., 2008; Wang et al., 2008) have been performed in different platforms (e.g., ground, on board ships, and airborne platforms) and environments (e.g., urban, marine) for which the effects of chemical composition and mixing state have been addressed.

Although reasonable CCN closure has been achieved for studies in which a simplified composition (aerosol composed of only $(NH_4)_2SO_4$ or NaCl) scheme has been used (Bigg, 1986; Quinn et al., 1993; Martin et al., 1994; VanReken et al., 2003; Vestin et al., 2007), it is evident that a more detailed chemical composition is needed to achieve a better CCN closure. To address this, different instruments have been used to obtain size averaged (e.g., filters, Micro Orifice Uniform Deposit Impactors (MOUDI), Hygroscopic

[12] Asa-Awuku, A., Moore, R. H., Brock, C. A., Bahreini, R., Middlebrook, A. M., Schwarz, J. P., Spackman, J. R., Holloway, J. S., Stickel, R., Tanner,D. J., Huey, L. G. and Nenes, A.: Airborne cloud condensation nuclei measurements during the 2006 Texas Air Quality Study, In Review.

[13] Lance, S., Gates, H., Varutbangkul, V., Rissman, T., Murphy, S., Sorooshian, A. Brechtel, F., Flagan, R. C., Seinfeld, J. H. and Nenes, A.: CCN activity, closure, and droplet growth kinetics of Houston aerosol during the Gulf of Mexico Atmospheric Composition and Climate Study (GoMACCS), In Review.

Tandem Differential Mobility Analyzers (HT-DMA), and Aerosol Mass Spectrometers) and size resolved (e.g., Aerosol Mass Spectrometers) chemical information. Results obtained from different studies show that having size resolved chemical composition tends to improve predictions since smaller particles tend to have more organics than the bigger ones. Studies have shown that knowledge of aerosol mixing state and chemical composition (Medina et al., 2007, Asa-Awuku et al., in review[12], Lance et al., in review[13]) are needed to achieve good closure.

In the present work, we present data for two types of air masses sampled in California aboard an aircraft. The two air masses were either downwind of a large ship container off the coast of Monterey or downwind of a major bovine source in the San Joaquin Valley. These two cases were chosen due to the different chemical composition and nature of the aerosols measured. Particles emitted from ships tend to be acidic while those found near bovine farms tend to be basic. For these two cases, we perform CCN closures and droplet growth kinetic studies in order to get a better understanding of the formation and growth of the CCN in two areas that are affected by different sources. Despite the numerous CCN closures studies done so far, this is the first time this type of analysis has been perform for such type of air masses. In this study, we pay particular attention to both the effects of chemical composition and mixing state of the aerosol on CCN closure. Finally, we address the effect of organics in the droplet growth kinetics and the possible existence of organic films.

6.2 Observation platform and instruments

During the MArine Stratus Experiment (MASE) II campaign, which took place in July 2007 in Monterey, CA, the Center for Interdisciplinary Remotely Piloted Aircraft Studies (CIRPAS) Twin Otter (http://www.cirpas.org) realized sixteen research flights to characterize the marine stratus clouds that form in this region. The flight plan consisted of twelve minute constant leg flights which allowed full characterization of the aerosols.

Table 6. 1 summarizes the instruments and the measurements performed aboard the Twin Otter. Due to meteorological conditions, not all the flights performed during the campaign characterized marine stratus clouds. As a consequence three distinct research flights were conducted: ship tracks, clear air masses, and polluted air masses. We focus on three research flights, one carried out downwind of a large ship container (July 16; Flight A) off the coast of Monterey and two downwind of a large bovine source (July 12 and 30; Flight B and C) in the San Joaquin Valley. These flights were chosen based on their different aerosol characteristics (basic or acidic) and emission sources affecting the locations.

6.2.1 Particle size distribution and total aerosol concentration

A Dual Automated Classifier Aerosol Detector (DACAD (Wang et al., 2003)) was used to measure the particle size distribution for particles having electrical mobility diameters (d_m) ranging from 10 to 807 nm and places them in 84 bins. The DACAD consists of two scanning Differential Mobility Analyzers (DMA) run in parallel, one at a dry relative humidity and another at a humid relative humidity. However, in this study both DMA's were run under dry relative humidity (RH) conditions. Due to the lack of higher relative humidity measurements no information of the aerosol hygroscopicity is available from this instrument. The DACAD was fully operational with both DMA's off the main inlet throughout both flights. The complete distribution takes 74 seconds.

Total aerosol concentrations were measure by three different Condensation Particle Counters (CPC's), two counters with a minimum diameter of 10 nm (TSI model 3010) and one ultrafine counter with a minimum diameter of 3 nm (TSI model 3025). Total aerosol concentration can also be obtained by integrating the DACAD size distributions however at a lower resolution than the CPC's (1 s). The aerosol concentrations measured by the CPC's were used to align the DACAD and CCN counter measurements due to temporal variations between the instruments.

Table 6. 1: Summary of Twin Otter Missions for MASE II campaign.

Instrument	Measurement
Aerodyne Aerosol Mass Spectrometer (AMS)*	Particle size and chemical composition: 50 nm to 800 nm
Cloud, Aerosol, and Precipitation Spectrometer (CAPS)	Particle size distribution: 0.4 μm to 50 μm
Cloud Condensation Nuclei counter (CCN)	CCN concentration S_c ranging from 0.1 to 1.6 %
Condensation Particle Counter (CPC)	Particle concentration
Counterflow Virtual Impactor (CVI)	Cloud droplet sampler
Differential Aerosol Sizing and Hygroscopicity Spectrometer Probe (DASH-SP)	Particle concentration and hygroscopicity for particle sizes: 120 to 250 nm and 0, 70, 85 and 90 % RH
Dual Automated Classifier Aerosol Detector (DACAD)	Particle size distribution: 10 – 807 nm
Forward Scattering Spectrometer Probe (FSSP)	Particle size distribution: 1.5 to 37 μm
Gerber Liquid Water Content probe (Gerber LWC)	Liquid water content
Multi-angle Light Scattering spectrometer (MLS)	Particle scattering (refractive index)
Passive Cavity Aerosol Spectrometer Probe (PCASP)	Particle size distribution: 0.1 to 2.5 μm
Phase Doppler Interferometer (PDI)	Cloud droplet size and updraft velocities
Particle-Into-Liquid Sampler (PILS) *	Particle chemical composition: 1 μm cut size
Particle Soot Absorption Photometer (PSAP)	Light absorption coefficient
Reverse Inlet (RI)	Interstitial aerosol

*Behind the CVI for cloudy days flights.

6.2.2 Aerosol chemical composition

Size-averaged and size-dependent chemical composition of non-refractory chemical species (ammonium (NH_4^+), SO_4^{2-}, nitrate (NO_3^-), and organics) were measured in real time by an Aerodyne compact Time of Flight Aerosol Mass Spectrometer (C-ToF-AMS; Drewnick et al., 2005) approximately every 24 seconds. The C-ToF-AMS focuses the aerosol samples into a vaporizer which then undergo electron impact ionization and produce a mass spectrum when detected by the mass spectrometer. Size-averaged assumes that all aerosol sizes have the same chemical composition; while for size resolved each aerosol size has a different chemical signature based on the distribution measured. The C-ToF-AMS measures the chemical composition for particles having particle vacuum aerodynamic diameters (d_a) ranging from 9 to 2500 nm and places them in 312 bins.

6.2.3 CCN and growth kinetic measurements

Cloud condensation nuclei concentration was measured with a Continuous Flow-Streamwise Thermal Gradient CCN counter (1 s resolution; Roberts and Nenes, 2005; Lance et al., 2006). The CCN instrument operates by applying a linear temperature gradient across a wetted column; water vapor diffuses more quickly than heat, resulting in a constant water supersaturation along a streamline (Roberts and Nenes, 2005). CCN flowing about the column centerline activate and grow into cloud droplets (D_p > 1 μm) and are counted at the exit with an optical particle counter (OPC; 0.18W and 500 THz). The CCN counter was running on a 12 minute cycle (consistent with constant leg flights) consisting of four to five supersaturations in the range from 0.1 to 0.5 %. The CCN instrument was calibrated five times during the mission with $(NH_4)_2SO_4$ to verify that it was operating properly.

The CCN instrument used in this study was calibrated with $(NH_4)_2SO_4$ similar to that performed in Sorooshian et al. (2008). The calibration procedure consisted of generating particles by atomizing a $(NH_4)_2SO_4$ solution with a high velocity air stream atomizer creating a polydisperse aerosol. The resulting polydisperse aerosol was then dried, charged, and size selected for analysis. The SMCA method (discussed in Chapters 3, 4, and 5) was applied to obtain the d_{p50} which determines the supersaturation in the column. The nominal supersaturation in the column (at d_{p50}) was determined using the traditional Köhler theory (Köhler, 1936) by assuming $(NH_4)_2SO_4$ has a van't Hoff factor of 2.5 (Brechtel and Kreidenweis, 2000) and the surface tension of water. The standard deviation in the supersaturation from Köhler theory was determined from the standard deviation observed in the d_{p50}. Since the supersaturation in the column depends on the temperature gradient, flowrate, and pressure (to a lower extent), calibrations were performed at different pressures (covering height range throughout study) and flow rates (500 and 1000 cm^3 min^{-1}). The resulting calibration curves (s_c versus ΔT; Figure 6. 1) are then interpolated for the temperature gradient and pressure to calculate the nominal supersaturation throughout the study.

Growth kinetics of the CCN can be determined from the CCN measurements; this is done by monitoring the change in droplet size measured at the OPC for all supersaturations studied. Since we sampled polydisperse aerosol, an average droplet diameter was determined from the droplet size distribution. To assess the impact of the aerosol composition and location within the plume, we compared the observed droplet diameters with ammonium sulfate calibration aerosol at two different pressures in order to evaluate the change in droplet diameter that would occur from different flight legs. This is important since pressure affects the supersaturation in the column and therefore the droplet size. For the calibration aerosol, we determine the droplet diameter (D_w) at the activation diameter (diameter at which an aerosol becomes a droplet) for each supersaturation and examine the relationship between supersaturation and D_w. The

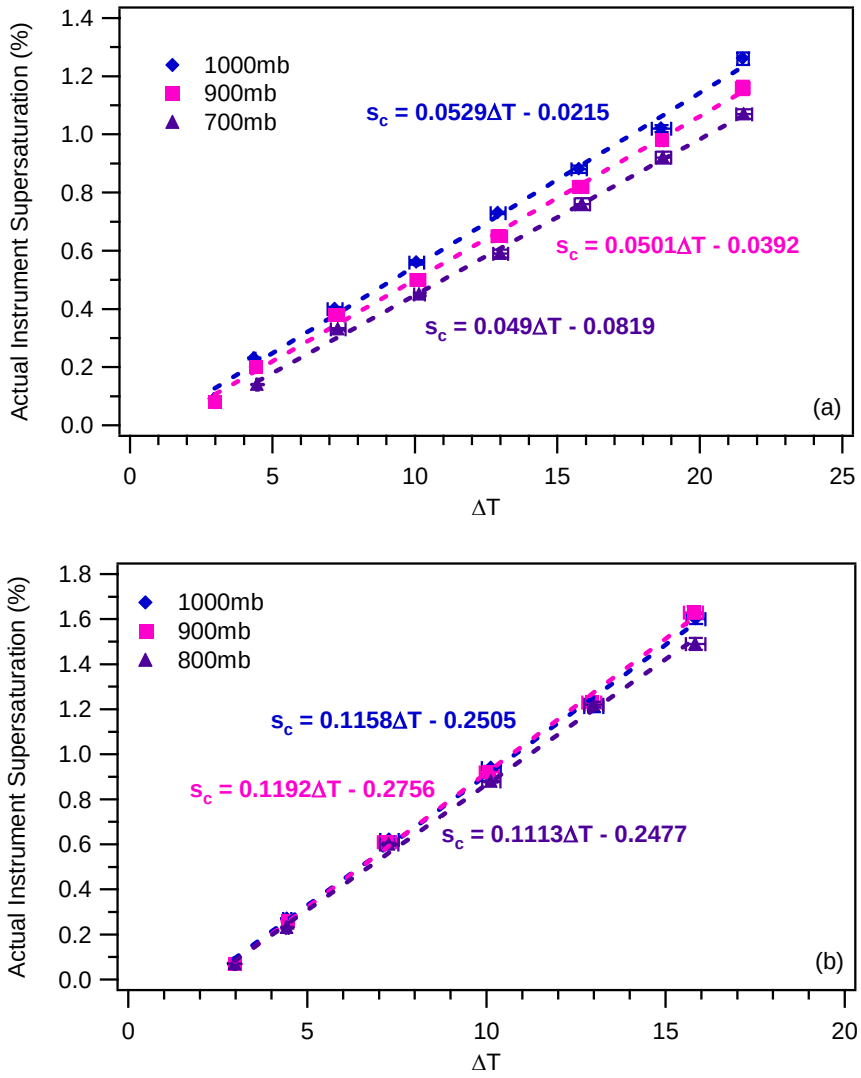

Figure 6. 1: Critical supersaturation versus delta T calibration for $(NH_4)_2SO_4$ aerosol. a) Calibration curve at a constant flowrate of 500 cm^3 min^{-1} and three different pressures: 1000 mb (blue diamonds), 900 mb (pink squares), and 700 mb (purple triangles). b) Calibration curve at a constant flowrate of 1000 cm^3 min^{-1} and three different pressures: 1000 mb (blue diamonds), 900 mb (pink squares), and 800 mb (purple triangles).

calibration growth curves are important since they provide a boundary; shows the minimum size expected for the activation of polydisperse particles that grow as fast as ammonium sulfate. Any points above the calibration curve correspond to particles that grow at least as fast as ammonium sulfate. Below the curve the particles grow more slowly than ammonium sulfate; the extent of delayed growth is reflected by how far away

from the calibration you are. Droplet growth delay can happen in the presence of an organic film which slows the growth of the droplet (Feingold and Chuang, 2002).

6.3 CCN closure

CCN closure is defined as a comparison between measured (from CCN counter) and predicted CCN concentrations, which purpose is to determine how well Köhler theory can predict CCN formation. To predict CCN concentrations, the supersaturation, the aerosol size distribution, and aerosol chemical composition (size averaged and size resolved) is needed. Data from the CCN counter (supersaturation and total CCN; 1 s), DACAD (particle size distribution; 74 s), and C-ToF-AMS (chemical composition; ~24 s) were used. Data from the CCN counter were filtered for pressure and temperature transients, since small perturbations in either can change the supersaturation in the column (Roberts and Nenes, 2005). For the closure analysis, the CCN and AMS measurements were averaged over 74 s intervals due to the lowest resolution of the DACAD. Since all the instruments had different temporal variations due to plumbing, these had to be aligned with the CPC data in order to assure we were sampling the same air mass. This was done by aligning the data to spikes in concentration observed during the flight.

The total CCN concentration at each supersaturation was determined by calculating the minimum aerosol diameter or the activation diameter, d_c, from Köhler theory (Köhler, 1936)

$$d_c = \left(\frac{256 M_w^3 \sigma^3}{27 R^3 T^3 \rho_w^3} \right)^{1/3} \left[\sum_i \left(\frac{M_w}{\rho_w} \right) \left(\frac{\rho_i}{M_i} \right) \varepsilon_i \upsilon_i \right]^{-1/3} s^{-2/3} \qquad (6.1)$$

where M_w is the molar mass of water, σ is the surface tension of the solution, R is the ideal gas constant, T is the temperature, ρ_w is the density of water, s is the supersaturation, and ρ_i, ε_i, υ_i, and M_i are the density, volume fraction, effective van't

Hoff factor and molar mass of the solute i (sulfuric acid (H_2SO_4), ammonium bisulfate (NH_4HSO_4), ammonium sulfate ($(NH_4)_2SO_4$), and ammonium nitrate (NH_4NO_3), and organic), respectively. ε_i is related to the mass fraction of i, x_i, as:

$$\varepsilon_i = \frac{x_i/\rho_i}{\sum_j (x/\rho)_j} \tag{6.2}$$

For the closure, the effective van't Hoff factor of organics was assumed to be 1 (Cruz and Pandis, 1997; Raymond and Pandis, 2002; Broekhuizen et al., 2004; Abbatt et al., 2005; Hartz et al., 2006), while for H_2SO_4, NH_4HSO_4, $(NH_4)_2SO_4$, and NH_4NO_3 values of 2, 2.5, 2.5 and 2 were used, respectively (Svenningsson et al., 2006; Murphy et al., 2009).

Since the DACAD measures d_m and the C-ToF-AMS measures d_a, these had to be related by the following relationship (DeCarlo et al., 2004)

$$d_m = d_a \frac{\rho_o}{\rho_p} \tag{6.3}$$

where ρ_o and ρ_p are the unit density (1 g cm^{-3}) and particle density, respectively. ρ_p was determined for each flight by aligning the particle mass (C-ToF-AMS) and volume distributions (DACAD). Knowledge about the particle density allows us to determine the mass composition in each DACAD bin as well as d_c. The total predicted CCN is obtained by integrating the aerosol size distribution for all diameters greater than d_c.

Four different CCN closure schemes, BULK-EX, BULK-INT, SR-EX, and SR-INT, can be performed based on the chemical composition given (size average or size resolved) and mixing state of the aerosol observed (C-ToF-AMS and hygroscopic growth measurements). Aerosols can be either externally mixed, each aerosol comes from a different source, or internally mixed, aerosols of the same size have a uniform mixture of components or have the same source (Figure 6. 2). For the size average chemical composition data the schemes BULK-EX and BULK-INT can be used; the difference

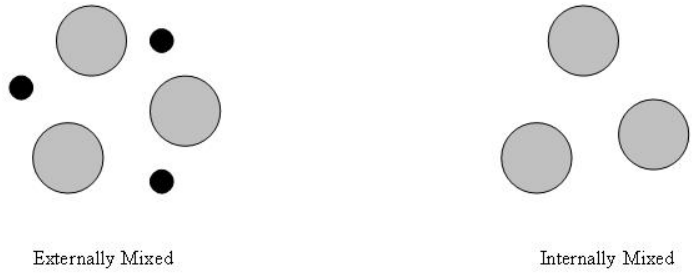

Figure 6. 2: Mixing state of aerosols.

between the two is in how the mixing state of the aerosol is addressed. For the BULK-EX, the aerosol population is considered to be externally mixed while for the BULK-INT, the aerosol is internally mixed. The two mixing states are also considered for the size resolved chemical composition data and these are SR-EX and SR-INT which address the externally and internally mixed aerosols, respectively. For the externally mixed cases (BULK-EX and SR-EX), the total predicted CCN is obtained by assuming the aerosol is composed of pure $(NH_4)_2SO_4$ and then multiplying it by the soluble components (inorganic salts, $(NH_4)_2SO_4$, NH_4HSO_4, H_2SO_4, and NH_4NO_3), which are assumed to be the only ones to contribute to the total CCN.

6.4 Results and discussion

6.4.1 CCN closures

Flight A consisted of following a ship off the coast of Monterey, CA and characterizing the aerosol properties in and out of the plume. For this particular flight, we divided the flight into two distinct air masses. We determined the air mass to be in plume when the total aerosol concentration was at least double the background concentration (~ 500/cm^{-3}). Two chemical composition scenarios were considered in the closure: a) bulk composition which assumes all the particles have the same composition, and, b) size

resolved composition which assigns a specific composition at each particle size. In each of these compositional scenarios, the sulfate molar ratio, SR = $[NH_4^+]/[SO_4^{2-}]$, was computed and used to determine the composition of the sulfate and ammonium particle fraction. When SR ≤ 1, the sulfate and ammonium are a mixture of NH_4HSO_4 and H_2SO_4, when 1 < SR < 2, the sulfate and ammonium are a mixture of NH_4HSO_4 and $(NH_4)_2SO_4$ and when SR ≥ 2, the sulfate and ammonium are composed of $(NH_4)_2SO_4$ and NH_4NO_3 (if NH_4^+ is in excess). In the plume (grey shaded area), the sulfate fraction consisted of mostly H_2SO_4 (Figure 6. 3); therefore it was acidic.

Due to the presence of H_2SO_4 in the plume, special attention had to be given to the particle size distributions to verify we were indeed sampling at low RH conditions. This is particularly important since H_2SO_4 can retain water even at low RH (below 20%, Seinfeld and Pandis, 1998) and can therefore affect the particle size distribution shifting it to larger sizes. After careful analysis it was found that during Flight A, the DACAD RH

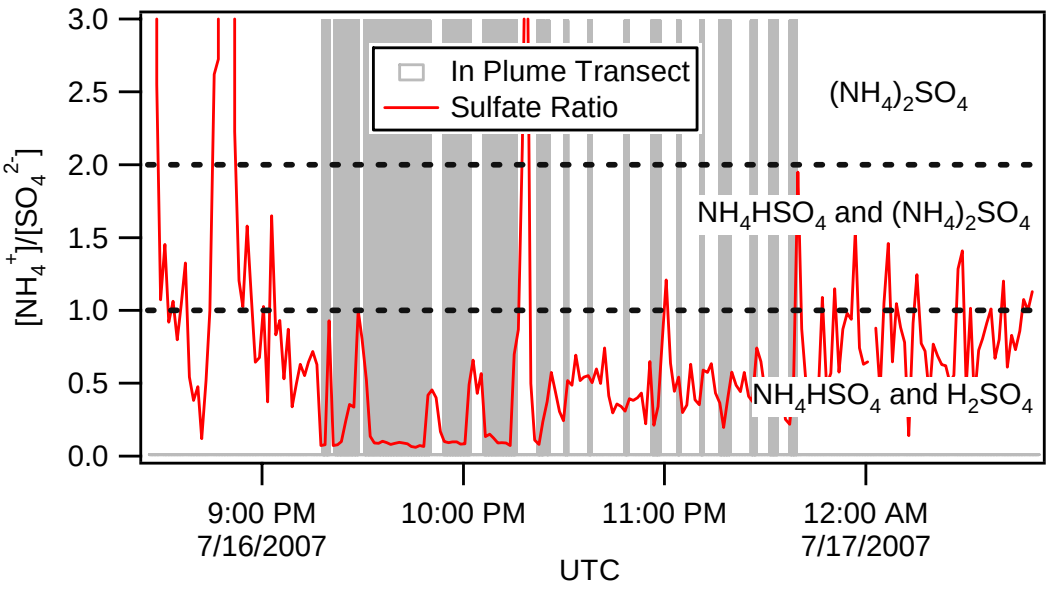

Figure 6. 3: Sulfate ratio as a function of time for Flight A (ship). The areas shaded in gray correspond to the times where we are "in plume".

remove the water associated with the H_2SO_4 (Figure 6. 4). It was found that in general the dry distributions were 15 to 28% smaller than the humid size distributions (Murphy et al., 2009). Besides the increase in size due to the addition of water associated to H_2SO_4, it was between 45 to 50%; thus corrections had to be done to the particle size distribution to was also important to correct for this high RH since the chemical composition reported was measured at dry RH and therefore it needed to be consistent to perform the analysis.

For this flight, CCN closure studies were performed only for the "in plume" case. The aerosol was treated as an internal mixture as supported by the C-ToF-AMS (Figure 6. 5) and the Differential Aerosol Sizing and Hygroscopicity Spectrometer Probe (DASH-SP) measurements (Murphy et al., 2009). In the closure, the organics were treated as hydrophobic (fresh emission) therefore contributing no moles, with the surface tension of water, and a density of 1.6 g/cm^3. The average aerosol density was 1.4 g/cm^3 and was used to convert d_a into d_m. We found that by assuming an internal mixture with

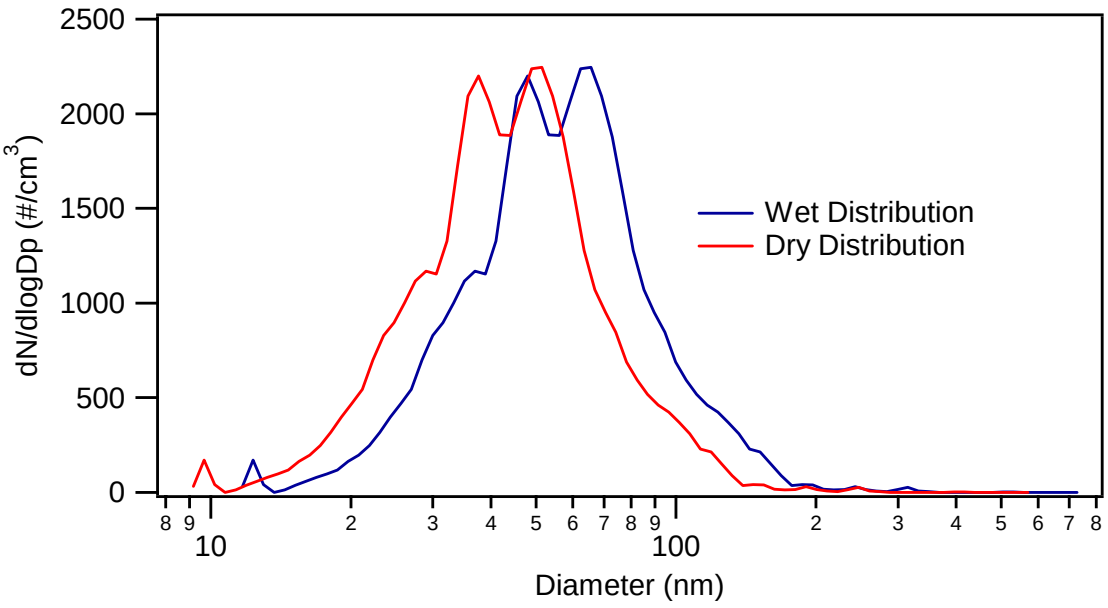

Figure 6. 4: Example of the effects of water retention by H_2SO_4 on the aerosol size distributions in Flight A. The wet distribution is shown in blue and the dry distribution is shown in red.

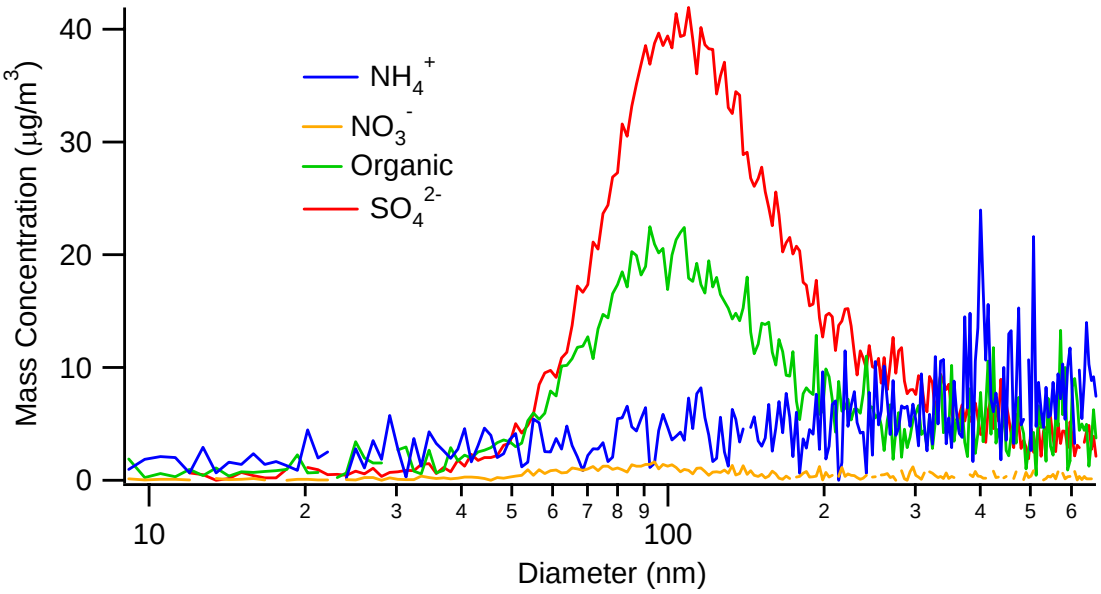

Figure 6. 5: Size resolved chemical composition within plume (Flight A).

bulk average composition the CCN was overpredicted by 23% (Figure 6. 6). We then performed the size resolved CCN closure which we found to improve the closure, where CCN is now overpredicted by only 16% (Figure 6. 7). Improvement is seen in the size-resolved CCN closure because particles below 100 nm have a higher organic volume fraction than at larger sizes but contribute much less to organic loading (Figure 6. 5); using a size averaged composition, hence underestimates the organic fraction in the CCN size range (30 – 100 nm), hence overpredicting CCN concentrations.

For Flight B, CCN closures studies were performed for the size averaged chemical composition scenario while looking at the effects of aerosol mixing. In contrast to Flight A, the aerosol in this flight was basic (Figure 6. 8) and the aerosol mass was dominated by organics. In the closure, the organics were treated as hydrophilic (aged with a van't Hoff factor of 1), with the surface tension of water, and a density of 1.4 g/cm^3. For this flight no distinction was done between the plume (bovine farm) and background aerosol since the ratio of *m/z* 57:44 was found to be nearly constant

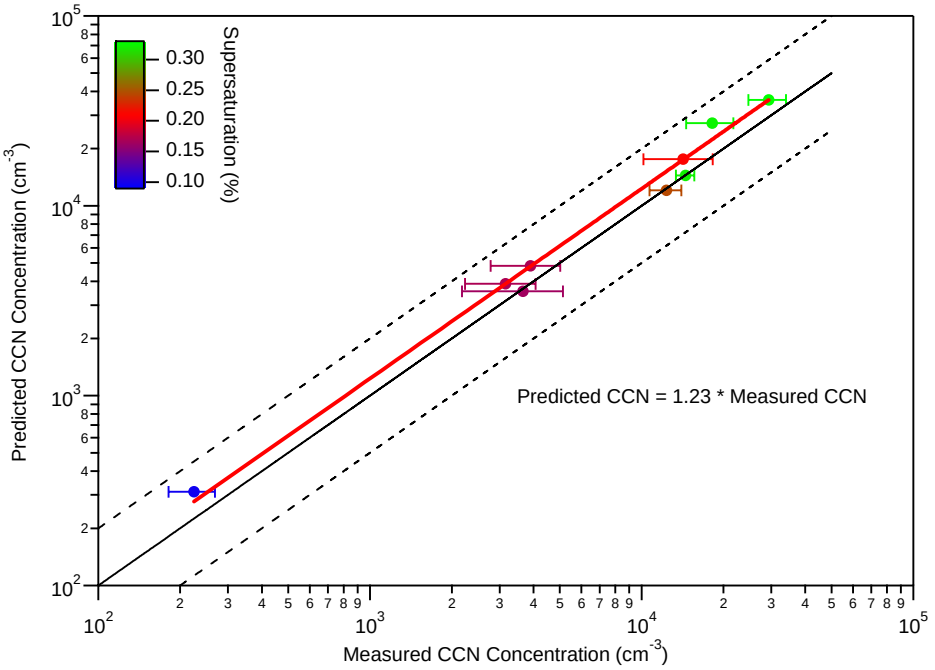

Figure 6. 6: Flight A in plume CCN closure for an internal mixture with size averaged composition. The color scheme refers to the supersaturation in the CCN instrument (Murphy et al., 2009).

throughout the flight (~ 0.07, Sorooshian et al., 2008). The *m/z* 57 peak is associated with the hydrocarbon-like (HOA) structures present in fresh emissions while the *m/z* 44 peak corresponds to oxygenated compounds (OOA) found in aged air masses (Alfarra et al., 2004; Cubison et al., 2006). We found that by assuming an external mixture with bulk average composition the CCN was underpredicted by 14% (Figure 6. 9), while assuming an internal mixture was overpredicted by 59% (Figure 6. 10). The better closure achieved for the external mixture is consistent with the reported externally mixture observed by the C-ToF-AMS during flight B (Sorooshian et al., 2008). Not accounting for the size-resolved chemical composition and residual water (associated with NH_4NO_3) are prime sources of CCN prediction error. The latter would bias the aerosol size distribution measurements to higher diameters which would increase the concentration of predicted CCN. Residual water is possible since the DACAD was found to be running at ~ 25%

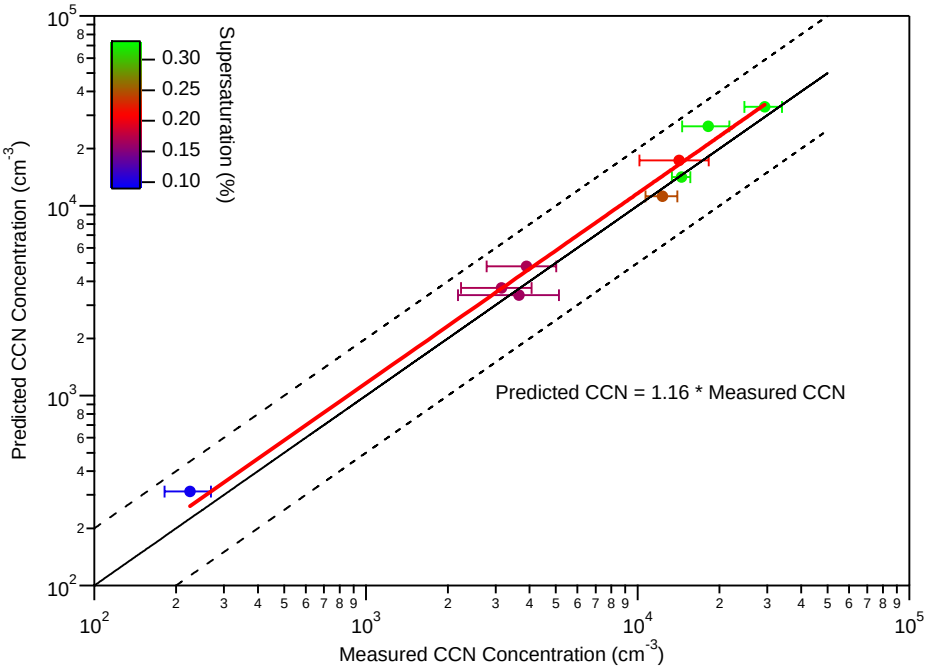

Figure 6. 7: Flight A in plume CCN closure assuming an internal mixture with size resolved composition. The color scheme refers to the supersaturation in the CCN instrument (Murphy et al., 2009).

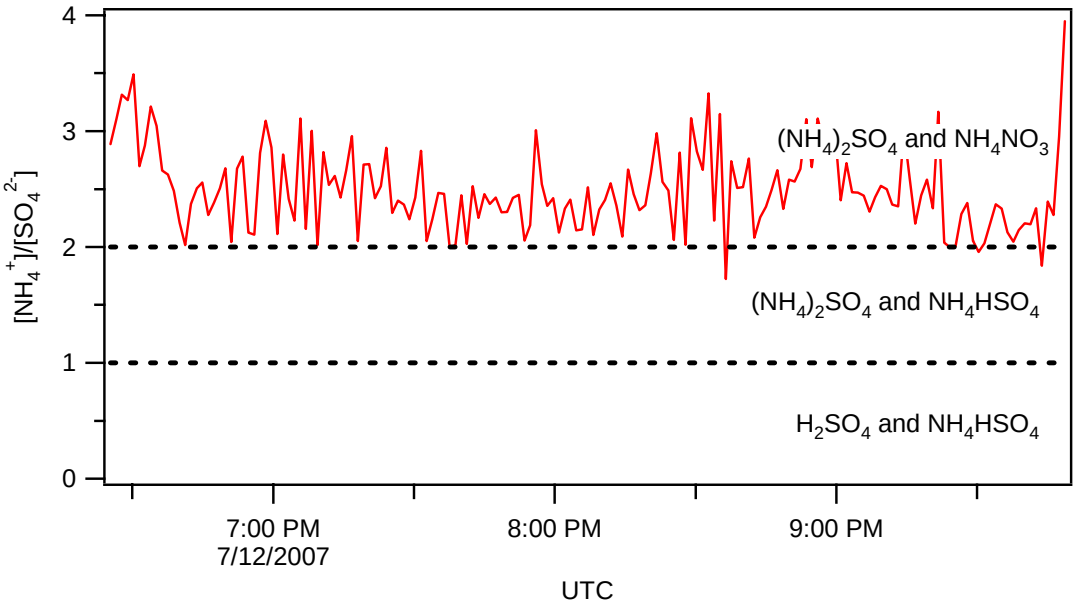

Figure 6. 8: Sulfate ratio as a function of time for Flight B.

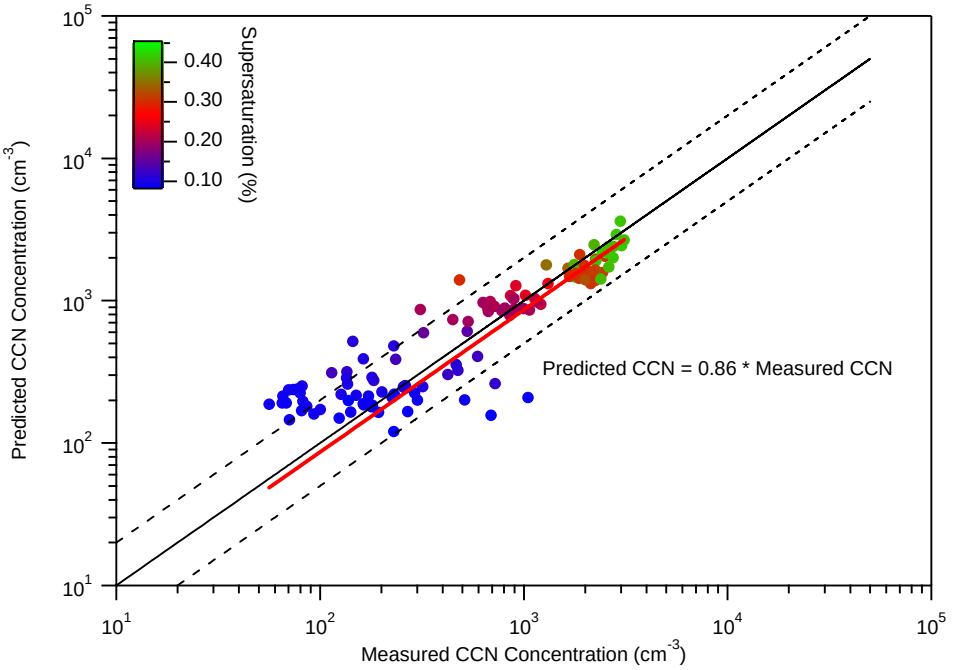

Figure 6. 9: Flight B in plume CCN closure for an external mixture with size averaged composition. The color scheme refers to the supersaturation in the CCN instrument.

RH which above the NH_4NO_3 efflorescence RH; however, should not be as substantial as for H_2SO_4.

6.4.2 Growth kinetics

Even though we just focused our attention to the in plume CCN closure for Flight A, we investigated the droplet growth kinetics in both air mass types: *i*) in plume (IP) and *ii*) out of plume (OP). For IP masses (Figure 6. 11), we found some particles to exhibit some growth delay. The observed droplet growth delay is probably due to the organics present which tend to be more hydrophobic due to the fresher emissions. As for OP masses (Figure 6. 11), we found the particles to exhibit droplet growth similar to ammonium sulfate consistent with aged organics which tend to be more hydrophilic. Whether the aerosols grow more quickly than ammonium sulfate, only size resolved data will tell. Since we are looking at polydisperse aerosols, particles that activate earlier

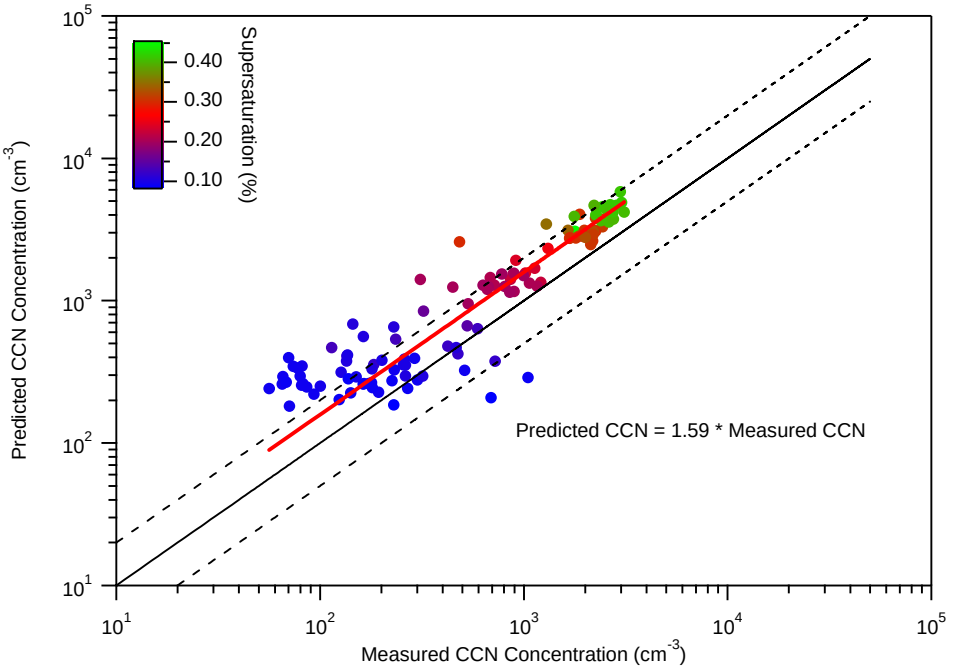

Figure 6. 10: Flight B in plume CCN closure for an internal mixture with size averaged composition. The color scheme refers to the supersaturation in the CCN instrument.

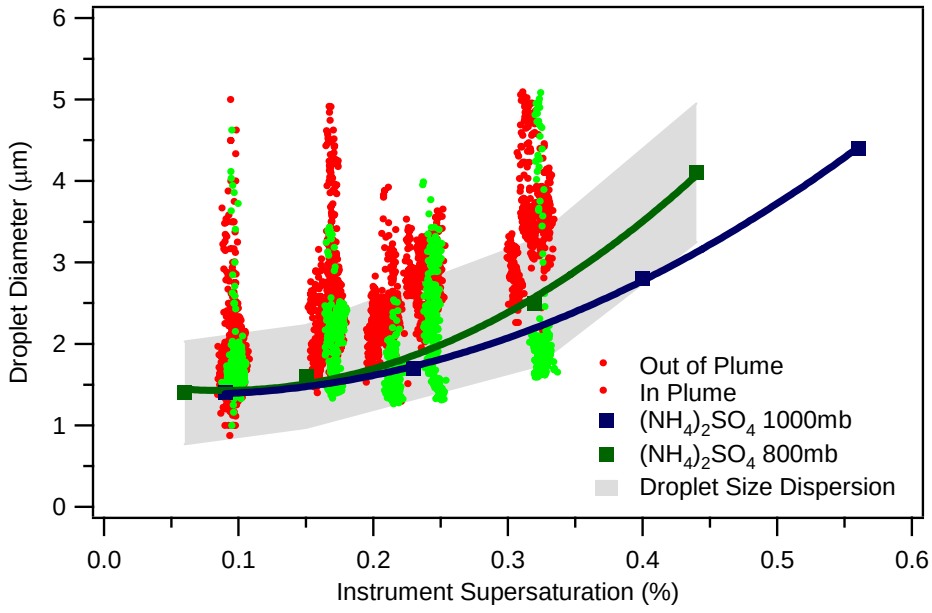

Figure 6. 11: Flight A droplet growth curves for the in plume (green) and out of plume (red) case. The lines correspond to the $(NH_4)_2SO_4$ calibration droplet diameter at 1000 (blue) and 800 (grey) mb (Murphy et al., 2009). The grey band represents the variability in the average droplet distribution.

(lower supersaturation) in the instrument will grow larger while the ones with supersaturation equal to that of the instrument will grow later and will be smaller compared to the first that activated. However, particles with the same critical supersaturation, when exposed to the same supersaturation profile will grow to be about the same size unless the mass transfer coefficient is different.

Additional droplet growth kinetic studies were performed for Flight B which consisted on characterizing the aerosols downwind of a cattle farm in the San Joaquin Valley on a clear sky day. While the ship flight (most of the time; Figure 6. 3) was dominated by H_2SO_4, organics dominated the aerosol mass in this location (Sorooshian et al., 2008) which could affect the growth of droplets by the presence of films. For this flight (Figures 6. 12 and 6. 13), some particles exhibit droplet growth delay especially for those containing relatively greater amounts of hydrophobic material (Sorooshian et al., 2008). This suggests kinetic limitations may play a role in suppressing aerosol water uptake in this region. The broader droplet size observed in Flight B is due to a lower flow (500 cm^3 min^{-1} versus 1000 cm^3 min^{-1}) being introduced into the CCN instrument therefore allowing the particles more time to grow.

6.5 Conclusions

Particle size distribution, chemical composition, and CCN measurements were performed aboard the CIRPAS Twin Otter during the MASE II 2007 campaign in California. This study focused on three flights with different pollution characteristics: one downwind of a large ship container off the coast of Monterey (acidic) and two downwind of a major bovine source in the San Joaquin Valley (basic). In the former H_2SO_4 was found to dominate the aerosol mass while organics dominated the latter. For the ship flight, the air masses were divided into in and out of plume to allow the characterization of fresh and aged aerosols. It was defined to be in plume when the concentration was at least double the background concentration.

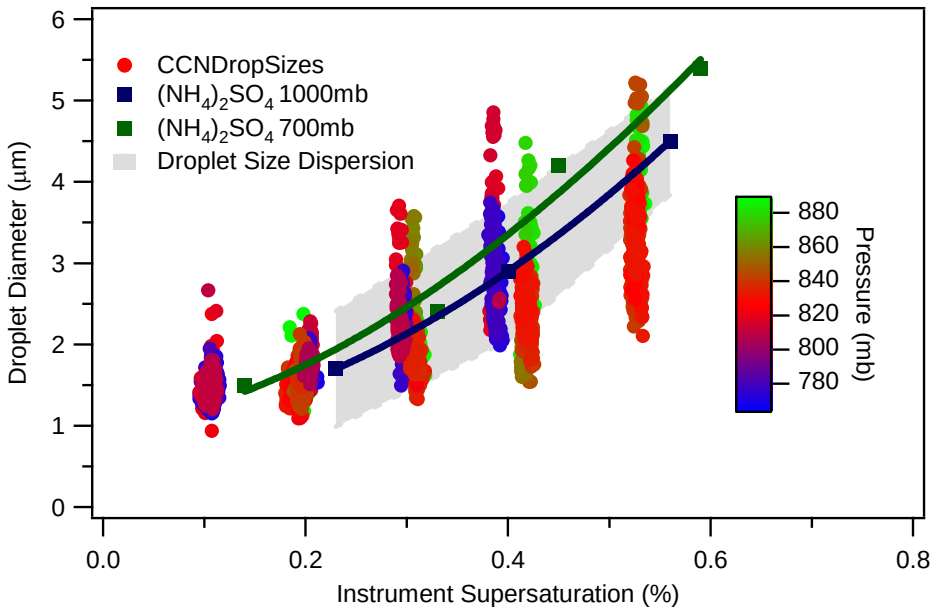

Figure 6. 12: Droplet growth curves for Flight B. The color scheme refers to the pressure (altitude) corresponding to that measurement. The grey band represents the variability in the average droplet distribution.

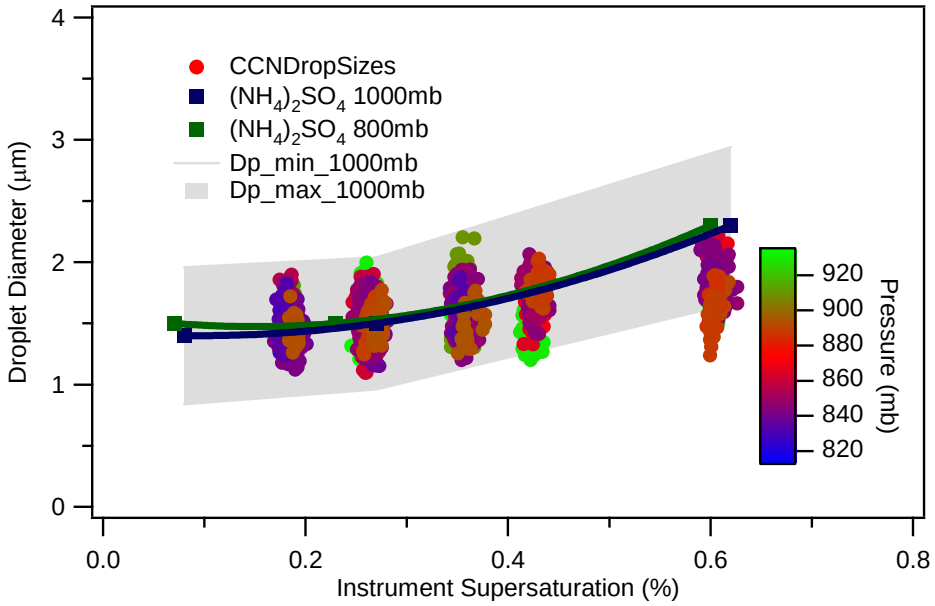

Figure 6. 13: Droplet growth curves for Flight C. The color scheme refers to the pressure (altitude) corresponding to that measurement. The grey band represents the variability in the average droplet distribution.

CCN concentrations were predicted by coupling the particle size distribution, chemical composition, and CCN measurements with Köhler theory. CCN predictions were then compared to the CCN measured through CCN closure plots. In order to perform the predictions in plume for the ship flight, corrections had to be made to the particle size distributions to remove the water associated with H_2SO_4 (always retains water even at low RH) due in part to the DACAD running at high RH. Two chemical composition schemes, size average and size resolved, were addressed through the closure. Introducing size averaged composition was found to overpredict CCN by 23%. A slight improvement in CCN prediction (16%) was achieved for the size average composition although the CCN was still being overpredicted. The improvement seen in the size resolved closure is due to particles smaller than 100 nm having a higher mass fraction of organic which does not contribute solute. For one of the San Joaquin flights (bovine source), size averaged closures of external and internal mixtures were performed. It was found that assuming an external mixture underpredicted CCN concentration by 46%, while assuming an internal mixture overpredicted by 59%. Based on the results of these analyses, it is important to know the composition and mixing state of aerosols to predict CCN more accurately.

Droplet growth kinetic studies for all flights were performed and compared to $(NH_4)_2SO_4$ calibration aerosol in order to access the effects of organics on droplet size. Within the ship plume, some droplet growth delay was observed consistent with the presence of fresher hydrophobic material behind the ship exhaust, while particles outside the plume were found to have growth similar to $(NH_4)_2SO_4$ consistent with the presence of more aged organics present (hydrophilic). For the flight downwind of the bovine source, some droplet growth delay was observed for those having greater amount of hydrophobic material.

6.6 References

Abbatt, J. P. D., Broekhuizen, K. and Kumal, P. P.: Cloud condensation nucleus activity of internally mixed ammonium sulfate/organic acid aerosol particles, Atmos. Environ., 39(26), 4767-4778, 2005.

Alfarra, M. R., Coe, H., Allan, J. D., Bower, K. N., Boudries, H., Canagaratna, M. R., Jimenez, J. L., Jayne, J. T., Garforth, A. A., Li, S. M. and Worsnop, D. R.: Characterization of urban and rural organic particulate in the lower Fraser valley using two aerodyne aerosol mass spectrometers, Atmospheric Environment Part a-General Topics, 38, 5745 - 5758, 2004.

Bigg, E. K.: Discrepancy between observation and prediction of concentrations of cloud condensation nuclei, Atmospheric Research, 20, 82 - 86, 1986.

Brechtel, F. J. and Kreidenweis, S. M.: Predicting particle critical supersaturation from hygroscopic growth measurements in the humidified TDMA. Part I: Theory and sensitivity studies, Journal of Atmospheric Science, 57(12), 1854-1871, 2000.

Broekhuizen, K., Chang, R. Y.-W., Leaitch, W. R., Li, S.-M. and Abbatt, J. P. D.: Closure between measured and modeled cloud condensation nuclei (CCN) using size-resolved aerosol compositions in downtown Toronto, Atmos. Chem. Phys., 6, 2513-2524, 2006.

Broekhuizen, K., Kumar, P. P. and Abbatt, J. P. D.: Partially soluble organics as cloud condensation nuclei: Role of trace soluble and surface active species, Geophys. Res. Lett., 31(1), Art. No. L01107, doi: 10.1029/2003GL018203, 2004.

Cantrell, W., Shaw, G., Cass, G., Chowdhury, Z., Hughes, L., Prather, K., Guazzotti, S. and Coffee, K.: Closure between aerosol particles and cloud condensation nuclei at Kaashidhoo climate observatory, Journal of Geophysical Research - Atmospheres, 106(D22), 28,711 - 28, 718, 2001.

Chang, R. Y.-W., Liu, P. S. K., Leaitch, W. R. and Abbatt, J. P. D.: Comparison between measured and predicted CCN concentrations at Egbert, Ontario: Focus on the organic aerosol fraction at a semi-rural site, Atmospheric Environment Part a-General Topics, 41(37), 8172 - 8182, 2007.

Covert, D., Gras, J., Wiedensohler, A. and Stratmann, F.: Comparison of directly measured CCN with modeled CCN from the number-size distribution in the marine

boundary layer during ACE 1 at Cape Grim, Tasmania, Journal of Geophysical Research - Atmospheres, 103(D13), 16597 - 16608, 1998.

Cruz, C. N. and Pandis, S. N.: A study of the ability of pure secondary organic aerosol to act as cloud condensation nuclei, Atmos. Environ., 31(15), 2205-2214, 1997.

Cubison, M. J., Alfarra, M. R., Allan, J., Bower, K. N., Coe, H., McFiggans, G. B., Whitehead, J. D., Williams, P. I., Zhang, Q., Jimenez, J. L., Hopkins, J. and Lee, J.: The characterisation of pollution aerosol in a changing photochemical environment, Atmos. Chem. Phys., 6, 5573 - 5588, 2006.

Cubison, M. J., Ervens, B., Feingold, G., Docherty, K. S., Ulbrich, I. M., Shields, L., Prather, K., Hering, S. and Jimenez, J. L.: The influence of chemical composition and mixing state of Los Angeles urban aerosol on CCN number and cloud properties, Atmos. Chem. Phys., 8, 5649-5667, 2008.

DeCarlo, P. F., Slowik, J. G., Worsnop, D., Davidovits, P. and Jimenez, J. L.: Particle morphology and density characterization by combined mobility and aerodynamic diameter measurements. Part 1: theory, Aerosol Sci. Technol., 38(12), 1185 - 1205, 2004.

Drewnick, F., Hings, S. S., DeCarlo, P., Jayne, J. T., Gonin, M., Fuhrer, K., Weimer, S., Jimenez, J. L., Demerjian, K. L., Borrmann, S. and Worsnop, D. R.: A new time-of-flight aerosol mass spectrometer (tof-ams) - instrument description and first deployment, Aerosol Sci. Technol., 39, 637 - 658, 2005.

Ervens, B., Cubison, M., Andrews, E., Feingold, G., Ogren, J. A., Jimenez, J. L., DeCarlo, P. and Nenes, A.: Prediction of cloud condensation nucleus number concentration using measurements of aerosol size distributions and composition and light scattering enhancement due to humidity, Journal of Geophysical Research - Atmospheres, 112, D10S32, doi:10.1029/2006JD007426, 2007.

Feingold, G. and Chuang, P. Y.: Analysis of the influence of film-forming compounds on droplet growth: Implications for cloud microphysical processes and climate, J. Atmos. Sci., 59(12), 2006-2018, 2002.

Hartz, K. E. H., Tischuk, J. E., Chan, M. N., Chan, C. K., Donahue, N. M. and Pandis, S. N.: Cloud condensation nuclei activation of limited solubility organic aerosol, Atmos. Environ., 40(4), 605-617, 2006.

Köhler, H.: The nucleus in and the growth of hygroscopic droplets, Transactions of the Faraday Society, 32(2), 1152-1161, 1936.

Lance, S., Medina, J., Smith, J. N. and Nenes, A.: Mapping the operation of the DMT continuous flow CCN counter Aerosol Sci. Technol., 40, 242-254, 2006.

Liu, P., Leaitch, W., Banic, C., Li, S., Ngo, D. and Megaw, W.: Aerosol observations at Chebogue Point during the 1993 North Atlantic Regional Experiment: Relationships among cloud condensation nuclei, size distribution, and chemistry, Journal of Geophysical Research - Atmospheres, 101, 28971 - 28990, 1996.

Martin, G. M., Johnson, D. W. and Spice, A.: The measurement and parameterization of effective radius of droplets in warm stratocumulus clouds, Journal of Atmospheric Science, 51, 1823 - 1842, 1994.

Medina, J., Nenes, A., Sotiropoulou, R. E. P., Cottrell, L. D., Ziemba, L. D., Beckman, P. J. and Griffin, R. J.: Cloud condensation nuclei closure during the International Consortium for Atmospheric Research on Transport and Transformation 2004 campaign: Effects of size-resolved composition, Journal of Geophysical Research - Atmospheres, 112, D10S31, doi:10.1029/2006JD007588, 2007.

Murphy, S. M., Agrawal, H., Sorooshian, A., Padro, L. T., Gates, H., Hersey, S., Welch, W. A., Jung, H., Miller, J. W., Cocker III, D. R., Nenes, A., Jonsson, H. H., Flagan, R. C. and Seinfeld, J. H.: Comprehensive simultaneous shipboard and airborne characterization of exhaust from a modern container ship at sea, Environmental Science & Technology, doi:10.1021/es802413j, 2009.

Quinn, P. K., Covert, D. S., Bates, T. S., Kapustin, V. N., Ramsey-Bell, D. C. and McInnes, L. M.: Dimethylsulfide/cloud condensation nuclei/climate system: relevant size-resolved measurements of the chemical and physical properties of atmospheric aerosol particles, Journal of Geophysical Research - Atmospheres, 98, 10411 - 10427, 1993.

Raymond, T. M. and Pandis, S. N.: Cloud activation of single-component organic aerosol particles, J. Geophys. Res.-A., 107(D24), Art. No. 4787, doi:10.1029/2002JD002159, 2002.

Rissman, T. A., VanReken, T. M., Wang, J., Gasparini, R., Collins, D. R., Jonsson, H. H., Brechtel, F. J., Flagan, R. C. and Seinfeld, J. H.: Characterization of ambient aerosol from measurements of cloud condensation nuclei during the 2003 Atmospheric Radiation Measurement Aerosol Intensive Observational Period at the Southern Great Plains site in

Oklahoma, Journal of Geophysical Research - Atmospheres, 111, D05S11,doi:10.1029/2004JD005695, 2006.

Roberts, G., Mauger, G., Hadley, O. and Ramanathan, V.: North American and Asian aerosols over the eastern Pacific Ocean and their role in regulating cloud condensation nuclei, J. Geophys. Res.-A., 111, D13205, doi:10.1029/2005JD006661, 2006.

Roberts, G. C., Artaxo, P., Zhou, J., Swietlicki, E. and Andreae, M. O.: Sensitivity of CCN spectra on chemical and physical properties of aerosol: A case study from the Amazon Basin, Journal of Geophysical Research - Atmospheres, 107, 8070, doi:10.1029/2001JD00583, 2002.

Roberts, G. C. and Nenes, A.: A continuous-flow streamwise thermal-gradient CCN chamber for atmospheric measurements, Aerosol Sci. Technol., 39(3), 206-211, 2005.

Roberts, G. C., Nenes, A., Seinfeld, J. H. and Andreae, M. O.: Impact of biomass burning on cloud properties in the Amazon Basin, Journal of Geophysical Research - Atmospheres, 108(D2), 4062, doi:10.1029/2001JD000985, 2003.

Seinfeld, J. H. and Pandis, S.: Atmospheric Chemistry and Physics, ed, John Wiley, New York, 1998.

Sorooshian, A., Murphy, S. M., Hersey, S., Gates, H., Padro, L. T., Nenes, A., Brechtel, F. J., Jonsson, H., Flagan, R. C. and Seinfeld, J. H.: Comprehensive airborne characterization of aerosol from a major bovine source, Atmos. Chem. Phys., 8, 5489 - 5520, 2008.

Stroud, C. A., Nenes, A., Jimenez, J. L., DeCarlo, P. F., Huffman, J. A., Bruintjes, R., Nemitz, E., Delia, A. E., Toohey, D. W., Guenther, A. B. and Nandi, S.: Cloud activating properties of aerosol observed during CELTIC, J. Atmos. Sci., 64(2), 441 - 459, 2007.

Svenningsson, B., Rissler, J., Swietlicki, E., Mircea, M., Bilde, M., Facchini, M. C., Decesari, S., Fuzzi, S., Zhou, J., Monster, J. and Rosenorn, T.: Hygroscopic growth and critical supersaturations for mixed aerosol particles of inorganic and organic compounds of atmospheric relevance, Atmos. Chem. Phys., 6, 1937-1952, 2006.

VanReken, T. M., Rissman, T. A., Roberts, G. C., Varutbangkul, V., Jonsson, H. H., Flagan, R. C. and Seinfeld, J. H.: Toward aerosol/cloud condensation nuclei (CCN) closure during CRYSTAL-FACE, J. Geophys. Res.-A., 108(D20), 2003.

Vestin, A., Rissler, J., Swietlicki, E., Frank, G. P. and Andreae, M. O.: Cloud-nucleating properties of the Amazonian biomass burning aerosol: Cloud condensation nuclei measurements and modeling, Journal of Geophysical Research - Atmospheres, 112, D14201, doi:10.1029/2006JD008104, 2007.

Wang, J., Flagan, R. C. and Seinfeld, J. H.: A differential mobility analyzer (DMA) system for submicron aerosol measurements at ambient relative humidity, Aerosol Sci. Technol., 37, 46-52, 2003.

Wang, J., Lee, Y.-N., Daum, P. H., Jayne, J. and Alexander, M. L.: Effects of aerosol organics on cloud condensation nucleus (CCN) concentration and first indirect aerosol effect, Atmos. Chem. Phys., 8, 6325 - 6339, 2008.

Zhou, J., Swietlicki, E., Berg, O. H., Aalto, P. P., Hämeri, K., Nilsson, E. D. and Leck, C.: Hygroscopic properties of aerosol particles over the central Artic Ocean during summer, Journal of Geophysical Research - Atmospheres, 106, 32111 - 32123, 2001.

CHAPTER 7

SUMMARY AND IMPLICATIONS

7.1 Synopsis

In this thesis, we study the CCN activity of laboratory and ambient aerosols with a significant fraction of carbonaceous material in an effort to improve our understanding of their role on droplet formation. Organics can affect CCN activity by lowering droplet surface tension (Shulman et al., 1996; Li et al., 1998; Facchini et al., 2000), altering the particle hygroscopicity (Shulman et al., 1996; Laaksonen et al., 1998), and potentially by retarding droplet activation kinetics by affecting the shape of the Köhler curve and impeding the condensation rate of water onto droplets (e.g., Shulman et al., 1996; Shantz et al., 2003;Feingold and Chuang, 2002;Ruehl et al, 2008;Asa-Awuku et al., 2009;Ruehl et al, in press). These complex interactions motivate the need to represent these effects in a comprehensive and simple manner, so that they can be incorporated in droplet formation parameterizations used in global model simulations of the aerosol indirect effect. The desired experimental information needed for parameterizations are surface tension depression, average molar properties (e.g., solubility) as well as the molar mass, chemical heterogeneity (mixing state) of the aerosol, and droplet growth kinetics. This thesis focuses on developing techniques and obtaining measurements required for constraining these parameters.

In Chapter 2, we studied the apparent solubility enhancement inferred from laboratory CCN activity experiments of sparingly soluble organics, and explore whether it could result from particle curvature effects on solubility. This phenomenon, termed Curvature Enhanced Solubility (CES), was investigated for nine organic compounds (using measurements of contact angle to infer the interfacial tension between substrate

and water) that have atmospheric relevance and have a wide range of solubility in water. It was shown that introducing CES into Köhler theory, could explain the unexpectedly high CCN activity, provided that the aerosol is initially wet (consistent with observations). If the original particle is completely dry, CCN activity is consistent with its "bulk" solubility. In terms of its implications for the atmosphere, CES may often occur in ambient particles as they almost always contain residual water. If true, then most hydrophilic organics could be assumed "completely soluble" when their effects are included in calculations of CCN activity.

In Chapter 3, we proposed a new method called Köhler Theory Analysis (KTA) to infer the molar volume (molar mass over density) of organics by combining surface tension, chemical composition, and CCN measurements. KTA was evaluated for six organic compounds in pure form and in mixtures with $(NH_4)_2SO_4$. We found KTA to predict the molar volume of the organics within 18% of the expected values when the organic mass fraction ranges between 50 and 90%; therefore proving the potential of this method for determining CCN characteristics of ambient samples. Besides the organic molar mass, KTA can also be used to determine the solubility and surfactant characteristics of organics which are also important to improve our understanding of aerosol-cloud formation. Köhler Theory Analysis has been applied to biomass burning WSOC (Asa-Awuku et al., 2008), secondary organic aerosol (Asa-Awuku et al., 2007; Engelhart et al., 2008; Asa-Awuku et al., 2009) and seawater organic matter (Moore et al., 2008) samples successfully.

In Chapter 4, KTA was applied to the water-soluble fraction of Mexico City aerosol collected during the MILAGRO campaign in March 2006. We characterized the water soluble fraction by performing surface tension, CCN activity, and droplet growth kinetic measurements. Filter samples were collected from two sites, one in downtown and another downwind of Mexico City, and analyzed the soluble material by water extraction. We found the organics in the Mexico City valley to act as surfactants, depressing surface

tension by about 10-15% from pure water. Surface tension depression in samples collected from downtown was slightly larger than that from downwind of Mexico City. In terms of CCN activity and hygroscopicity, the water soluble extracts from both sites exhibited remarkable similarity, corresponding to a hygroscopicity parameter between 0.22 and 0.37. The aerosol hygroscopicity did not strongly correlate with organic mass fraction, suggesting that the surface tension depression compensates for the lack of solute whenever the organic fraction increases. The CCN activation kinetic for all samples considered are similar to $(NH_4)_2SO_4$ and therefore the presence of water-soluble organics do not seem to impact the kinetics of droplet formation. The organic molar mass for the downwind site was found to range from 118 to 473 g mol^{-1} which changed depending on the sample time period, meteorology, and airmass characteristics. The invariance of hygroscopicity of the water-soluble material may help explain why CCN closure studies are often insensitive to assumption of chemical composition; it also suggests that key towards a successful closure is knowledge of the soluble fraction of the aerosol (inorganic and organics combined) and size distribution.

Finally, in Chapters 5 and 6, we explored the CCN activity and growth kinetics of CCN sampled in polluted environments and quantified the impact of chemical composition and mixing state variability on CCN closure. Using measurements of size distribution, chemical composition (size averaged and size resolved), CCN concentrations were predicted and compared against observed CCN concentration. Chapter 5 focuses on ground-based measurements of Atlanta aerosol; while Chapter 6, focuses on airborne sampling of plumes emitted from ship and bovine sources. These studies represent the first time in which CCN closures for such sources were carried out. Based on the results of the CCN closures, it is evident that an accurate chemical composition (size resolved versus size averaged) and mixing state of the aerosol is needed to predict CCN more accurately since these parameters control their ability to become cloud droplets. Some droplet growth delay, especially at the higher

supersaturations (smaller activation diameters), was observed in these polluted environments consistent with having greater amount of hydrophobic or less hygroscopic organic material.

From our analysis and results, we suggest the modeling community to assume the organics present in the aerosol to be completely soluble; especially in regions were the relative humidity is high and the organics present are surfactant. As shown from the different CCN closures, the chemical composition and mixing state of the aerosol are critical to obtain good closure, which one is more important however depends on the location. Since studies have found the predicted cloud droplet number error to be at most half of the CCN prediction error (obtained from closure studies; Sotiropoulou et al., 2006), we suggest that modelers treat the aerosol as completely soluble and in conjuction with an assumed chemical composition (size resolved or size averaged) and mixing state scenario since we found this parameters tend to provide good closure (within 30%). Although having size-resolved mixing state gives excellent CCN closure, we do not suggest this analysis to be included in models since it is computationally expensive.

In conclusion, we have shown (together with mounting evidence in the literature) that the organic effects on cloud droplet number, although potentially complex, can still be described in a relatively comprehensive and simple manner, ideally suited for cloud droplet formation parameterizations used in atmospheric models. Furthermore, the CCN closure studies carried out suggest that CCN prediction error associated with simplifying composition assumptions is constrained, and may not be prohibitively large for global indirect forcing assessments. Although further research is required to explore the link between CCN and chemical ageing, mixing state, volatility, and aerosol phase, the work presented here suggests that the aerosol-CCN link can be sufficiently described in atmospheric models.

7.2 References

Asa-Awuku, A., Engelhart, G. J., Lee, B. H., Pandis, S. N. and Nenes, A.: Relating CCN activity, volatility, and droplet growth kinetics of β-caryophyllene secondary organic aerosol, Atmos. Chem. Phys., 9, 795-812, 2009.

Asa-Awuku, A., Nenes, A., Gao, S., Flagan, R. C. and Seinfeld, J. H.: Alkene ozonolysis SOA: inferences of composition and droplet growth kinetics from Köhler theory analysis, Atmos. Chem. Phys. Discuss., 7, 8983-9011, 2007.

Asa-Awuku, A., Nenes, A., Sullivan, A. P., Hennigan, C. and Weber, R. J.: Investigation of Molar Volume and Surfactant Characteristics of Water-Soluble Organic Compounds in Biomass Burning Aerosol Atmos. Chem. Phys., 8, 799 - 812, 2008.

Engelhart, G. J., Asa-Awuku, A., Nenes, A. and Pandis, S. N.: CCN activity and droplet growth kinetics of fresh and aged monoterpene secondary organic aerosol, Atmos. Chem. Phys., 8, 3937 - 3949, 2008.

Facchini, M. C., Decesari, S., Mircea, M., Fuzzi, S. and Loglio, G.: Surface tension of atmospheric wet aerosol and cloud/fog droplets in relation to their organic carbon content and chemical composition, Atmos. Environ., 34(28), 4853-4857, 2000.

Laaksonen, A., Korhonen, P., Kulmala, M. and Charlson, R. J.: Modification of the Köhler equation to include soluble trace gases and slightly soluble substances, J. Atmos. Sci., 55(5), 853-862, 1998.

Li, Z. D., Williams, A. L. and Rood, M. J.: Influence of soluble surfactant properties on the activation of aerosol particles containing inorganic solute, J. Atmos. Sci., 55(10), 1859-1866, 1998.

Moore, R. H., Ingall, E. D., Sorooshian, A. and Nenes, A.: Molar mass, surface tension, and droplet growth kinetics of marine organics from measurements of CCN activity, Geophys. Res. Lett., 35, L07801, doi:10.1029/2008GL033350, 2008.

Ruehl, C. R., Chuang, P. Y. and Nenes, A.: How quickly do cloud droplets form on atmospheric particles?, Atmos. Chem. Phys., 8, 1043 – 1055, 2008.

Ruehl, C. R., Chuang, P. Y. and Nenes, A.: Distinct CCN activation kinetics above the marine boundary layer along the California coast, Geophys. Res. Lett., in press.

Shantz, N. C., Leaitch, W. R. and Caffrey, P. F.: Effect of organics of low solubility on the growth rate of cloud droplets, J. Geophys. Res.-A., 108(D5), 2003.

Shulman, M. L., Jacobson, M. C., Carlson, R. J., Synovec, R. E. and Young, T. E.: Dissolution behavior and surface tension effects of organic compounds in nucleating cloud droplets, Geophys. Res. Lett., 23(3), 277-280, 1996.

Sotiropoulou, R. E., Medina, J. and Nenes, A.: CCN predictions: Is theory sufficient for assessments of the indirect effect?, Geophys. Res. Lett., 33(L05816), doi:10.1029/2005GL025148, 2006.

VITA

LUZ TERESA PADRÓ MARTÍNEZ

Luz Teresa Padró Martínez was born in Rio Piedras, Puerto Rico. She graduated from Colegio Rosa-Bell in 1999 and received a B. S. in Chemical Engineering (*Cum Laude*) from Virginia Polytechnic Institute and State University in Blacksburg, VA in 2004 before coming to Georgia Institute of Technology to pursue a doctorate in Chemical Engineering with a minor in Atmospheric Chemistry.